The dual role of the desmosomal regulator Plakophilin 3

in cellular adhesion and cell cycle progression

Dissertation

zur Erlangung des

Doktorgrades der Naturwissenschaften (Dr. rer. nat.)

der

Naturwissenschaftlichen Fakultät I – Biowissenschaften –

der Martin-Luther-Universität Halle-Wittenberg,

vorgelegt

von Frau Lisa Müller

geboren am 01.11.1990 in Halle

Gutachter*innen: Herr Prof. Dr. Stefan Hüttelmaier

Frau Prof. Dr. Mechthild Hatzfeld

Herr Prof. Dr. Rudolf Leube

Tag der Verteidigung: 17.02.2023

„Für einen Forscher sind die unvergessenen Momente seines Lebens jene seltenen, die nach Jahren mühsamer Arbeit entstanden sind, wenn das Geheimnis um die Natur plötzlich gelüftet ist und wenn das, was dunkel und chaotisch war, in einem klaren und schönen Licht und Muster erscheint."

(Gerty Cori, Biochemikerin)

This doctoral thesis is based on two research publications.

TABLE OF CONTENTS

Danksagung

Curriculum Vitae

List of publications, presentations, and posters

Eidesstattliche Erklärung

1. ABSTRACT

Maintaining skin integrity is crucial for life. Under normal conditions, the skin surface is in a constant state of renewal, whereas deregulation can result in a variety of skin diseases, including cancer. In the epidermis, proliferation is restricted to the basal layer whereas the suprabasal layers are critical for barrier formation. This implies that adhesion between these layers must be different. Desmosomes are cell structures specialized for cell-to-cell adhesion. While cell type specific expression of desmosomal proteins including the plakophilins (PKPs) has been known for years, little is known about how PKP isoforms affect desmosomal properties and how desmosomal localization of these isoforms is regulated. It has previously been shown that insulin like growth factor 1/insulin signaling phosphorylates PKP1, which results in translocation from the desmosome into the cytoplasm leading to decreased adhesive strength. At the same time, this activates PKP1's function in translation, which promotes proliferation.

How PKP3 localization and function are regulated in keratinocytes and during epidermal differentiation is not clear to date. To elucidate the roles of PKP3 in adhesion and in signaling, PKP3-dependent adhesive properties and modifications by growth factor signaling were analyzed in murine keratinocytes and human A431 cells. Here, I show that epidermal growth factor but not insulin like growth factor 1/insulin signaling is important for phosphorylation of PKP3 and its recruitment to the plasma membrane to facilitate desmosome assembly. PKP3 associates with ribosomal S6 kinases with a preference for the isoform 1 resulting in the accumulation of PKP3 at tricellular contacts, which correlates with the stabilization of intercellular adhesion. This indicates that PKP1 and PKP3 sense signals from different growth factors and interpret these signals in distinct ways that either promote (PKP3) or prevent (PKP1) their desmosomal localization.

PKPs perform additional functions in the nucleus and the cytoplasm. For PKP3, these functions have not yet been well characterized. Since the ratio of PKP3 to PKP1 is much higher in the proliferating basal cells compared to suprabasal cells, I asked how PKP3 contributes to the control of proliferation. To test this, I used non-transformed murine keratinocytes to avoid bias from disturbed cell cycle control in cancer cells and to focus on the mechanistic basis of PKP3's role in proliferation. In this thesis, I have identified PKP3 as a scaffold in epidermal growth factor receptor signaling, which promotes ribosomal S6 kinase activation. In addition, I show that PKP3 acts as a signaling hub modulating the retinoblastoma pathway via an epidermal growth factor receptor – runt-related transcription factor 3 – p21 axis to promote cell cycle progression.

ABSTRACT

These data challenge the view of desmosomes as static structures and show how signaling pathways balance PKP functions to regulate adhesive strength and allow desmosomes to adapt to their environment in a context-dependent manner. This implicates that desmosomal proteins are active signaling hubs that receive signals (phosphorylation of PKP1 by insulin like growth factor 1/insulin and of PKP3 by epidermal growth factor, respectively) and transduce this information to modulate adhesive strength and control proliferation. This supports the accurate balance of proliferation and differentiation which is required to control tissue homeostasis in the epidermis.

2. INTRODUCTION

2.1. Structure and function of the skin

The skin is the outermost layer of the body and thus separates the internal tissues from the external environment. It consists of three layers: hypodermis, dermis, and epidermis (Figure 1A). The three skin layers are composed of distinct cell types and imply a strong as well as a flexible physical structure, to ensure both integrity and flexibility of the skin (Goodarzi *et al.*, 2018).
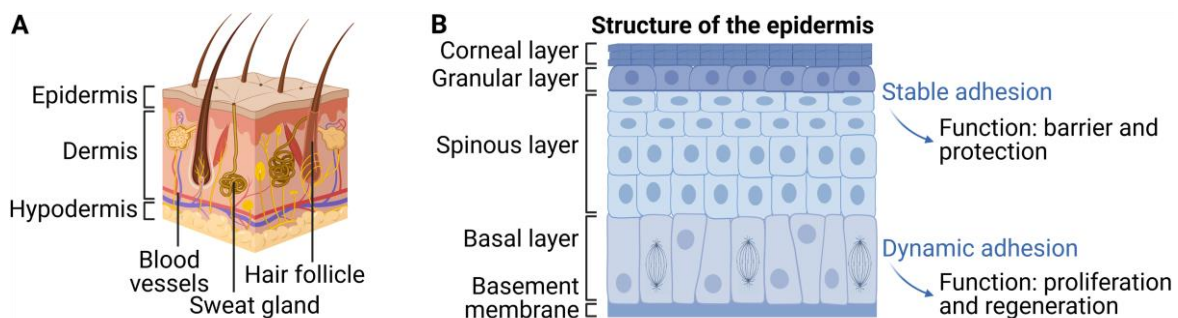
Figure 1 │ Structure and function of the skin and the epidermis. Created with biorender.com, modified from (Delva *et al.*, 2009). **(A)** The skin is composed of three main layers: the epidermis, dermis, and hypodermis. **(B)** The stratified epidermis is comprised of four distinct layers – corneal, granular, spinous, and basal layer, which are attached to the basement membrane. The high proliferative character of the basal layer is represented by mitotic spindles in these cells. Epidermal integrity is based on stable and dynamic intercellular adhesion, which maintain the barrier and regeneration function of the epidermis.

The lowest layer is the hypodermis (subcutis), which contains mainly adipose and connective tissue and thus serves as a heat and nutrient reservoir as well as a shock absorber. The overlying dermis contains blood vessels, sweat glands, and hair follicles and consists of a dense network of tear-resistant collagen fibers, elastic fibers, and connective tissue cells, which give the skin stability while simultaneously allowing elasticity. In contrast, the epidermis is a stratified squamous epithelium composed primarily of keratinocytes, which by virtue of their morphological and metabolic characteristics are divided into four layers (Figure 1B): The basal layer, which is attached to a non-cellular basement membrane, consists of epidermal stem cells that continuously divide by mitosis to give rise to keratinocytes (Alonso and Fuchs, 2003). Basal keratinocytes form a single layer and are composed of basophilic cytoplasm and a chromatin-rich nucleus in an elliptical shape. During the differentiation process called keratinization, new cells generated by stem cells in the basal layer push the keratinocytes upward into the spinous layer and granular layer, where they differentiate (Watt, 1989). During continuous keratinization, the typical cellular structure is replaced by keratin accumulation. In these multilayers, keratinocytes are shaped like a polyhedron, have prominent cytoplasm and round-oval nuclei.

In the corneal layer, terminally differentiated keratinocytes are filled with keratin intermediate filaments, leaving these metabolic inactive cells flat and anucleated. These cells are finally shed in a process called desquamation. Thus, the epidermis is a dynamic structure whose integrity is based on the constant generation of new cells and their outward transport with associated differentiation. Keratinocyte adhesion plays a central role and is present in a dynamic low affinity state in the lower proliferating layers, whereas in the upper layers the differentiated keratinocytes show a high affinity adhesive state (Garrod and Chidgey, 2008). This organization as a stratified epithelium maximizes the structural barrier on the one hand and guarantees flexibility during embryonic development and wound healing on the other hand.

2.2. Epidermal cell-cell contacts

To maintain the functions of the epidermis, a cellular network is necessary to ensure both adhesion and flexibility. This is regulated by cell-cell junctions, which include the tight junctions (Figure 2A), adherens junctions (Figure 2B), and desmosomes (Figure 3). These connect and organize the cytoskeleton of adjacent cells, thereby forming a structural continuum across the tissue (Garcia *et al.*, 2018; Zimmer and Kowalczyk, 2020).
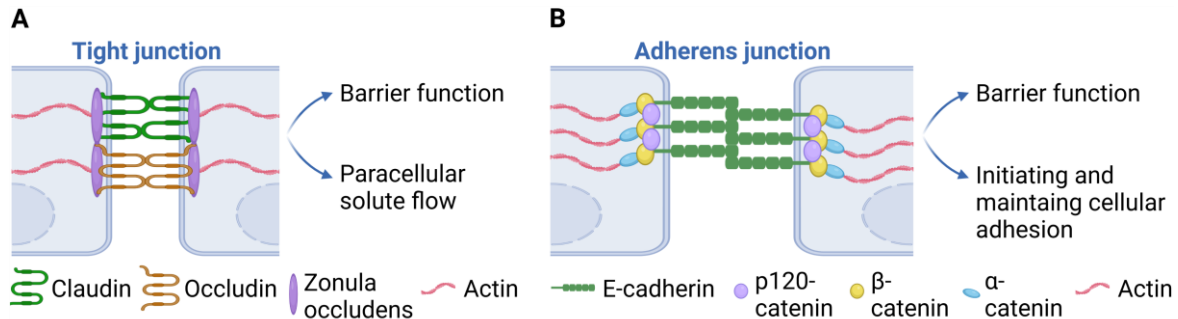
Figure 2 │ Structure, composition, and main functions of the tight junction and adherens junction. Created with biorender.com, modified from (Zimmer and Kowalczyk, 2020). **(A)** Tight junctions are intercellular adhesion complexes composed of claudin and occludin, which are linked to the actin cytoskeleton by the adaptor proteins zonula occludens. Tight junctions control paracellular permeability by forming a diffusion barrier. **(B)** Adherens junctions consist of classical cadherins such as E-cadherin which is linked to actin cytoskeleton by a group of catenins (p120-, β-, α-catenin). Adherens junctions regulate barrier function, initiate cell-cell contacts, and mediate the maturation and maintenance of the contact.

Tight junctions (Figure 2A) seal adjacent keratinocytes in the granular layer and are thus mainly responsible for barrier function and regulation of paracellular solute flow (Zihni *et al.*, 2016). They consist of two families of transmembrane proteins, claudin and occludin, which form homotypic complexes between cells. They connect the actin cytoskeleton via the cytoplasmic adaptor proteins zonula occludens. The adherens junctions (Figure 2B) also connect the actin cytoskeleton but consist of classical cadherins such as E-cadherin, which are associated via their cytoplasmic domains with p120-catenin, β-catenin, and α-catenin,

to which actin is connected in a tension-dependent manner (Hartsock and Nelson, 2008). Thus, adherens junctions regulate the barrier function and initiate and maintain cellular adhesion via actin-cytoskeleton connections. Mechanical cohesion is further strengthened by the connection of intermediate filaments such as keratin. This is accomplished by desmosomes, which are the main junction type in stratified epithelia, including the epidermis (Niessen, 2007). Desmosomes are found in all epidermal layers with the exception of the corneal layer where desmosomes are transformed to corneodesmosomes. The major compositional distinction from desmosomes is the presence of corneodesmosin in the extracellular portion (Ishida-Yamamoto and Igawa, 2015). The desmosome can be divided into three morphologically distinct regions (Figure 3): the extra-cellular core region, the outer dense plaque, and the inner dense plaque (Yin and Green, 2004; Delva *et al.*, 2009; Nekrasova and Green, 2013).
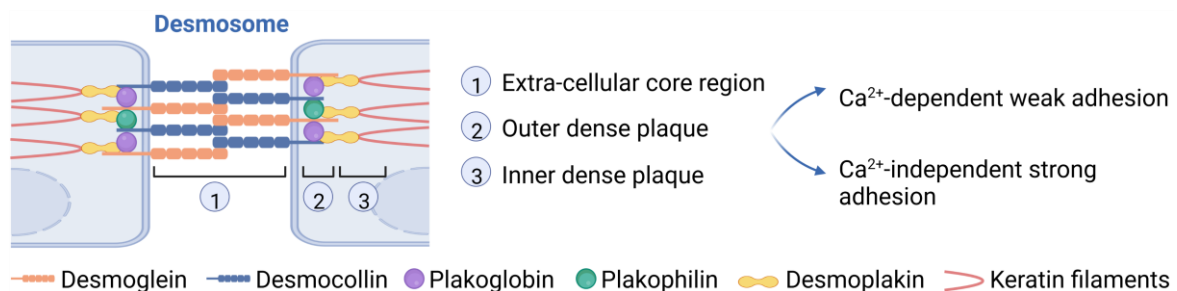
Figure 3 │ **Structure, composition, and main functions of the desmosome.** Created with biorender.com, modified from (Zimmer and Kowalczyk, 2020). Desmoglein and desmocollin extent into the extra-cellular core region and the outer dense plaque to establish contact between adjacent cells. In the outer dense plaque, desmosomal cadherins associate with the linker proteins plakoglobin, plakophilin, and desmoplakin. Within the inner dense plaque, desmoplakin binds to keratin intermediate filaments, serving to tether the intermediate filaments to the plasma membrane. Desmosomes have two distinct adhesive states, a Ca^{2+}-dependent state and a Ca^{2+}-independent hyper-adhesive state, which balance tissue plasticity and strength.

The extracellular core region mediates adhesion and is formed by the extracellular domains of the desmosomal cadherins, which are transmembrane glycoproteins of the desmoglein and desmocollin families. These are associated via their cytoplasmic ends with the desmosomal plaque proteins plakophilin (PKP) and plakoglobin, which are members of the armadillo protein family. PKPs and plakoglobin bind to plakin family proteins such as desmoplakin to form the outer dense plaque. The plakin proteins interact with keratin filaments in the inner dense plaque, tethering the adhesion complex with the cytoskeleton. Desmosomes show Ca^{2+}-dependent assembly and adhesion (Garrod *et al.*, 2005; Kimura *et al.*, 2007). In the presence of extracellular Ca^{2+}, desmosomes as well as Ca^{2+}-dependent adherens junctions, show intercellular adhesions, but these are relatively weak. Desmosomes are the only cell-cell contacts that have the ability to become Ca^{2+}-independent, thereby adopting a strong hyper-adhesive state. In tissue culture, they thus

show resistance to dissociation by chelating agents (Garrod *et al.*, 2005). In tissues, the hyper-adhesive state of desmosomes enables resistance to disruption by mechanical forces (Hatzfeld *et al.*, 2017; Hsu *et al.*, 2018). Thus, desmosomes are increasingly found as adhesive cell-cell junctions in tissues exposed to strong mechanical stresses such as the skin, myocardium, bladder, and in gastrointestinal mucosa.

Another difference from adherens junctions is that desmosomes have a highly organized disc-like plaque, the formation of which is ensured by PKP1-3 (Garrod and Chidgey, 2008). PKPs act as scaffolds in two ways. First, they cluster desmosomal cadherins in the plane of the plasma membrane. Second, they recruit the cytoskeleton to the desmosomal plaque through interaction with desmoplakin. PKPs are thus not only involved in the formation as well as maturation of desmosomes, but also support the connection to the cytoskeleton. In the following chapter, the focus on PKPs will reveal their structure and expression pattern as well as their role in maintaining tissue integrity.

2.3. Plakophilins

PKP1-3 are desmosomal members of the armadillo-related protein family, which are characterized by a series of repeated motifs of about 45 amino acid residues called arm repeats (Hatzfeld, 2007). These arm repeats are flanked by a large N-terminal head domain and a short C-terminal tail (Figure 4A).
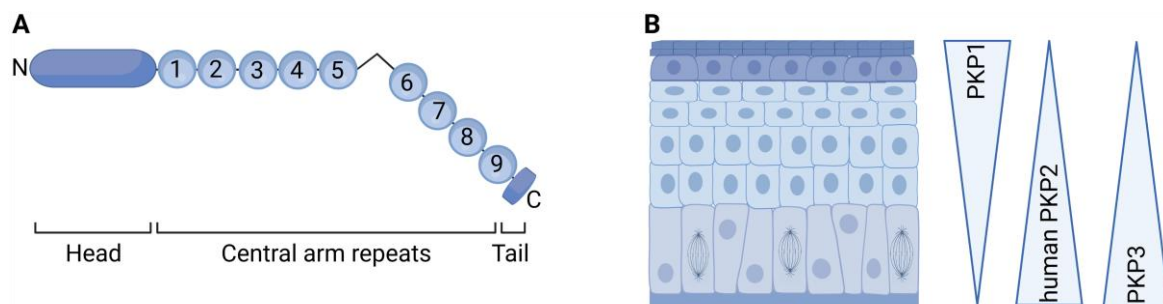
Figure 4 │ Structure and epidermal expression pattern of PKPs. Created with biorender.com, modified from (Delva *et al.*, 2009). **(A)** Structure of PKPs, which belongs to the armadillo-related protein family. PKPs contain an amino-terminal head domain, a central arm repeat domain with 9 repeats and an insert between repeat 5 and 6, and a carboxyl-terminal tail. **(B)** Relative expression profiles of various PKPs in the epidermal layers. PKP1 is concentrated in the desmosomes of the superficial epidermal layers, whereas human PKP2 is more abundant in desmosomes of the basal layer. PKP2 is not expressed in murine epidermis. PKP3 shows decreased expression from basal to suprabasal layers.

In detail, the basic amino terminal end of PKPs is followed by the long head domain, which has no obvious homology to other head domains providing a structural difference among PKP1-3. Except for a small conserved α-helical stretch, the head domain reveals no secondary structure. Followed the head domain, the arm repeats are organized to an elongated superhelical structure. A small spacer sequence between arm repeat five and

six leads to a characteristic bend in the domain structure. The arm repeats are terminated with the short carboxyl terminal end. Both the head and arm repeat domains may play a role in interactions with junctional and non-junctional proteins (Hatzfeld *et al.*, 2000; Chen *et al.*, 2002; Bonne *et al.*, 2003). Protein domains are defined as structurally, functionally, and evolutionarily distinct units, which can be altered in their architecture by alternative splicing. As a result, PKP1 and PKP2 exist in two isoforms each, whereas no alternative splice products have been characterized for PKP3 so far (Hatzfeld, 2007). Distinct protein isoforms and the rather diverse head domain suggest that PKP1-3 differ in their expression patterns and properties. Like other desmosomal proteins, PKPs reveal a tissue specific und epidermal differentiation specific expression pattern (Neuber *et al.*, 2010) (Figure 4B). PKP1 is highly expressed in stratified epithelia where it localizes predominantly in the suprabasal compartment of the epidermis suggesting a role in differentiation. PKP2 is the only PKP that is also expressed in non-epithelial tissues such as the myocardium and lymph nodes. Human PKP2 also shows decreasing expression from basal to suprabasal epidermal layers, whereas no PKP2 protein is detected in mouse skin. PKP3 is found in most simple and stratified epithelia. In contrast to PKP1, PKP3 shows decreased expression from basal to suprabasal epidermal layers (Schmidt and Jager, 2005).

Desmosomes contain at least one PKP isoform. The importance of PKPs in maintaining desmosomal integrity is demonstrated by the development of diseases and dysregulated cellular processes due to mutations in the genes encoding PKP1 and PKP2. In the autosomal recessive genetic disorder ectodermal dysplasia-skin fragility syndrome, a loss of function mutation in the PKP1 gene causes detachment of desmoplakin and intermediate filaments from desmosomes (Doolan *et al.*, 2020). The resulting loss of desmosomal adhesion leads to the disruption of tissue integrity, which is shown by cutaneous blistering and erosions. Due to the predominant expression of PKP2 in cells of the myocardium, the disease patterns reveal the function of the heart. In the potentially life-threatening disorder arrhythmogenic right ventricular dysplasia, PKP2 mutations cause fibrofatty infiltration of the myocardium and inflammatory infiltrates (Costa *et al.*, 2021). For PKP3, no human disorder has been described so far. Nonetheless, PKP3-knockout mice show morphological abnormalities in the hair follicles and a disturbed cutaneous inflammation (Sklyarova *et al.*, 2008). Moreover, PKP3-knockout mice were considerably smaller than their wildtype littermates pointing to a role in growth control.

Due to the lack of PKP2 expression in mouse skin, PKP1 and PKP3 are responsible for maintaining the structural integrity of the murine epidermis. Besides the function of PKP as

a structural scaffold that increases mechanical strength, they regulate junction assembly and cytoskeletal dynamics through their role as signaling scaffolds (Bass-Zubek *et al.*, 2009; Broussard *et al.*, 2015). Thus, they control tissue homeostasis in important cellular processes such as proliferation and migration while maintaining barrier function. However, the molecular mechanisms of desmosomal protein regulation have been poorly studied. For elucidating the complex role of PKPs, the present work focuses on PKP3 and its desmosomal role as a scaffold for junction proteins as well as its extra-desmosomal role as a scaffold in cell signaling.

2.4. Plakophilin 3

PKP3 is the most widely expressed PKP family member. In the following chapter, I summarize the current state of knowledge about PKP3 regulation including the transcriptional and post-transcriptional level as well as post-translational modifications which may control PKP3 localization and function (Figure 5). Current knowledge about the desmosomal and extra-desmosomal roles of PKP3 support the hypothesis that PKP3 acts as a multifunctional protein in regulating junctional and signaling processes. Data on the role of PKP3 in cancer corroborate the assumption that PKP3 has important extra-desmosomal functions.
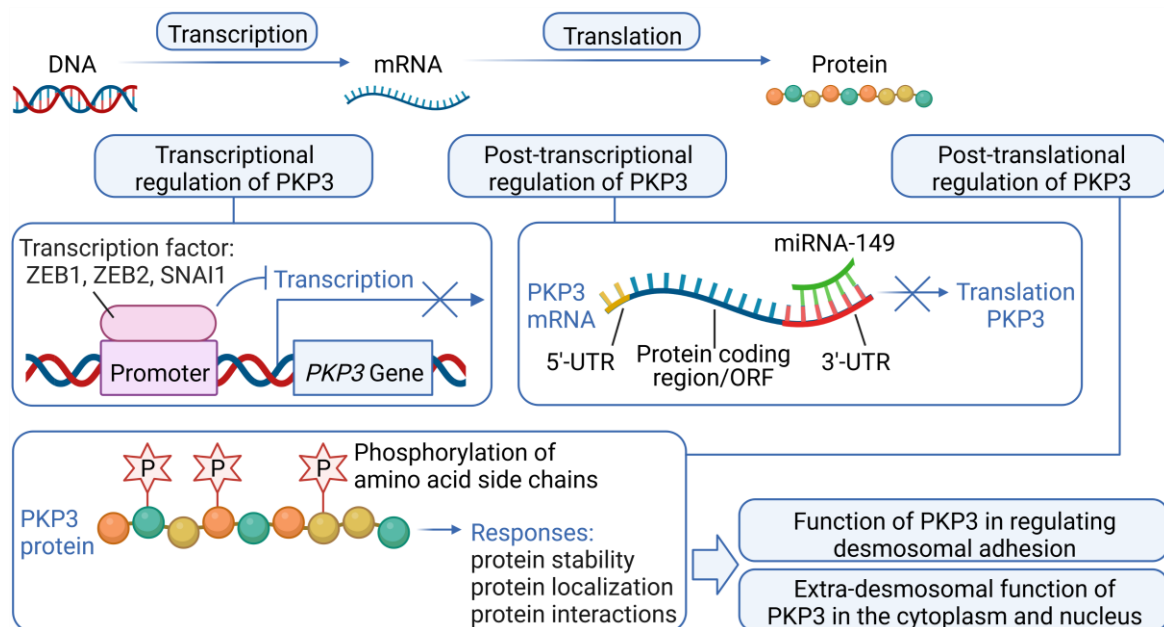
Figure 5 │ **Transcriptional, post-transcriptional, and post-translational regulation of PKP3.** Created with biorender.com. The central dogma of molecular biology reveals that during transcription DNA is copied to mRNA, which directs protein synthesis in the process called translation (upper panel). PKP3 expression is negatively regulated at transcriptional level by binding of transcription factors (e.g. ZEB1, ZEB2, SNAI1) in the PKP3 promoter (mid left panel, (Aigner *et al.*, 2007; Burks *et al.*, 2021)). Post-transcriptional control of PKP3 expression is negatively regulated by binding of miRNA-149 in the 3'-UTR of PKP3 mRNA (mid right panel, (Li *et al.*, 2018)). Post-translational modifications such as phosphorylation of amino acid side chains might

affect PKP3 protein stability, localization, and interactions (lower left panel, (Roberts *et al.*, 2013; Neuber *et al.*, 2015)), which regulate the function of PKP3 in desmosomal adhesion as well as its extra-desmosomal function in the cytoplasm and nucleus (lower right panel).

2.4.1. Transcriptional and post-transcriptional regulation

Gene expression is regulated at the transcriptional and post-transcriptional level. Regulation of gene transcription is central to the control of cell differentiation and dysregulation can lead to diseases such as cancer. In the epidermis, the expression of desmosomal genes is thought to be controlled by a variety of transcription factors. So far, the control of PKP3 gene transcription and expression remain incompletely understood. However, it has been shown that PKP3 expression is repressed by the transcription factor zinc finger E-box binding homeobox 1 (ZEB1) which binds with two conserved E-box elements in the human and murine PKP3 promoter (Aigner *et al.*, 2007). The homologue ZEB2 (Burks *et al.*, 2021) as well as snail family transcriptional repressor 1 (SNAI1) (Aigner *et al.*, 2007) have also been reported to repress PKP3 expression.

Post-transcriptional control of gene expression involves the regulation of messenger RNA (mRNA) degradation as well as mRNA translation and, in some cases, directed subcellular transport of mRNAs. 3'-untranslated regions (3'-UTR) are best known to regulate these mRNA-based processes. Most functions of the 3'-UTRs are mediated by RNA-binding proteins and non-coding RNAs, particularly microRNAs (miRNAs) (Zanzoni *et al.*, 2019). Databases for RNA-binding protein- and miRNA target prediction identify several putative binding sites in the PKP3 3'-UTR. The atlas of UTR regulatory activity (http://aura.science.unitn.it, 2022) predicted 16 RNA-binding proteins that bind at the human PKP3 3'-UTR. However, these predicted RNA-binding proteins by large scale approaches based on crosslinking immunoprecipitations require further validation to examine the functional consequences. In addition, the 3'-UTR of the PKP3 transcript is predicted to be targeted by 11 miRNAs (http://www.mirdb.org/cgi-bin/search.cgi, 2022). In nasopharyngeal carcinoma, upregulated miRNA-149 decreased PKP3 expression by direct binding to the PKP3 3′-UTR (Li *et al.*, 2018). This suggests that miRNA-149 may facilitate carcinoma metastasis by down-regulating PKP3. Post-transcriptional control of PKP3 expression appears to play a role in modulating desmosome composition and function. However, further studies are required to identify the RNA-binding proteins and non-coding RNAs involved and to understand the context and mechanisms of transcriptional and post-transcriptional regulation of PKP3.

2.4.2. Post-translational modifications: Phosphorylation of PKP3

Control of protein stability and protein localization, as well as that of protein interactions, is achieved by post-translation modifications. These reversible modifications include acetylation, methylation, palmitoylation, sumoylation, ubiquitylation, and phosphorylation of specific amino acid side chains. Especially tyrosine and serine/threonine phosphorylation are thought to be key regulators of desmosomal protein function. For PKP3, phosphorylation at Ser^{285} induced the binding to stratifin in the cytoplasm, which regulates the incorporation of PKP3 into desmosomes (Roberts *et al.*, 2013). Furthermore, phosphorylation at Tyr^{195} by cellular sarcoma (c-Src) kinase in response to oxidative stress has been reported (Neuber *et al.*, 2015). This phosphorylation had a fast turn-over by phosphatases but phosphatase inhibition altered PKP3 subcellular distribution. Phosphorylated PKP3 was released from the desmosomes and appeared in the cytoplasm, suggesting that this phosphorylation might play a role in desmosome disassembly. The detailed mechanism of this modification remain to be determined. However, this already suggests that PKP3 not only functions as a desmosomal plaque protein but may also have an extra-desmosomal function. In the next paragraph, the desmosomal and extra-desmosomal functions of PKP3 known so far will be discussed in more detail.

2.4.3. Function of PKP3 in regulating desmosomal adhesion

PKP3 is an important component of the desmosomal plaques. Although loss of PKP3 did not provoke a severe adhesion defect (Sklyarova *et al.*, 2008), PKP3 regulates desmosome function and maintains desmosome structure (Figure 6).
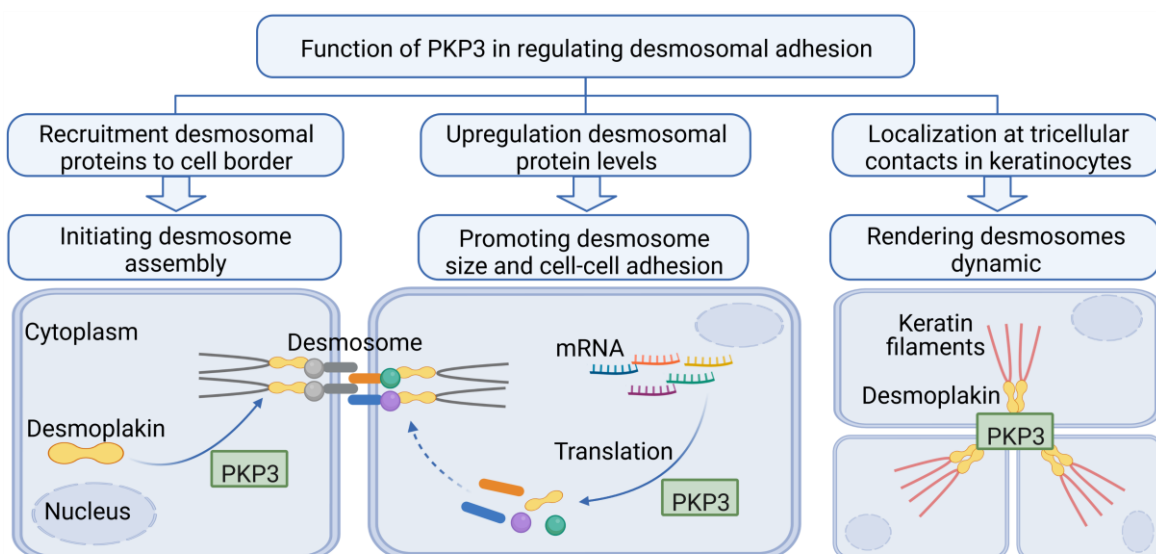
Figure 6 │ **Main functions of PKP3 in regulating desmosomal adhesion.** Created with biorender.com. PKP3 initiates desmosome assembly by recruitment of desmosomal proteins such as desmoplakin to cell borders (left panel, (Todorovic *et al.*, 2014)), which is further promoted by PKP3 through increasing

desmosomal protein levels (mid panel, (Gurjar *et al.*, 2018)). In keratinocytes, tricellular localization of PKP3 renders desmosomes more dynamic by tethering keratin filaments in high tension (right panel, (Keil *et al.*, 2016)).

PKP3 facilitates the recruitment of other desmosomal proteins to the cell border (Bonne *et al.*, 2003; Gosavi *et al.*, 2011), suggesting a role in initiation of desmosome assembly. The presence of pre-formed adherens junctions is required for the formation of new desmosomes, which is initiated by a complex of E-cadherin with PKP3 and plakoglobin (Gosavi *et al.*, 2011). Localization of this complex at the cell border prior to desmosome formation promotes the PKP3-dependent initial recruitment of multiple desmosomal proteins. Since desmosomes change from a Ca^{2+}-dependent to a Ca^{2+}-independent adhesive state, the localization of PKPs in the absence or presence of Ca^{2+} is essential for the initiation of desmosome assembly. A time course analysis of desmosome assembly in murine keratinocytes showed that PKP3, unlike PKP1, is present at the cell border in early stages of Ca^{2+} treatment (Keil *et al.*, 2016). Only after long Ca^{2+} treatment, PKP1 is recruited to the cell border. This suggests that PKP3 is required for the initial recruitment of desmosomal proteins to the cell border, and that desmosomes are further stabilized by other PKP family members including PKP1. The exact mechanism by which PKP3 mediates desmosome assembly is still unclear. Recent reports show that PKP3 formed a functional complex with rat sarcoma virus-related protein 1 guanosine triphosphatase (RAP1 GTPase), thereby mediating desmoplakin accumulation during desmosome formation (Todorovic *et al.*, 2014). Localization of desmosomal proteins at cell borders is further increased by PKP3 through upregulation of their protein levels. Thus, PKP3 increases desmosome size and cell-cell adhesion (Gurjar *et al.*, 2018). Cellular adhesion depends on desmosomal protein localization at both lateral and tricellular contacts. In keratinocytes, PKP3 accumulated at tricellular contacts, whereas PKP1 was excluded from these regions (Keil *et al.*, 2016; Rietscher *et al.*, 2018). Tricellular contacts are formed at sites where three cells make contact to each other. By holding three cells together, tricellular contacts are hotspots of tension and contribute to mechanical integrity and maintenance of the epithelial barrier function. Recent studies have uncovered a role of tricellular contacts in the regulation of the epithelial cell division orientation, which is essential for morphogenesis and the maintenance of tissue polarity (Bosveld *et al.*, 2016; Nestor-Bergmann *et al.*, 2019; Higashi and Chiba, 2020). In addition, tricellular localization of PKP3 renders desmosomes more dynamic (Keil *et al.*, 2016), which facilitates tissue remodeling as required during wound healing and regeneration.

2.4.4. Extra-desmosomal functions of PKP3 in the cytoplasm and nucleus

Besides its role in junction formation, PKP3 reveals an extra-desmosomal function reflected by its subcellular distribution in the cytoplasm and nucleus (Bonne *et al.*, 1999; Hofmann *et al.*, 2006). Interaction of PKP3 with proteins that are not directly linked to cell-cell adhesion reveals a role of PKP3 as a scaffold for signaling complexes, through which PKP3 might participate in signal transduction pathways (Figure 7).
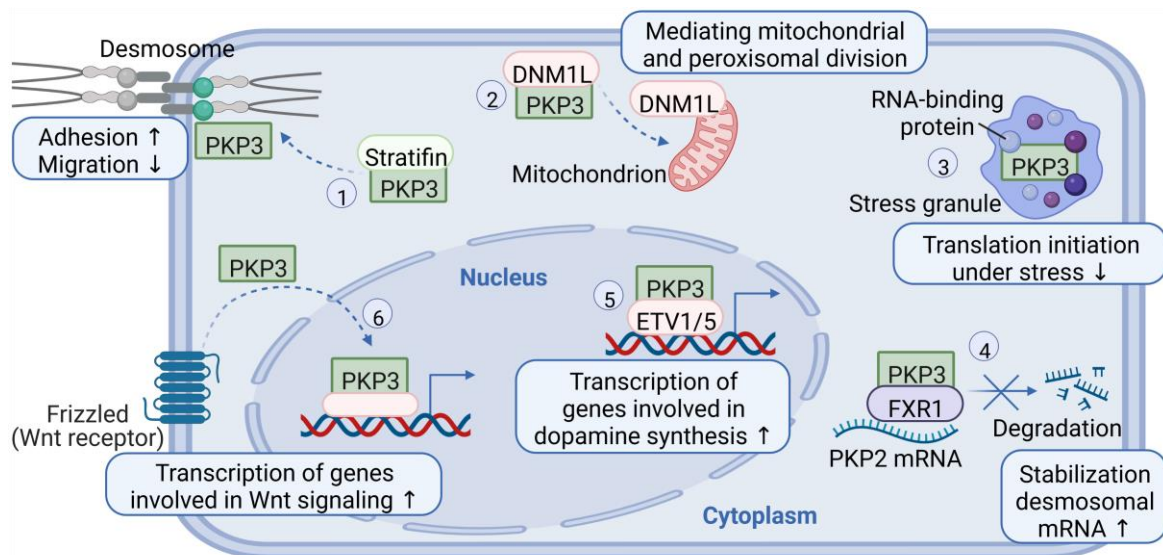
Figure 7 │ **Main extra-desmosomal functions of PKP3 in the cytoplasm and nucleus.** Created with biorender.com. (1) Cytoplasmic PKP3 interacts with stratifin to promote PKP3 incorporation into the desmosomal plaque resulting in increased adhesion and decreased migration (Roberts *et al.*, 2013; Rietscher *et al.*, 2018). (2) Binding of cytosolic PKP3 with DNM1L regulates mitochondrial and peroxisomal division (Furukawa *et al.*, 2005). (3) PKP3 interacts with RNA-binding proteins in cytoplasmic stress granules, which regulate mRNA translation and turnover upon stress resulting in inhibited translation initiation in response to stress (Hofmann *et al.*, 2006). (4) Cytosolic PKP3 associates with the RNA-binding protein FXR1 to stabilize the PKP2 mRNA thereby acting as a post-transcriptional regulator of desmosomal gene expression (Fischer-Keso *et al.*, 2014). (5) Nuclear PKP3 reveals an association with the transcription factors ETV1 and ETV5 to activate genes involved in dopamine synthesis (Munoz *et al.*, 2014). (6) Wnt signaling promotes re-localization of PKP3 from the cytoplasm to the nucleus, which further increases the activation of genes involved in Wnt signaling (Hong *et al.*, 2021).

Due to its high soluble pool, PKP3 occurs dispersed in cytoplasmic particles where it may serve as an interaction partner for stratifin (Roberts *et al.*, 2013; Rietscher *et al.*, 2018). As a consequence of the cytosolic PKP3-stratifin binding, stratifin regulates the dynamic incorporation of PKP3 into the desmosomal plaque, resulting in increased cell-cell adhesion and decreased migration. In addition to stratifin binding, cytoplasmic PKP3 interacted with dynamin-1-like protein (DNM1L, also known as DRP1) in lung cancer cells (Furukawa *et al.*, 2005) and may thereby regulates mitochondrial and peroxisomal division as well as mitochondria-dependent apoptosis. Besides the interaction of PKP3 with stratifin and DNML1, PKP3 is a part of stalled translation initiation complexes in the cytoplasm. Under environmental stress, PKP3 associated with RNA-binding proteins such as

polyadenylate binding protein 1 (PABPC1), fragile X mental retardation syndrome-related protein 1 (FXR1), or ras GTPase-activating protein-binding protein 1 (G3BP) in stress granules, where blocked translation initiation complexes accumulate (Hofmann *et al.*, 2006). Furthermore, cytoplasmic PKP3 binding to FXR1 stabilized the PKP2 mRNA (Fischer-Keso *et al.*, 2014), suggesting that PKP3 acts as post-transcriptional regulator of gene expression. Besides its role in RNA metabolism and post-transcriptional control of gene expression, PKP3 appears to have an additional role in gene transcription. Nuclear PKP3 reveals an association and functional interaction with the ETS variant transcription factors 1 and 5 (ETV1, ETV5), thereby activating genes involved in dopamine synthesis which are essential for regulating dopaminergic neural differentiation (Munoz *et al.*, 2014). How PKP3 can translocate into the nucleus is still unclear. A recent study show that endogenous PKP3 entered the nucleus after activation of the Wnt pathway, which might increase the activation of Wnt pathway gene control regions (Hong *et al.*, 2021). Although future work is required to examine the exact mechanism, the Wnt pathway is one of the key signaling pathways in regulating cell proliferation, motility, and differentiation, suggesting a role of PKP3 in these fundamental cellular processes.

2.4.5. Role of PKP3 in cancer

Homeostasis in healthy tissues strongly relies on cell-cell adhesion, which is regulated by PKP3 through its function in desmosome assembly. Disruption of cellular adhesion leads to changes in the morphological organization of a tissue and is a hallmark of cancer (Janiszewska *et al.*, 2020). Loss of cell-cell adhesion and the desquamation of cells from the underlying lamina allows malignant cells to detach from their site of origin and acquire a more motile phenotype allowing cells to metastasize and invade into other tissues, which corresponds with poor prognosis. Reduced expression of PKP3, which may contribute to the weakening of cell-cell adhesion observed in cancer cells, was shown in bladder cancer (Takahashi *et al.*, 2012) or oropharyngeal tumors (Papagerakis *et al.*, 2003). However, there are numerous examples where PKP3 was overexpressed in tumor tissue. Although this could represent a compensatory mechanism for the loss of adhesive strength, more recent data point to an adhesion-independent role, suggesting that the subcellular localization of PKP3 could be involved in cancer progression. Overexpression of PKP3 in prostate and prostatic adenocarcinoma cells revealed not only desmosomal but also cytoplasmic localization and an increased cell proliferation rate (Breuninger *et al.*, 2010). In non-small lung carcinoma, increased PKP3 expression has also been shown to be consistent with poor prognosis and reduced survival. In these cells, PKP3 knockdown led

to reduced growth (Furukawa *et al.*, 2005). Based on a putative cancer promoting role of PKP3, its mRNA was proposed as a biomarker for the detection of circulating cells in the blood of gastrointestinal cancer or ovarian cancer patients (Valladares-Ayerbes *et al.*, 2010; Gao *et al.*, 2020). Besides the cancer-related role of PKP3 due to its subcellular localization and function in adhesion, PKP3 might also act as signaling scaffold in promoting carcinogenic effects. Bioinformatic tool-based analysis of PKP3 in ovarian cancer revealed a multifunctional role of PKP3 in junctional organization and keratinocyte proliferation as well as in signaling pathways including cytokine-mediated pathways and receptor signaling pathways (Gao *et al.*, 2020). In a recent study, a pan-cancer analysis of PKP3 revealed a function of PKP3 in carcinogenesis and aggressiveness in multiple human tumors, which seems to be regulated by PKP3 expression, DNA methylation, and protein phosphorylation (Ruan *et al.*, 2021). However, the role of PKP3 as a tumor progressor or tumor suppressor seems to be context-dependent (Hatzfeld *et al.*, 2014). In addition, the abnormal proliferative signaling of cancer cells may also be partially controlled by desmosomes via their accessory components, including tyrosine kinases, which are frequently upregulated in cancer.

2.5. Growth factor signaling

Kinase cascades and phosphorylation of target proteins are well known to modulate localization and function of numerous proteins. Desmosomal proteins are highly modified by phosphorylation, which in turn is regulated by signaling cascades that are activated by growth factors, mechanical signals, or cytokines. Growth factors are endogenous signaling molecules that stimulate cellular growth, proliferation, and differentiation under controlled conditions (Park *et al.*, 2017). Experiments with cultured keratinocytes as well as animal models showed that a variety of growth factors are involved in the regulation of keratinocyte growth. Most studies deal with insulin-like growth factor 1 (IGF-1) and its pleiotropic hormone insulin as well as epidermal growth factor (EGF) (Ward *et al.*, 2007; Seeger and Paller, 2015). In the skin, IGF-1 and EGF are secreted by dermal myeloid cells such as fibroblasts and macrophages and the signal can be taken up by epidermal keratinocytes via their receptors (Nguyen and Soulika, 2019). Binding of the ligands to their corresponding receptors causes phosphorylation and thus activation of downstream kinases. These signaling cascades regulate cellular processes such as proliferation, differentiation, and apoptosis. In addition, growth factor signaling also determines the structure and function of desmosomal proteins via post-translational modifications, such as phosphorylation. For example, PKP1 has previously been shown to be phosphorylated via

the IGF-1/insulin signaling pathway, affecting its localization and function (Wolf *et al.*, 2013) (Figure 8A). Insulin signaling phosphorylates and activates AKT2, which in turn phosphorylated PKP1. In the phosphorylated state, PKP1 no longer localized to cell contacts. Instead its cytoplasmic localization led to increased proliferation. PKP1 controlled proliferation and cell-size in an adhesion-independent manner by promoting protein synthesis through its association with the eukaryotic translation initiation factor (eIF) 4A (Wolf *et al.*, 2010). These studies indicate that PKP1 regulates desmosomal adhesion and is further involved in extra-desmosomal regulation of proliferation. The shift from a function in strengthening adhesion to an adhesion-independent function in promoting proliferation was controlled by the IGF-1/insulin signaling pathway.
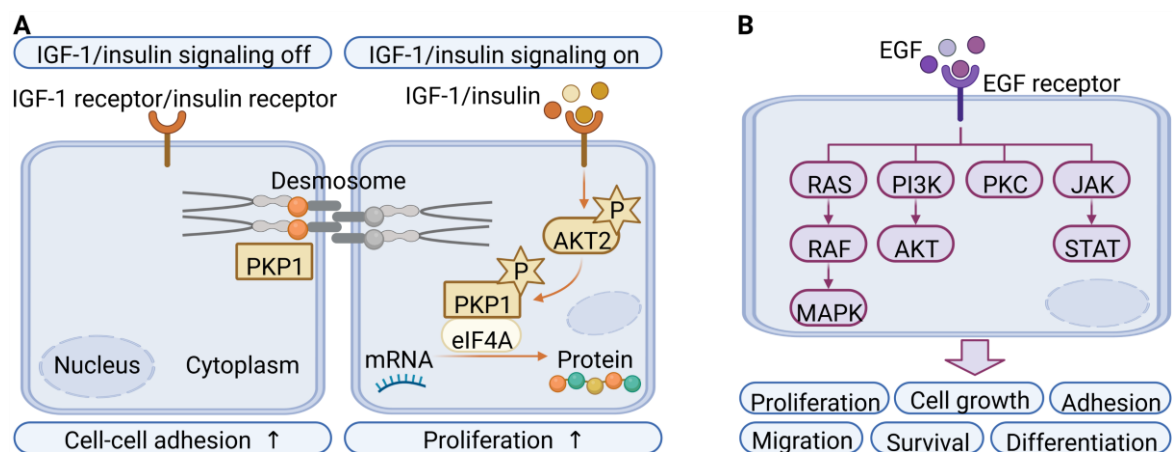
Figure 8 │ The role of insulin and EGF signaling in regulating fundamental physiological processes. Created with biorender.com, modified from (Wolf *et al.*, 2013; Müller *et al.*, 2021). **(A)** IGF-1/insulin signaling affects localization and function of PKP1. Unphosphorylated PKP1 incorporates into the desmosomal plaque to increase cell-cell adhesion. By IGF-1/insulin signaling activated AKT2 phosphorylates PKP1 and translocates it into the cytoplasm. Association of cytoplasmic PKP1 with eIF4A promotes protein synthesis, resulting in enhanced proliferation. **(B)** EGF binding to EGFR triggers four canonical EGFR trafficking pathways: RAS/RAF/MAPK pathway, PI3K/AKT pathway, PKC signaling cascade, and JAK/STAT pathway. These transmit the cellular response to mediate various cellular activities, including proliferation, growth, adhesion, migration, survival, and differentiation.

The pathways that coordinate PKP3 dynamic are poorly understood. PKP3 is phosphorylated at Tyr[195] via c-Src kinase, a component of the EGF receptor (EGFR) pathway (Neuber *et al.*, 2015), suggesting an EGFR-dependent regulation of PKP3 function. However, this modification was only detected after phosphatase inhibition raising the question how such a transient modification can affect cell behavior. The mammalian EGFR has been proposed as a key modulator of desmosomal post-translational modifications (Gaudry *et al.*, 2001; Lorch *et al.*, 2004; Bektas *et al.*, 2013). The EGFR is activated by binding of its specific ligands, including EGF. Ligand-induced dimerization of the receptor monomer initiates the downstream "canonical" EGFR signaling pathways (Figure 8B): the rat sarcoma virus (RAS)/rapidly accelerated fibrosarcoma (RAF)/mitogen

activated protein kinase (MAPK) pathway, the phosphoinositide 3 kinase (PI3K)/AKT pathway, the protein kinase C (PKC) signaling cascade, and the janus kinase (JAK)/signal transducer and activator of transcription (STAT) pathway (Müller *et al.*, 2021). These pathways regulate a series of important keratinocyte functions including proliferation, cell growth, adhesion, migration, survival, and differentiation. In human skin, the response to EGF is determined by the localization and number of EGFR molecules. Basal cells show an enrichment of receptors, whereas diminished EGFR activity correspond to stratification and differentiation (Gazel and Blumenberg, 2013; Joly-Tonetti *et al.*, 2021). This suggest a role of EGFR signaling in keratinocyte transition from the proliferative basal layer to the differentiating suprabasal compartment. Abnormal epidermal expression of EGFR and/or its ligands are common features of several hyper-proliferative and inflammatory diseases (Gottlieb *et al.*, 1988; Nanney *et al.*, 1992). EGFR activation is a frequent event in many cancers and EGFR inhibitors are an important treatment option for patients with malignant carcinoma (Klijn *et al.*, 1992; Shir *et al.*, 2006; Keysar *et al.*, 2013). In squamous cell carcinoma, EGFR inhibition promotes desmosome assembly, resulting in increased cell-cell adhesion (Lorch *et al.*, 2004). On the other hand, EGFR signaling is controlled by desmosomal proteins as well. PKP3 might be an effector of the RAS/RAF/MAPK pathway, thereby regulating proliferation and invasion in ovarian cancer cells (Lim *et al.*, 2019). In light of these observations, it might be predicted that EGFR signaling modulates the junctional function of PKP3 in cell-cell adhesion as well as its extra-desmosomal role in terms of proliferation.

2.6. Proliferation

Regulation of proliferation via desmosomal proteins plays a major role in establishing homeostasis and is associated with their function in cell-cell adhesion, signaling pathways, and activation of transcriptional factors. Desmosomal dysfunction can promote cancer development, which is further affected by enhanced cell cycle progression, resulting in hyper-proliferation and abnormal tumor growth.

High cell density or confluency prompts cells to cease proliferation and cell division, a phenomenon known as contact inhibition of proliferation (CIP) (McClatchey and Yap, 2012). In normal epithelial cells, the arrest of cell proliferation is associated with decreased cell division and the initiation of differentiation. CIP is overcome in rapidly growing tissues during embryonic development, wound healing, or tissue regeneration. Pathologically, loss of CIP leads to uncontrolled cell growth and might participate in the tissue dysmorphogenesis displayed by cancers. Many molecular mechanisms have been

proposed to contribute to CIP. It is widely accepted that cell-cell adhesion molecules are key drivers of CIP by sensing mechanical forces and crowding (Miroshnikova *et al.*, 2018). Whereas the role of adherens junctions and E-cadherin in CIP has been extensively studied (Mendonsa *et al.*, 2018), the role of desmosomal proteins in controlling proliferation versus differentiation is only beginning to emerge.

Besides the junctional regulation of CIP, the proliferation arrest is also mediated by signaling pathways. Computational modelling shows that the Wnt pathway is involved in CIP (Dunn *et al.*, 2016). Due to the role of Wnt signaling in regulating PKP3 localization (Hong *et al.*, 2021) it is possible that PKP3 might contribute to the loss of contact inhibition as well. Furthermore in the stratified squamous epithelium of esophagus, PKP3 remains cytoplasmic in the basal layer and lower parts of the suprabasal layers (Schmidt and Jager, 2005), which might correspond to the high proliferation rate of these cells. However, the participation of PKP3 in regulating proliferation is not well understood despite its pro-proliferative role in prostate cancer cells (Breuninger *et al.*, 2010) and its growth-promoting activity in lung cancer cells (Furukawa *et al.*, 2005). The molecular mechanism by which PKP3 modulates proliferation pathway components is still unclear in both transformed cancer cells and non-transformed cells.

2.7. Aims of the thesis

Desmosomes are essential for strong intercellular adhesion but at the same time they need to be dynamic to allow for remodeling of epithelia during regeneration and wound healing. The tight control of proliferation and adhesion is therefore essential for tissue integrity. While the steady-state composition of desmosomes has been well characterized, the mechanisms that regulate junction assembly and stability are poorly understood.

It is known that desmosomes from the basal and the suprabasal layers of the epidermis differ in subtype composition. For example, PKP isoforms reveal distinct localization patterns with basal desmosomes depending primarily on PKP3 and suprabasal desmosomes containing predominantly PKP1. In two-dimensional cell culture, PKP3 accumulates at the most dynamic point of cell contacts, the tricellular contacts, whereas PKP1-containing desmosomes seal lateral membranes. The exchange rates of desmosomal PKP3 are much higher than those of PKP1, implicating that PKP3-containing desmosomes are best suited for dynamic adhesion whereas PKP1 facilitates the transition to stable hyper-adhesive desmosomes.

Elucidating how PKP isoform localization and function are regulated in keratinocytes would considerably improve the understanding of how desmosomes adapt to different conditions

in the epidermis. The molecular mechanisms underlying the control of PKP1 have been elucidated. IGF-1/insulin signaling via AKT2 phosphorylates PKP1 and translocates it into the cytoplasm to enable its function in translation, resulting in reduced adhesive strength and enhanced proliferation. Thus, desmosomes may also act as signaling hubs, thereby participating in fundamental processes such as proliferation and differentiation.

In contrast to PKP1, the regulation of PKP3 localization and function in keratinocytes and during epidermal differentiation are not well understood. PKP3 is not only a constituent of cell-cell contacts, but it is also found dispersed in the cytoplasm and the nucleus. This dual localization suggests that in addition to establishing and maintaining cell adhesive functions, PKP3 may also play a role in cytoplasmic and nuclear processes including proliferation. Numerous serine/threonine- and tyrosine phosphorylation sites in PKP3 suggest that phosphorylation of this protein by growth factor signaling (e.g. IGF-1/insulin or EGF signaling) might induce changes in its subcellular localization and function. Thus, the role of PKP3 as a multifunctional scaffold for adhesion and signaling requires further investigation.

The here presented thesis focuses on two major aims:

I) The desmosomal role of PKP3 as a scaffold for adhesion: Identification of the growth factor signaling pathway that induces PKP3 modifications and elucidating of the effects on PKP3-dependent adhesive properties.

II) The extra-desmosomal role of PKP3 as a scaffold for signaling: Elucidation of PKP3 contribution to the control of proliferation.

3. MATERIALS AND METHODS

3.1. Materials

3.1.1. Cell lines

All cell lines used in this thesis are listed in Table 1. Immortalized keratinocytes from wildtype (WT) and PKP3-knockout (PKP3-KO) mice have been described (Keil *et al.*, 2016). Generation of all stable cell lines by lentiviral transduction was kindly performed by Dr. René Keil and Dr. Katrin Rietscher (Hatzfeld lab, Martin Luther University) and has been described previously (Rietscher, 2018).

Table 1 │ **Cells lines.** FUCCI = fluorescent ubiquitination-based cell cycle indicator, GFP = green fluorescent protein, h = human, KO = knockout, MKC = murine keratinocytes, PKP = plakophilin, WT = wildtype.

Cell line	Description	Source
A431	epidermoid carcinoma cells	(Giard *et al.*, 1973)
WT MKC	spontaneously immortalized murine keratinocytes derived from PKP3+/+ mice	generated by Dr. René Keil (Hatzfeld lab)
PKP3-KO MKC	spontaneously immortalized murine keratinocytes derived from PKP3-/- mice	generated by Dr. René Keil (Hatzfeld lab)
WT + hPKP3-GFP MKC	generated by lentiviral transduction of WT MKC and puromycin selection	generated by Dr. René Keil (Hatzfeld lab)
GFP MKC	generated by lentiviral transduction of WT MKC and puromycin selection	generated by Dr. Katrin Rietscher (Hatzfeld lab)
WT MKC FUCCI	generated by lentiviral transduction of WT MKC and puromycin selection	generated by Dr. René Keil (Hatzfeld lab)
PKP3-KO MKC FUCCI	generated by lentiviral transduction of PKP3-KO MKC and puromycin selection	generated by Dr. René Keil (Hatzfeld lab)

3.1.2. Chemicals, reagents, and cell culture consumables

All chemicals used throughout this thesis were purchased from Cayman Chemical (Ann Arbor, USA), Carl Roth (Karlsruhe, Germany), Invitrogen (Waltham, USA), New England Biolabs (Frankfurt, Germany), Roche Diagnostics (Indianapolis, USA), Santa Cruz Biotechnology (Dallas, USA), Selleck Chemicals (Houston, USA), Sigma-Aldrich (St. Louis, USA), and Thermo Fisher Scientific (Waltham, USA). Cell culture media and consumables were acquired from Corning (Glendale, USA), Pan Biotech (Aidenbach, Germany), Roche Diagnostics, and Sigma-Aldrich. Compositions of buffers and stock solutions are summarized in Table 2. Inhibitors including working concentration are listed in Table 3.

Table 2 │ **Application and composition of buffers and stock solutions.** EDTA = ethylenediamine-tetraacetic acid, EGF = epidermal growth factor, EGTA = ethylene bis(oxyethylenenitrilo)tetraacetic acid, HCM = high calcium medium, IP = immunoprecipitation, LCM = low calcium medium, MKC = murine keratinocytes, MT = microtubule stabilization, PBS = phosphate-buffered saline, PBSE = phosphate-buffered saline with ethylenediaminetetraacetic acid, RIPA = radioimmunoprecipitation assay, SDS = sodium dodecyl sulfate, SDS-PAGE = sodium dodecyl sulfate polyacrylamide gel electrophoresis, TBS = tris-buffered saline, TBST = tris-buffered saline with Tween 20.

Name	Application	Composition of stock solution
1 µM Choleratoxin	Cell cultivation	1 mg choleratoxin; 1.18 ml sterile water

Name	Application	Composition of stock solution
1 mg/ml Hydrocortisone	Cell cultivation	500 mg hydrocortisone; 50 ml ethanol
2 M CaCl$_2$	Cell cultivation	29.4 g CaCl$_2$ (x2 water); 100 ml sterile water
3.7% Formaldehyde	Immunofluorescence	18.5 g paraformaldehyde; 430 ml aqua bidest; 1 M sodium hydroxide; 50 ml 10xPBS; pH 7.3
4x SDS loading buffer	SDS-PAGE	250 mM Tris/HCl; 8% (v/v) SDS; 10% (v/v) β-mercaptoethanol; 30% (v/v) glycerol; 0.25% (w/v) bromophenol blue; pH 6.8
10 µg/ml EGF	Cell cultivation	0.1 mg EGF; 10 ml serum-free LCM
90 mM Adenine	Cell cultivation	0.304 g adenine; 75 ml 150 mM HCl
Blotting buffer I	Western blotting	0.3 M Tris/HCl; 20% (v/v) methanol; pH 10.4
Blotting buffer II	Western blotting	25 mM Tris/HCl; 20% (v/v) methanol; pH 10.4
Blotting buffer III	Western blotting	25 mM Tris/HCl; 40 mM ε-aminocaproic acid; 20% (v/v) methanol; pH 9.4
Chemiluminescence solution 1	Western blotting	100 mM Tris/HCl; 25 mM luminol; 0.4 mM coumaric acid; pH 8.5
Chemiluminescence solution 2	Western blotting	100 mM Tris/HCl; 0.02% (v/v) H$_2$O$_2$; pH 8.5
Dispase solution	Dispase assay	serum-free HCM; 2.4 U/ml dispase II; 25 mM HEPES; 1.2 mM Ca^{2+}
Hypotonic buffer A	Nucleus/cytoplasm fractionation	10 mM HEPES; 10 mM KCl; 0.1 mM EDTA; 0.1 mM EGTA; pH 7.9
Hypertonic buffer C	Nucleus/cytoplasm fractionation	20 mM HEPES; 0.42 M NaCl; 1 mM EDTA; 1 mM EGTA; pH 7.9
IP buffer	Immunoprecipitation	20 mM Tris/HCl; 137 mM NaCl; 2 mM EDTA; 10% (v/v) glycerol; 1% (v/v) NP-40 (IPEGAL); pH 7.5
IP buffer II	Phospho-antibody validation	20 mM Tris/HCl; 137 mM NaCl; 10% (v/v) glycerol; 1% (v/v) NP-40 (IPEGAL); pH 7.5
Mowiol	Immunofluorescence	5% (w/v) Mowiol; 30% (v/v) glycerol; 0.25% (w/v) 1,4- diazabicyclo[2.2.2]octane (DABCO)
MT buffer	Immunofluorescence	100 mM pipes; 4 M glycerol; 2 mM EDTA; 1 mM EGTA; 0.5% (v/v) triton X-100; pH 6.9
PBS	Cell cultivation, Immunofluorescence	135 mM NaCl; 2.5 mM KCl; 10 mM Na$_2$HPO$_4$; 1 mM KH$_2$PO$_4$; pH 7.4
PBSE	Cell cultivation	135 mM NaCl; 2.5 mM KCl; 10 mM Na$_2$HPO$_4$; 1 mM KH$_2$PO$_4$; 0.5 mM EDTA; pH 7.4
Ponceau S staining solution	Western blotting	2% (w/v) Ponceau S; 30% trichloroacetic acid; 30% sulfosalicylic acid
Propidium iodide solution	Cell cycle analyzes	1 mg/ml sodium citrate; 0.1 mM EDTA; 50 µg/ml propidium iodide; 50 ml PBS
RIPA buffer	Immunoprecipitation	150 mM NaCl; 1% (v/v) NP-40 (IGEPAL); 0.5% (w/v) sodium desoxycholate; 0.1% (v/v) SDS; 50 mM Tris/HCl; pH 8.0
SDS electrophoresis buffer	SDS-PAGE	25 mM Tris/HCl; 19.2 mM glycine; 0.1% (v/v) SDS; pH 8.3
SDS lysis buffer	Protein extraction	20 mM Tris/HCl; 1% (w/v) SDS; pH 7.5
Separating gel buffer	SDS-PAGE	1.5 M Tris/HCl; pH 8.8
Stacking gel buffer	SDS-PAGE	0.5 M Tris/HCl; pH 6.8
Stripping buffer	Western blotting	0.2 M glycerol/HCl; 0.05% (v/v) tween20; pH 2.5
TBS	Western blotting	10 mM Tris/HCl; 100 mM NaCl; pH 7.6
TBST	Western blotting	10 mM Tris/HCl; 100 mM NaCl; 0.1% (v/v) tween20; pH 7.6

Name	Application	Composition of stock solution
TRIzol	RNA extraction	0.8 M guanidine isothiocyanate; 0.4 M ammonium thiocyanate; 0.1 M sodium acetate; 5% (v/v) glycerol; 48% (v/v) roti-aqua-phenol; pH 5.0
Trypsin A431	Cell cultivation	0.02% (v/v) ES-EDTA-Solution; 0.05% (w/v) trypsin; sterile PBS
Trypsin MKC	Cell cultivation	0.02% (v/v) ES-EDTA-Solution; 0.025% (w/v) trypsin; sterile PBS
Wet blot buffer	Western blotting	2.5 mM Tris/HCl; 19.2 mM glycerol; 20% methanol; pH 8.3

Table 3 │ Inhibitors including working concentrations.

Inhibitor	Company	Working concentration
FR180204	Selleck Chemicals	25 µM
Gefitinib	Sigma-Aldrich	10 µM
LJH685	Cayman Chemical	50 µM
Osu-03012	Selleck Chemicals	10 µM
PF-4708671	Sigma-Aldrich	10 µM
Rapamycin	Sigma-Aldrich	100 nm
U0126	Sigma-Aldrich	10 µM

3.1.3. Antibodies

Primary as well as secondary antibodies and dilutions used for western blotting and immunofluorescence analyses are listed in Table 4 and Table 5, respectively.

Table 4 │ Primary antibodies including dilutions used in western blotting and immunofluorescence.
CDK = cyclin-dependent kinase, EGFR = epidermal growth factor receptor, ERK = extracellular-signal regulated kinase, GFP = green fluorescent protein, HA = human influenza hemagglutinin, IF = immunofluorescence, MEK = mitogen-activated protein kinase kinase, PKP = plakophilin, RB = retinoblastoma, RSK = ribosomal S6 kinase, RUNX = runt-related transcription factor, S6K = s6 kinase; WB = western blotting.

Antigen / Clone	Company (Catalog number)	Host and clonality	WB	IF
AKT / 40D4	Cell Signaling (#2920)	Mouse monoclonal	1.1,000	
CDK2 / 78B2	Cell Signaling (#2546)	Rabbit monoclonal	1:100	
CDK4 / DCS-35	Santa Cruz Biotechnology (#sc-23896)	Mouse monoclonal	1:50	
CDK6 / DCS83	Cell Signaling (#3136)	Mouse monoclonal	1:500	
c-MYC / D84C12	Cell Signaling (#5605)	Rabbit monoclonal	1:500	
Corneodesmosin	Sigma-Aldrich (#HPA044730)	Rabbit polyclonal	1:500	
Cyclin D1 / 92G2	Cell Signaling (#2978)	Rabbit monoclonal	1:1,000	
Cyclin D2 / D52F9	Cell Signaling (#3741)	Rabbit monoclonal	1:1,000	
Cyclin E1 / D7T3U	Cell Signaling (#20808)	Rabbit monoclonal	1:250	
Desmoglein1 / 3.10	Progen (#61002)	Mouse monoclonal	1:1,000	
Desmoplakin	Hatzfeld lab (Keil *et al.*, 2016; Rietscher *et al.*, 2018)	Rabbit polyclonal		1:500
E2F1	Abcam (#ab137415)	Rabbit polyclonal	1:250	
EGFR / D38B1	Cell Signaling (#4267)	Rabbit monoclonal	1:500	
ERK1/2 / L34F12	Cell Signaling (#9102)	Mouse monoclonal	1:1,000	
FLAG M2	Sigma-Aldrich (#F1804)	Mouse monoclonal	1:1,000	1:500
GFP	Rockland (#600-401-215)	Rabbit polyclonal	1:2,000	
HA	Biomol (#600-401-384)	Rabbit polyclonal		1:500
Involucrin / SY5	Santa Cruz Biotechnology (#sc-21748)	Mouse monoclonal	1:100	

Antigen / Clone	Company (Catalog number)	Host and clonality	WB	IF
Keratin1 / peptide VKFVSTSYSRGTK	Magin lab (PSL, customized peptide-specific antibodies)	Rabbit polyclonal	1:20,000	
Keratin10	Magin lab (PSL, customized peptide-specific antibodies)	Rabbit polyclonal	1:10,000	
Loricrin	GenTex (#GTX116013), Biozol	Rabbit polyclonal	1:500	
MEK1/2 / L38C12	Cell Signaling (# 4694)	Mouse monoclonal	1:500	
p16	Thermo Fisher Scientific (#PA1-49749)	Rabbit polyclonal	1:250	
p21	Cell Signaling (#64016)	Rabbit polyclonal	1:250	1:50
P54nrb / 3/p54nrb	Transduction (#611279)	Mouse monoclonal	1:500	
Phospho-AKT-Ser^{473}	Cell Signaling (#9271)	Rabbit polyclonal	1:500	
Phospho-AKT substrate (RXXpS/pT) / 110B7E	Cell Signaling (#9614)	Rabbit monoclonal	1:500	
Phospho-CDK2-Thr^{160}	Cell Signaling (#2561)	Rabbit polyclonal	1:100	
Phospho-CDK4-Thr^{172}	Thermo Fisher Scientific (#PA5-64482)	Rabbit polyclonal	1:100	
Phospho-CDK6-Thr^{177} / 16HCLC	Thermo Fisher Scientific (#711588)	Rabbit monoclonal	1:50	
Phospho-CDK6-Tyr^{24}	Thermo Fisher Scientific (#PA5-104683)	Rabbit polyclonal	1:100	
Phospho-EGFR-Tyr^{992}	Cell Signaling (#2235)	Rabbit polyclonal	1:500	
Phospho-EGFR-Tyr^{1045}	Cell Signaling (#2237)	Rabbit polyclonal	1:500	
Phospho-EGFR-Tyr^{1068} / D7A5	Cell Signaling (#3777)	Rabbit monoclonal	1:500	
Phospho-ERK1/2-Thr^{202}/Tyr^{204} / D13.14.4E	Cell Signaling (#4370)	Rabbit monoclonal	1:1,000	
Phospho-MEK1/2-Ser$^{217/221}$ / 41G9	Cell Signaling (# 9154)	Rabbit monoclonal	1:500	
Phospho-RB-Ser$^{807/811}$ / D20B12	Cell Signaling (#8516)	Rabbit monoclonal	1:1,000	
Phospho-RSK-Ser^{380} / D3H11	Cell Signaling (#11989)	Rabbit monoclonal	1:500	
Phospho-S6-Ser$^{235/236}$ / D57.2.2E	Cell Signaling (#4858)	Rabbit monoclonal	1:500	
Phospho-S6K-Thr^{389} / 108D2	Cell Signaling (#9234)	Rabbit monoclonal	1:500	
PKP1	Hatzfeld lab (Keil *et al.*, 2016; Rietscher *et al.*, 2018)	Guinea pig polyclonal		1:1,000
PKP3 / peptide GGAQPTPPM-PTRPVSFHER	Hatzfeld lab (PSL, customized peptide-specific antibodies)	Guinea pig polyclonal	1:20,000	1:4,000
RB / D20	Cell Signaling (#9313)	Rabbit monoclonal	1:500	
RB-Alexa Fluor546 / IF8	Santa Cruz Biotechnology (#sc-102 AF546)	Mouse monoclonal		1:100
RSK1 / D6D5	Cell Signaling (#8408)	Rabbit monoclonal	1:1,000	
RSK1/2/3 / 32D7	Cell Signaling (#9355)	Rabbit monoclonal	1:1,000	
RSK2 / D21B2	Cell Signaling (#5528)	Rabbit monoclonal	1:1,000	
RSK3	Cell Signaling (#9343)	Rabbit polyclonal	1.1,000	
RSK4 / JS-31	Santa Cruz Biotechnology (#sc-377501)	Mouse monoclonal	1:1,000	
RUNX3 / D9K6L	Cell Signaling (#13089)	Mouse monoclonal	1:500	
S6 / 5G10	Cell Signaling (#2217)	Rabbit monoclonal	1:2,000	
S6K	Cell Signaling (#9202)	Rabbit polyclonal	1:1,000	

Antigen / Clone	Company (Catalog number)	Host and clonality	WB	IF
α-tubulin / DM1A	Sigma-Aldrich (#T6199)	Mouse monoclonal	1:1,000	
β-actin / AC-74	Sigma-Aldrich (#A2228)	Mouse monoclonal	1:2,000	

Table 5 │ Secondary antibodies including dilutions used in western blotting and immunofluorescence.
IF = immunofluorescence, IgG = immunoglobulin G, WB = western blotting.

Antigen / Clone	Company (Catalog number)	Host and clonality	Dilution
anti-guinea pig-IgG conjugated to horseradish peroxidase	Dianova, Hamburg, Germany (#706-035-148)	Donkey polyclonal	1:15,000 (WB)
anti-guinea pig-IgG conjugated to Alexa488	Dianova (#706-546-148)	Donkey polyclonal	1:400 (IF)
anti-mouse-IgG conjugated to Cyanine3	Dianova (#715-586-151)	Donkey polyclonal	1:200 (IF)
anti-mouse-IgG conjugated to horseradish peroxidase	Dianova (#715-035-150)	Donkey polyclonal	1:20,000 (WB)
anti-rabbit-IgG conjugated to Alexa647	Dianova (#711-606-152)	Donkey polyclonal	1:200 (IF)
anti-rabbit-IgG conjugated to Cyanine3	Dianova (#711-515-152)	Donkey polyclonal	1:200 (IF)
anti-rabbit-IgG conjugated to horseradish peroxidase	Dianova (#711-035-152)	Donkey polyclonal	1:40,000 (WB)

3.1.4. Vectors and plasmids

Plasmids ordered from Addgene company (Watertown, USA) are listed in Table 6. Cloning of all constructs was kindly performed by Andrej Mun, Dr. Christina Kießling, and Dr. René Keil (Hatzfeld lab, Martin Luther University), or by Dr. Marcel Köhn (Köhn lab, Martin Luther University). Cloning strategies including plasmids and restriction enzymes are summarized in Table 7. All constructs have been validated by Sanger sequencing (Eurofins Genomics GmbH, Ebersberg, Germany).

Table 6 │ Plasmids ordered from Addgene including the catalog number, principle investigator, and the reference in which the plasmids were described. CDK = cyclin-dependent kinase, h = human, HA = human influenza hemagglutinin, p = promoter, RB = retinoblastoma, RSK = ribosomal S6 kinase, WT = wildtype.

Name	Addgene plasmid	Deposited by
hCDK4-HA	#1876	Sander van den Heuvel (van den Heuvel and Harlow, 1993)
hCDK6-HA	#1868	Sander van den Heuvel (van den Heuvel and Harlow, 1993)
pCMV-HA-hRBΔCDK	#58906	Steven Dowdy (Narasimha *et al.*, 2014)
pCMV-HA-hRB-WT	#58905	Steven Dowdy (Narasimha *et al.*, 2014)
pKH3-hRSK1	#13841	John Blenis (Richards *et al.*, 2001)
pWZL-Neo-Myr-FLAG-RSK2	#20627	William Hahn and Jean Zhao (Boehm *et al.*, 2007)

Table 7 │ Plasmids for expression in cell lines. CDK = cyclin-dependent kinase, CDT = chromatin licensing and DNA replication factor, EGFP = enhanced green fluorescent protein, FUCCI = fluorescent ubiquitination-based cell cycle indicator, GEM = geminin, h = human, HA = human influenza hemagglutinin, ORF = open reading frame, p = promoter, PKP = plakophilin, RB = retinoblastoma, RSK = ribosomal S6 kinase, WT = wildtype.

Name	Expressed protein	Vector	Source or restriction enzymes
FUCCI-Puro	hCDT1 and hGEM	FUCCI-Puro	Dr. Marcel Köhn (Köhn lab)

Name	Expressed protein	Vector	Source or restriction enzymes
hCDK4-HA	hCDK4-HA	pCMV-neo-BamHI	Addgene #1876
hCDK6-HA	hCDK6-HA	pCMV-neo-BamHI	Addgene #1868
pEGFP-C2	EGFP	pEGFP-C2	Takara Bio Inc. (Kusatsu, Japan)
hPKP3-pEGFP	hPKP3-GFP	pLVX-IRES-puro containing EGFP ORF	EcoRI/SalI in EcoRI/XhoI by Dr. René Keil (Hatzfeld lab)
hPKP3-pVenus1-FLAG-C2	hPKP3-Venus1-FLAG	pVenus1-FLAG-C2	EcoRI/SalI by Dr. Christina Kießling (Hatzfeld lab)
hRB-ΔCDK-pEGFP-C2	hRBΔCDK	pEGFP-C2	XhoI/SalI, subcloned from Addgene #58906 by Andrej Mun (Hatzfeld lab)
hRB-WT-pEGFP-C2	hRB-WT	pEGFP-C2	SalI/BamHI, subcloned from Addgene #58905 by Andrej Mun (Hatzfeld lab)
hRSK1-pEGFP-C2	hRSK1	pEGFP-C2	EcoRI/SalI, subcloned from Addgene #13841 by Andrej Mun (Hatzfeld lab)
hRSK1-pVenus2-HA-C2	hRSK1-Venus2-HA	pVenus2-HA-C2	EcoRI/SalI, subcloned from Addgene #13841 by Andrej Mun (Hatzfeld lab)
hRSK2-pVenus2-HA-C2	hRSK2-Venus2-HA	pVenus2-HA-C2	EcoRI/SalI, subcloned from Addgene #20627 by Andrej Mun (Hatzfeld lab)
pVenus2-HA-C2	Venus2-HA	pVenus2-HA-C2	Hüttelmaier lab
pVenus1-FLAG-C2	Venus1-FLAG	pVenus1-FLAG-C2	Hüttelmaier lab

3.1.5. Oligonucleotids for qRT-PCR

Primer pairs were selected using Primer Blast (https://www.ncbi.nlm.nih.gov/tools/primer-blast/, 2019) and were ordered from Sigma-Aldrich. All primer pair sequences used in quantitative real-time polymerase chain reaction (qRT-PCR) are listed in Table 8.

Table 8 │ **Primer pair sequences used in qRT-PCR.** A primer pair consists of a forward primer and a reverse primer. CDK = cyclin-dependent kinase, EIF3K = eukaryotic translation initiation factor 3 subunit k, FEN = flap endonuclease, fw = forward primer, MCM = minichromosome maintenance complex component, PKP = plakophilin, RB = retinoblastoma, rev = reverse primer, RSK = ribosomal S6 kinase, RUNX = runt-related transcription factor, TYMS = thymidylate synthase.

Primer	Sequence 5' → 3'
CDK1-mouse_fw	ACAGAGAGGGTCCGTCGTAAC
CDK1-mouse_rev	CCGAATTGCAGTACTGGGCAC
CDK6-mouse_fw	ACGTGGTCAGGTTGTTTGATG
CDK6-mouse_rev	AAAGTCCAGACCTCGGAGAAGC
C-MYC-mouse_fw	GTTGGAAACCCCGCAGACAG
C-MYC-mouse_rev	GGGCTGTACGGAGTCGTAGT
CyclinA2-mouse_fw	TTCCTTACCCAGTACTTCCTGCAC
CyclinA2-mouse_rev	CCAATGACTCAGGCCAGCTCTGT
CyclinB1-mouse_fw	CAAATTGCAGCTGGGGCTTTC
CyclinB1-mouse_rev	TACTTGTTCTTGACAGTCATGTGCT
E2F3-mouse_fw	CCCACCGGCAAAGCGAAG
E2F3-mouse_rev	AGGGACGTATCATACCGCGT
EIF3K-mouse_fw	TCGACAGGTACCAGTTCAACCC
EIF3K-mouse_rev	GCCGCTCTTCTTGATGTGCC

Primer	Sequence 5' → 3'
FEN1-mouse_fw	GAACATTCCTCTTCGCCGGT
FEN1-mouse_rev	CATCGATGGCCACTTTGCGA
MCM3-mouse_fw	GGGCACAGTAGTGCTGGATGA
MCM3-mouse_rev	CATTGTTCAGGAGGCGGTTAGC
MCM6-mouse_fw	ATCAATGGCCCGCATGCACT
MCM6-mouse_rev	GCTGTCGGCATGACCATTGAC
P15-mouse_fw	CCGGCGAAGGACCATTTCTG
P15-mouse_rev	CTGCCCATCATCATGACCTGGA
P16-mouse_fw	TCGCAGGTTCTTGGTCACTGT
P16-mouse_rev	GCCCATCATCATCACCTGGTC
P18-mouse_fw	TGTGAACAAGGGACCCTAAAGAAT
P18-mouse_rev	CTCTGAGGAGAAGCCTCCTGG
P19-mouse_fw	CTGGAAGAAGTCTGCGTCGG
P19-mouse_rev	CTTCCAAACATCATGACCTGCAA
P21-mouse_fw	TCCAGACATTCAGAGCCACAGG
P21-mouse_rev	ACGGGACCGAAGAGACAACG
P27-mouse_fw	TTAGCGGAGCAGTGTCCAGG
P27-mouse_rev	CTTAATTCGGAGCTGTTTACGTCTG
P57-mouse_fw	CCAATCAGCCAGCAGAACAGC
P57-mouse_rev	GCTACGCGCTATCACTGGGA
PKP3-mouse_fw	GAAGAGGGATAGCCCCGACA
PKP3-mouse_rev	AGTCACGGTGGAGCTTGCTG
RB-mouse_fw	CACAACCCAGCAGTGCGTTA
RB-mouse_rev	TGGCTCTCTGAGTAGTGCAGG
RSK1-human_fw	GGAGAATGGACAGACCTCAGGG
RSK1-human_rev	AGCTCGAAATGGGATGGATCA
RSK1-mouse_fw	GAAGAAGCTGGACTTCAGCCAT
RSK1-mouse_rev	ATACAAGTGCCCACTGTCAGGC
RSK2-human_fw	GACAGCGCTGAGAATGGACA
RSK2-human_rev	TTCCAAATGATCCCTGCCCT
RSK2-mouse_fw	ACCTATGGGAGAGGAGGAGA
RSK2-mouse_rev	GCTGTCTAGCATCAGAGCCT
RSK3-human_fw	CCTATGGAAATAGAGACATCTTGGC
RSK3-human_rev	CCAGCTCAGCCAGGTAGAAC
RSK3-mouse_fw	TGGGCAGTGAGAGATGATCAGG
RSK3-mouse_rev	CCTCACCAAGAACACCTTTCCA
RSK4-human_fw	GCGGCGAGGTAAATGGTCTT
RSK4-human_rev	GAGCAACTCAAACTGTGCAGG
RSK4-mouse_fw	GGATGAGTCAGCCCATCCAG
RSK4-mouse_rev	TCACAGGCAGCATCATATCCC
RUNX3-mouse_fw	CTGTGGATGGACCCCGGGAA
RUNX3-mouse_rev	TTCAGGTCTGAGGAGCCTTGGATT
TYMS-mouse_fw	GCACGATACAGCCTGAGAGATGA
TYMS-mouse_rev	CCTGTCGGGCAGAAAATCCC

3.1.6. siRNAs

siRNAs were ordered from siTOOLs Biotech GmbH (Planegg, Germany). To minimize off-target effects and to guarantee a robust knockdown, siPOOLs were used, which are a pool of 30 selected siRNAs (Hannus *et al.*, 2014).

3.1.7. Kits and ready-to-use reagents

All Kits and ready-to-use reagents were ordered from ChromoTek GmbH (Martinsried, Germany), Sigma-Aldrich, Takara Bio Inc. (Kusatsu, Japan), and Thermo Fisher Scientific, respectively, and are listed in Table 9.

Table 9 │ Kits and ready-to-use reagents.

Kit/Reagent	Company
Cell Proliferation ELISA, BrdU Kit	Sigma-Aldrich
ChromoTek GFP-trap®	ChromoTek GmbH
Halt™ protease and phosphatase inhibitor cocktail	Thermo Fisher Scientific
Lipofectamin® RNAiMAX reagent	Thermo Fisher Scientific
PageRuler™ Plus Prestained Protein ladder	Thermo Fisher Scientific
Pierce™ BCA Protein Assay Kit	Thermo Fisher Scientific
Pierce™ Protein A Plus Agarose	Thermo Fisher Scientific
Xfect™ transfection reagent	Takara Bio Inc.

The ready-to-use 100x Halt™ protease and phosphatase inhibitor cocktail contains a mixture of several potent inhibitors, which are listed in Table 10.

Table 10 │ Protease and phosphatase inhibitors included in the 100x Halt™ protease and phosphatase inhibitor cocktail (Thermo Fisher Scientific). The protease inhibitors target aminopeptidases, cysteine and serine proteases. The phosphatase inhibitors target serine/threonine and protein tyrosine phosphatases.

Inhibitor	Target Protease/Phosphatase
Aprotinin	Serine Proteases
Bestatin	Aminopeptidase Proteases
E-64	Cysteine Proteases
Leupeptin	Serine and Cysteine Proteases
Sodium Fluoride	Serine and Threonine Phosphatases
Sodium Orthovanadate	Tyrosine Phosphatases
Sodium Pyrophosphate	Serine and Threonine Phosphatases
β-glycerophosphate	Serine and Threonine Phosphatases

As a protein standard for sodium dodecyl sulfate (SDS) polyacrylamide gel electrophoresis (PAGE), the PageRuler™ Plus Prestained Protein Ladder was used (Figure 9).
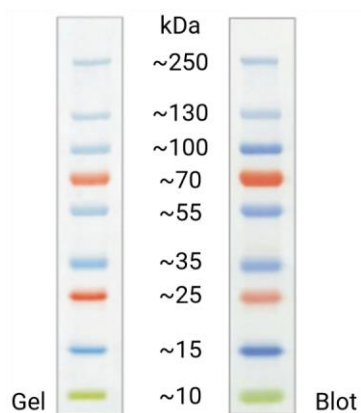
Figure 9 │ SDS-PAGE band profile of the PageRuler™ Plus Prestained Protein Ladder. Image was adapted from https://www.thermofisher.com/order/catalog/product/26620, 2022.

3.1.8. Instruments and general lab material

Plastic ware (cell scraper, cryogenic tubes, hypodermic needles, pipet tipes, cell culture ware, filters, syringes, tubes) was purchased from B. Braun (Melsungen, Germany), Becton Dickinson (Franklin Lakes, USA), Biozym Scientific GmbH (Hessisch Oldendorf, Germany), Carl Roth, Corning Diagonal GmbH & Co. KG (Münster, Germany), Greiner AG (Kremsmünster, Austria), Sarstedt (Nümbrecht, Germany), Starlab International GmbH (Hamburg, Germany), and TPP Techno Plastic Products AG (Trasadingen, Switzerland). Glass coverslips were purchased from Hartenstein (Würzburg, Germany), glass slides from Glaswarenfabrik Karl Hecht GmbH & Co. KG (Sondheim, Germany), immersion oil for microscopy from Leica (Wetzlar, Germany), nitrocellulose blotting membrane from Thomas Geyer (Renningen, Germany), and filter paper from Carl Roth.

All instruments were purchased from Analytik Jena (Jena, Germany), Bio-Rad Laboratories (Hercules, USA), Carl Zeiss Microscopy GmbH (Jena, Germany), Cole-Parmer (Staffordshire, USA), Epson (Suwa, Japan), Hettich Benelux B.V. (Geldermalsen, Netherlands), Hettich GmbH & Co. KG (Tuttlingen, Germany), IKA (Staufen, Germany), LaboGene (Lillerød, Denmark), Lauda GmbH & Co. KG (Lauda-Königshofen, Germany), Miltenyi Biotec (Bergisch-Gladbach, Germany), Nikon (Minato, Japan), Peqlab (Erlangen, Germany), Roche (Basel, Switzerland), Sartorius (Göttingen, Germany), Scientific Industries (New York, USA), Sony (Minato, Japan), Tecan (Männedorf, Switzerland), and VWR (Radnor, USA). Instruments including manufacturer are listed in Table 11.

Table 11 │ **Instruments.**

Instrument	Company
Centrifuge (Mikro 220 R)	Hettich GmbH & Co. KG
Centrifuge (Universal 320 R)	Hettich GmbH & Co. KG
CO_2 incubator 1 (Thermo Haraeus Cytosperm 2)	Thermo Fisher Scientific
CO_2 incubator 2 (Heracell^{TM} 240i)	Thermo Fisher Scientific
Digital shaker with microtiter attachment (IKA vortex 4 digital)	IKA
Heating thermo shaker (MHR 23)	Hettich Benelux B.V.
IncuCyte® S3 System	Sartorius
Inverted microscope 1 (Primovert)	Carl Zeiss Microscopy GmbH
Inverted microscope 2 (Nikon Eclipse Ts2)	Nikon
LightCycler 480 II Real Time PCR system	Roche
MACSQuant® flow cytometer	Miltenyi Biotec
Mini centrifuge (Rotilabo®)	Carl Roth
Mini-Protean Tetra vertical electrophoresis cell	Bio-Rad Laboratories
Mini Trans-Blot cell for wet blot approach	Bio-Rad Laboratories
Overhead rotator (Stuart rotator SB3)	Cole-Parmer
PCR thermal cycler (Biometra TRIO)	Analytik Jena
PerfectBlue Semi-Dry blotter	Peqlab
Plate reader Infinite® M PLEX	Tecan
Power supply	Bio-Rad Laboratories
Rocking shaker (VWR 12620 platform rocker)	VWR
Safety workbench (LaboGene Scanlaf Mars 1200 Runner Cl. II)	LaboGene

Instrument	Company
Scanner (Epson Perfection V600 Photo)	Epson
Sony DSC-H300 camera	Sony
Vortex mixer (Vortex-Genie 2)	Scientific Industries
Water bath (Lauda Aqualine AL 18)	Lauda GmbH & Co. KG

3.2. Methods

The following chapter deals with the cell biological, biochemical, and molecular biological methods used in this thesis. At the beginning of each experimental procedure, relevant lab equipment, chemicals, and software are listed. The entire chapter ends with information about image processing and quantification as well as statistical analysis.

3.2.1. Cell biological methods

3.2.1.1. Cultivation of cell lines

Lab equipment: Centrifuge (Universal 320 R); CO_2 incubator 1 (Thermo Haraeus Cytosperm 2); CO_2 incubator 2 (Heracell^{TM} 240i); Inverted microscope 1 (Primovert); Inverted microscope 2 (Nikon Eclipse Ts2); Safety workbench (LaboGene Scanlaf Mars 1200 Runner Class II); Water bath (Lauda Aqualine AL 18). Chemicals: Cell culture medium and consumables (see Table 2 and Table 12); 50 µg/µl Collagen I rat tail (Corning) in 0.02 N acidic acid; PBS (see Table 2); PBSE (see Table 2); Trypsin for A431 (see Table 2); Trypsin for MKC (see Table 2).

All cells used in this thesis are listed in Table 1. Composition of cell culture medium is shown in Table 12.

Table 12 │ Composition of cell culture medium. DMEM = Dulbecco's modified Eagle medium, DMSO = dimethyl sulfoxide, FCS = fetal calf serum, HCM = high calcium medium, LCM = low calcium medium, MKC = murine keratinocytes.

Cell line	Medium	Composition
A431	Standard DMEM	DMEM supplemented with 4.5 g/L glucose, 0.584 g/L L-glutamine (Sigma-Aldrich); 10% (v/v) FCS Superior (Sigma-Aldrich)
	Serum-free DMEM	DMEM supplemented with 4.5 g/L glucose, 0.584 g/L L-glutamine
MKC	LCM	DMEM/Ham's F12 (3.5 : 1.1) supplemented with 3.096 g/L NaHCO₃ (Pan Biotech); 10% (v/v) Ca²⁺-free FCS Superior (chelex-treated, Sigma-Aldrich); 1 mM sodium pyruvate (Sigma-Aldrich); 1 mM L-alanyl-L-glutamine (Sigma-Aldrich); 0.18 mM adenine (see Table 2); 0.5 µg/ml hydrocortisone (see Table 2); 5 µg/ml insulin (Sigma-Aldrich); 10 ng/ml EGF (see Table 2); 100 nM choleratoxin (see Table 2); 1 g/L glucose (Sigma-Aldrich)
	HCM	LCM; 1.2 mM CaCl₂ (see Table 2)
	Serum-free LCM	DMEM/Ham's F12 (3.5 : 1.1) supplemented with 3.096 g/L NaHCO₃ (Pan Biotech)
	Serum-free HCM	DMEM/Ham's F12 (3.5 : 1.1) supplemented with 3.096 g/L NaHCO₃ (Pan Biotech); 1.2 mM CaCl₂ (see Table 2)
A431, MKC	Freezing medium	90% (v/v) FCS Superior (Sigma-Aldrich); 10% (v/v) DMSO (Sigma-Aldrich)

A431 cells were cultured on 10 cm dishes in standard Dulbecco's modified Eagle medium (DMEM) at 37°C, 5% CO_2, and 90% humidity. Murine keratinocytes were grown on collagen I-coated 10 cm dishes in low calcium medium (LCM) at 32°C, 5% CO_2, and 90% humidity. Every 2-3 days, the medium was discarded and A431 cells were washed twice in phosphate-buffered saline with EDTA (PBSE), murine keratinocytes with phosphate-buffered saline (PBS), respectively. Cells were incubated with trypsin at 37°C until they detached from the dish. Fresh medium was added to stop the detachment. Cells were pelleted by low speed centrifugation (3 min; 1,000 x *g*; room temperature) and the supernatant was aspirated. Cells were resuspended in fresh medium and replated at the required density.

To induce differentiation of keratinocytes, murine keratinocytes were grown in high calcium medium (HCM) for the indicated time points. To analyze growth factor effects, A431 cells were grown in serum-free DMEM and murine keratinocytes were grown in serum-free LCM or serum-free HCM for the indicated time points.

To freeze cells, cell pellets were resuspended in freezing medium, aliquoted in cell culture cryogenic tubes and stored at -80°C. To thaw cells, vials were placed in a 37°C water bath, immediately transferred to a centrifuge tube containing 6 ml medium and pelleted by low speed centrifugation (3 min; 1,000 x *g*; room temperature). The cells were resuspended in fresh medium and plated on 10 cm dishes.

3.2.1.2. DNA transfection of murine keratinocytes

Lab equipment: Lab equipment for cultivation of cell lines (see chapter 3.2.1.1.); Mini centrifuge (Rotilabo®); Vortex mixer (Vortex-Genie 2).
Chemicals: Plasmid DNA (see Table 6 and Table 7); Xfect™ transfection reagent (Takara Bio Inc.) including Xfect reaction buffer and Xfect polymer.

Transfection of plasmid DNA was performed using Xfect™ transfection reagent. Plasmids used in this thesis are listed in Table 6 and Table 7. The amount of growth medium, DNA, and transfection reagent mixture is shown in Table 13. Murine keratinocytes were grown in LCM for 24 h to allow 50-70% confluency at the time of transfection. In a microcentrifuge tube, the appropriate µg of plasmid DNA was diluted with Xfect reaction buffer. Xfect polymer was added to the diluted plasmid DNA and mixed by vortexing for 10 sec at high speed. To allow formation of nanoparticle complexes, the solution was incubated for 10 min at room temperature. The solution was spinned down and the entire nanoparticle complex solution was added dropwise to the medium of adherent keratinocytes. The plate was incubated at 32°C for 4 h. Nanocomplex particles were removed by aspiration and replaced with fresh LCM or HCM for 24 h until further processing of transfected keratinocytes.

Table 13 │ DNA transfection by Xfect reagent.

Culture vessel	Growth medium	DNA	Xfect reaction buffer	Xfect polymer
24-well plate	250 µl	0.5-1 µg	25 µl	
12-well plate	500 µl	2 µg	50 µl	0.3 µl for every
6-well plate	1 ml	5 µg	100 µl	1 µg of plasmid
10 cm dish	8 ml	30 µg	600 µl	

3.2.1.3. RNA interference in murine keratinocytes

Lab equipment: Lab equipment for cultivation of cell lines (see chapter 3.2.1.1.); Mini centrifuge (Rotilabo®); Vortex mixer (Vortex-Genie 2).
Chemicals: Lipofectamin® RNAiMAX reagent (Thermo Fisher Scientific); siRNA pools generated by siTools Biotech GmbH.

For knockdown analysis in murine keratinocytes, siRNA pools (defined pools of 30 selected siRNAs) were generated by siTools Biotech GmbH (Hannus *et al.*, 2014). Murine keratinocytes were transfected in suspension with 2 pmol of non-targeting (Ctrl), p21, PKP3, ribosomal s6 kinase 1 (RSK1), RSK2, or runt-related transcription factor 3 (RUNX3) directed siRNAs with Lipofectamine® RNAiMAX. The cells were plated in the appropriate density just prior to preparing RNA-lipid transfection complexes. For each sample, two microcentrifuge tubes were prepared. Lipofectamine® RNAiMAX reagent and siRNA were diluted separately in serum-free medium as described in Table 14, combined in a 1:1 ratio, vortexed at medium speed for 10 sec, and incubated for 5 min at room temperature. After adding the entire siRNA-lipid complex to the freshly plated cell suspension, keratinocytes were incubated at 32°C until further proceeding. For analyzing the role of PKP3 in adhesion, keratinocytes were transfected with siRNA, switched to HCM at 48 h after transfection, and kept in HCM for another 24 h. For analysis of the extra-desmosomale role of PKP3, transfected cells were kept in LCM for 72 h.

Table 14 │ siRNA transfection by Lipofectamin® RNAiMax. LCM = low calcium medium.

Culture vessel	Dilution Lipofectamin® RNAiMAX in serum-free LCM		Dilution siRNA in serum-free LCM	
	Volume serum-free LCM	Volume Lipofectation RNAiMAX	Volume serum-free LCM	Volume siRNA
24-well plate	50 µl	3 µl	50 µl	1 µl (10 pmol)
12-well plate	100 µl	6 µl	100 µl	2 µl (20 pmol)
6-well plate	150 µl	9 µl	150 µl	3 µl (30 pmol)

3.2.1.4. Growth factor, inhibitor, and EGTA treatment

Lab equipment: Lab equipment for cultivation of cell lines (see chapter 3.2.1.1.); Mini centrifuge (Rotilabo®); Vortex mixer (Vortex-Genie 2).
Chemicals: DMSO (Sigma-Aldrich); 100 ng/ml EGF; 3.3. mM EGTA (Carl-Roth); Inhibitors (see Table 3); 50 µg/ml Insulin.

Murine keratinocytes grown for 24 h in HCM were starved in serum-free HCM for 5 h and stimulated with growth factors insulin or EGF for the indicated times. A431 cells were serum-starved for 24 h before stimulation with growth factors.

Inhibitors and corresponding working concentration used in this thesis are listed in Table 3. For application of inhibitors, keratinocytes were treated with the indicated inhibitor for 1 h or 24 h. In experiments with simultaneously EGF treatment, inhibitors were applicate before stimulation with EGF for 15 min. Dimethyl sulfoxide (DMSO) was used as control treatment. For application of ethylene bis(oxyethylenenitrilo)tetraacetic acid (EGTA), keratinocytes were treated with 3.3 mM EGTA for 1 h or 3 h.

3.2.1.5. Actinomycin D and cycloheximide treatment

Lab equipment: Lab equipment for cultivation of cell lines (see chapter 3.2.1.1.); Mini centrifuge (Rotilabo®); Vortex mixer (Vortex-Genie 2).
Chemicals: 10 µg/ml Actinomycin D (Sigma-Aldrich); 200 µg/ml Cycloheximide (Sigma-Aldrich).

To perform a mRNA decay or cycloheximide chase assay, murine keratinocytes were treated with actinomycin D or cycloheximide, respectively. The working principle is described in Figure 10.
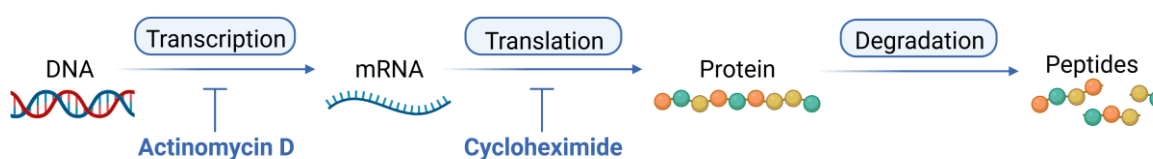
Figure 10 │ Analyzing mRNA and protein stability by using actinomycin D and cycloheximide. Created with biorender.com. During transcription, DNA is copied to mRNA, which directs protein synthesis in the process called translation. The levels of proteins within cells are determined not only by rates of synthesis, but also by rates of degradation, which results in protein breakdown into smaller polypeptides or amino acids. Actinomycin D is widely used in mRNA stability assays. Actinomycin D is a transcription inhibitor which intercalates into DNA, thereby inhibiting synthesis of new mRNA, allowing the assessment of mRNA decay by measuring mRNA abundance following transcription inhibition. By blocking the translational elongation phase, cycloheximide is used to analyze protein stability over a time course.

The mRNA stability within cells can be measured indirectly by analysing the mRNA half-life following transcription inhibition. Treatment with actinomycin D results in changes in mRNA levels that are assumed to reflect mRNA degradation. Murine keratinocytes were grown in LCM for 24 h followed by treatment with actinomycin D in LCM for 1 h, 3 h, 5 h, and 8 h. Subsequently, cells were harvested at indicated times and samples were prepared for RNA isolation, cDNA synthesis, and qRT-PCR (see chapter 3.2.3.).

To measure steady-state protein stability, a cycloheximide chase assay was performed. The *de novo* protein synthesis was blocked by cycloheximide due to the prevention in translational elongation. For analysis of protein stability, murine keratinocytes were treated with cycloheximide for 8 h or 16 h. Subsequently, cells were harvested at indicated times.

Samples were prepared for SDS-PAGE and western blotting (see chapter 3.2.2.2. and chapter 3.2.2.3.).

3.2.1.6. Cell proliferation assay

Lab equipment: IncuCyte® S3 System; Lab equipment for cultivation of cell lines (see chapter 3.2.1.1.).
Software: IncuCyte® S3 Software (version 2021C, Sartorius).

For the assessment of cell proliferation, murine keratinocytes were grown for up to 96 h in LCM or HCM. Live cell images were automatically taken every 24 h by using an IncuCyte® S3 System with 20x magnification and the corresponding IncuCyte® S3 Software. Cell proliferation was determined by analyzing the occupied area of individual nuclei over time.

3.2.1.7. Cell cycle analyzes

Lab equipment: IncuCyte® S3 System; Lab equipment for cultivation of cell lines (see chapter 3.2.1.1.); MACSQuant® flow cytometer.
Chemicals: 70% Ethanol; PBS (see Table 2); Propidium iodide solution (see Table 2); RNAse A (Sigma-Aldrich); Trypsin MKC (see Table 2).
Software: FlowJo™ Software (version 10.6.0, Dickinson and Company, Ashland, USA); IncuCyte® S3 Software (version 2021C, Sartorius); MACSQuantify™ Software (version 2.11, Miltenyi Biotec).

For cell cycle analyzes, cells were harvested by trypsinization and pelleted by centrifugation (3 min; 1,000 x g; room temperature). The pellet was washed three times in PBS and fixed overnight in 70% ethanol at -20°C. Cells were pelleted by centrifugation (5 min; 3,200 x g; room temperature), washed three times in PBS, and incubated with 40 µg/ml RNAse and propidium iodide solution to stain DNA at 37°C for 10 min in the dark. The DNA content of about 10,000 cells per sample was measured by flow cytometry using a MACSQuant® flow cytometer and the MACSQuantify™ Software and was analyzed using FlowJo™ Software. Flow cytometry was kindly performed by Dr. Nadine Bley (Core Facility Imaging of the Medical Faculty, Martin Luther University).

The fluorescent ubiquitination-based cell cycle indicator (FUCCI) system was used to analyze the duration of cell cycle phases. Cell cycle phases of WT FUCCI and PKP3-KO FUCCI cells were monitored based on their fluorescence using an IncuCyte® S3 System with 20x magnification starting 4 h after seeding. Live cell images were automatically taken every hour. Individual FUCCI cells were identified and tracked visually in every cell cycle phase for their duration using the IncuCyte® S3 Software.

3.2.1.8. BrdU assay

Lab equipment: Lab equipment for cultivation of cell lines (see chapter 3.2.1.1.); Plate reader Infinite® M PLEX.
Chemicals: Cell Proliferation ELISA, BrdU Kit (Sigma-Aldrich) including BrdU, fixation solution, anti-BrdU peroxidase coupled antibody, and tetramethylbenzidine containing substrate solution; PBS (see Table 2).

To analyze DNA replication, a colorimetric 5-bromo-2'-desoxyuridine (BrdU) assay was performed using the Cell Proliferation ELISA, BrdU Kit. The working principle is described in Figure 11.
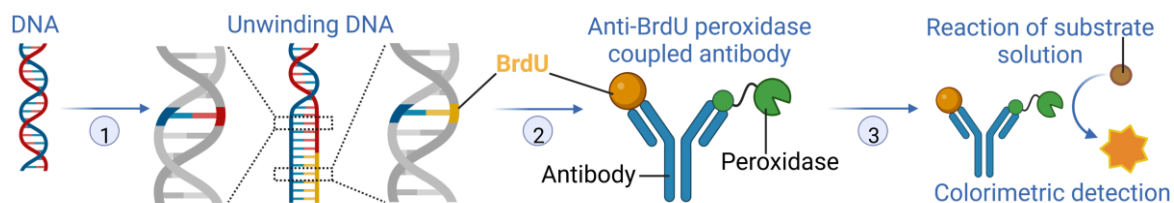
Figure 11 │ Colorimetric BrdU assay principle. Created with biorender.com. (1) Cells were treated with the non-radioactive pyrimidine analogue 5-bromo-2'-desoxyuridine (BrdU) to allow its incorporation in place of thymidine into new synthesized DNA of proliferating cells. (2) Cells were fixed and incubated with the anti-BrdU peroxidase coupled antibody to detect the level of BrdU incorporation. (3) Incubation with substrate solution enables color development for photometric detection.

Murine keratinocytes were grown in LCM for 24 h, 48 h, and 72 h. At the indicated times, the medium was discarded, cells were washed twice in PBS, and maintained in LCM supplemented with BrdU (100 µM) for 6 h at 32°C. Cells were fixed for 30 min at room temperature using the fixation solution provided in the kit, incubated with the anti-BrdU peroxidase coupled antibody for 90 min, and washed three times in PBS to remove unbound antibodies. Tetramethylbenzidine containing substrate solution was added for 100 min until color development was sufficient for photometric detection. The absorbance of all samples was measured at 370 nm (reference wavelength 492 nm) using a plate reader Infinite® M PLEX. The blank control (assay performed in wells without cells) was subtracted from all other values.

3.2.1.9. Epithelial sheet assay (Dispase assay)

Lab equipment: Digital shaker with microtiter attachment (IKA vortex 4 digital); Lab equipment for cultivation of cell lines (see chapter 3.2.1.1.); Sony DSC-H300 camera.
Chemicals: Dispase solution (see Table 2); 3.3 mM EGTA (Carl-Roth); PBS (see Table 2).
Software: Fiji, tool "Cell Counter" (version 1.51h; (Schindelin *et al.*, 2012)).

For analysis of intercellular adhesion, murine keratinocytes were grown to confluence in HCM, washed twice in PBS, and maintained in Dispase solution for 30 min at 37°C. After detachment, 3.3 mM EGTA was added to the medium for additional 30 min to facilitate disruption of Ca^{2+}-sensitive cell contacts. Free floating monolayers were submitted to mechanical stress on a digital shaker at 750 rpm. Images were taken using a Sony DSC-H300 camera. Image processing and counting of fragments were performed with the Fiji tool "Cell Counter".

3.2.1.10. Immunofluorescence

Lab equipment: Glass coverslips (12 mm); Glass slides; Lab equipment for cultivation of cell lines (see chapter 3.2.1.1.); Tweezer.
Chemicals: Aqua bidest; 50 µg/µl Collagen I rat tail (Corning) in 0.02 N acidic acid; Ethanol; Fluorochrome-coupled primary antibody (see Table 4); 3.7% (w/v) Formaldehyde; Hoechst 33342 (Thermo Fisher Scientific); Methanol; Mowiol (see Table 2); MT buffer (see Table 2); PBS (see Table 2); Poly-L-lysine; Primary antibodies (see Table 4); Secondary antibodies (see Table 5); 1% (w/v) Skimmed BSA/PBS; 1% (w/v) Skimmed milk/PBS.

In indirect immunofluorescence, a two-step incubation is performed (Figure 12A). Firstly, a specific primary antibody recognizes the target structure. In a second incubation step, a fluorescence-coupled secondary antibody is applied which specifically binds to the primary antibody. Directing the secondary antibody against the species in which the primary antibody was raised obtains the specificity.

Murine keratinocytes were grown on collagen I-coated coverslips and A431 cells were grown on poly-L-lysine-coated coverslips and proceeded according to the experiment. The medium was discarded and cells were washed twice in PBS. Cells were fixed for 10 min in methanol at −20°C or for 20 min in 3.7% (w/v) formaldehyde in PBS at room temperature or on ice. Formaldehyde fixation results in crosslinking of cellular proteins via their free amino groups, which enables good visualization of soluble components. Methanol has a dehydrogenating effect and precipitate proteins, thereby fixing them in their cellular context. Next, the plasma membrane was permeabilized in detergent buffer (microtubule stabilization (MT) buffer) for 15 min at room temperature to enable the accessibility of intracellular structures for the antibody. Cells were washed three times in PBS and blocked in 1% (w/v) skimmed milk/PBS or 1% (w/v) skimmed bovine serum albumin (BSA)/PBS (depending on primary antibody) for 30 min at room temperature to minimize the unspecific binding of antibodies to non-target structures. Primary antibodies (see Table 4) were diluted in blocking solution and incubated overnight at 4°C in a humid chamber. The next day, coverslips were washed three times for 10 min in PBS, briefly blocked in blocking solution, and incubated for 1 h at room temperature with the fluorophore-conjugated secondary antibody (see Table 5). DNA was stained with Hoechst 33342 (1:1,000 in blocking solution). Again, coverslips were washed three times for 10 min in PBS, briefly washed in aqua bidest as well as ethanol. After drying at room temperature, coverslips were mounted in Mowiol and stored at a dark, dry place at room temperature until image processing.

Direct immunofluorescence was used to visualize total RB in murine WT keratinocytes (Figure 12B). In direct immunofluorescence, the specific primary antibody is linked to a fluorochrome, which visualizes the target structure under the microscope. Cells were fixed in 3.7% (w/v) formaldehyde in PBS on ice, permeabilized in MT buffer, blocked in 1% (w/v)

skimmed BSA/PBS, and incubated with the fluorochrome-coupled primary antibody overnight at 4°C. The next day, coverslips were washed, DNA was stained with Hoechst 33342, and coverslips were mounted in Mowiol.
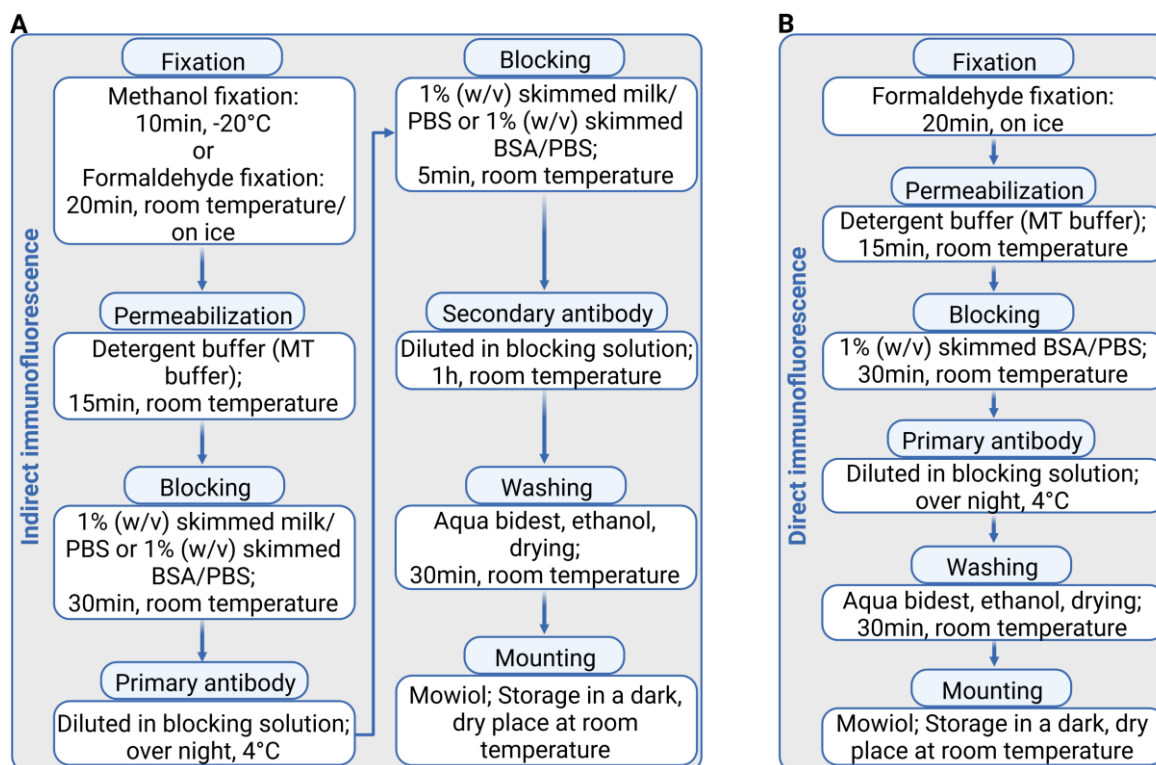
Figure 12 │ **Workflow of indirect and direct immunofluorescence principle.** Created with biorender.com. Detailed information about incubation times and temperatures are given in the figure. **(A)** In indirect immunofluorescence, on coverslips coated cells were methanol or formaldehyde fixed, permeabilized in detergent buffer, blocked in blocking solution, and incubated with the primary antibody. In a next step, coverslips were incubated with the appropriate fluorophore-conjugated secondary antibody, washed, and mounted. Indirect immunofluorescence was used to visualize all in this thesis mentioned proteins except retinoblastoma protein. **(B)** In direct immunofluorescence, the specific primary antibody is linked to a fluorochrome, resulting in a workflow similar to that of indirect immunofluorescence but without additional secondary antibody incubation. Direct immunofluorescence was used to visualize retinoblastoma protein.

3.2.1.11. BiFC

Lab equipment: Glass coverslips (12 mm); Glass slides; Lab equipment for cultivation of cell lines (see chapter 3.2.1.1.); Tweezer.
Chemicals: Aqua bidest; 50 µg/µl Collagen I rat tail (Corning) in 0.02 N acidic acid; Ethanol; 3.7% (w/v) Formaldehyde; Hoechst 33342 (Thermo Fisher Scientific); Mowiol (see Table 2); MT buffer (see Table 2); PBS (see Table 2); Plasmid DNA (see Table 7); Primary antibodies (see Table 4); Secondary antibodies (see Table 5); 1% (w/v) Skimmed BSA/PBS; 1% (w/v) Skimmed milk/PBS; Xfect™ transfection reagent (Takara Bio Inc.) including Xfect reaction buffer and Xfect polymer.
Software: Fiji (version 1.51h; (Schindelin *et al.*, 2012))

Bimolecular fluorescence complementation (BiFC) enables visualization of protein-protein associations by using a single fluorescent protein. This fluorescent protein is split into two fragments that individually lack fluorescence. When they are brought in proximity to each

other by an association between proteins fused to the fragments, the fragments form the complete fluorescent protein resulting in a fluorescent signal that can be detected by a fluorescence microscope.

For BiFC analysis, murine keratinocytes were grown on collagen I-coated coverslips for 24 h in LCM. The medium was discarded and cells were co-transfected with the indicated pVenus1 and pVenus2 constructs (see Table 7) using Xfect™ transfection reagent (for details see chapter 3.2.1.2.). At 4 h after transfection, LCM was switched to HCM and cells were incubated for 24 h before fixation in 3.7% (w/v) formaldehyde/PBS on ice. Further steps were performed as described above (for details see chapter 3.2.1.10.). Cells were immunostained with FLAG and human influenza hemagglutinin (HA) tag-directed antibodies. BiFC images of cells expressing both FLAG- and HA-tagged fusion proteins were taken with identical exposure times (2 s) to enable a comparison of BiFC efficiencies. Image processing and mean BiFC fluorescence intensities of individual transfected cells were determined using Fiji.

3.2.2. Biochemical methods

3.2.2.1. Preparation of protein lysates and determination of protein concentration

Lab equipment: Cell scraper; Centrifuge (Mikro 220 R); Heating thermo shaker (MHR 23); Hypodermic needles (0.45 x 25 mm); Plate reader Infinite® M PLEX; Syringes (1 ml).
Chemicals: Benzonase (Santa Cruz Biotechnology); 1x Halt™ protease and phosphatase inhibitor cocktail (Thermo Fisher Scientific); Pierce™ BCA Protein Assay Kit (Thermo Fisher Scientific) including BSA, BCA reagent A and B; PBS (see Table 2); SDS lysis buffer (see Table 2); 4x SDS loading buffer (see Table 2).
Software: Microsoft Excel (version 2016; Microsoft Corporation, Redmond, USA).

For protein expression analyses, cells were washed twice in PBS and lysed in SDS lysis buffer (supplemented with 1x Halt™ protease and phosphatase inhibitor cocktail). The cells were scraped off using a cell scraper and stored in a microcentrifuge tube at -80°C. After thawing, cells were homogenized using hypodermic needles by about 10 iterations of up and down passes of the syringe. Lysates were cleared by centrifugation (15 min; 13,000 x g; room temperature). The supernatant was transferred into a new microcentrifuge tube and the protein concentration was determined using the Pierce™ bicinchoninic acid (BCA) Protein Assay Kit. This assay combines the reduction of Cu^{2+} to Cu^+ by proteins in an alkaline medium (also known as biuret reaction) with the ability of BCA to form an intense purple complex with the cuprous cation Cu^+. To perform the colorimetric BCA protein assay, standard BSA solutions were prepared according to the manufacturer's instructions (see Table 15). 25 µl of each standard and unknown sample (1:10 dilution) were pipetted into a microplate. The working reagent was prepared by mixing 50 parts of BCA reagent A with 1 part of BCA reagent B (50:1, reagent A:B). After adding

200 µl of the working reagent to each well, the plate was incubated at 37°C for about 30 min. The absorbances of the standard BSA solutions and the unknown samples were measured at 562 nm on a plate reader Infinite® M PLEX. The evaluation was performed using the software Microsoft Excel. The absorbance measurement of the blank standard was subtracted from measurements of all other individual standard and unknown samples. The responses of the standards were used to prepare a standard curve by plotting the average blank-corrected measurement for each BSA standard versus its concentration in µg/ml. The standard curve was used to determine the protein concentration of each unknown sample. For an adjustment of protein concentration, the samples were provided with the corresponding amount of SDS buffer. After adding Benzonase and 4x SDS loading buffer to a partial sample volume, samples were heated to 95°C for 5 min, stored at -20°C, separated by SDS-PAGE, and analyzed by western blotting.

Table 15 │ Preparation of standard BSA solutions. BSA = bovine serum albumin.

Vial	Volume of BSA	Volume of aqua bidest	Final BSA concentration
A	2,000 µl of stock	2,000 µl	1,000 µg/ml
B	1,500 µl of vial A dilution	500 µl	750 µg/ml
C	750 µl of vial B dilution	250 µl	500 µg/ml
D	500 µl of vial C dilution	500 µl	250 µg/ml
E	500 µl of vial D dilution	500 µl	125 µg/ml
F	200 µl of vial E dilution	800 µl	25 µg/ml
G	0 µl	800 µl	0 µg/ml = blank

3.2.2.2. SDS-PAGE

Lab equipment: Mini-Protean Tetra vertical electrophoresis cell including buffer tank, lid with cables, electrode assembly, and companion running module; Power supply.

Chemicals: Chemicals for preparation of polyacrylamide gels including acrylamide/bis-solution (29:1; Carl Roth), separating gel buffer (see Table 2), stacking gel buffer (see Table 2), 10% SDS (Carl Roth), tetramethylethylenediamine (Carl Roth), and 10% ammonium persulfate (Carl Roth); PageRuler™ Plus Prestained protein ladder (Thermo Fisher Scientific); SDS electrophoresis buffer (see Table 2).

To separate proteins under denaturing conditions, SDS-PAGE was performed. The SDS-polyacrylamide (SDS-PAA) gels consist of two layers. A stacking gel with a low acrylamide concentration and pH value lined up all the loaded protein samples. In the separating gel, proteins are separated solely based on polypeptide chain length. Proteins migrate at different rate depending on the concentration of the separating gel. The appropriate gel concentrations were as follows:

Visualization of proteins with a size of	Separating gel concentration
<30 kDa	15%
30-120 kDa	10%
>120 kDa	8%

Separating and stacking gel were prepared as described in Table 16. After gel polymerization and assembly of the electrophoresis system, 20 µl of each sample mixed with 4x SDS loading buffer were loaded in pockets of the stacking gel. 4 µl of the PageRuler™ Plus Prestained protein ladder was loaded as protein standard. The buffer tank was filled with SDS electrophoresis buffer and electrophoresis was carried out at 80 V for 30 min and 100 V for approximately 2-3 h.

Table 16 │ Preparation of polyacrylamide gels. SDS = sodium dodecyl sulfate, TEMED = tetramethyl-ethylenediamine.

Component	For final concentration of separating gel			Stacking gel
	8%	10%	15%	
30% Acrylamide / 0.8% bisacrylamide	20 ml	25 ml	37.5 ml	3.9 ml
Separating gel buffer	18.75 ml			-
Stacking gel buffer	-			7.5 ml
10% SDS	750 µl			300 µl
Aqua bidest	35.75 ml	30.75 ml	18.25 ml	18.6 ml
TEMED	50 µl			30 µl
10% Ammonium persulfate	500 µl			600 µl

3.2.2.3. Western blotting

Lab equipment: Filter paper (Rotilabo®; thickness 0.35 mm); Fusion-SL 3500.WL imaging system; Mini Trans-Blot cell for wet blot approach including tank, lid with cables, holder cassettes, foam pads, electrode module, and cooling unit; Nitrocellulose blotting membrane (Amersham™ Protan™; pore size 0.2 µm); Overhead rotator (Stuart rotator SB3); PerfectBlue Semi-Dry blotter including blotting lid and blotting system; Power supply; Rocking shaker (VWR 12620 platform rocker); Scanner (Epson Perfection V600 Photo).
Chemicals: Blotting buffer I, II, and III (see Table 2); Chemiluminescence solution 1 and 2 (see Table 2); Horseradish peroxidase-conjugated secondary antibodies (see Table 5); Ponceau S solution (see Table 2); Primary antibodies (see Table 4); 3% Skimmed BSA/TBST; 3% Skimmed milk/TBST; 100 nM Sodium azide (Sigma-Aldrich); Stripping buffer (see Table 2); TBS (see Table 2); TBST (see Table 2); Western Blot Ultra Sensitive HRP Substrate (Takara); Wet blot buffer (see Table 2).

Following SDS-PAGE, proteins were transferred to a nitrocellulose blotting membrane using a PerfectBlue Semi-Dry blotter or Mini Trans-Blot cells for a wet blot approach. Semi-dry blotting provides more convenience compared to wet blot transfer, but the wet blot approach offers a higher efficiency of transfer from gel to blot (Ghosh *et al.*, 2014). The composition of the blotting devices is described in Figure 13.
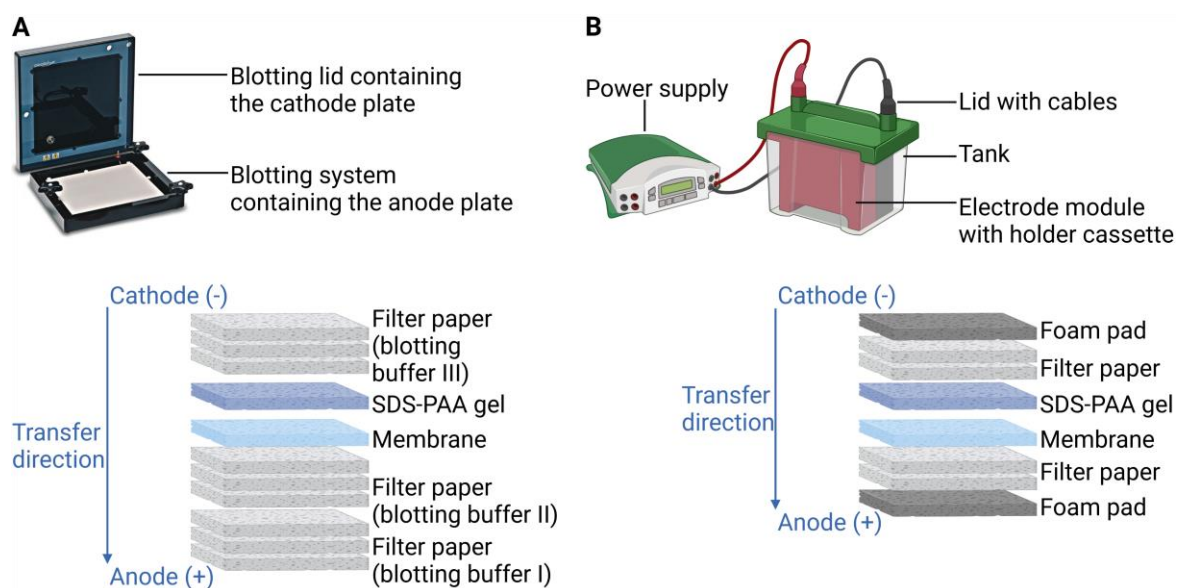
Figure 13 │ Assembly of a semi-dry and wet blot approach. Created with biorender.com. Image of the semi-dry blotting system (upper left panel) was adapted from https://de.vwr.com/store/product/15248668/perfect bluetm-semi-dry-blotter-sedectm#gallery, 2022. **(A)** In the semi-dry approach, one stack of paper, each containing three single sheets, were pre-soaked in blotting buffer I, II, or III, respectively. The stacks of in blotting buffer I and II pre-soaked filter papers were placed in the center of the base of the blotting system. A blotting membrane was put on top of the filter paper stack. The sodium dodecyl sulfate polyacrylamide (SDS-PAA) gel was placed at the top of the membrane. Any air bubbles between gel and membrane were removed. A stack of in blotting buffer III pre-soaked filter papers were stacked on top. After assembling the gel sandwich, the lid was closed, fixed with the screwing knobs, and the transfer was started. **(B)** In the wet blot approach, filter paper, the gel, and membrane were thoroughly saturated with wet blot buffer before blotting. A foam pad was placed on the inner side of the holder cassette. Two sheets of filter paper were put on top of the foam pad. A blotting membrane was placed on top of the filter paper stack and the gel was put at the top of the membrane. The gel sandwich was completed by placing two sheets of filter paper on the membrane and adding the second foam pad. After every single step, air bubbles were removed. The holder cassette was closed and placed in the electrode module. The tank was filled with wet blot buffer, a frozen cooling unit was added, the lid was closed, and the transfer was started.

The transfer performed with a semi-dry blotter was at 1 mA/cm² for 45 min followed by 1.5 mA/cm² for 30 min. Proteins were transferred using the wet blot approach at 110 V for 70 min. After transfer, membranes were stained in Ponceau S solution for 5 min, destained in distilled water, and documented using a scanner. Membranes were cut, briefly washed in tris-buffered saline with Tween20 (TBST), and blocked using 3% (w/v) skimmed milk/ TBST or 3% (w/v) BSA/TBST on a rocking shaker for 30 min. Membranes were probed overnight at 4°C on an overhead rotator with the appropriate primary antibodies (see Table 4). Next day, membranes were washed in TBST (three times for 10 min) and incubated for 1 h at room temperature on a rocking shaker with the appropriate horseradish peroxidase-conjugated secondary antibodies (diluted in 3% (w/v) skimmed milk/TBST, see Table 5). After washing twice in TBST for 10 min and once in tris-buffered saline (TBS) for 10 min, membranes were treated with enhanced chemiluminescence (ECL) Western Blotting Substrate (equal parts chemiluminescence solution 1 and 2) or Western Blot Ultra Sensitive HRP Substrate. Signals were detected using a Fusion-SL 3500.WL imaging

system. If staining with additional antibodies was required, the membranes were washed in TBST (three times, each for 10 min), incubated in stripping buffer (fresh supplemented with 100 nM sodium azide) for 1 h, washed again in TBST (three times, each for 10 min), blocked, and treated with antibodies as described above. β-actin or ponceau S staining was used as loading control.

3.2.2.4. Nucleus/cytoplasm fractionation

Lab equipment: Cell scraper; Centrifuge (Mikro 220 R); Heating thermo shaker (MHR 23); Hypodermic needles (0.45 x 25 mm); Overhead rotator (Stuart rotator SB3); Syringes (1 ml).
Chemicals: 0.5 mM DTT (Roche); 1x Halt^{TM} protease and phosphatase inhibitor cocktail (Thermo Fisher Scientific); Hypotonic buffer A (see Table 2); Hypertonic buffer C (see Table 2); NP-40 (Sigma-Aldrich); PBS (see Table 2); 4x SDS loading buffer (see Table 2).

For nucleus/cytoplasm fractionation, 6x 10^5 murine keratinocytes were used. All preparation steps were performed on ice. The principle of nucleus/cytoplasm fractionation is described in Figure 14 (Caspi *et al.*, 2008). Cells were washed twice in PBS and lysed in hypotonic buffer A (supplemented with 1x Halt^{TM} protease and phosphatase inhibitor cocktail and 0.5 mM DTT). The cells were scraped off using a cell scraper and transferred into a microcentrifuge tube. The lysate was incubated for 10 min at 4°C on an overhead rotator. After adding NP-40 to a final concentration of 3%, the solutions were kept for 10 min. Cells were homogenized using hypodermic needles by about 10 iterations of up and down passes of the syringe. Lysates were cleared by centrifugation (30 sec; 14,000 x *g*; 4°C). The supernatant was collected as cytoplasmic fraction and stored at -20°C. The pellet was washed three times in buffer A and incubated in hypertonic buffer C (supplemented with 1x Halt^{TM} protease and phosphatase inhibitor cocktail) for 30 min at 4°C on an overhead rotator. Lysates were cleared by centrifugation (30 min; 18,000 x *g*; 4°C). The supernatant was collected as nuclear fraction and stored at -20°C. For SDS-PAGE analysis, cytoplasmic and nuclear fractions were mixed with 4x SDS loading buffer, heated to 95°C for 5 min, separated by SDS-PAGE, and analyzed by western blotting. P54nrb and α-tubulin were used as positive controls for the nuclear and cytoplasmic fractions, respectively.
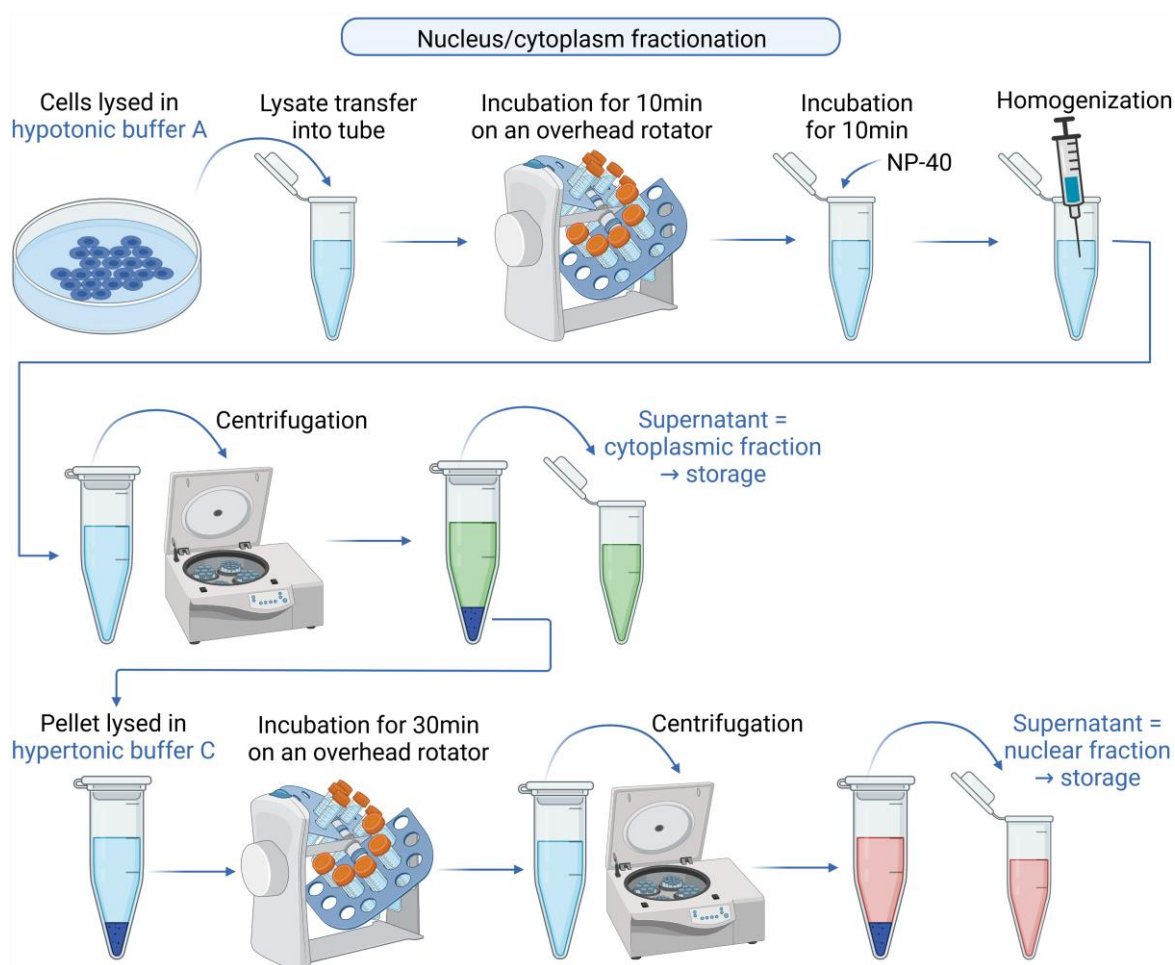
Figure 14 │ Workflow of nucleus/cytoplasm fractionation principle. Created with biorender.com, modified from (Caspi *et al.*, 2008). Cells were lysed and incubated in hypotonic buffer A. After adding NP-40 and homogenization of the cells, the lysate was cleared by centrifugation. The supernatant was collected as cytoplasmic fraction, whereas the pellet was incubated with hypertonic buffer C. After centrifugation, the supernatant was collected as nuclear fraction.

3.2.2.5. Immunoprecipitation

Lab equipment: Cell scraper; Centrifuge (Mikro 220 R); Heating thermo shaker (MHR 23); Hypodermic needles (0.45 x 25 mm); Overhead rotator (Stuart rotator SB3); Syringes (1 ml).
Chemicals: Anti-E2F1 antibody and anti-PKP3 antibody (see Table 4); Benzonase (Santa Cruz Biotechnology); GFP-Trap Agarose beads (ChromoTek); 1x Halt™ protease and phosphatase inhibitor cocktail (Thermo Fisher Scientific); IP buffer (see Table 2); Normal rabbit IgG (Santa Cruz Biotechnology #sc-2027) and guinea pig serum (Sigma-Aldrich #G9774); PBS (see Table 2); Protein A agarose beads (Thermo Fisher Scientific); 1x and 4x SDS loading buffer (see Table 2).

For each immunoprecipitation reaction, 6x 10^5 murine keratinocytes were used. All preparation steps were performed on ice. Cells were washed twice in PBS and lysed in immunoprecipitation (IP) buffer (supplemented with 1x Halt™ protease and phosphatase inhibitor cocktail). The cells were scraped off using a cell scraper and stored in a microcentrifuge tube at -80°C. After thawing, cells were homogenized using hypodermic needles by about 10 iterations of up and down passes of the syringe. Lysates were cleared

by centrifugation (15 min; 13,000 x g; 4°C). 1/6 of the lysate was mixed with 4x SDS loading buffer and Benzonase, heated to 95°C for 5 min, and stored at -20°C for an input control. The residual lysate was incubated with anti-E2F1 or anti-PKP3 antibody overnight at 4°C on an overhead rotator. Normal rabbit immunoglobulin G (IgG) or guinea pig serum was used as an isotype control. Protein A agarose beads were washed in IP buffer and added to the lysate for 1 h at 4°C on an overhead rotator. Lysates were pelletized by centrifugation (3 min; 4,000 x g; 4°C). The pellet was washed three times in IP buffer and bound proteins were eluted in 1x SDS loading buffer. Both input and eluate samples were separated by SDS-PAGE and analyzed by western blotting.

For GFP-Trap, WT cells expressing GFP-tagged PKP3 were lysed and pelleted as described before. Cell lysates were incubated with GFP-Trap Agarose beads for 1 h at 4°C on an overhead rotator. Further preparation of the samples was as described before.

3.2.2.6. Lambda protein phosphatase treatment

Lab equipment: Cell scraper; Centrifuge (Mikro 220 R); Heating thermo shaker (MHR 23); Hypodermic needles (0.45 x 25 mm); Syringes (1 ml).
Chemicals: 1x Halt™ protease and phosphatase inhibitor cocktail (Thermo Fisher Scientific); IP buffer II (see Table 2); Lambda PP (New England Biolabs), supplied with Lambda PP buffer (50 mM HEPES; 100 mM NaCl; 2 mM DTT; 0.01% Brij 35; freshly supplemented with 1 mM MnCl$_2$; pH 7.5); PBS (see Table 2); 4x SDS loading buffer (see Table 2).

To validate the phospho-RB Ser[807/811] antibody in murine keratinocytes, WT cells were treated with Lambda protein phosphatase (Lambda PP). Lambda PP is an Mn^{2+}-dependent protein phosphatase with activity towards phosphorylated serine, threonine, and tyrosine residues. All preparation steps were performed on ice. Cells were washed twice in PBS and lysed in IP buffer II (supplemented with 1x Halt™ protease and phosphatase inhibitor cocktail). IP buffer II contains no EDTA in order to avoid inhibition of Lambda PP. The cells were scraped off using a cell scraper and stored in a microcentrifuge tube at -80°C. After thawing, cells were homogenized using hypodermic needles by about 10 iterations of up and down passes of the syringe. Lysates were cleared by centrifugation (15 min; 13,000 x g; 4°C). The entire 80 µl WT cell lysate was incubated with 4 µl Lambda PP in 20 µl Lambda PP buffer at 30°C for 30 min on a heating thermo shaker at 900 U/min. Negative control was performed in the same experimental condition without Lambda PP. Subsequently, the lysate was mixed with 4x SDS loading buffer to inhibit the enzyme, and heated to 95°C for 5 min. The samples were stored at -20°C, separated by SDS-PAGE, and analyzed by western blotting.

3.2.3. Molecular biological methods

3.2.3.1. RNA isolation

Lab equipment: Cell scraper; Centrifuge (Mikro 220 R); DNase/RNase-free 2.0ml microcentrifuge tubes.
Chemicals: Chloroform (Carl Roth); DNase/RNase-free distilled water (Invitrogen); Ice-cold 75% ethanol (Sigma-Aldrich); Ice-cold isopropanol (Sigma-Aldrich); β-Mercaptoethanol (Carl Roth); PBS (see Table 2); RNA-grade glycogen (20 mg/ml; Thermo Fisher Scientific); Trizol (see Table 2).

Total RNA was isolated from murine keratinocytes and A431 cells grown for 3 days in LCM or standard DMEM, respectively. Cells were washed twice in PBS, homogenized in 1,500 µl Trizol supplemented with β-mercaptoethanol (1:100), scratched from the dish, and transferred into a DNase/RNase-free 2.0 ml microcentrifuge tube. The sample was frozen and stored at -80°C. After thawing, the RNA was isolated by phenol/chloroform extraction and isopropanol precipitation. 1/5 vol chloroform was added to homogenized cells, mixed by shaking for 15 sec, incubated for 3 min, and separated by centrifugation (15 min; 13,000 x g; 4°C). The RNA-containing aqueous phase was transferred into a new RNase-free microcentrifuge tube, mixed with 1 vol chloroform, and separated by centrifugation (15 min; 13,000 x g; 4°C). Again, the RNA-containing aqueous phase was transferred into a new RNase-free microcentrifuge tube, mixed with 1 vol ice-cold isopropanol and 1 µl glycogen. RNA was incubated overnight at -20°C for precipitation. Next day, RNA was pelletized by centrifugation (10 min; 13,000 x g; 4°C) and washed for three times with ice-cold 75% ethanol by centrifugation (5 min; 5,000 x g; 4°C). After removal of the ethanol by pipetting, the RNA was dried for 10 min at room temperature, resolved within nuclease-free distilled water, and stored at -80°C.

3.2.3.2. cDNA synthesis

Lab equipment: PCR thermal cycler (Biometra TRIO); Plate reader Infinite® M PLEX.
Chemicals: DNase/RNase-free distilled water (Invitrogen); dNTP mix (10 mM); DTT (0.1 M; Invitrogen); First-Strand buffer (5x; Invitrogen); Random hexamer primer (0.2 µg/µl; Thermo Fisher Scientific); SuperScript® II Reverse Transcriptase (Invitrogen).

For the synthesis of complementary DNA (cDNA), a reverse transcription reaction was performed. RNA concentration was quantified using a plate reader Infinite® M PLEX. Absorbance of RNA samples was measured at 260 nm. To assess the RNA purity, an additional measurement at 280 nm was performed to indicate proteins in the sample. In each sample, a 260/280 ratio of about 1.9 was considered as "pure" for RNA. 1 µg isolated total RNA was incubated with 1 µl random hexamer primer, 1 µl dNTP mix, and nuclease-free distilled water to a final volume of 12 µl for 5 min at 65°C to denature any secondary structures of the RNA. For reverse transcription, the following reaction mix was added: 4 µl 5x First-Strand buffer, 2 µl 0.1 M DTT, 1 µl SuperScript® II Reverse Transcriptase,

1 µl nuclease-free distilled water. The reactions were run in a PCR thermal cycler and performed with the following program:

Step	Temperature	Time
Denaturation	65°C	5 min
Cool down	4°C	hold
Addition of 8 µl reaction mix		
Primer annealing	25°C	10 min
Reverse transcription	42°C	50 min
Inactivation	70°C	15 min
End	4°C	hold

The synthesized cDNA was diluted in 180 µl nuclease-free distilled water and stored at -20°C.

3.2.3.3. qRT-PCR

Lab equipment: 384 well plate; LightCycler 480 II Real Time PCR system.
Chemicals: Maxima SYBR Green/ROX qPCR Master Mix (Thermo Fisher Scientific).

To assess the relative abundance of mRNAs, qRT-PCR was performed. Primer pairs were selected using Primer Blast (https://www.ncbi.nlm.nih.gov/tools/primer-blast/, 2021). Primer sequences are listed in Table 8. In wells of a 384 well plate, 2.4 µl cDNA was mixed with 0.1 µl primer pairs, and 2.5 µl Maxima SYBR Green/ROX qPCR Master Mix. The PCR runs on a LightCycler 480 II Real Time PCR system with the following conditions:

Step	Temperature	Time	
DNA polymerase activation	95°C	15 min	
Denaturation	95°C	15 sec	
Primer annealing	62°C	15 sec	40 cycles
Elongation	72°C	20 sec	

3.2.4. Image processing and quantification

3.2.4.1. Image processing of immunofluorescence and BiFC

Immunofluorescence and BiFC images were taken on a Nikon Eclipse E600 microscope, with a charge-coupled device camera and a Plan APO 60x/1.40 NA oil objective, controlled with the NIS-Elements AR software (version 4.12.00, Nikon). For comparisons between different treatments within the same experiment, samples were treated in parallel and images were captured with the same exposure times. Image processing of BiFC experiment is described in chapter 3.2.1.11. The Fiji software was used for image processing (Schindelin *et al.*, 2012).

3.2.4.2. Quantification of immunofluorescence images

To determine the enrichment factors for PKP3 and desmoplakin at lateral contacts as well as PKP3 at tricellular contacts, fluorescence intensities were measured in segments of equal length (~100 pixel) and width (bicellular, 40 pixel; tricellular, 10 pixel) covering the cytoplasm as well as lateral and tricellular contacts as illustrated in Figure 15A. All cell contacts of the entire image were evaluated, with the exception of mitotic, polynuclear, or overgrowing cells. Each line scan results in a histogram depicting the fluorescence intensities along the bar. The enrichment factors for PKP3 and desmoplakin at lateral contacts were calculated by dividing the mean junctional value (10 pixel length of the 100 pixel scan line) by the mean cytoplasmic value (both ends of a scan line, each 10 pixel length) for each line scan. To quantify PKP3 fluorescence intensities at tricellular contacts, the mean tricellular value (10 pixel length at the middle of the 100 pixel scan line) was divided by the mean lateral value (one end of a scan line, 10 pixel length).
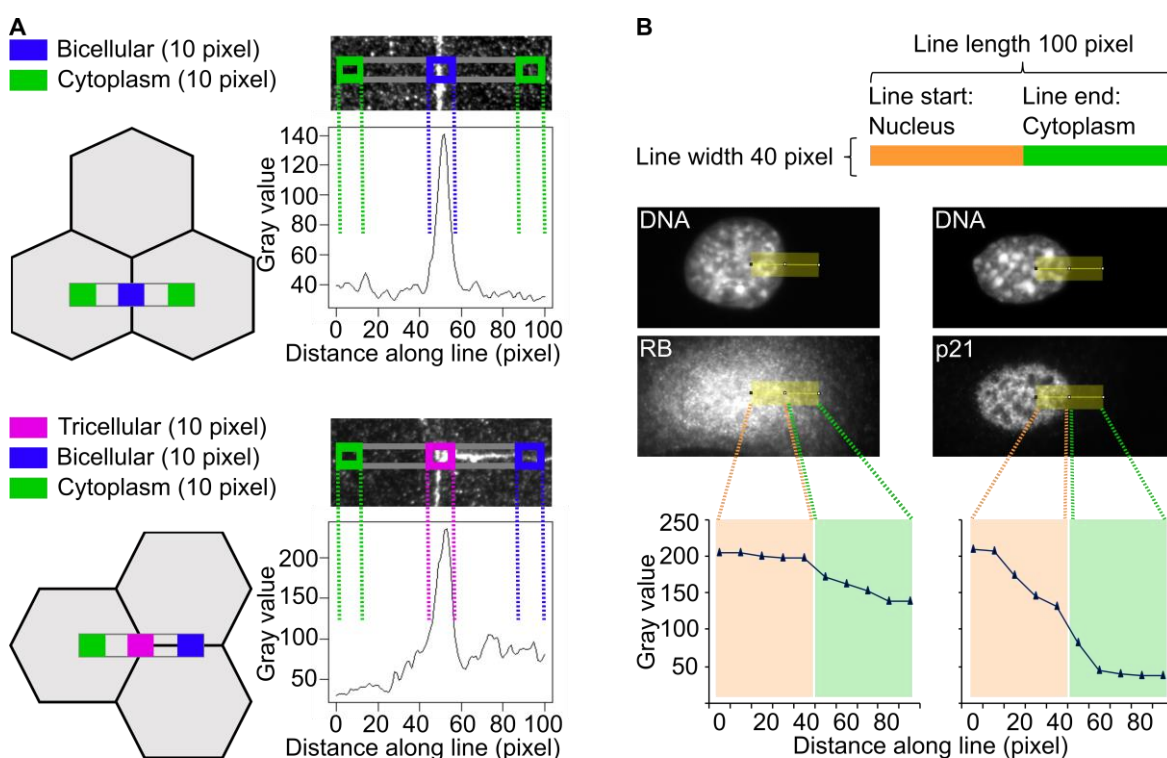
Figure 15 │ Quantification of immunofluorescence images. (A) Quantification of PKP3 and desmoplakin immunofluorescence intensities at lateral contacts (upper panel) and tricellular contacts (lower panel). PKP3 and desmoplakin fluorescence intensities were determined in immunofluorescence images using Fiji by measuring segments of equal length (about 100 pixel) and width (bicellular, 40 pixel; tricellular, 10 pixel) across individual bicellular or tricellular contacts as illustrated by the colored bars in the schematics and immunofluorescence images. Each line scan results in a histogram depicting the fluorescence intensities along the bar [bicellular (blue), cytoplasm (green), tricellular (pink)]. **(B)** Quantification of RB and p21 immunofluorescence intensities. RB (left panel) and p21 (right panel) fluorescence intensities were calculated from images using Fiji by measuring segments of equal length (100 pixel) and width (40 pixel) across individual nuclei as illustrated by the colored bars. An image of the nuclear marker Hoechst33342 was used to generate a mask that segments nuclei. The start of the line was in the nucleus, the end of the line was in the cytoplasm. The lines were positioned in such a way that their center was at the transition from nucleus to cytoplasm. Each

line scan resulted in a histogram depicting the fluorescence intensities along the bar [nucleus (orange), cytoplasm (green)].

To determine the enrichment factors for RB and p21 in the nucleus and the cytoplasm, fluorescence intensities were measured in segments of equal length (100 pixel) and width (40 pixel) across individual nuclei as illustrated in Figure 15B. All nuclei of the entire image were evaluated, with the exception of mitotic, polynuclear, or overgrowing cells. Each line scan results in a histogram depicting the fluorescence intensities along the bar. The enrichment factors for RB were calculated by dividing the mean cytoplasmic value (50 pixel length at the end of the 100 pixel scan line) by the mean nuclear value (50 pixel length at the start of the 100 pixel scan line) for each line scan. To quantify p21 fluorescence intensities, the mean nuclear value was divided by the mean cytoplasmic value. At least 250 cells per condition from two independent experiments were analyzed.

3.2.4.3. Quantification of western blots

For quantification of western blots, the Fiji tool "Gel analysis" was used. Signals were normalized to the internal loading control β-actin. If β-actin protein level varied due to experimental conditions, Ponceau S staining was used as loading control. Details concerning normalization procedures are given in the figure legends.

3.2.4.4. Calculation of mRNA levels

Raw cycle threshold (C_t) values for the gene of interest and the housekeeping gene were used to determine the relative RNA abundance by the $\Delta\Delta C_t$ method with the following equation: $\Delta\Delta C_t = \Delta C_t \text{ (experimental conditions)} - \Delta C_t \text{ (control conditions)}$

where $\Delta C_t = \text{mean } C_t \text{ (gene tested)} - \text{mean } C_t \text{ (housekeeping gene)}$ for experimental conditions and control conditions, respectively. In a next step, the $\log_2$ fold changes were determined by the following equation: $\log_2 \text{ fold change} = -\Delta\Delta C_t$

For validation of knockdown efficiency, the fold changes were calculated by the following formula: $\text{fold change} = 2^{-\Delta\Delta C_t}$

3.2.4.5. Calculation of mRNA half-life

Murine keratinocytes were treated with actinomycin D to analyze RNA stability (see chapter 3.2.1.5.). To assess mRNA decay kinetics, one-phase exponential decay curve analysis was performed using Graphpad Prism Software (version 9). The mRNA half-life was obtained with the following equation:

$t_{1/2} = \frac{\ln(2)}{k_{decay}}$ where $t_{1/2}$ is the half-life of mRNA

and k_{decay} is the rate constant for decay (i.e., percent change over time). An exponential decay equation model was fit to determine k_{decay} using the following equation for one-phase decay: $Y = (Y0 - Plateau) * \exp(-k_{decay} * X) + plateau$ where X is the time and Y is the mRNA level, starting at Y0 and decaying (with one phase) down to Plateau (Y value at infinite times) as described in the following plot:
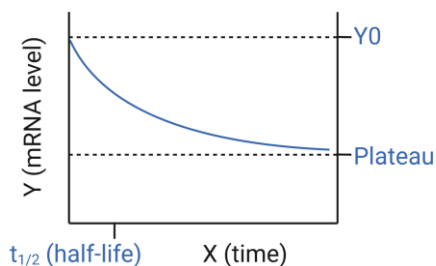
3.2.4.6. RNA sequencing and GSEA

Total RNA (≥ 2 µg) isolated from murine keratinocytes (see chapter 3.2.3.1.) was sequenced and analyzed to reveal mRNA expression profiles. Library preparation (Poly(A) tail RNA selection) and sequencing was performed by LC Sciences (Houston, USA). Calculation of $\log_2$ fold changes and gene set enrichment analysis (GSEA) were kindly performed by Dr. Markus Glaß (Core Facility Imaging of the Medical Faculty, Martin Luther University). GSEA was performed using the R-package clusterProfiler (version 4.4.4, (Yu *et al.*, 2012)), and MSigDB (version 7.5.1, (Liberzon *et al.*, 2015)) gene sets utilizing the fgsea algorithm and setting the exponent parameter to 0 for unweighted analyses of $\log_2$ fold change sorted gene lists from RNA sequencing data. Murine gene names were converted to human homolog equivalents using the R-package biomaRt (version 2.52.0, (Durinck *et al.*, 2005)).

3.3. Statistical analysis

Statistical analysis and preparation of plots were performed using Graphpad Prism Software (version 9). Details on how data and error bars are presented can be found in the figure legends. In bar plots, all individual data points are shown. Boxplots display the first to third quartile; whiskers extend to the minimum and maximum. For two independent data sets, statistically significant differences were determined with a student's unpaired two tailed *t*-test. To compare more than two independent data sets with normal distribution, one-way analysis of variance (ANOVA) followed by a Tukey's multiple comparison test was used. Asterisks indicate statistical significance (*p<0.05, **p<0.01, ***p<0.001). ns represents no significant difference.

4. RESULTS

4.1. The desmosomal role of PKP3 as a scaffold for adhesion

The first part of the results chapter deals with the desmosomal role of PKP3 as a scaffold for adhesion. As PKP1 promotes desmosome maturation to a Ca-independent "hyper-adhesive" state and PKP3 facilitates desmosome assembly, I wondered if these distinct functions are regulated by distinct signals that would lead to specific post-translational modifications. Therefore, I analyzed the effects of growth factor signaling pathways on PKP3-dependent adhesive properties using non-transformed murine keratinocytes and A431 cells as model systems.

4.1.1. EGF signaling induces PKP3 phosphorylation

Keratinocyte proliferation, differentiation, and migration depend on growth factors such as IGF-1/insulin and EGF (Krane *et al.*, 1991; Sadagurski *et al.*, 2006; Seeger and Paller, 2015). To test the effect of insulin and EGF on PKP3 phosphorylation, murine keratinocytes and A431 cells were treated with insulin and EGF, respectively, and compared to untreated serum-starved cells. The activity of both growth factors was validated by testing downstream kinase activation of the PI3K/AKT and the RAS/RAF/MAPK signaling pathways using phospho-specific antibodies (Figure 16A, 16B). AKT, S6 kinase (S6K), mitogen-activated protein kinase kinase (MEK), extracellular signal regulated kinase (ERK), ribosomal S6 kinase (RSK), and the ribosomal protein S6, which is a common target of S6K and RSKs, were all phosphorylated after insulin and/or EGF stimulation in murine keratinocytes. Immunoprecipitated PKP3 was then tested for its phosphorylation using an antibody that recognizes the AGC-kinase motif RXXpS/pT (see Figure S1 for putative antibody recognition sites). In murine keratinocytes, PKP3 was phosphorylated at such motifs only after EGF but not after insulin treatment. In contrast, PKP1 was phosphorylated in response to insulin stimulation but not after EGF treatment (Wolf *et al.*, 2013). To further validate these data, PKP3 modification by EGF was analyzed in human A431 cells (Figure 16A), which reveal high protein levels of the EGFR. Again, activation of the PI3K/AKT and the RAS/RAF/MAPK signaling pathways was confirmed by phospho-specific antibodies to AKT, S6K, MEK, ERK, and RSK. Phosphorylation of PKP3 at the AGC-kinase motif RXXpS/pT was strongly increased after EGF but not after insulin treatment.

These date show that EGF stimulates PKP3 phosphorylation at AGC-consensus sites in murine keratinocytes and human A431 cells. In contrast, insulin, which promoted PKP1 phosphorylation and its cytoplasmic accumulation, had no effect on PKP3 phosphorylation.
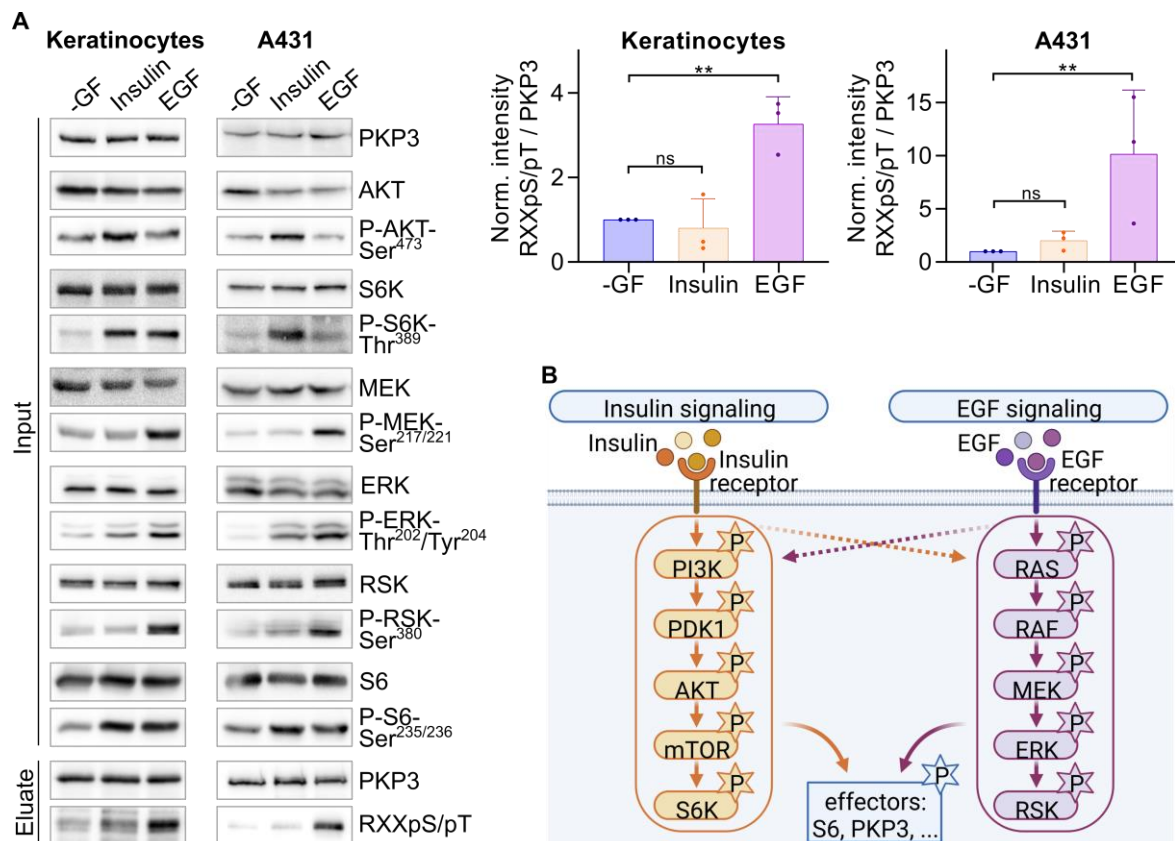
Figure 16 │ EGF induces PKP3 phosphorylation. (A) For analyzing growth factor signaling on PKP3 phosphorylation, murine keratinocytes were grown in HCM for 24 h, maintained in serum-free HCM without any supplements for 5 h (without growth factors, -GF), and treated with Ca^{2+} in combination with growth factors (50 µg/ml insulin, 100 ng/ml EGF) for 15 min. A431 cells were grown in standard DMEM for 24 h, maintained in serum-free DMEM for additional 24 h (-GF), and stimulated with growth factors (50 µg/ml insulin, 100 ng/ml EGF) for 15 min. Kinase activation was verified by western blotting with the indicated antibodies (input). Immunoprecipitated PKP3 (eluate) was probed for growth factor-specific phosphorylation with an antibody that recognizes RXX-phospho-serine or phospho-threonine motif (RXXpS/pT). Insulin had no effect on the respective motif, whereas EGF stimulated PKP3 phosphorylation at these AGC-kinase consensus sites (RXXS/T motif) in murine keratinocytes and A431 cells. The bar plots (upper right panel) depicts the mean intensity ratios (+ s.d.; n=3) of eluate RXXpS/pT versus precipitated PKP3 normalized to untreated cells (-GF). Statistical significance was determined by one-way ANOVA with Tukey's multiple comparisons test. **(B)** Schematic of insulin and EGF signaling pathways (created with biorender.com). Insulin interacts with the insulin receptor to activate the PI3K/AKT signaling pathway, whereas EGF activates the EGF receptor followed by activation of the RAS/RAF/MAPK signaling pathway. In addition, both downstream pathways are secondary branches of insulin or EGF signaling, respectively. A phosphorylation cascade leads to the phosphorylation of downstream effectors such as S6 protein, thereby modulating their function. PKP3 might be an effector of the EGF signaling pathway.

4.1.2. EGF signaling improves PKP3 cell contact association

Phosphorylation alters the structural conformation of proteins (Ardito *et al.*, 2017) and can modify their functions due altered subcellular localization and interactions (Lee and Yaffe, 2016). To analyze whether EGF induced PKP3 phosphorylation affects its localization, serum-starved murine keratinocytes were treated with insulin, EGF, or complete medium and processed for immunofluorescence (Figure 17). In untreated serum-starved cells, PKP3 and desmoplakin were hardly found at cell contact sites. Whereas PKP3 and

desmoplakin lateral localization remained essentially unaltered upon insulin treatment, EGF considerably improved PKP3 and desmoplakin association at lateral membranes similar to the incubation in complete medium. This suggests that EGF-induced PKP3 phosphorylation affects its localization resulting in improved lateral membrane association of PKP3.
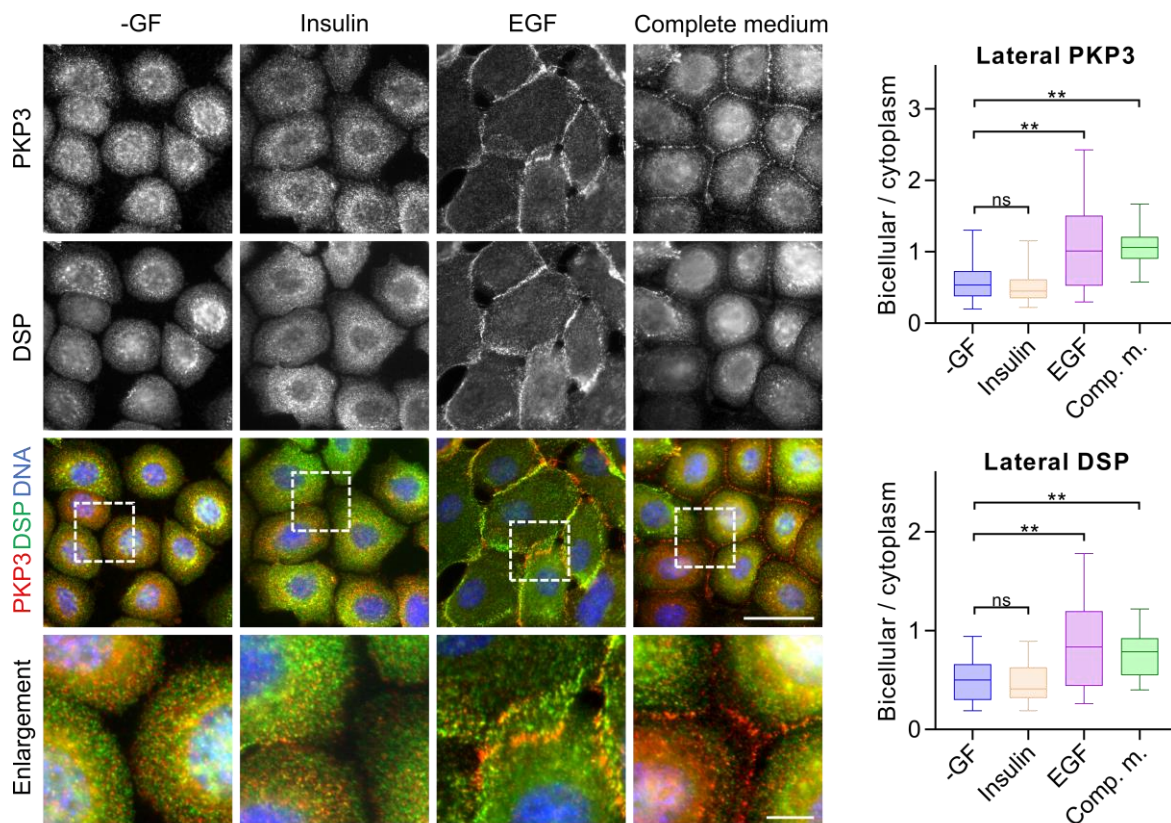
Figure 17 │ EGF improves lateral PKP3 membrane recruitment in murine keratinocytes. For analyzing EGF induced effects on PKP3 localization, murine keratinocytes were grown in HCM for 24 h, maintained in serum-free HCM without any supplements for 5 h (without growth factors, -GF), and treated with Ca^{2+} in combination with growth factors (50 µg/ml insulin, 100 ng/ml EGF) or complete medium (HCM; comp. m.) for 15 min. Cells were fixed in methanol at -20°C and immunostained for PKP3 and desmoplakin (DSP). Immunofluorescence images show PKP3 and desmoplakin localization in stimulated compared to non-stimulated cells. The enlargements highlight the effects of the respective treatments on PKP3 and desmoplakin localization. Scale bars: 50 µm, enlargement 10 µm. Insulin had no effect on PKP3 or desmoplakin membrane association, whereas stimulation with EGF or complete medium improves PKP3 and desmoplakin recruitment to lateral membranes. The boxplots (right panels) depict the enrichment factor of PKP3 or desmoplakin at lateral contacts (n≥200). The Whiskers extend to the minimum and maximum values. Statistical significance was determined by one-way ANOVA with Tukey's multiple comparisons test.

As clustering of PKP3 at tricellular contacts depends on its displacement from lateral membranes by PKP1 (Keil *et al.*, 2016), I analyzed whether a brief EGF stimulation would be sufficient to induce PKP3 recruitment to tricellular contacts or whether a longer time period would allow PKP3 distribution to cell corners even in the absence of complete medium. Therefore, PKP3 localization at tricellular contacts was analyzed in murine keratinocytes after a short EGF stimulation followed by 6 h incubation without growth

factors or a prolonged incubation with either EGF or complete medium for 6 h (Figure 18). Immunofluorescence analysis showed that short EGF stimulation was not sufficient to induce PKP3 accumulation at tricellular contacts. In contrast, prolonged EGF treatment resulted in increased tricellular PKP3 localization. However, EGF alone was clearly less efficient than complete medium. This suggests that EGF supports desmosome formation by facilitating the incorporation of phosphorylated PKP3 into nascent desmosomes, but that their full maturation requires additional signals.
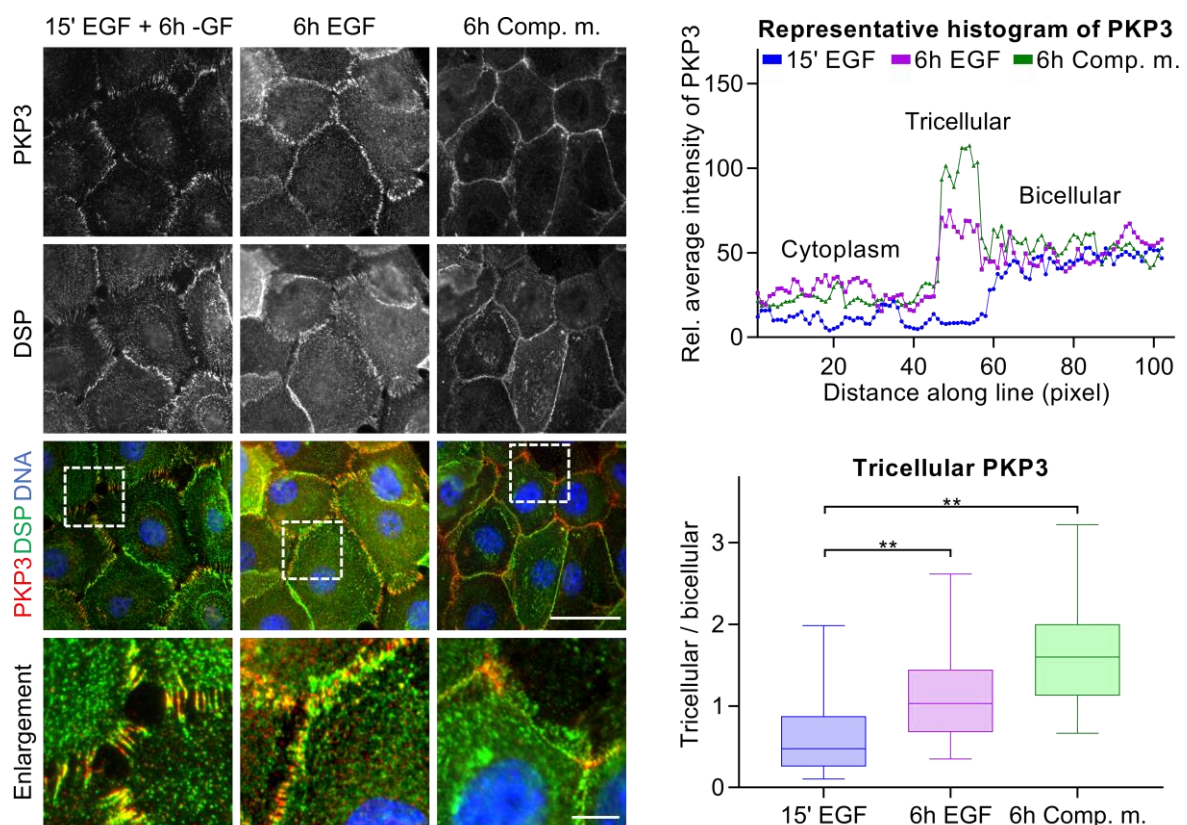
Figure 18 │ EGF improves tricellular PKP3 cell contact association in murine keratinocytes. For analyzing EGF induced tricellular PKP3 localization, murine keratinocytes were grown in HCM for 24 h, maintained in serum-free HCM without any supplements for 5 h, and treated with Ca^{2+} in combination with EGF (100 ng/ml) for 15 min followed by 6 h incubation in serum-free HCM without any supplements (without growth factors, -GF), or with Ca^{2+} in combination with EGF (100 ng/ml) or complete medium (HCM; comp. m.) for 6 h. Cells were fixed in methanol at -20°C and immunostained for PKP3 and desmoplakin (DSP). Immunofluorescence images show PKP3 and desmoplakin localization in prolonged EGF stimulated compared to short EGF stimulated cells. The enlargements highlight the effects of the respective treatments on PKP3 and desmoplakin localization. Scale bars: 50 μm, enlargement 10 μm. A short EGF stimulation for 15 min followed by 6 h incubation without growth factors was not sufficient for PKP3 accumulation at tricellular contacts. After prolonged EGF treatment for 6 h, tricellular PKP3 localization was increased. A strong enrichment of PKP3 at tricellular contact sites was observed after 6 h incubation in complete medium. Representative line scans of PKP3 fluorescence intensities across tricellular contact regions (upper right panel) illustrate the different distribution of PKP3 after short EGF treatment followed by incubation without growth factors (15' EGF) and prolonged EGF (6 h EGF) or complete medium (6 h comp. m.) treatment. The boxplot (lower right panel) depicts the enrichment factor of PKP3 at tricellular versus bicellular contacts (n≥200). The Whiskers extend to the minimum and maximum values. Statistical significance was determined by one-way ANOVA with Tukey's multiple comparisons test.

Similar effects were observed in human A431 cells, although due to the low expression of PKP1 in these cells, PKP3 does not accumulate at tricellular contacts. Nonetheless, to analyze whether EGF induced PKP3 phosphorylation affect its lateral localization, serum-starved A431 cells were treated with insulin, EGF, or complete medium (standard DMEM containing FCS) and processed for immunofluorescence (Figure 19). In untreated serum-starved and insulin treated A431 cells, PKP3 and desmoplakin were hardly found at cell contact sites. In contrast, EGF and complete medium considerably improved PKP3 and desmoplakin association at lateral membranes.
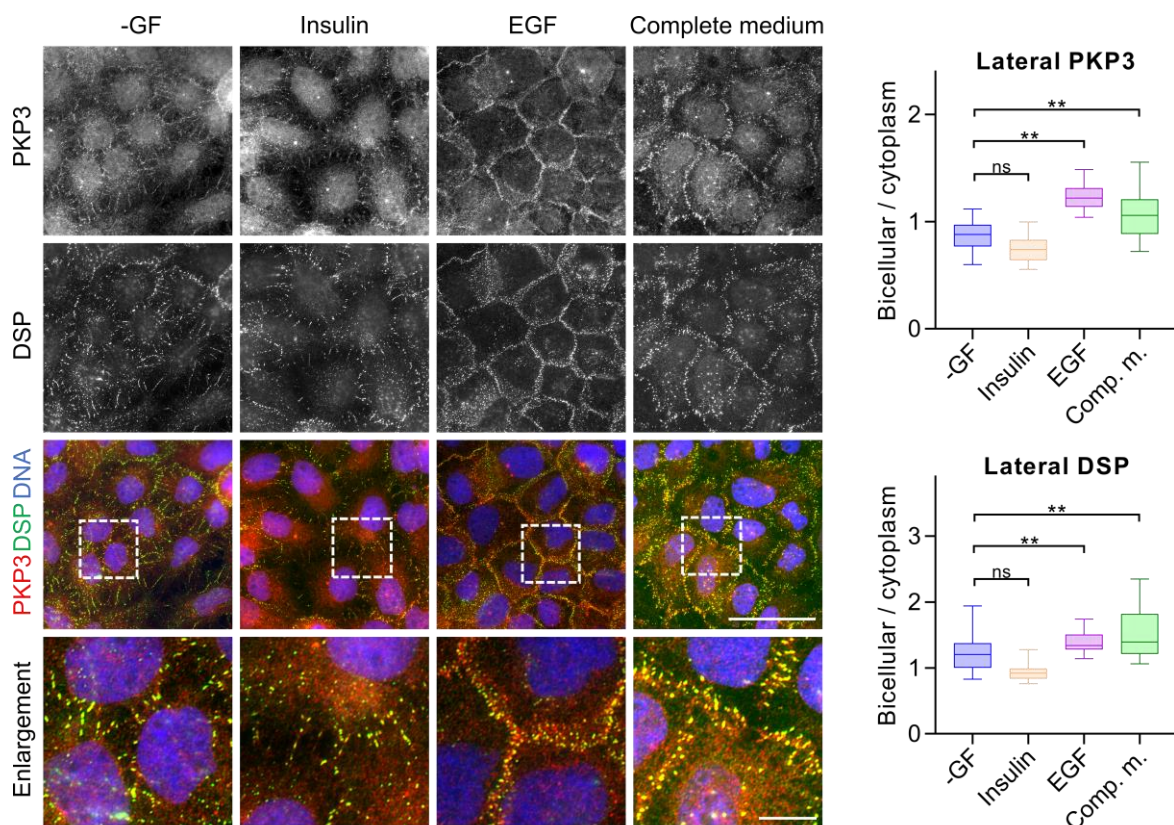
Figure 19 │ **EGF improves lateral PKP3 membrane recruitment in A431 cells.** For analyzing EGF induced effects on PKP3 localization, A431 cells were grown in standard DMEM for 24 h, maintained in serum-free DMEM for additional 24 h (without growth factors, -GF), and stimulated with growth factors (50 µg/ml insulin, 100 ng/ml EGF) or standard DMEM with FCS (complete medium) for 15 min. Cells were fixed in methanol at -20°C and immunostained for PKP3 and desmoplakin (DSP). Immunofluorescence images show PKP3 and desmoplakin localization in stimulated compared to non-stimulated cells. The enlargements highlight the effects of the respective treatments on PKP3 and desmoplakin localization. Scale bars: 50 µm, enlargement 10 µm. Insulin had no effect on PKP3 or desmoplakin membrane association, whereas stimulation with EGF or complete medium improves PKP3 and desmoplakin recruitment to lateral membranes. The boxplots (right panels) depict the enrichment factor of PKP3 or desmoplakin at lateral contacts (n≥100). The Whiskers extend to the minimum and maximum values. Statistical significance was determined by one-way ANOVA with Tukey's multiple comparisons test.

Taken together, these data show that short EGF treatment for 15 min was sufficient to promote desmosome assembly by recruiting PKP3 to lateral membranes in murine keratinocytes as well as in A431 cells. However, additional signals are necessary for PKP3 sorting into tricellular contacts in murine keratinocytes.

4.1.3. The effect of EGF on early desmosomes depends on PKP3

Short EGF treatment resulted in lateral PKP3 accumulation, suggesting a role of PKP3 in desmosome assembly by recruiting other junctional proteins such as desmoplakin and PKP1 to lateral membranes. To test whether EGF-mediated desmosome assembly depended indeed on PKP3, desmosome formation in wild-type (WT) and PKP3-knockout (PKP3-KO) keratinocytes was compared. Ca^{2+} was added to induce desmosome formation and cells were either kept without growth factors or stimulated with insulin, EGF, or complete medium and processed for immunofluorescence (Figure 20A). In WT cells, lateral desmoplakin membrane association was significantly improved in the presence of EGF or complete medium, supporting the notion that EGF promotes early desmosome formation in WT keratinocytes. In contrast, desmoplakin accumulation at lateral contacts was not enhanced in PKP3-KO keratinocytes, neither in the presence nor in the absence of EGF or complete medium, indicating that the effect of EGF signaling in facilitating desmosome initiation depended on PKP3.

Collectively these results show that EGF-induced PKP3 phosphorylation improves its localization at lateral cell contacts as well as its role in desmosome assembly by recruiting desmoplakin to lateral membranes (Figure 20B).
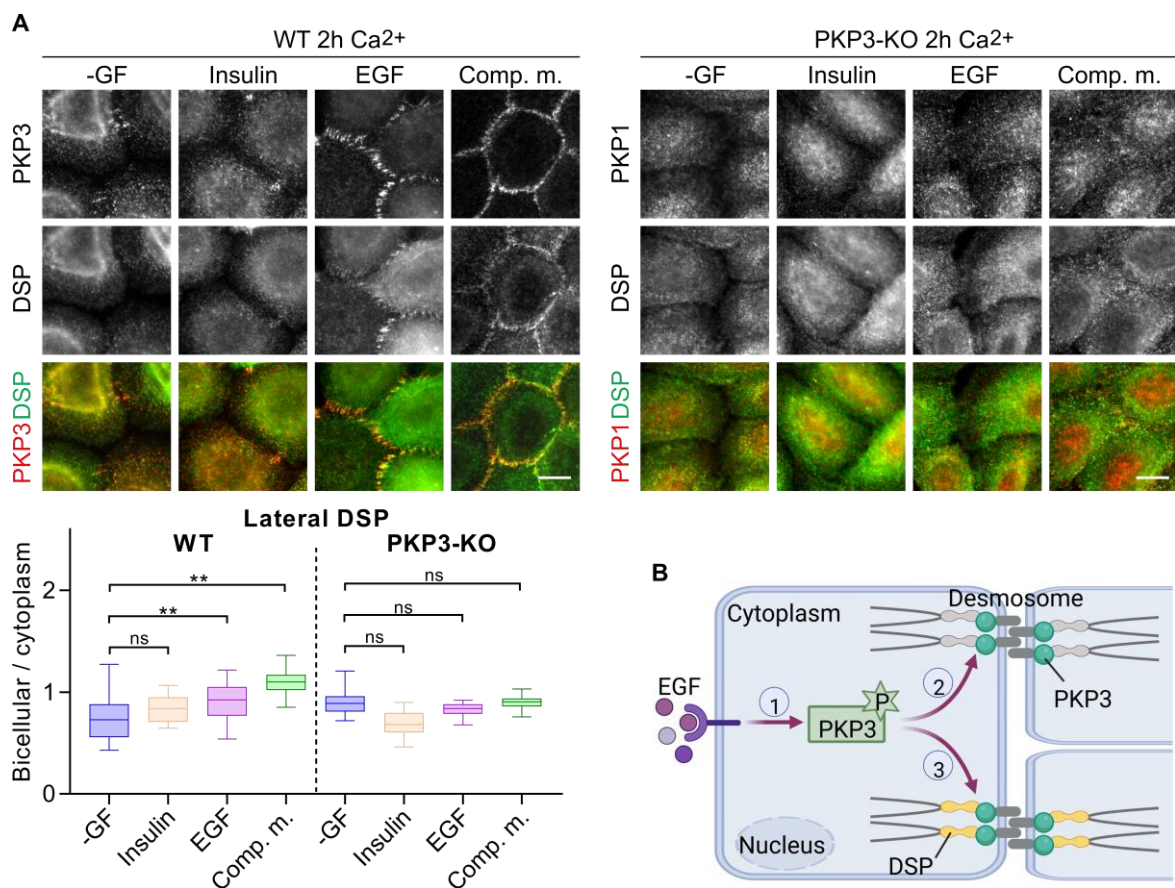
Figure 20 │ Early desmosome formation is mediated by EGF and depends on PKP3 in murine keratinocytes. (A) For analyzing PKP3's effect on EGF-mediated desmosome assembly, murine keratinocytes were grown in LCM for 24 h, maintained in serum-free LCM without any supplements for 5 h (without growth factors, -GF), and treated with Ca^{2+} in combination with growth factors (50 µg/ml insulin, 100 ng/ml EGF) or complete medium (HCM; comp. m.) for 2 h. Cells were fixed in methanol at -20°C and immunostained for PKP3 and desmoplakin (DSP) in WT cells or PKP1 and desmoplakin in PKP3-KO cells. Immunofluorescence images show PKP3, desmoplakin, and PKP1 localization in stimulated compared to non-stimulated cells. Scale bars: 10 µm. In WT cells, stimulation with EGF or complete medium for 2 h improves desmoplakin recruitment to lateral membranes. In PKP3-KO cells, lack of lateral desmoplakin membrane association after EGF stimulation or incubation with complete medium indicates a delayed cell contact formation. The boxplot (lower left panel) depicts the enrichment factor of desmoplakin at lateral contacts (n≥20) in WT and PKP3-KO cells. The Whiskers extend to the minimum and maximum values. Statistical significance was determined by one-way ANOVA with Tukey's multiple comparisons test. **(B)** Schematic of EGF-dependent PKP3 function based on the previous results (created with biorender.com). (1) EGF induces PKP3 phosphorylation, which affects its localization. (2) EGF improves lateral PKP3 membrane recruitment. (3) The effect of EGF on desmosome assembly depends on PKP3, which might recruits desmoplakin to lateral membranes.

4.1.4. RSKs mediate EGF-induced PKP3 phosphorylation

EGF activates the RAS/RAF/MAPK kinase cascade as well as PI3K/AKT mediated signaling. In order to identify the kinase(s) responsible for PKP3 phosphorylation, a series of inhibitors for kinases of both pathways was used. Therefore, serum-starved murine keratinocytes were treated with EGF in the absence or presence of Gefitinib (EGFR inhibitor), Rapamycin (mechanistic target of rapamycin (mTOR) inhibitor), PF-4708671 (S6K inhibitor), Osu03012 (3-phosphoionositide-dependent protein kinase 1 (PDK1)

inhibitor), U0126 (MEK inhibitor), FR180204 (ERK inhibitor), or LJH685 (RSK inhibitor). Pathway activation by EGF and impact of inhibitors were validated by probing cell lysates with phospho-specific antibodies as indicated (Figure 21A, 21B). PKP3 was immunoprecipitated and its phosphorylation determined using the RXXpS/pT motif antibody. PKP3 phosphorylation was increased in EGF stimulated cells, but was slightly reduced upon inhibition of EGFR, MEK, and ERK, as well as strongly impaired upon inhibition of RSK. In contrast, inhibition of mTOR, S6K, or PDK1 did not interfere with PKP3 phosphorylation. This confirms the importance of EGF signaling via the MEK/ERK/RSK axis and strongly suggests a role of RSKs in the regulation of PKP3.
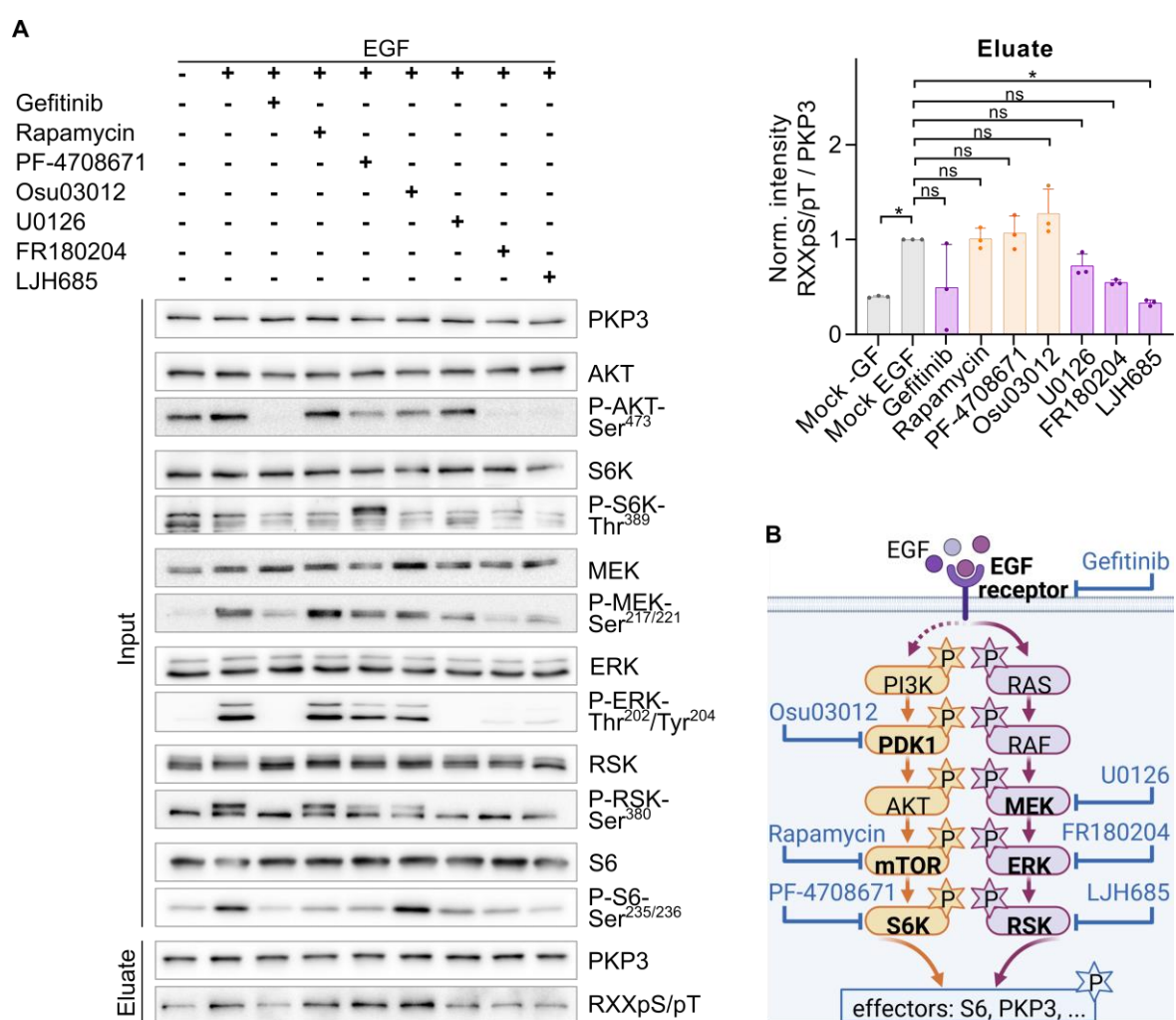
Figure 21 │ **PKP3 phosphorylation is mediated by the MEK-ERK-RSK axis. (A)** For analyzing the kinase(s) responsible for PKP3 phosphorylation, murine keratinocytes were grown in HCM for 24 h, maintained in serum-free HCM without any supplements for 5 h (without growth factors, -GF), incubated with the indicated inhibitors (EGFR, 10 µM Gefitinib; mTOR, 100 nM Rapamycin; S6K, 10 µM PF-4708671; PDK1, 10 µM Osu03012; MEK, 10 µM U0126; ERK, 25 µM FR180204; RSK, 50 µM LJH685) for 1 h, and treated with Ca^{2+} in combination with EGF (100 ng/ml) for 15 min. Impact of inhibitors was verified by western blotting with the indicated antibodies (input). Immunoprecipitated PKP3 (eluate) was probed for phosphorylation with an antibody that recognizes RXX-phospho-serine or phospho-threonine motif (RXXpS/pT). EGF-stimulated PKP3 phosphorylation at these AGC-kinase consensus sites (RXXS/T motif) was slightly reduced upon inhibition of EGFR, MEK, and ERK

and strongly impaired upon RSK inhibition. The bar plot (upper right panel) depicts the mean intensity ratios (+ s.d.; n=3) of RXXpS/pT versus PKP3 normalized to EGF stimulation without inhibitor (mock EGF). Orange colored bars indicate the PI3K/AKT signaling pathway, purple colored bars indicate the RAS/RAF/MAPK signaling pathway. Statistical significance was determined by one-way ANOVA with Tukey's multiple comparisons test. **(B)** Schematic of PI3K/AKT (orange colored) and RAS/RAF/MAPK (purple colored) signaling pathways with indicated inhibitors (created with biorender.com).

The RSK family of proteins consists of four isoforms: RSK1 (gene name *RPS6KA1*), RSK2 (*RPS6KA3*), RSK3 (*RPS6KA2*), and RSK4 (*RPS6KA6*). To identify the kinase(s) responsible for PKP3 phosphorylation in murine keratinocytes and A431 cells, the mRNA levels of all four RSKs were analyzed (Figure S2). RSK1 and RSK2 were highly expressed in both cell types, whereas RSK3 and RSK4 were rare or undetectable at the mRNA level. Thus, the focus was set on RSK1 and RSK2.

To distinguish between unique or overlapping roles of RSK1 and RSK2, knockdown studies in EGF stimulated murine keratinocytes were performed and the effects compared to LJH685 treatment (Figure 22A). Pathway activation by EGF was validated by probing cell lysates with phospho-specific antibodies as indicated. S6 phosphorylation was reduced after RSK1 or RSK2 knockdown and completely abolished upon RSK inhibition by LJH685. PKP3 was immunoprecipitated and its phosphorylation determined using the RXXpS/pT motif antibody. PKP3 phosphorylation was increased in EGF stimulated cells, but was decreased in RSK1-depleted cells as well as upon RSK inhibition by LJH685 treatment. In contrast, RSK2 depletion did not affect PKP3 phosphorylation. Therefore, RSK1 appears to be the predominant kinase responsible for PKP3 phosphorylation at RXXpS/pT motif. However, due to the incomplete depletion of RSK2, RSK2 cannot yet be completely ruled out and in the following experiments RSK1 as well as RSK2 were analyzed.

For further validation of an association between PKP3 and RSK1 or RSK2, BiFC analysis were performed (Figure 22B). Murine keratinocytes were co-transfected with FLAG-Venus1 tagged PKP3 and HA-Venus2 tagged RSK1/RSK2. Association of PKP3 with RSK brought the fragments of the fluorescent protein Venus within close proximity, allowing the Venus protein to fold in its native three-dimensional conformation and emit a fluorescent signal. This experiment confirmed a strong association of PKP3 with RSK1 at cell borders and in the cytoplasm. In contrast, the BiFC signal for PKP3 and RSK2 was low.

Collectively these results show that EGF-induced PKP3 phosphorylation was mediated by the MEK/ERK/RSK signaling axis. The downstream effectors RSKs appear to regulate PKP3 via the association of RSK1 with PKP3 at the cell membrane and in the cytoplasm (Figure 22C). In the following chapter, the role of RSKs in modulating PKP3 localization and cellular adhesion will be analyzed.
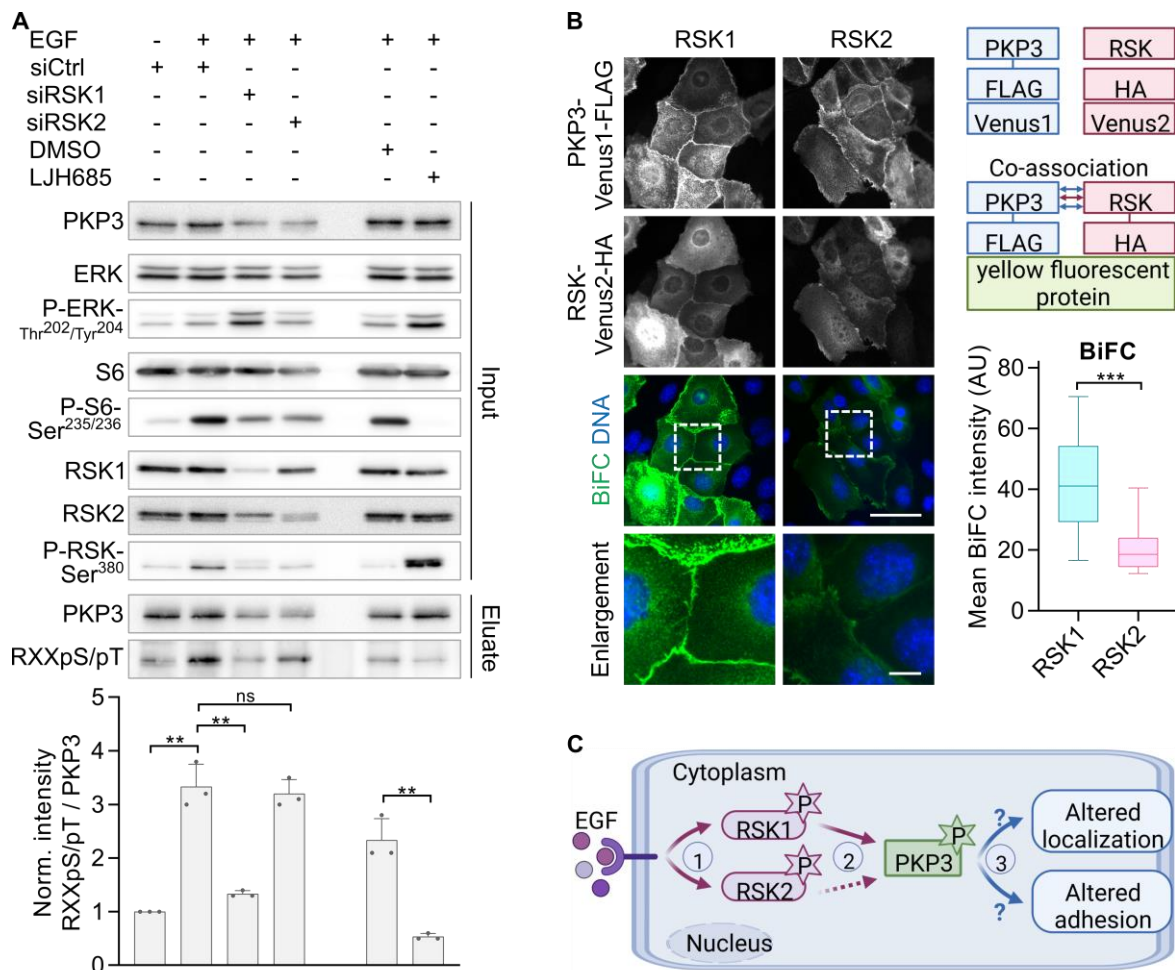
Figure 22 │ RSKs mediate PKP3 phosphorylation at RXXS/T motif. (A) For analyzing RSK isoform specific effects on PKP3 phosphorylation, murine keratinocytes transfected with non-targeting (siCtrl), RSK1, or RSK2 (siRSK1, siRSK2, respectively) directed siRNAs were grown in HCM for 24 h, maintained in serum-free HCM without any supplements for 5 h, and treated with Ca^{2+} in combination with EGF (100 ng/ml) for 15 min. Furthermore, murine keratinocytes were grown in HCM for 24 h, maintained in serum-free HCM without any supplements for 5 h, incubated with the RSK inhibitor LJH685 (50 μM) for 1 h, and treated with Ca^{2+} in combination with EGF (100 ng/ml) for 15 min. Knockdown effciency, kinase activation, and impact of inhibitor were verified by western blotting with the indicated antibodies (input). Immunoprecipitated PKP3 (eluate) was probed for phosphorylation with an antibody that recognizes RXX-phospho-serine or phospho-threonine motif (RXXpS/pT). EGF-stimulated PKP3 phosphorylation at these AGC-kinase consensus sites (RXXS/T motif) was strongly increased, whereas RSK1 depletion and RSK inhibtion led to impaired PKP3 phosphorylation. In contrast, RSK2 depletion did not prevent PKP3 phosphorylation. The bar plot (lower panel) depicts the mean intensity ratios (+ s.d.; n=3) of RXXpS/pT versus PKP3 normalized to non-stimulated cells. Statistical significance was determined by one-way ANOVA with Tukey's multiple comparisons test. **(B)** For BiFC analysis, murine keratinocytes were co-transfected with the indicated pVenus1 and pVenus2 constructs, LCM was switched to HCM, and cells were maintained in HCM for 24 h before fixation in formaldehyde on ice and immunostaining with FLAG- and HA-directed antibodies. Images of cells expressing both FLAG- and HA-tagged fusion proteins were taken with identical exposure times (2 s) to enable a comparison of BiFC efficiencies. Scale bars: 50 μm, enlargement 10 μm. BiFC shows an association of PKP3 with RSK1 at cell borders as well as in the cytoplasm. In contrast, the association of PKP3 with RSK2 was low. The boxplot (right panel) depicts the mean fluorescence intensity (in area units, AU) of BiFC signals of ~ 70 individual transfected cells. The Whiskers extend to the minimum and maximum values. Statistical significance was determined by a student's unpaired two tailed *t*-test. **(C)** Schematic of EGF-dependent PKP3 function based on the previous results (created with biorender.com). (1) EGF induces RSK phosphorylation by activation of the RAS/RAF/MAPK signaling pathway. (2) RSK1 and to a lesser extent RSK2, mediate PKP3 phosphorylation via association. (3) RSK-dependent modulation of PKP3 might affect its localization resulting in altered cellular adhesion.

4.1.5. RSKs modulate PKP3 localization and intercellular adhesion

Based on the observation that PKP3 and RSK1 associate and depletion of RSK1 resulted in decreased PKP3 phosphorylation, I asked if this is reflected by changes in PKP3 localization and desmosome structure. To analyze the effect of RSK1 and RSK2 on PKP3 localization, plasmids encoding human RSK1 or RSK2 cDNA were transiently transfected into murine keratinocytes, resulting in RSK1 or RSK2 overexpression in these cells (Figure 23). Lateral desmosomes appeared as straight lines as observed after desmosome maturation in both RSK1 and RSK2 overexpressing cells. Despite the different appearance, the amount of lateral PKP3 was not considerably affected. In contrast, overexpression of RSK1 was compatible with strong PKP3 tricellular accumulation, whereas overexpression of RSK2 did not promote its tricellular localization.
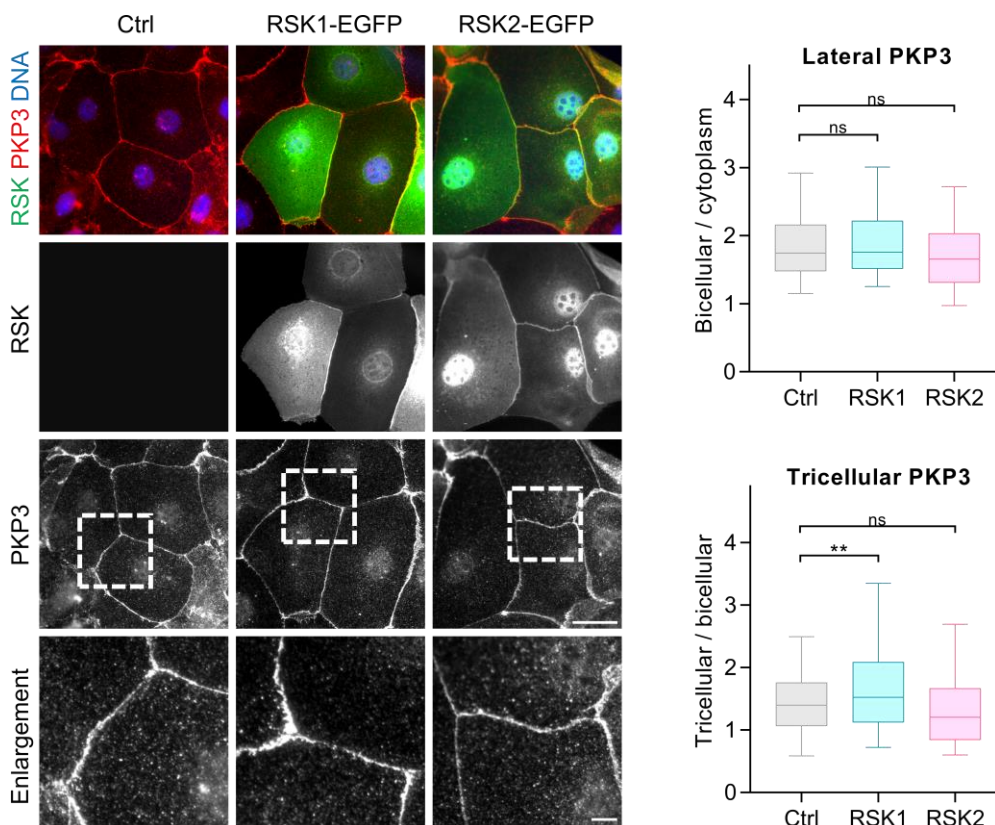
Figure 23 │ RSK1 overexpression improves tricellular PKP3 localization. For analyzing the effect of RSK1/2 overexpression on PKP3 localization, murine keratinocytes were transfected with the indicated GFP-RSK constructs or a plasmid without insert (Ctrl) and grown in HCM for 24 h. Cells were fixed in methanol at -20°C and immunostained for PKP3. Immunofluorescence images show RSK1/2 and PKP3 localization in control and in RSK1- or RSK2-overexpressing cells. The enlargements highlight the effects of the respective treatments on PKP3 localization. Scale bars: 50 μm, enlargement 10 μm. Lateral localization of PKP3 was not affected by RSK1 or RSK2 overexpression, whereas RSK1 overexpression led to increased tricellular PKP3 localization. The boxplots (right panels) depict the enrichment factor of PKP3 at lateral contacts (n≥100) or at tricellular versus bicellular contacts (n≥100). The Whiskers extend to the minimum and maximum values. Statistical significance was determined by one-way ANOVA with Tukey's multiple comparisons test.

Given that overexpression of RSK1 promoted tricellular PKP3 localization, I investigated the effect of RSK1 or RSK2 depletion on PKP3 localization in murine keratinocytes (Figure 24A). Knockdown of RSK1 and RSK2 was validated by western blotting (Figure S3A). Lateral PKP3 and desmoplakin appeared in a punctate pattern in RSK1- or RSK2-depleted cells, which is a characteristic of native immature desmosomes. Furthermore, the knockdown of either RSK1 or RSK2 resulted in decreased tricellular PKP3 localization. To further validate these results, RSK activity was inhibited by LJH685 treatment (Figure 24B, for validation of inhibitor impact see Figure S3B). Inhibition of RSKs strongly prevented the tricellular localization of PKP3.
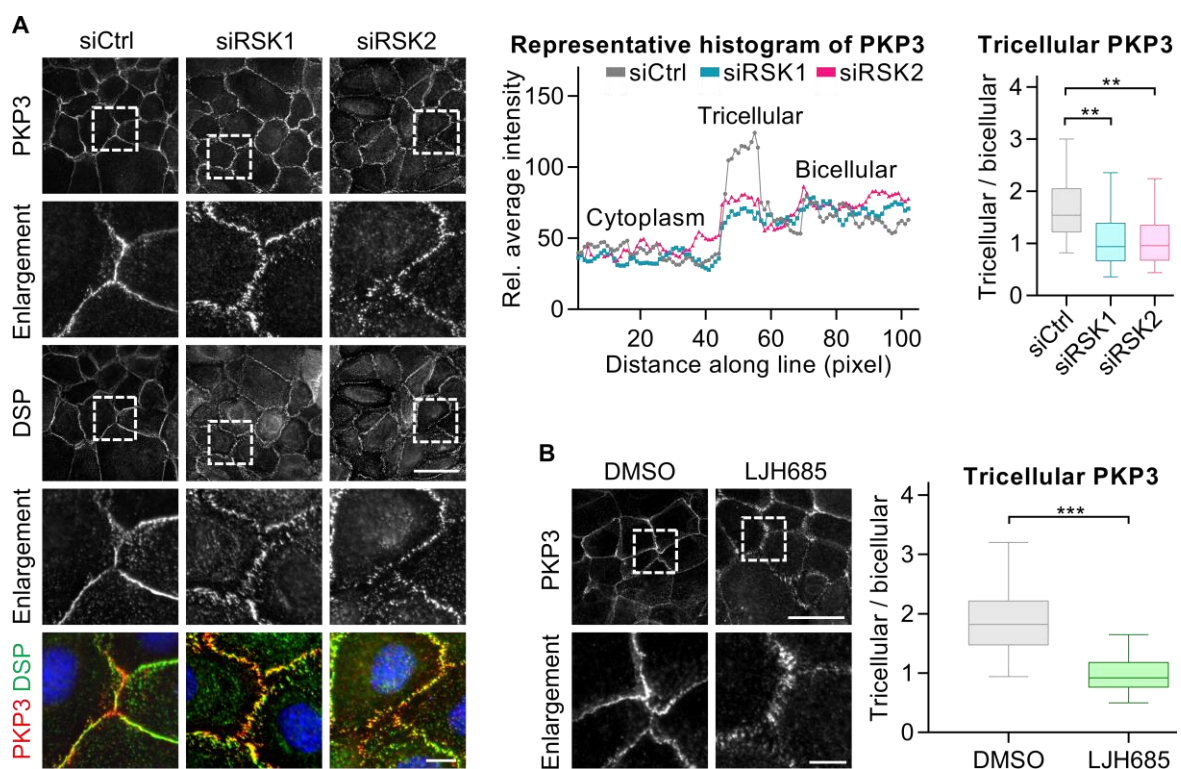
Figure 24 | RSK knockdown and inhibition interfere with PKP3 localization at tricellular contacts. (A) For analyzing the effect of RSK1/2 depletion on PKP3 localization, murine keratinocytes transfected with non-targeting (siCtrl), RSK1, or RSK2 (siRSK1, siRSK2, respectively) directed siRNAs were switched to HCM at 48 h after transfection and kept in HCM for another 24 h. Cell were fixed in methanol at -20°C and immunostained for PKP3 and desmoplakin (DSP). Immunofluorescence images show PKP3 and desmoplakin localization in control and in RSK1- or RSK2-depleted cells. The enlargements highlight the effects of the respective siRNAs on PKP3 and desmoplakin localization. Scale bars: 50 μm, enlargement 10 μm. Knockdown of RSK1 or RSK2 led to punctate desmosomes at lateral membrane and decreased tricellular PKP3 localization. Representative line scans of PKP3 fluorescence intensities across tricellular contact regions (upper mid panel) illustrate the different distribution of PKP3 in control and RSK1- or RSK2-depleted cells. The boxplot (upper right panel) depicts the enrichment factor of PKP3 at tricellular versus bicellular contacts (n≥300). The Whiskers extend to the minimum and maximum values. Statistical significance was determined by one-way ANOVA with Tukey's multiple comparisons test. **(B)** For analyzing the effect of RSK inhibition on PKP3 localization, murine keratinocytes were grown in HCM for 24 h before control treatment with DMSO or treatment with the RSK inhibitor LJH685 (50 μM) for 1 h. Cells were fixed in methanol at -20°C and immunostained for PKP3. Immunofluorescence images show PKP3 localization in control and in LJH685 treated cell. The enlargements highlight the effects of the respective treatments on PKP3. Scale bars: 50 μm, enlargement 10 μm. RSK inhibition resulted in a punctate pattern of lateral PKP3 and a strongly reduced tricellular PKP3 localization. The boxplot (right panel) depicts the enrichment factor of PKP3 at tricellular versus bicellular contacts (n≥100). The

Whiskers extend to the minimum and maximum values. Statistical significance was determined by a student's unpaired two tailed *t*-test.

These experiments confirmed a specific role of RSKs in regulating PKP3 localization. RSK depletion or inhibition led to a switch of PKP3 localization from tricellular contacts to a more diffuse lateral membrane association (Figure 24), whereas overexpression of RSK1 but not RSK2 promote tricellular PKP3 localization (Figure 23). Due to the stronger effect of RSK1 overexpression on PKP3 localization, RSK1 and not RSK2 seems to be the key driver (Figure 25A).

As strong localization of PKP1 at lateral cell borders and PKP3 accumulation at tricellular contacts was described to correlate with increased intercellular adhesion (Keil *et al.*, 2016), I asked whether RSK-dependent regulation of PKP3 localization affects the intercellular adhesion. An epithelial sheet assay (also known as dispase assay) was performed to measure the strength of intercellular adhesion (Figure 25B). Cell monolayers released by dispase were subjected to mechanical stress and the number of cell fragments were counted. In murine WT keratinocytes, RSK1/2 depletion as well as RSK inhibition resulted in an increased number of fragments, suggesting reduced intercellular adhesion (Figure 25C). This was in line with the altered lateral and tricellular localization of PKP3. In contrast, PKP3-KO cells showed an unaltered number of fragments after RSK1/2 depletion or RSK inhibition compared to control treated cells (Figure 25D). These results confirm that the effect of RSKs on desmosomes depend on PKP3.
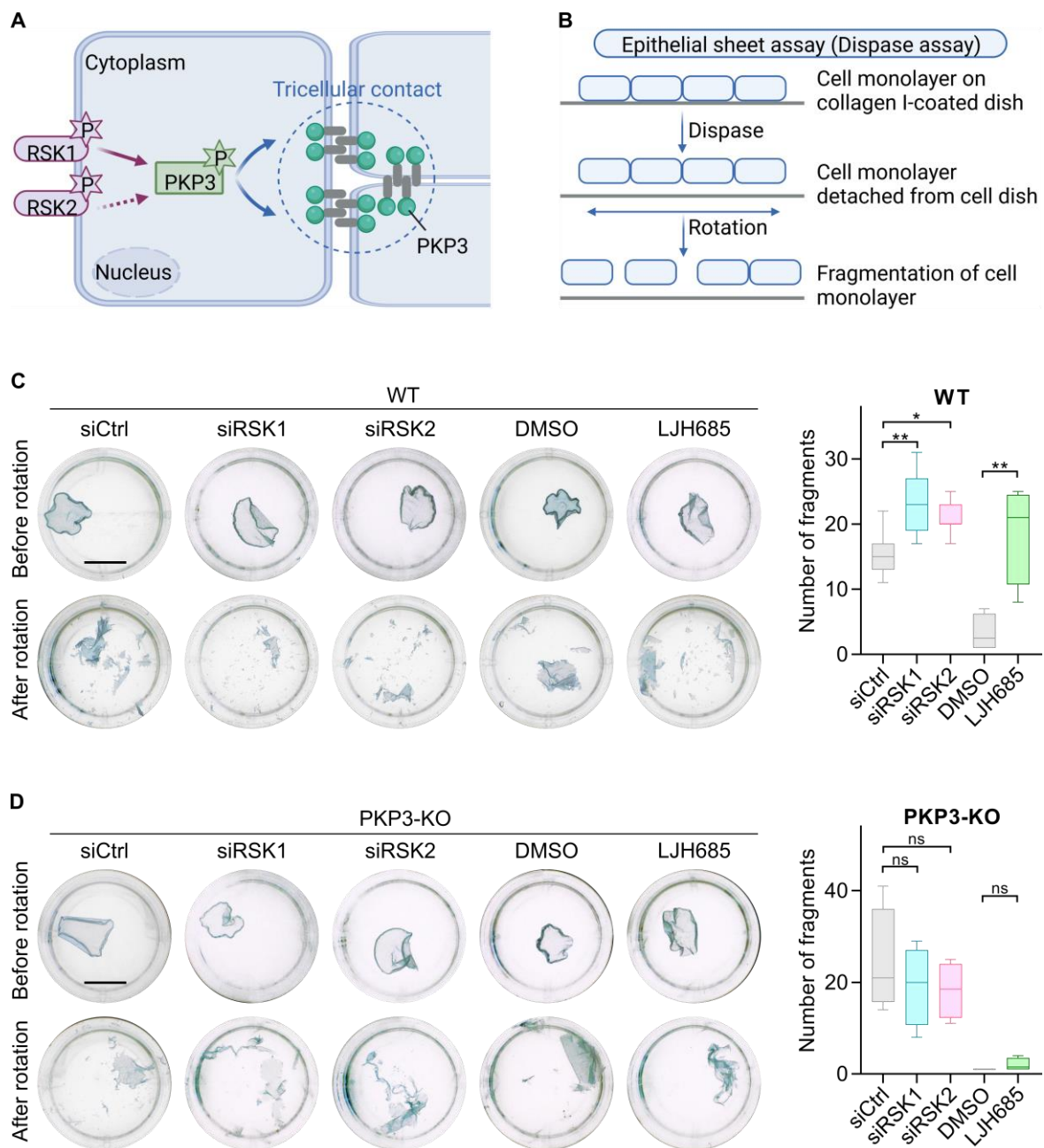
Figure 25 │ **Impaired tricellular PKP3 localization by RSK knockdown and inhibition correlate with reduced intercellular adhesion. (A)** Schematic of RSK-dependent PKP3 function based on the previous results (created with biorender.com). RSK1 and to a lesser extent RSK2, phosphorylate PKP3 to promote tricellular localization. **(B)** Schematic of the epithelial sheet assay (also known as dispase assay, created with biorender.com). Cells were grown to confluence on collagen-I coated cell culture dishes. After detaching of monolayers by dispase, the monolayers were subjected to mechanical stress on a digital shaker. Cell plates were documented and fragments were counted. **(C, D)** Epithelial sheet assay performed in (C) WT cells and (D) PKP3-KO cells. Murine keratinocytes transfected with non-targeting (siCtrl), RSK1, or RSK2 (siRSK1, siRSK2, respectively) directed siRNAs were switched to HCM at 24 h after transfection. Alternatively, RSK inhibitor LJH685 (50 µM) was applied for 1 h to keratinocytes kept in HCM for 24 h before performing epithelial sheet assay. Cells were detached using dispase solution (serum-free medium supplemented with dispase, HEPES, and Ca^{2+}) and treated with EGTA (3.3 mM) for 30 min to facilitate disruption of Ca^{2+}-sensitive cell contacts. Monolayers were documented using a digital camera and subjected to mechanical stress for a maximum of 20 min on a digital shaker at 750 *rpm*. Fragments were documented and counted. Representative images before rotation (upper panels) and after rotation (lower panels) are shown. Scale bars: 0.7 cm. Knockdown of RSK1/2 (n=7) or RSK inhibition (n=4) led to increased number of fragments in WT cells. This effect was completely lost in PKP3-KO cells (n=4). The boxplots (right panels) depict the number of fragments.

The Whiskers extend to the minimum and maximum values. Statistical significance was determined by one-way ANOVA with Tukey's multiple comparisons test.

To further validate the stability of adhesion, cells were treated with the chelator EGTA. As tricellular regions are more dynamic than lateral contacts, EGTA treatment induces small gaps at tricellular regions as described previously (Takasawa *et al.*, 2013; Keil *et al.*, 2016). Murine keratinocytes were treated with EGTA and immunostained for desmoplakin in both WT and PKP3-KO cells (Figure 26). In WT cells transfected with non-targeting siRNA (siCtrl), EGTA induced the dissociation of tricellular contacts but lateral contacts remained intact. In RSK1-depleted WT cells, the area of gaps between adjacent cells was significantly larger compared to control treated WT cells resulting in the extensive separation of neighboring cells after 3 h of EGTA treatment. In agreement with the loss of contact, RSK1 depletion resulted in the extensive loss of desmoplakin from lateral membranes. This indicates that RSK1 promotes cellular adhesion by stabilizing lateral contacts. In order to analyze if this phenomenon was PKP3-dependent, the experiment was performed in PKP3-KO cells. In the absence of PKP3, tricellular gaps remained small even after prolonged EGTA treatment in RSK1 depleted cells. This suggests a PKP3-dependent stabilization of cell adhesion by RSK1.
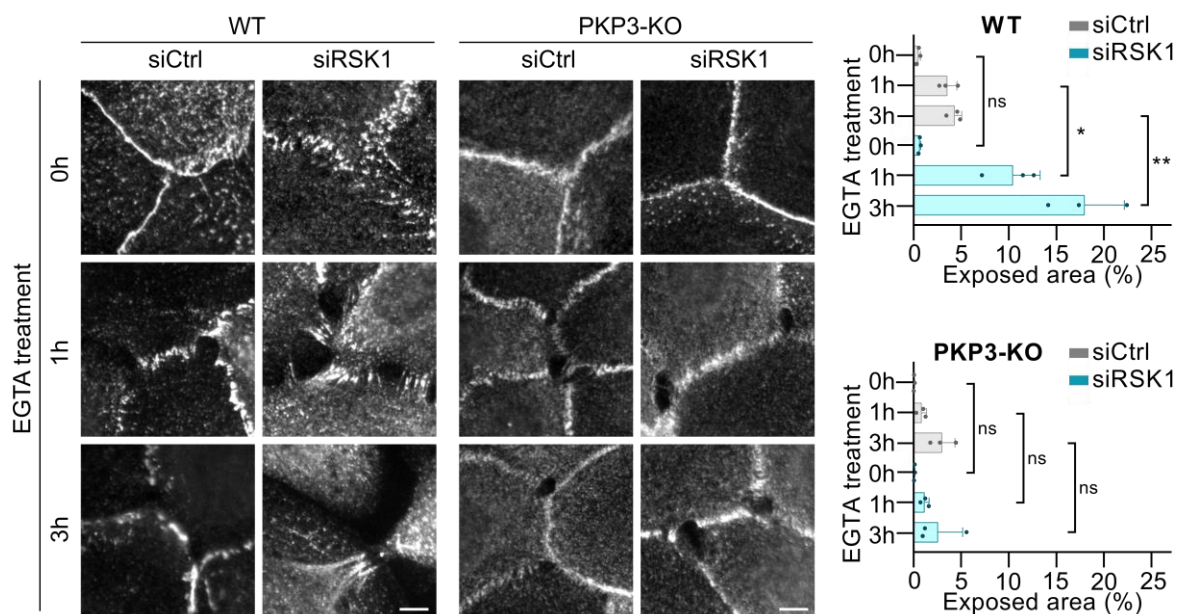
Figure 26 │ **PKP3 promotes stabilization of cellular adhesion by RSK1.** Murine WT and PKP3-KO keratinocytes transfected with non-targeting (siCtrl) or RSK1 (siRSK1) directed siRNAs were switched to HCM at 48 h after transfection and kept in HCM for another 24 h. Cell were treated with EGTA (3.3 mM) for 1 h or 3 h, fixed in methanol at -20°C, and immunostained for desmoplakin. Immunofluorescence images show desmoplakin localization in control and in RSK1-depleted cells. Scale bars: 10 µm. In WT cells, EGTA treatment resulted in small gaps between adjacent cells that expanded after RSK1 depletion. The loss of PKP3 (PKP3-KO cells) led to small gaps even after prolonged EGTA treatment. RSK1 knockdown did not affect gap size of neighboring PKP3-KO cells. The bar plots (right panels) depict the exposed area in percent per image (+ s.d.; n=3; 30 images each). Statistical significance was determined by one-way ANOVA with Tukey's multiple comparisons test.

4.1.6. Summary

In this chapter, murine keratinocytes and human A431 cells were used to analyze the desmosomal role of PKP3 as a scaffold for adhesion. Whereas PKP1 desmosome association is negatively regulated by IGF-1/insulin, this signaling pathway did not affect PKP3 phosphorylation or localization. In contrast, EGF signaling supported desmosome formation via PKP3, which was identified as a direct target of RSKs downstream of the EGFR. This effect of EGF on desmosomes was completely lost in PKP3-KO keratinocytes indicative of the essential role of PKP3 in mediating desmosome assembly in response to EGFR activation. PKP3 associated with RSKs with a preference for the RSK1 isoform resulting in altered PKP3 localization and function. Overexpression of RSK1 or RSK2 supported desmosome formation and maturation with the accumulation of PKP3 at tricellular contacts. In contrast, depletion of RSKs by siRNAs or their inhibition interfered with normal desmosome maturation. In RSK-depleted or inhibited cells, PKP3 displayed a punctate or frayed appearance along lateral membranes whereas tricellular regions not only lacked PKP3 but in addition did not become sealed. This correlated with the destabilization of intercellular cohesion. Taken together, this chapter focused on the regulation of PKP3 in terms of adhesion and reports several novel findings that considerably improve the understanding of desmosomal regulation. The next chapter addresses the extra-desmosomal role of PKP3 as a scaffold for signaling.

4.2. The extra-desmosomal role of PKP3 as a scaffold for signaling

The second part of the results chapter deals with the extra-desmosomal role of PKP3 as a scaffold for signaling. The occurrence of PKP3 in different and distant locations suggests that PKP3 plays roles in cytoplasmic and nuclear processes in addition to its involvement in cell-cell adhesive interactions. These additional functions in the cytoplasm and the nucleus are less well characterized. As nuclear and cytoplasmic proteins can induce signaling pathways to regulate cell growth and differentiation, I started to elucidate how PKP3 contributes to the control of proliferation.

Since proliferation is upregulated in cancer cells which correlates with disturbed cell cycle progression due to mutations for example in the tumor suppressor genes *RB* and/or *p53* (Engeland, 2022), I performed all the following experiments in non-transformed murine keratinocytes to focus on the mechanistic basis of PKP3's role in proliferation. As a model system, I used established WT keratinocytes (Sklyarova *et al.*, 2008; Keil *et al.*, 2016) and PKP3-KO keratinocytes, which do not express PKP3 protein (Sklyarova *et al.*, 2008; Keil *et al.*, 2016), as well as PKP3-GFP overexpressing WT cells (WT+PKP3, (Keil *et al.*,

2016)). Unless otherwise stated, all experiments were performed in LCM to keep PKP3 in a soluble, cytoplasmic pool in order to analyze its extra-desmosomal function.

4.2.1. PKP3 affects proliferation and cell cycle progression

To explore putative extra-desmosomal functions of PKP3, I analyzed PKP3-dependent protein coding gene expression patterns using various bioinformatic tools and databases. RNA sequencing of WT, PKP3-KO, and WT+PKP3 cells grown for 24 h in LCM was performed followed by assessment of a GSEA of all expressed protein coding genes to identify differentially regulated biological processes and molecular functions. Signaling pathways associated with PKP3 were identified using the REACTOME and KEGG databases, which are collections of various protein interaction networks such as pathways and complexes (Kanehisa *et al.*, 2004; Yu *et al.*, 2015). To further analyze the role of PKP3, the HALLMARK database was mapped, which represents biological states or processes (Liberzon *et al.*, 2015). GSEA-based REACTOME (Figure 27), KEGG (Figure S4), and HALLMARK analyses (Figure S5) highlight the top ten downregulated gene sets in PKP3-KO versus WT cells as well as the top ten upregulated gene sets in WT+PKP3 versus WT cells. The downregulated genes in PKP3-KO cells and the upregulated genes in WT+PKP3 cells were mainly associated with cell cycle regulation and related pathways. This suggests that PKP3 positively correlates with cell cycle progression.
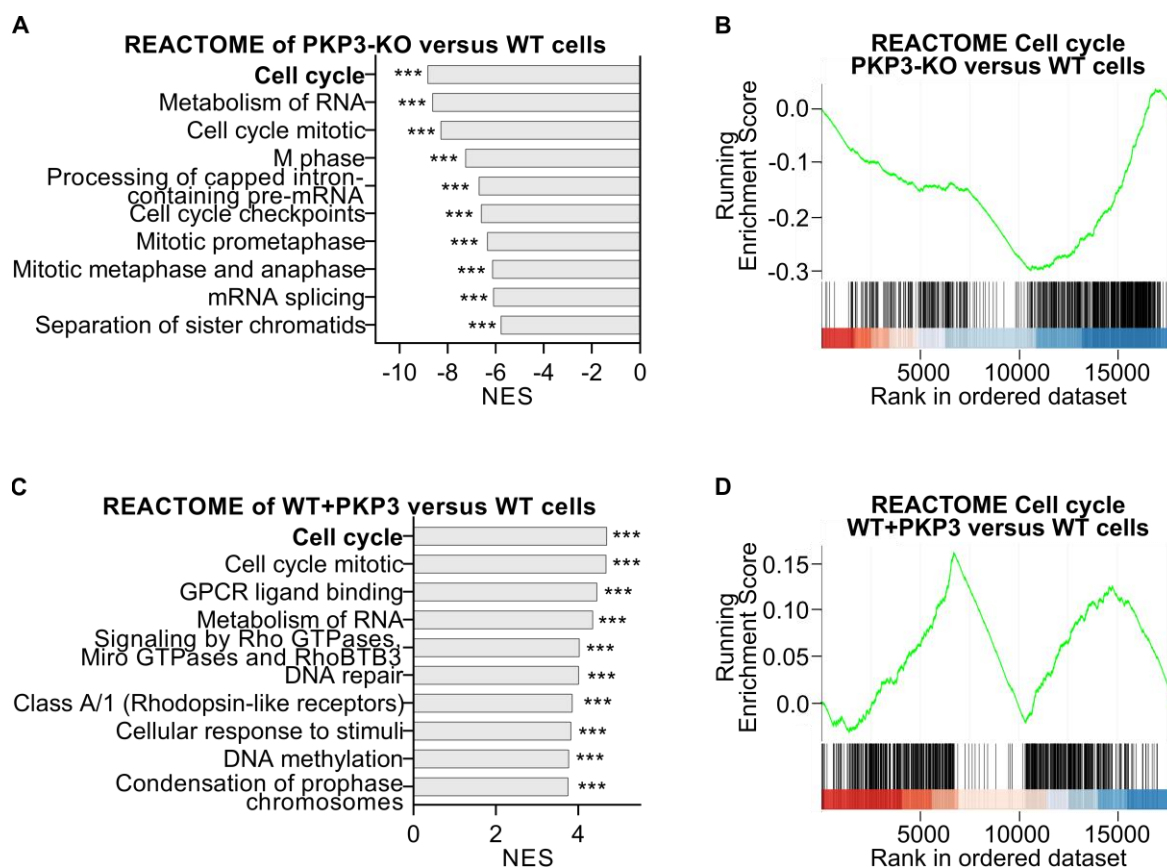
Figure 27 │ Gene set enrichment analysis links PKP3 to cell cycle regulation. For analyzing PKP3-dependent protein coding gene expression patterns, WT, PKP3-KO, and WT+PKP3 cells were grown for 24 h in LCM and prepared for RNA sequencing. Based on a list of all protein coding genes ranked according to $\log_2$ fold changes, a GSEA was performed mapping the REACTOME database. The GSEA-based REACTOME shows that downregulated protein coding genes in PKP3-KO cells and upregulated protein coding genes in WT+PKP3 cells were mainly involved in cell cycle regulation. Calculation of $\log_2$ fold changes and GSEA were kindly performed by Dr. Markus Glaß (Core Facility Imaging of the Medical Faculty, Martin Luther University). **(A, C)** The bar plots depict the normalized enriched scores (NES) of (A) the top ten most negatively enriched gene sets among protein coding genes in PKP3-KO versus WT cells or (C) the top ten most positively enriched gene sets among protein coding genes in WT+PKP3 versus WT cells. A positive NES reflects enrichment of the gene set at the top of the ranked list, i.e. gene sets overrepresented among induced genes. A negative NES indicates enrichment of the gene set at the bottom of the ranked list, i.e. gene sets overrepresented among repressed genes. The adjusted p-value estimates the statistical significance of the NES for a single gene set. The representative gene set which is further analyzed in (B) and (D) is marked in bold. **(B, D)** The GSEA enrichment plots for "REACTOME Cell cycle" for (B) PKP3-KO versus WT cells and (D) WT+PKP3 versus WT cells shows the running enrichment score (green curve), which increases as a gene within the set is present while the GSEA walks down the rank ordered list of $\log_2$ fold changes of protein coding genes. Vertical black lines indicate the positions of genes in the ranked dataset. Genes on the far left (red) correlates with the most upregulated cell cycle-associated genes, whereas genes on the far right (blue) correlates with the most downregulated cell cycle-associated genes.

To further analyze the role of PKP3 in cell cycle regulation, cell proliferation of the adherent growing murine keratinocytes was tracked by live cell images automatically taken by an IncuCyte S3 system (Figure 28). Relative confluence was monitored for 4 days. In supporting of the GSEA data, growth behavior differed between WT, PKP3-KO, and WT+PKP3 cells. WT and WT+PKP3 cells revealed a similar growth pattern with continuous proliferation, as indicated by a steep ascent of the relative confluence over time. Up to

day 3, their proliferation appeared indistinguishable. After 3 days, however, a flattening of the curve revealed a tendency of WT cells to become non-proliferative at high cell density, whereas WT+PKP3 cells continued to proliferate, suggesting that these cells might be able to overcome contact inhibition. Loss of PKP3 (PKP3-KO cells) resulted in a flat curve with reduced relative confluence even after 96 h. These data further suggest that PKP3 promotes proliferation in non-transformed keratinocytes.
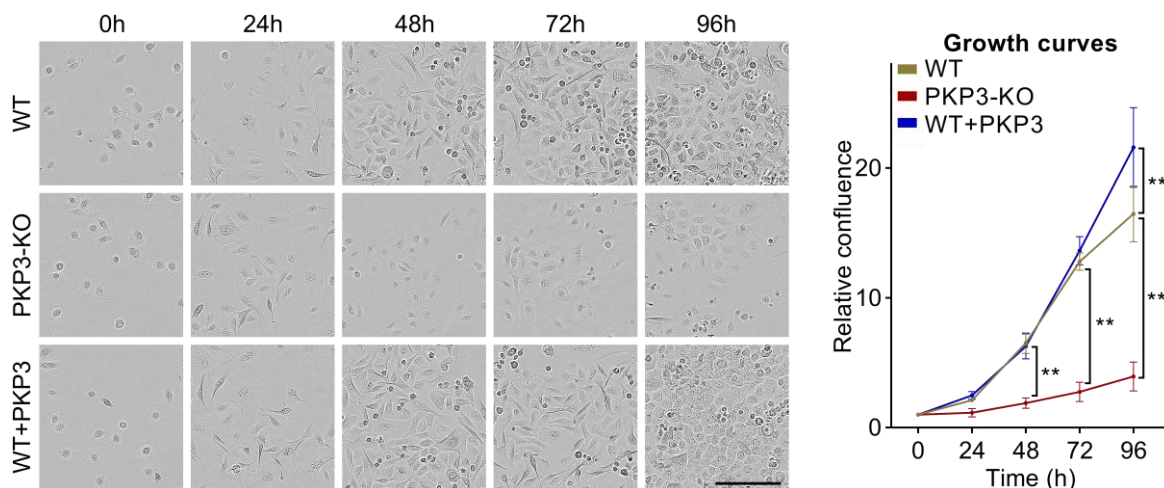
Figure 28 │ **PKP3 promotes proliferation in non-transformed murine keratinocytes.** For analyzing cell proliferation rates, murine WT, PKP3-KO, and WT+PKP3 keratinocytes were grown for up to 96 h in LCM. Live cell images were automatically taken from day 0 on every day by using an IncuCyte S3 System. Representative images (left panels) showing the confluence of WT, PKP3-KO, and WT+PKP3 cells at the indicated time points. Scale bar: 200 µm. WT and WT+PKP3 cells revealed a similar growth pattern with continuous proliferation, but WT+PKP3 cells continued to proliferate at high cell density. In contrast, PKP3-KO cells showed delayed confluence even after 96 h. The graph (right panel) depicts the averages of relative confluence, which was determined by analyzing the occupied area of individual nuclei over time (± s.d.; n=5; 12 images each). Statistical significance was determined by one-way ANOVA with Tukey's multiple comparisons test.

Cell proliferation involves cell growth and cell division, and is tightly organized by cell cycle phases (Schafer, 1998). During G0 phase, cells exist in a quiescent state. Proliferation begins with the first period of growth (G1 phase) during which DNA synthesis is prepared. In this phase, the cells grow in size and synthesize mRNA and proteins required for DNA synthesis. In the synthesis phase (S phase), the cells replicate their DNA. Once the cells have duplicated their chromosomes, they enter a second period of growth (G2 phase) during which the division into two daughter cells is prepared. Finally, the cell partitions its replicated DNA into two daughter cells in mitosis (M phase). After completing the cell cycle, the cell either starts the process again starting from G1 phase or it exits from the cell cycle through G0 phase. To determine more directly which phase of the cell cycle was primarily affected by PKP3, flow cytometry using propidium iodide to label DNA was performed (Figure 29). This allows measurement of cellular DNA content and reveals the distribution of cells in the cell cycle phases G0/G1 versus S versus G2/M. However, G0 and G1 as well

as G2 and M phase cannot be discriminated due their identical DNA content. Nonetheless, this analysis showed an enrichment of PKP3-KO cells in G0/G1 phase and a reduction of WT+PKP3 cells in this phase.
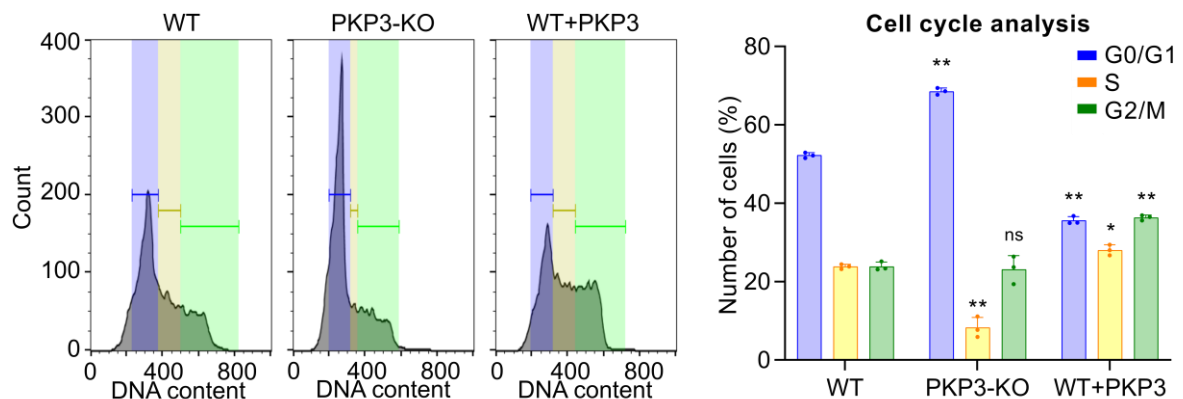
Figure 29 │ Loss of PKP3 increases the number of cells in G0/G1 phase. For analyzing the PKP3-affected cell cycle phase, WT, PKP3-KO, and WT+PKP3 cells were grown for 24 h in LCM. Cells were fixed overnight in 70% ethanol, pelleted by centrifugation, and labelled with propidium iodide at 37°C for 10 min. The DNA content of about 10,000 cells per sample was measured by flow cytometry to analyze cell cycle. Flow cytometry was kindly performed by Dr. Nadine Bley (Core Facility Imaging of the Medical Faculty, Martin Luther University). Representative population histograms (left panels) showing the cell cycle distribution of WT, PKP3-KO, and WT+PKP3 cells. Blue, G0/G1 phase; yellow, S phase; green, G2/M phase. Whereas PKP3-KO cells were enriched in G0/G1 phase, WT+PKP3 cells revealed a reduction in this phase. The bar plot (right panel) depicts the number of cells in cell cycle phases (+ s.d.; n=3). Statistical significance was determined by one-way ANOVA with Tukey's multiple comparisons test.

Analysis of cell cycle specific events in murine keratinocytes is challenging because cell cycle synchronization using chemicals does not induce a synchronized division pattern (data not shown, experiment performed by Dr. René Keil and Gunther Kahl, Hatzfeld lab). To overcome this limitation, the FUCCI system was used. The FUCCI technology is based on the expression of two proteins, which show cell cycle regulated oscillations (Figure 30). Chromatin licensing and DNA replication factor 1 (CDT1) tagged with red fluorescent protein is present in G1 phase, whereas GFP tagged geminin accumulates in G2 and M phase. During S phase, both proteins are highly expressed resulting in a yellow fluorescence signal. Thus, changes in fluorescence allow to determine the duration of G1 and G2 phases. WT and PKP-3KO cells were stably transfected with FUCCI probes and fluorescence was visualized by live cell images automatically taken by an IncuCyte S3 system (Figure 30). This allowed monitoring of cell cycle progression at the single cell level. The loss of PKP3 (PKP3-KO FUCCI cells) prolonged G1 phase approximately twofold compared to WT FUCCI cells whereas other phases of the cell cycle were unaffected. This considerable enrichment of PKP3-KO FUCCI cells in G0/G1 phases suggested a delay in S phase entry.
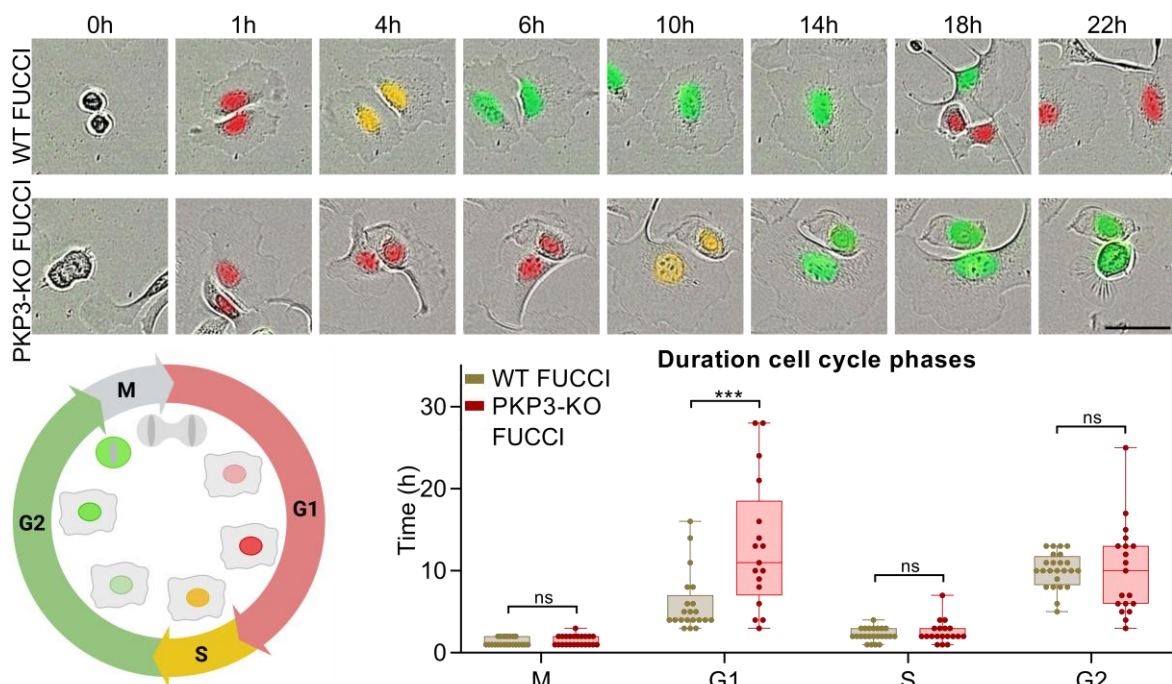
Figure 30 │ Loss of PKP3 increases the duration in G1 phase. To determine the duration in cell cycle phases, WT and PKP3-KO cells were stable transfected with FUCCI probes. Cell cycle phases of WT FUCCI and PKP3-KO FUCCI cells were monitored based on their fluorescence using an IncuCyte S3 system starting 4 h after seeding. Live cell images were automatically taken every hour. The FUCCI system (lower left panel, schematic created with biorender.com) consists of two fluorescent polypeptides that are degraded in a cell cycle dependent manner. In G1 phase, only CDT1 tagged with red fluorescent protein is present, whereas in G2 and early M phase, only geminin tagged with green fluorescent protein remains. As cells progress into S phase, both proteins are present in the nuclei as indicated by yellow fluorescence. Representative images of WT FUCCI and PKP3-KO FUCCI cells with segmentation mask overlays (upper panels) showing the fluorescence at the indicated time points. Red, G1 phase; yellow, S phase; green, G2 phase. Scale bar: 50 µm. In PKP3-FUCCI cells, G1 phase was prolonged approximately twofold compared to WT FUCCI cells. Other phases of the cell cycle were unaffected. The boxplot (lower right panel) depicts the duration of the cell cycle phases in WT FUCCI compared to PKP3-KO FUCCI cells (n=2; 17 cells per condition). The Whiskers extend to the minimum and maximum values. Statistical significance was determined by a student's unpaired two tailed *t*-test.

To compare the amount of cells in S phase, the incorporation of BrdU into newly synthesized DNA was measured (Figure 31). WT+PKP3 cells showed increased BrdU incorporation. In contrast, BrdU incorporation was diminished in PKP3-KO cells, indicating a decrease in the number of cells in S phase. This finding correlates with the growth curves and further supports a delay in G1-S phase transition in PKP3-KO keratinocytes.
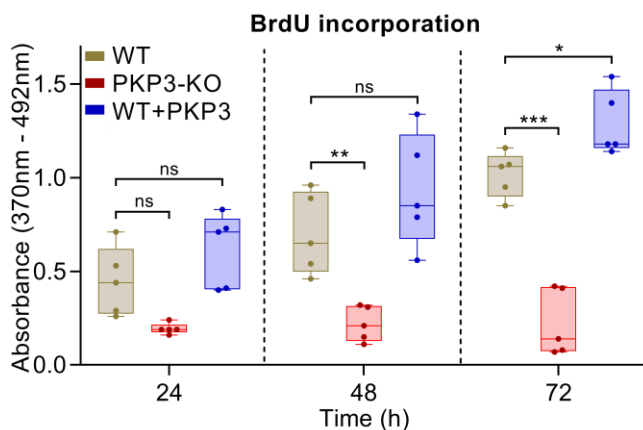
Figure 31 │ Loss of PKP3 reduces BrdU incorporation into the DNA. For analyzing DNA replication, WT, PKP3-KO, and WT+PKP3 cells were grown for 24 h, 48 h, or 72 h in LCM. Afterwards, a colorimetric BrdU assay was performed. Cells were labelled with BrdU and incubated with the anti-BrdU peroxidase coupled antibody. After adding of substrate solution, photometric detection was based on blue color development. BrdU incorporation into newly synthesized DNA was decreased in PKP3-KO cells but increased in WT+PKP3 cells compared to WT cells. The boxplot depicts the absorbance (n=5). The Whiskers extend to the minimum and maximum values. Statistical significance was determined by one-way ANOVA with Tukey's multiple comparisons test.

In the skin, epidermal stem cells of the single basal layer differentiate upon stratification to form the suprabasal layers for maintaining the architecture of the mature epidermis. Thus in keratinocytes, a "slow-down" in cell cycle progression is commonly associated with the induction of differentiation. When cells stop to proliferate, they can undergo reversible quiescence by entering temporarily the non-proliferative state G0 or the cells irreversible enter G0 phase, which induces terminal differentiation with the simultaneous inability to proliferate (Marescal and Cheeseman, 2020). The expression of differentiation-specific markers enables reversible quiescence and terminal differentiation of epidermal keratinocytes to be distinguished. Early epidermal differentiation is characterized by increased levels of desmoglein 1, keratin 1, and keratin 10 in the spinous layer of the epidermis, whereas corneodesmosin, involucrin, and loricrin are expressed in the upper corneal and granular layers (Matsui and Amagai, 2015) (Figure 32). The protein levels of these differentiation markers were analyzed to examine whether reduced proliferation correlated with increased differentiation in PKP3-KO cells. WT and PKP3-KO keratinocytes were grown for 72 h in LCM or HCM to induce differentiation (Figure 32). WT cells grown in HCM expressed all differentiation markers. In contrast, protein levels of differentiation markers were unaltered or decreased in PKP3-KO cells grown in HCM. Thus, growth retardation in PKP3-KO cells was not a consequence of premature differentiation.
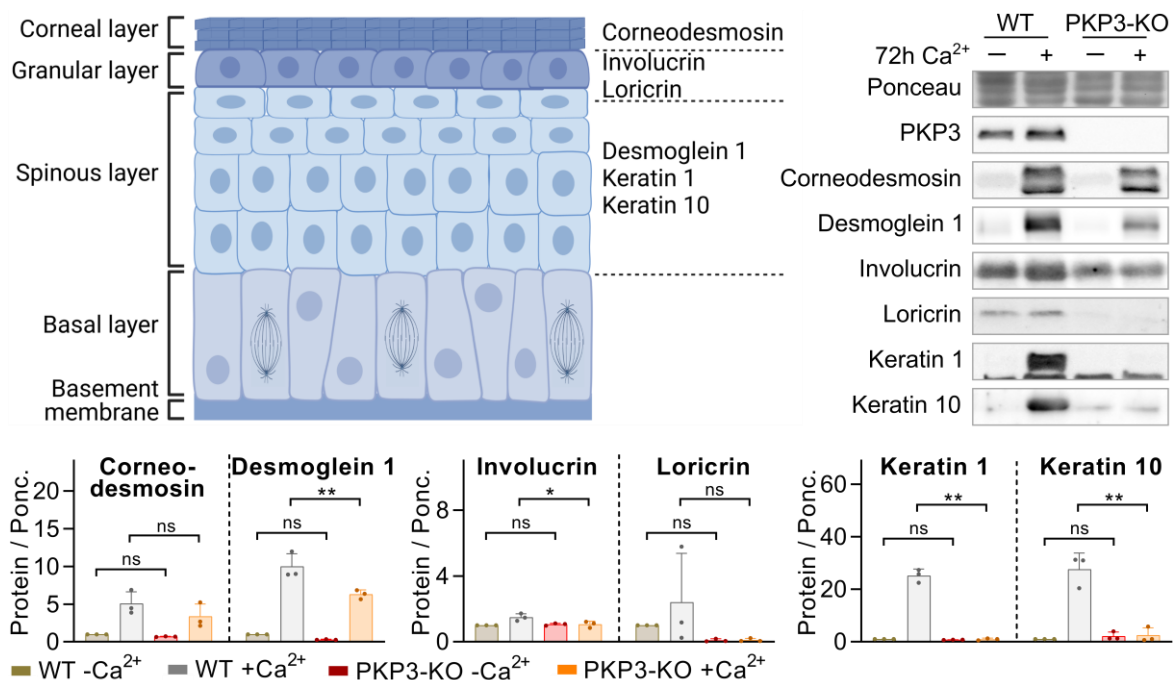
Figure 32 | Growth retardation is not a consequence of premature differentiation. A schematic of the epidermis demonstrates the expression of differentiation markers in distinct epidermal layers (upper left panel, created with biorender.com, modified from (Matsui and Amagai, 2015). Desmoglein 1, keratin 1, and keratin 10 are highly expressed in the spinous layer, whereas corneodesmosin, involucrin, and loricrin show increased expression in the upper corneal and granular layers. For analysis of the PKP3-dependent expression pattern of differentiation markers, WT and PKP3-KO cells were grown for 72 h in medium with or without Ca^{2+} and lysed in SDS lysis buffer. Total cell extracts were analyzed by western blotting with the indicated antibodies. Representative western blots (upper right panel) showing the protein levels of PKP3 and epidermal differentiation markers. Ponceau S staining was used as a loading control. PKP3-KO cells grown in HCM showed unaltered or decreased protein levels of all differentiation markers compared to WT cells. The bar plots (lower panels) depict the protein amounts (+ s.d.; n=3) normalized to Ponceau S staining and relative to WT cells grown in medium without Ca^{2+} (first lane in western blot). Statistical significance was determined by one-way ANOVA with Tukey's multiple comparisons test.

Collectively these results show that loss of PKP3 led to an enrichment of cells in G0/G1 phase and a prolonged G1 phase. As a consequence, S phase entry was retarded. These data indicate that PKP3 promotes proliferation and cell cycle progression in murine keratinocytes. In the following chapter, the mechanistic basis of PKP3's role in the G1-S phase transition will be analyzed.

4.2.2. PKP3 promotes RB phosphorylation and E2F1 activity

G1 to S phase transition is primarily controlled by the RB pathway (Figure 33A). The RB protein is a tumor suppressor, which plays a central role in the negative control of the cell cycle (Giacinti and Giordano, 2006). In G0 and early G1 phase, un-phosphorylated RB binds to members of the E2F family of transcriptions factors, including E2F1, in the nucleus and represses its transcriptional activity. In late G1 phase, mitogenic signals induce the synthesis of cyclins D and E, which form complexes with cyclin-dependent kinase

(CDK)4/CDK6 and CDK2, respectively. These activated complexes promote RB phosphorylation which leads to E2F dissociation. The priming hypo-phosphorylation is mediated by cyclin D-CDK4/6, which mono-phosphorylate RB. Subsequently, cyclin E-CDK2 completes RB phosphorylation and its inactivation. Hyper-phosphorylated RB dissociates from E2F1 and can be translocated into the cytoplasm in an exportin-1 dependent manner (Jiao *et al.*, 2008). The release of E2F1 leads to its full activation and allows the expression of E2F1 target genes that encode proteins necessary for S phase transition.
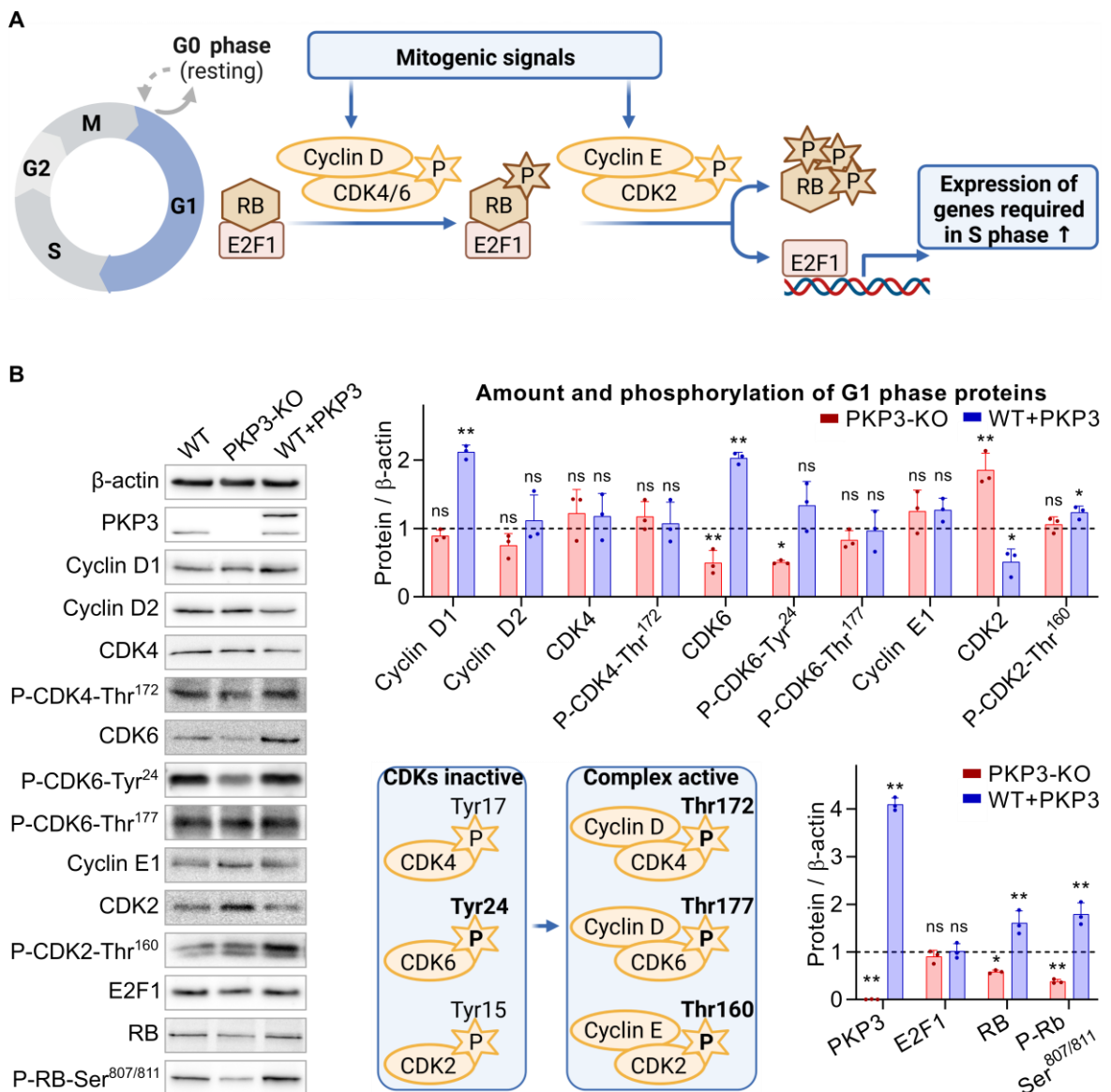
Figure 33 │ PKP3 regulates G1 phase in murine keratinocytes. (A) A schematic of the key events initiating G1-S phase progression demonstrates RB pathway as a central control mechanism (created with biorender.com, modified from (Giacinti and Giordano, 2006)). Un-phosphorylated, activated RB binds to E2F1 transcription factor, which represses its transcriptional activity and blocks cell cycle progression. When a cell receives mitogenic signals, complex formation of CDK4/6 and CDK2 with their corresponding cyclins is triggered, leading to their full activation. Activated cyclin-CDK complexes partially deactivate RB by

phosphorylation. Subsequently, E2F1 is released and mediates expression of genes that encode proteins necessary for G1-S phase transition. **(B)** For analysis of the putative effect of PKP3 on the RB pathway, WT, PKP3-KO, and WT+PKP3 cells were grown for 24 h in LCM and lysed in SDS lysis buffer. Total cell extracts were analyzed by western blotting with the indicated antibodies. Representative western blots (left panel) showing the protein level of PKP3 and distinct G1 phase markers. In the PKP3 blot, the lower lane represents endogenous PKP3, the upper lane reflects PKP3-GFP. β-actin was used as a loading control. PKP3-KO cells showed unaltered protein levels of cyclin D1, D2, and E1, as well as CDK4, phospho-CDK4-Thr^{172}, and E2F1 compared to WT cells. CDK6 protein amount was reduced in PKP3-KO cells, but the level of its active form, phospho-CDK6-Thr^{177}, was unaltered. CDK2 protein level was increased in PKP3-KO cells and decreased in WT+PKP3 cells, but the amount of its activated form (phospho-CDK2-Thr^{160}) was unaltered or slightly increased. Importantly, RB and phospho-RB-Ser$^{807/811}$ revealed PKP3-dependent levels, as shown by decreased amounts in PKP3-KO cells and increased levels in WT+PKP3 cells. A schematic of CDK activation (lower mid panel, created with biorender.com) demonstrates CDK4/6 and CDK2 phosphorylation sites, with indicated analyzed phosphosites (marked in bold). The bar plots (upper panel and lower right panel) depict the protein amounts (+ s.d.; n=3) normalized to β-actin and relative to WT cells (first lane in western blot). Statistical significance was determined by one-way ANOVA with Tukey's multiple comparisons test.

To analyze the putative effect of PKP3 on the RB pathway, the amount and activity of distinct proteins involved in RB regulation were quantified by western blotting (Figure 33B). In PKP3-KO cells, protein levels of cyclin D1, D2, and E1 were unaltered. Furthermore, CDK4 protein amount and activity (i.e., phosphorylation at Thr^{172}) were not affected by the loss of PKP3. However, CDK6 protein level and its phosphorylation at Tyr^{24}, which inhibits cyclin D-CDK6 association and prevents cell cycle progression, were decreased in PKP3-KO cells, suggesting low levels of inactive CDK6. Despite its reduced protein level, activation of CDK6 by phosphorylation at Thr^{177} was not affected by PKP3. In contrast, the CDK2 protein level was significantly increased in PKP3-KO cells, but the amount of activated CDK2 (i.e., phosphorylation at Thr^{160}) was unaltered. WT+PKP3 cells showed decreased CDK2 protein levels without a decrease in its activation. This suggests that PKP3 primarily affects the amount of CDK6 and CDK2 protein levels without significant effects on their activation.

Even though the activities of the cyclin-CDK complexes were essentially unaltered, I investigated whether RB and/or E2F1 activity was affected by PKP3. The most dramatic effect was observed downstream of cyclin-CDKs. Total RB levels were significantly reduced in PKP3-KO and increased in WT+PKP3 cells. To analyze the effect on RB phosphorylation, I used an antibody raised against human phospho-RB-Ser$^{807/811}$, a well-known CDK4/CDK6 and CDK2 phosphorylation site (Rubin, 2013; Narasimha *et al.*, 2014). To validate this antibody in murine keratinocytes, WT cells were treated with Lambda PP, which is active towards phosphorylated serine, threonine, and tyrosine residues (Figure S6). Treatment with Lambda PP did not alter PKP3 or RB levels, but the phospho-RB signal was abolished confirming the antibody's specificity for phospho-RB. Not only total RB was affected by PKP3, phospho-RB also revealed PKP3-dependent changes (Figure 33B). PKP3-KO cells showed an even more pronounced reduction in phospho-RB

compared to total RB, whereas WT+PKP3 cells showed elevated levels of phospho-RB. These data suggest that PKP3 might contribute to the regulation of RB phosphorylation.

PKP3-KO cells were obtained from PKP3-KO mice, which were generated by the Cre/loxP-site specific recombination system and were specified by the depletion of the mouse *Pkp3* exon 2-4 (Figure 34A) (Sklyarova *et al.*, 2008). PKP3-KO cells were characterized by the loss of PKP3 protein (Figure 33B) and, surprisingly, by high levels of non-protein coding PKP3 RNA (Figure 34B). To analyze whether this non-protein coding RNA might affect the expression and regulation of components of the RB pathway, WT and PKP3-KO cells were treated with control or PKP3-directed (siPKP3) siRNAs. Depletion of PKP3 resulted in decreased PKP3 mRNA levels in both WT and PKP3-KO cells. Nonetheless, the loss of the non-protein coding PKP3 RNA in PKP3-KO cells did not affect CDK6 and RB mRNA levels, which were reduced to the same extent as in PKP3-KO cells with high levels of the truncated PKP3 RNA. This excludes that the observed effects on cell cycle associated genes were caused by the non-protein coding PKP3 RNA but are due to the loss of the PKP3 protein.
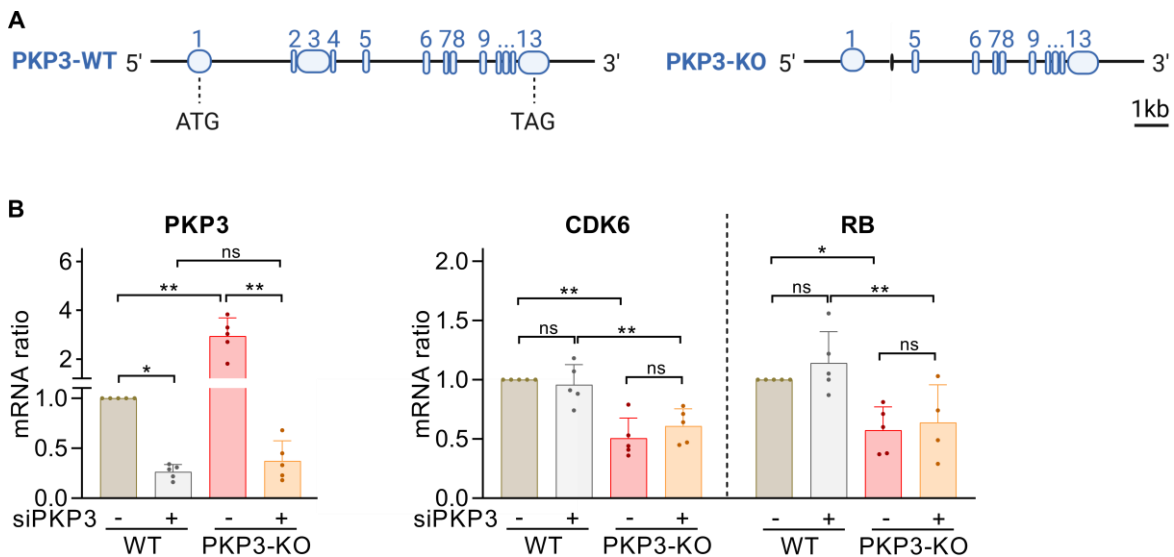
Figure 34 │ Increased non-coding PKP3 RNA levels in PKP3-KO cells does not affect CDK6 and RB mRNA amount. (A) Schematic of *Pkp3*-WT allele and mutated *Pkp3* allele with depletion of exon 2-4 (created with biorender.com, modified from (Sklyarova *et al.*, 2008)). Exons are indicated as numbered blue boxes. Exon 1 starts with the ATG start codon, exon 13 ends with the TAG stop codon. PKP3-KO cells were obtained from PKP3-KO mice, which were generated by knockout of exon 2-4. **(B)** WT and PKP3-KO cells were transfected with non-targeting (siCtrl) or PKP3-directed (siPKP3) siRNAs, grown for 72 h in LCM, and processed for qRT-PCR. PKP3-KO cells showed increased levels of non-protein coding RNA, which was reduced to the same extent as in WT cells after PKP3 knockdown (left panel). CDK6 and RB mRNA were reduced in siCtrl and siPKP3 treated PKP3-KO cells compared to WT cells (right panel). The bar plots depict the mRNA amounts (+ s.d.; n=5) normalized to *Eif3k* as an invariant endogenous control (reference gene) and relative to WT cells. Statistical significance was determined by one-way ANOVA with Tukey's multiple comparisons test.

Although PKP3-KO cells showed altered CDK6 and RB protein levels (Figure 33B), PKP3 depletion in WT cells was not sufficient to decrease CDK6 and RB mRNA levels (Figure 34B), which might be due to the short time frame of the knockdown experiment. To analyze this effect in detail, protein stability of PKP3, CDK6, and RB was determined. WT, PKP3-KO, and WT+PKP3 cells were treated with cycloheximide, an inhibitor of protein biosynthesis which prevents translational elongation. After treatment and lysis of the cells, the protein abundance was analyzed by western blotting (Figure 35). The highly unstable protein c-MYC was used as positive control (Welcker *et al.*, 2004; Li *et al.*, 2015). Even after prolonged cycloheximide treatment, protein abundance of CDK6 and RB were only slightly decreased in WT cells, suggesting high protein stability. Highly stable proteins do not need continuous translation from mRNA, which might contribute to smaller effects of PKP3 knockdown in WT cells compared to its depletion in PKP3-KO cells. Moreover, CDK6 and RB protein levels after cycloheximide treatment were unaltered in PKP3-KO and WT+PKP3 cells compared to WT cells. Thus, it seems that PKP3 does not affect protein stability of CDK6 and RB.
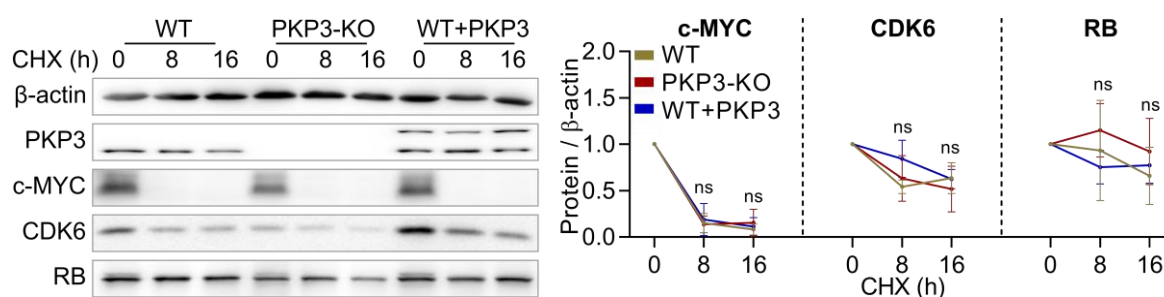
Figure 35 │ PKP3 does not affect protein stability of CDK6 and RB. A cycloheximide chase assay was performed to measure steady-state protein stability. WT, PKP3-KO, and WT+PKP3 cells were grown for 24 h in LCM and treated with cycloheximide (CHX, 200 µg/ml) for 8 h or 16 h. Cells were lysed in SDS lysis buffer. Total cell extracts were analyzed by western blotting with the indicated antibodies. Representative western blots (left panel) showing the protein level of PKP3, CDK6, and RB. In the PKP3 blot, the lower lane represents endogenous PKP3, the upper lane reflects PKP3-GFP. β-actin was used as a loading control. c-MYC was used as positive control. Whereas c-MYC showed dramatically reduced protein amounts in all three cell lines, PKP3, CDK6, and RB protein levels were unaltered even after 16 h cycloheximide. The graph (right panels) depicts the protein abundance (± s.d.; n=3) normalized to β-actin and relative to 0 h cycloheximide. Statistical significance was determined by one-way ANOVA.

As CDK6 can phosphorylate RB and PKP3-KO cells showed diminished protein levels of CDK6 and phospho-RB, I determine whether increased expression of CDK4 or CDK6 can rescue RB phosphorylation in PKP3-KO cells. Thus, HA-tagged CDK4 or CDK6 were expressed in all three cell lines (Figure 36). Neither the ectopic expression of CDK4 nor expression of CDK6 increased RB phosphorylation in PKP3-KO cells. This suggests that the reduced CDK6 protein level in PKP3-KO cells is not the main driver of the prolonged G1 phase.
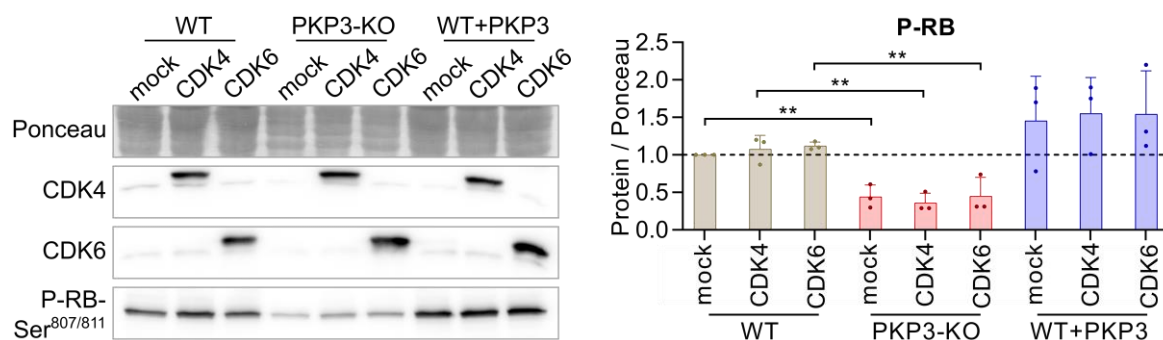
Figure 36 │ Ectopic expression of CDK4 or CDK6 does not rescue RB phosphorylation in PKP3-KO cells. For analyzing the effect of CDK4 and CDK6 overexpression, WT, PKP3-KO, and WT+PKP3 cells were transfected with the indicated Venus2-HA-CDK constructs or a plasmid without insert (mock) and grown for 24 h in LCM. Cells were lysed in SDS lysis buffer. Total cell extracts were analyzed by western blotting with the indicated antibodies. Representative western blots (left panel) showing the protein level of CDK4/6 and phospho-RB. Ponceau S staining was used as a loading control. Amount of phospho-RB was not increased in PKP3-KO cells after ectopic expression of CDK4 or CDK6. The bar plot (right panel) depicts the level of phospho-RB (+ s.d.; n=3) normalized to Ponceau S staining and relative to mock treatment in WT cells (first lane in western blot). Statistical significance was determined by one-way ANOVA with Tukey's multiple comparisons test.

RB phosphorylation is the key event in G1-S phase transition by promoting E2F1 release and regulating its transcriptional activity. E2F1 protein level was not affected by PKP3 (Figure 33B). As PKP3-KO cells showed impaired RB phosphorylation, I hypothesized that E2F1 activity might also be reduced. To analyze the transcriptional activity of E2F1, mRNA levels of selected E2F1 target genes involved in cell cycle control, such as *E2F3*, *CCNA2* (cyclin A2), *CCNB1* (cyclin B1), *CDK1,* minichromosome maintenance complex components 3 and 6 (*MCM3*, *MCM6*), thymidylate synthase *(TYMS*), and flap endonuclease *1 (FEN1*), were quantified by qRT-PCR (Figure 37). In PKP3-KO cells, mRNA levels of these E2F1 target genes were decreased. This indicates that the loss of PKP3 resulted in reduced transcriptional activity of E2F1 and was further supported by GSEA-based HALLMARK data (Figure S5), in which downregulated protein coding genes in PKP3-KO cells and upregulated protein coding genes in WT+PKP3 cells were highly associated with E2F targets.
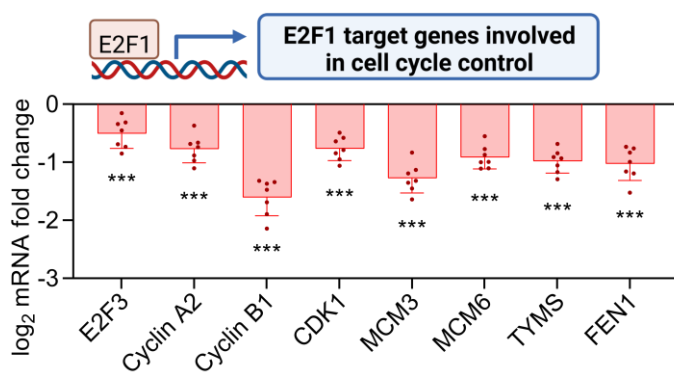
Figure 37 │ PKP3 promotes transcriptional activity of E2F1. For analyzing the transcriptional activity of E2F1, WT and PKP3-KO cells were grown for 24 h in LCM and processed for qRT-PCR. Analysis of mRNA of E2F1 targets involved in cell cycle control revealed decreased levels in PKP3-KO cells compared to WT cells. The bar plot depicts the $\log_2$ mRNA fold changes (+ s.d.; n=7) normalized to *Eif3k* as an invariant endogenous control (reference gene) and relative to WT cells. Statistical significance was determined by a student's unpaired two tailed *t*-test.

Taken together, these data show that PKP3 promotes the G1-S phase transition by increasing RB phosphorylation, thereby enhancing E2F1 activity. In the following chapter, the molecular mechanism underlying the regulation of the G1 to S phase transition by PKP3 will be analyzed.

4.2.3. PKP3 captures RB to promote E2F1 release

Cell cycle research continues to focus heavily on the molecular mechanisms to understand the modulators of the RB pathway. To test whether PKP3 contributes to RB pathway regulation by association with proteins involved in G1-S phase transition, immunoprecipitations were performed. PKP3-GFP was affinity purified from WT+PKP3 cells (Figure 38A). CDK4, CDK6, cyclin E1, and CDK2 did not co-purify with PKP3. In contrast, RB and phospho-RB co-precipitated, suggesting an association with PKP3. To validate these data, endogenous RB was immunoprecipitated from WT cells (Figure 38B). Co-purification of PKP3 supports a putative association of PKP3 with RB. The interaction of PKP3 with RB may facilitate the dissociation of RB from E2F1. According to this hypothesis, the amount of RB-E2F1 complex would decrease in the presence of PKP3. To verify this hypothesis, endogenous E2F1 was immunoprecipitated from WT and PKP3-KO cells (Figure 38C). As expected, phospho-RB did not co-purify with E2F1, whereas RB co-precipitated. In agreement with my hypothesis, the amount of RB forming a complex with E2F1 was reduced in WT cells. This supports the assumption that PKP3 disturbs the interaction of RB with E2F1. In contrast, the significantly greater amount of RB-E2F1 complex in PKP3-KO cells suggests that the loss of PKP3 increased the association of RB with E2F1, leading to reduced E2F1 activity.
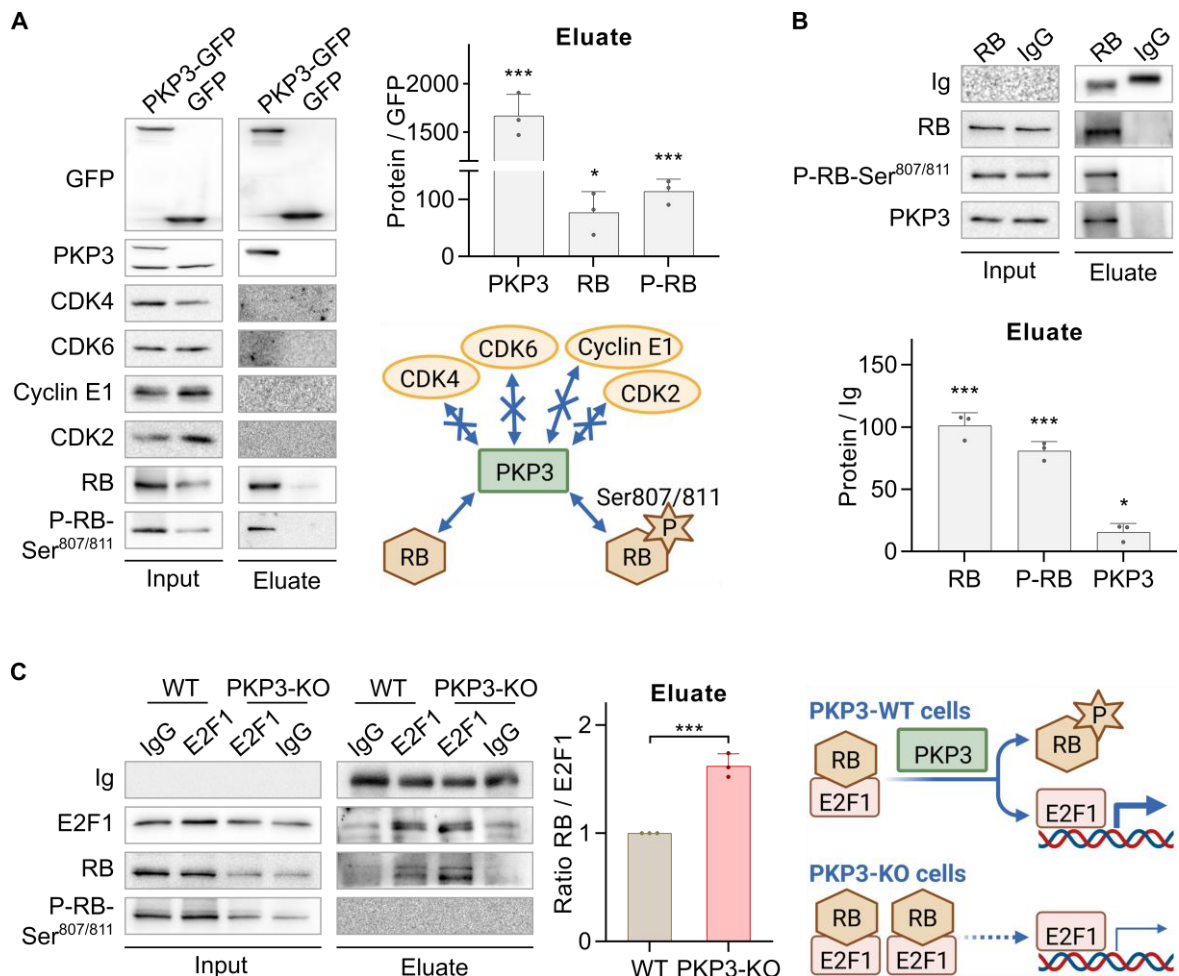
Figure 38 │ PKP3 captures RB to promote E2F1 release. (A) For analyzing putative PKP3 binding partners, PKP3-GFP or GFP were precipitated from ectopically expressing WT cells using GFP-trap agarose and probed for interaction by western blotting with the indicated antibodies. Representative western blots (left panel) showing total protein lysates labeled input, and immunoprecipitates which are eluated from the beads after the immunoprecipitation labeled eluate. In the PKP3 blot, the lower lane represents endogenous PKP3, the upper lane reflects PKP3-GFP. Whereas CDK4, CDK6, cyclin E1, and CDK2 did not co-purify with PKP3, RB and phospho-RB co-precipitated. The bar plot (upper right panel) depicts the level of eluate proteins (+ s.d.; n=3) normalized to precipitated GFP and relative to the values of GFP-only cells (second lane in western blot). Statistical significance was determined by a student's unpaired two tailed *t*-test. The schematic (lower right panel, created with biorender.com) shows the role of PKP3 as a putative interaction partner of G1 phase regulating proteins. **(B)** For analyzing putative RB binding partners, endogenous RB was affinity purified from WT cells and probed for interaction by western blotting with the indicated antibodies. Representative western blots (upper panel) showing total protein lysates labeled input, and immunoprecipitates which are eluated from the beads after the immunoprecipitation labeled eluate. Normal rabbit IgG served as a negative control. PKP3 did co-purify with endogenous RB. The bar plot (lower panel) depicts the level of eluate proteins (+ s.d.; n=3) normalized to precipitated IgG heavy chain (Ig) and relative to values in control cells (second lane in western blot). Statistical significance was determined by a student's unpaired two tailed *t*-test. **(C)** For analyzing the E2F1-RB complex, endogenous E2F1 was affinity purified from WT cells or PKP3-KO cells and probed for interaction by western blotting with the indicated antibodies. Representative western blots (left panel) showing total protein lysates labeled input, and immunoprecipitates which are eluated from the beads after the immunoprecipitation labeled eluate. Normal rabbit IgG served as a negative control. Whereas phospho-RB did not co-purify with endogenous E2F1, RB did co-purify in WT and PKP3-KO cells. The bar plot (mid panel) depicts the RB/E2F1 ratio in the eluate (+ s.d.; n=3) normalized to precipitated IgG heavy chain (Ig) and relative to WT cells (second lane in western blot). Statistical significance was determined by a student's unpaired two tailed *t*-test. The schematic (right panel, created with biorender.com) shows that PKP3 might promotes E2F1 release and its increasing transcriptional activity in WT cells, whereas in PKP3-KO cells, the higher amount of RB-E2F1 complex may results in impaired transcriptional activity of E2F1.

As subcellular localization and phosphorylation status of RB change during the cell cycle (Mittnacht and Weinberg, 1991; Stokke *et al.*, 1993), the effects of PKP3 on intracellular RB localization were analyzed. Nucleus/cytoplasm fractionation were used to identify the localization of PKP3, RB, and phospho-RB in WT as well as PKP3-KO cells (Figure 39A). PKP3 was detected in both cytoplasmic and nuclear fractions, with a slight preference for cytoplasmic localization. Total RB was primarily detected in the nucleus of WT and PKP3-KO cells. In contrast, phospho-RB was primarily detected in the cytoplasmic fraction of WT cells, with a strong reduction in PKP3-KO cells. Thus, PKP3 might capture phospho-RB in the cytoplasm to promote G1-S phase transition. To test this assumption, nucleus/cytoplasm fractionation was combined with immunoprecipitation. Nuclear and cytoplasmic fractions were prepared from WT+PKP3 cells and PKP3-GFP was affinity purified from these fractions (Figure 39B). PKP3 was isolated from both fractions but it localized preferentially in the cytoplasm. RB co-isolated with PKP3 not only from the nuclear fraction but also from the cytoplasm. Although RB localized primarily in the nucleus, its interaction with PKP3 was detected mainly in the cytoplasm, suggesting a preferred association of PKP3 with the phosphorylated form of RB that translocates into the cytoplasm. Because nucleus/cytoplasm fractionation may not accurately reflect subcellular localization of proteins in living cells (e.g., redistribution after cell breakage of molecules not tightly bound to nuclear or cytoplasmic structures), immunofluorescence studies were performed to validate the PKP3-dependent localization of RB. WT and PKP3-KO cells were processed for immunofluorescence studies of PKP3 and RB (Figure 39C). In agreement with fractionation studies, RB was predominantly localized in the nucleus with a weaker cytoplasmic signal. The ratio of cytoplasmic to nuclear RB fluorescence was further decreased in PKP3-KO cells. Thus, PKP3 might increase the amount of cytoplasmic RB.
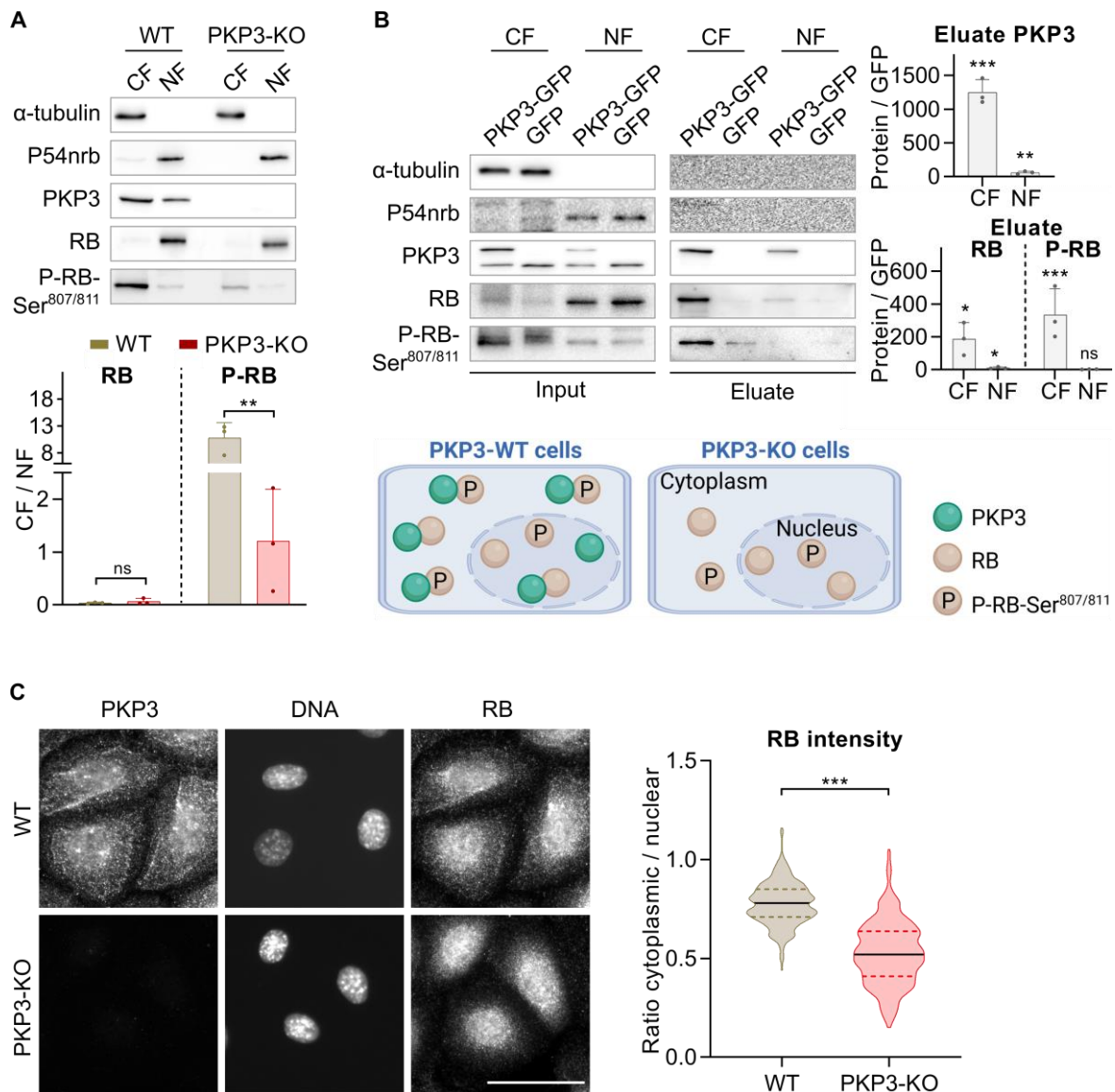
Figure 39 │ PKP3 promotes cytoplasmic localization of phospho-RB. (A) For analyzing intracellular localization, WT and PKP3-KO cells were grown for 24 h in LCM, processed for nucleus/cytoplasm fractionation, and analyzed by western blotting with the indicated antibodies. Representative western blots (upper panel) showing cytoplasmic fractions (CF) and nuclear fractions (NF). α-tubulin was used as CF control, p54nrb was used as NF control. Whereas PKP3 showed cytoplasmic and nuclear localization, RB localized predominantly nuclear. Phospho-RB was primarily detected in the cytoplasm of WT cells, with a strong reduction in PKP3-KO cells. The bar plot (lower panel) depicts the CF/NF ratio (+ s.d.; n=3) in WT and PKP3-KO cells. Statistical significance was determined by a student's unpaired two tailed t-test. **(B)** For analyzing putative PKP3 binding partners in the cytoplasm and the nucleus, PKP3-GFP or GFP were precipitated from ectopically expressing WT cells using GFP-trap agarose after nucleus/cytoplasm fractionation and probed for interaction by western blotting with the indicated antibodies. Representative western blots (upper left panel) showing total protein lysates labeled input, and immunoprecipitates which are eluated from the beads after the immunoprecipitation labeled eluate. In the PKP3 blot, the lower lane represents endogenous PKP3, the upper lane reflects PKP3-GFP. CF, cytoplasmic fraction; NF, nuclear fraction. PKP3 was isolated from both fraction. RB was co-isolated from the cytoplasm and to a lesser extent from the nucleus. Phospho-RB was co-isolated with PKP3 only from the cytoplasm. The bar plots (upper right panel) depict the level of eluate proteins (+ s.d.; n=3) normalized to precipitated GFP and relative to the values of GFP-only cells (second and fourth lane in western blot, respectively). Statistical significance was determined by a student's unpaired two tailed t-test. The schematic (lower panel, created with biorender.com) shows that PKP3 prefers cytoplasmic binding with phospho-RB in WT cells, whereas in PKP3-KO cells, the loss of PKP3 results in decreased cytoplasmic levels of phospho-RB. **(C)** For analyzing intracellular RB localization, WT and PKP3-KO cells were grown for 24 h in LCM, and processed for immunofluorescence. Cells were fixed in formaldehyde on ice and immunostained for

PKP3 and RB. Immunofluorescence images (left panel) show RB localization in PKP3-KO cells compared to WT cells. PKP3 fluorescence depicts the loss of PKP3 in PKP3-KO cells. Scale bar: 50 µm. RB localized primarily nuclear with a weaker cytoplasmic signal. In PKP3-KO cells, cytoplasmic RB localization was further decreased. The truncated violin plot (right panel) depicts the cytoplasmic/nuclear ratio of RB fluorescence intensity (n≥300 cells per condition from two independent experiments). The violin plot shows medium smoothed data distribution for each subgroup, a black horizontal line representing the median of each subgroup, and colored horizontal lines representing the 75th percentile or the 25th percentile, respectively, of each subgroup. Statistical significance was determined by a student's unpaired two tailed *t*-test.

These data show a preferred interaction of PKP3 with the phosphorylated form of RB that translocates into the cytoplasm. To understand whether the association depended on RB phosphorylation or whether it was rather regulated by RB localization, a RB-ΔCDK construct was used. RB-ΔCDK is a mutant version of RB lacking all 15 CDK phosphorylation sites, which have been exchanged to alanine (Narasimha *et al.*, 2014). GFP-tagged RB-WT and RB-ΔCDK were expressed in WT keratinocytes and both proteins were affinity purified (Figure 40). Using the phospho-RB-Ser$^{807/811}$ antibody, a lack of Ser$^{807/811}$ phosphorylation in the RB-ΔCDK mutant was confirmed. However, PKP3 co-precipitated with RB-WT as well as RB-ΔCDK. This suggests no preference of PKP3 for phosphorylated or unphosphorylated RB. Therefore, RB localization, not its phosphorylation, determines its interaction with PKP3.
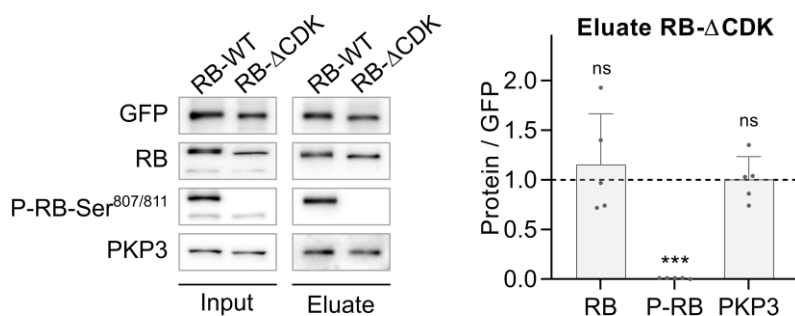
Figure 40 │ RB phosphorylation does not determine its interaction with PKP3. GFP-RB-WT or GFP-RB-ΔCDK were precipitated from ectopically expressing WT cells using GFP-trap agarose and probed for interaction by western blotting with the indicated antibodies. Representative western blots (left panel) showing total protein lysates labeled input, and immunoprecipitates which are eluated from the beads after the immunoprecipitation labeled eluate. In the RB and P-RB-Ser$^{807/811}$ blots, the lower lane represents endogenous RB, the upper lane reflects RB-GFP. The RB-ΔCDK mutant was characterized by a lack of phosphorylation. PKP3 was co-isolated with RB-WT and RB-ΔCDK. The bar plot (right panel) depicts the level of eluate proteins (+ s.d.; n=5) normalized to precipitated GFP and relative to the values of RB-WT (first lane in western blot). Statistical significance was determined by a student's unpaired two tailed *t*-test.

Collectively these results uncover a role of PKP3 in the regulation of RB. Mechanistically, PKP3 interacts with phosphorylated RB in the cytoplasm, which may contribute to reducing RB in the nucleus and decrease the inhibitory RB-E2F1 interaction.

4.2.4. PKP3 regulates p21 expression, localization, and function

The previous data show that PKP3 sequesters RB in the cytoplasm which might promote E2F1 activity. However, these data do not explain why RB phosphorylation was reduced in PKP3-KO cells. Therefore, the regulation of G1-S phase transition upstream of the RB-E2F1 complex was analyzed. RB phosphorylation is tightly controlled by CDKs. Their activity is regulated by the cyclin-dependent kinase inhibitor (CDKN) family of genes which code for proteins that bind and inhibit the activity of CDKs (Lutful Kabir *et al.*, 2015). The inhibitors of CDK4 (INK4) family members p16 (gene name *CDKN2A*), p15 (*CDKN2B*), p18 (*CDKN2C*), and p19 (*CDKN2D*) primarily target cyclin D-CDK4/CDK6, whereas the CDK interacting protein/kinase inhibitory protein (CIP/KIP) family members p21 (*CDKN1A*), p27 (*CDKN1B*), and p57 (*CDKN1C*) inhibit both cyclin D-CDK4/CDK6 and cyclin E-CDK2 complexes (Figure 41A). Analysis of mRNA levels in WT, PKP3-KO, and WT+PKP3 cells demonstrated decreased p16, p15, and p27 mRNA levels in both PKP3-KO and WT+PKP3 cells (Figure 41B). Importantly, mRNA levels of p21 were increased in PKP3-KO cells and slightly decreased in WT+PKP3 cells. mRNA of p19 was unaltered in PKP3-KO cells. p57 and p18 were not expressed in murine keratinocytes (data not shown). As p21 mRNA was inversely correlated with PKP3, the role of p21 in cell cycle regulation was further analyzed. First, I addressed the question if regulation of the stability of the p21 mRNA may contribute to its inhibitory effect on cell cycle progression. Thus, WT and PKP3-KO cells were treated with actinomycin D to inhibit synthesis of new mRNA, allowing the analysis of the p21 mRNA half-life (Figure 41C). The highly unstable c-MYC mRNA was used as a positive control (Dani *et al.*, 1984). Whereas c-MYC revealed a mRNA half-life of about 1 h, the mRNA half-life of p21 was about 5.04 h in WT cells and 4.52 h in PKP3-KO cells. Thus, the mRNA stability of p21 was essentially unaltered in PKP3-KO cells, suggesting that PKP3 does not contribute to p21 mRNA decay. To test for a correlation of mRNA levels with protein abundance, protein levels of p16 and p21 were analyzed in WT, PKP3-KO, and WT+PKP3 cells (Figure 41D). In accordance to mRNA levels, p16 protein levels were decreased in PKP3-KO and WT+PKP3 cells. Furthermore, p21 protein levels were inversely correlated with PKP3 levels. This identifies p21 as the main inhibitory protein revealing a PKP3-dependent expression pattern.
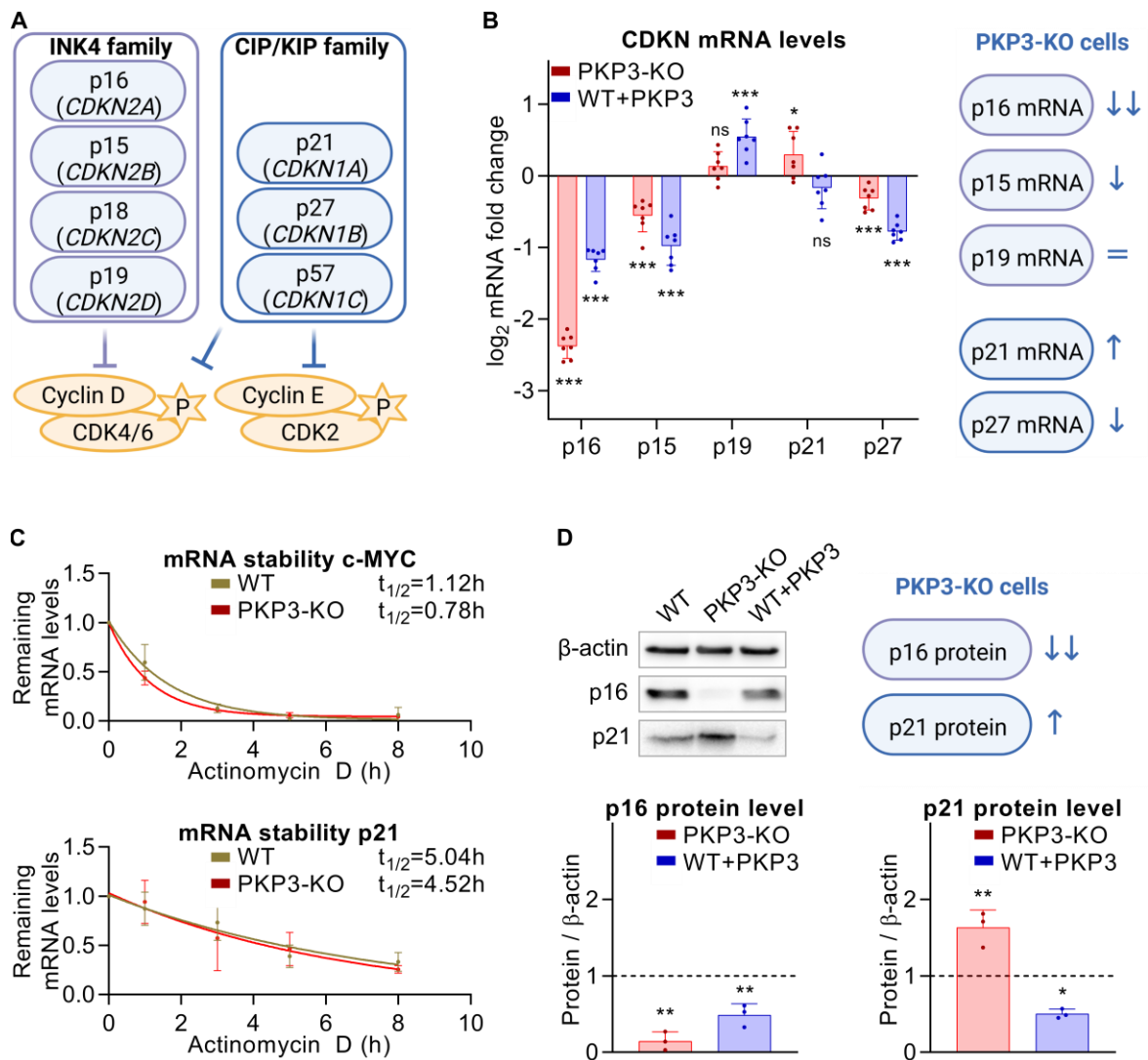
Figure 41 │ PKP3 inhibits p21 mRNA and protein levels. (A) A schematic of the regulation of CDKs activity by the CDKN protein family (created with biorender.com, modified from (Lutful Kabir *et al.*, 2015). The INK4 family members p16 (gene name *CDKN2A*), p15 (*CDKN2B*), p18 (*CDKN2C*), and p19 (*CDKN2D*) primarily bind and inactivate cyclin D-CDK4/CDK6, whereas the CIP/KIP family members p21 (*CDKN1A*), p27 (*CDKN1B*), and p57 (*CDKN1C*) inhibit both cyclin D-CDK4/CDK6 and cyclin E-CDK2 complexes. **(B)** For analyzing CDKN mRNA levels, WT, PKP3-KO, and WT+PKP3 cells were grown for 24 h in LCM and processed for qRT-PCR. Analysis of CDKN mRNA revealed increased levels of p21 in PKP3-KO cells and slightly decreased levels in WT+PKP3 cells. mRNA of p16, p15, p19, and p27 were not inversely correlated with PKP3 levels. The bar plot (left panel) depicts the $\log_2$ mRNA fold change (+ s.d.; n=7) normalized to *Eif3k* as an invariant endogenous control (reference gene) and relative to WT cells. Statistical significance was determined by a student's unpaired two tailed *t*-test. A schematic (right panel, created with biorender.com) demonstrates CDKN mRNA levels in PKP3-KO cells compared to WT cells. **(C)** A mRNA decay assay was performed to measure mRNA stability. WT and PKP3-KO cells were grown for 24 h in LCM, treated with actinomycin D (10 µg/ml) for up to 8 h, and processed for qRT-PCR. The mRNA fold change was calculated normalized to *Eif3k* as an invariant endogenous control (reference gene) and relative to values at 0 h actinomycin D treatment. Subsequently, an one-phase exponential decay curve analysis was performed to determine the mRNA half-life of p21. C-MYC was used as positive control. The graphs depict the remaining mRNA levels (± s.d.; n=3) relative to 0 h actinomycin D and the calculated half-life ($t_{1/2}$) of c-MYC or p21 mRNA in WT and PKP3-KO cells, respectively. mRNA stability of p21 was unaltered in PKP3-KO cells. **(D)** For analysis of the protein levels, WT, PKP3-KO, and WT+PKP3 cells were grown for 24 h in LCM and lysed in SDS lysis buffer. Total cell extracts were analyzed by western blotting with the indicated antibodies. Representative western blots (upper left panel) showing the protein levels of p16 and p21. β-actin was used as a loading control. PKP3-KO and WT+PKP3 cells showed impaired p16 protein levels compared to WT cells. In contrast, p21 protein level was increased in PKP3-KO cells and decreased in WT+PKP3 cells. A schematic (upper right panel, created with biorender.com)

demonstrates CDKN protein levels in PKP3-KO cells compared to WT cells. The bar plots (upper panels) depict the protein amounts (+ s.d.; n=3) normalized to β-actin and relative to WT cells (first lane in western blot). Statistical significance was determined by one-way ANOVA with Tukey's multiple comparisons test.

To determine the role of p21 in controlling the RB pathway, its localization and function were analyzed in more detail. The function of p21 as inhibitor of cell cycle progression depends on its subcellular localization. Cytoplasmic localization of p21 promotes cell growth, whereas p21 inhibits proliferation and acts as a tumor suppressor when localized in the nucleus (Georgakilas *et al.*, 2017; Shamloo and Usluer, 2019). The localization of p21 in WT and PKP3-KO cells was determined by immunofluorescence studies (Figure 42A). In order to validate the specificity of the antibody on murine keratinocytes, a knockdown of p21 was performed in parallel. In both WT and PKP3-KO cells, p21 localized predominately in the nucleus. However, the nuclear to cytoplasmic ratio of fluorescence intensity was 3-fold higher in PKP3-KO cells than in WT cells. This PKP3-dependent localization of p21 might be driven by its interaction with PKP3, which was confirmed by immunoprecipitations. PKP3-GFP was affinity purified from WT+PKP3 cells (Figure 42B). p16 did not co-purify with PKP3, whereas p21 co-precipitated, suggesting an association of PKP3. As PKP3 interacts with p21, PKP3 might sequesters p21 in the cytoplasm to prevent its inhibitory activity.
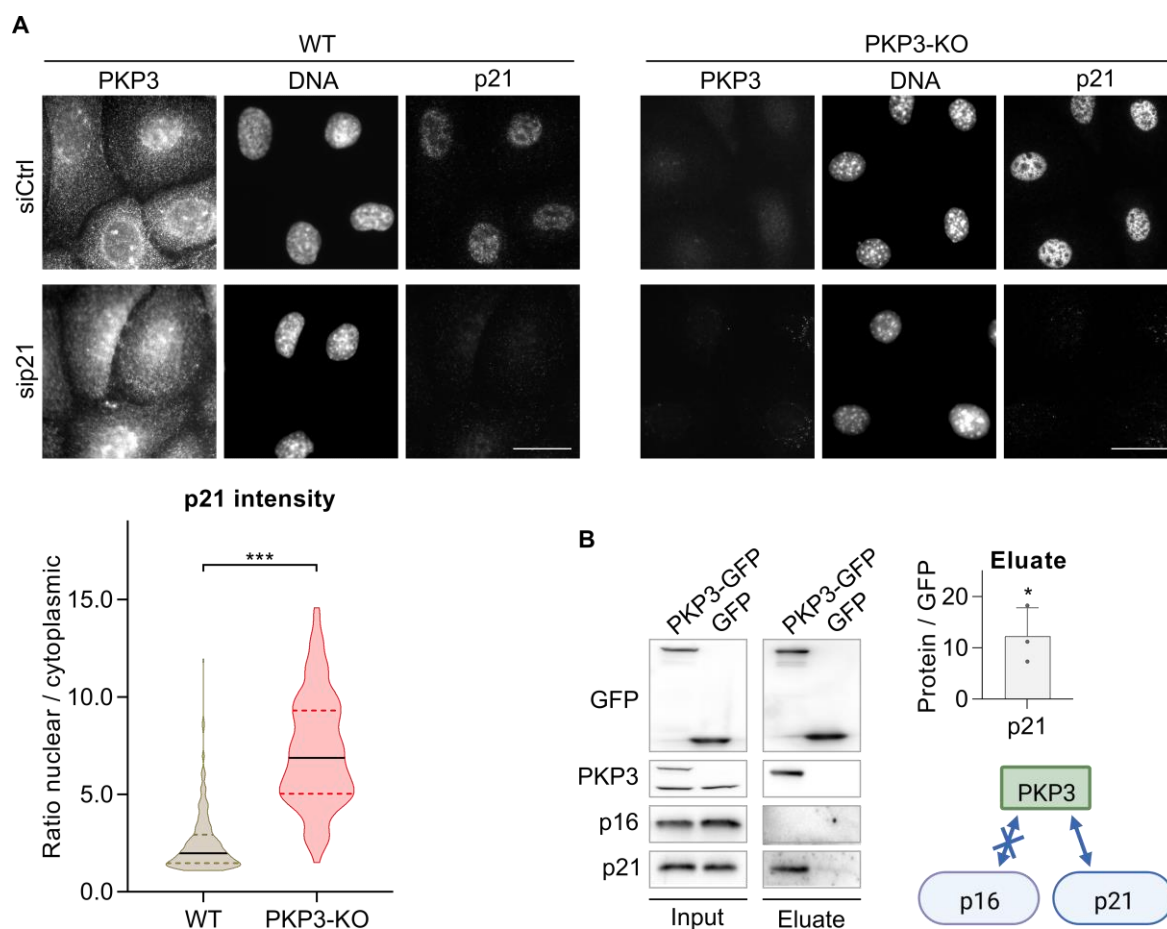
Figure 42 │ PKP3 prevents nuclear localization of p21. (A) For analyzing intracellular p21 localization, WT and PKP3-KO cells were transfected with non-targeting (siCtrl) or p21-directed (sip21) siRNAs, grown for 72 h in LCM, and processed for immunofluorescence. Cells were fixed in formaldehyde on ice and immunostained for PKP3 and p21. Immunofluorescence images (upper panel) show p21 localization in siCtrl-treated PKP3-KO cells compared to siCtrl-treated WT cells. p21 fluorescence depicts successful siRNA treatment. Scale bars: 50 μm. In siCtrl-treated WT cells, p21 localized primarily nuclear. In contrast in siCtrl-treated PKP3-KO cells, nuclear p21 localization was further enhanced. The truncated violin plot (lower left panel) depicts the nuclear/cytoplasmic ratio of p21 fluorescence intensity in siCtrl-treated cells (n≥250 cells per condition from two independent experiments). The violin plot shows medium smoothed data distribution for each subgroup, a black horizontal line representing the median of each subgroup, and colored horizontal lines representing the 75th percentile or the 25th percentile, respectively, of each subgroup. Statistical significance was determined by a student's unpaired two tailed *t*-test. **(B)** For analyzing putative PKP3 binding partners, PKP3-GFP or GFP were precipitated from ectopically expressing WT cells using GFP-trap agarose and probed for interaction by western blotting with the indicated antibodies. Representative western blots (left panel) showing total protein lysates labeled input, and immunoprecipitates which are eluated from the beads after the immunoprecipitation labeled eluate. In the PKP3 blot, the lower lane represents endogenous PKP3, the upper lane reflects PKP3-GFP. Whereas p16 did not co-purify with PKP3, p21 co-precipitated. The bar plot (upper right panel) depicts the level of eluate p21 protein (+ s.d.; n=3) normalized to precipitated GFP and relative to the values of GFP-only cells (second lane in western blot). Statistical significance was determined by a student's unpaired two tailed *t*-test. The schematic (lower right panel, created with biorender.com) shows PKP3's role as a putative interaction partner of CDKN proteins.

In PKP3-KO cells, nuclear p21 might act as a tumor suppressor. To investigate whether elevated nuclear localization of p21 in PKP3-KO cells resulted in impaired RB phosphorylation, WT and PKP3-KO cells were transfected with non-targeting or p21-directed siRNAs (Figure 43). Depletion of p21 in PKP3-KO cells diminished the p21 protein

to a level similar to that detected in WT cells. Importantly, downregulation of p21 in PKP3-KO cells resulted in increased levels of phospho-RB. This partial rescue of RB phosphorylation after p21 knockdown in PKP3-KO cells suggested that p21 is critically involved in PKP3-mediated regulation of cell cycle progression.
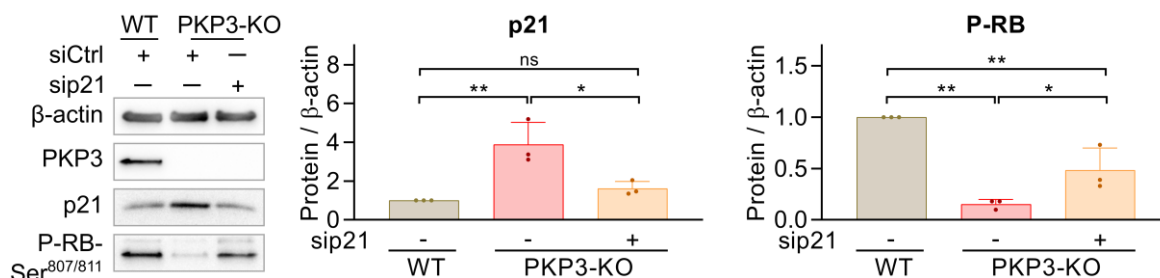
Figure 43 │ **RB phosphorylation is determined by p21 level.** For analyzing p21 depletion, WT and PKP3-KO cells were transfected with non-targeting (siCtrl) or p21-directed (sip21) siRNAs, grown for 72 h in LCM, and lysed in SDS lysis buffer. Total cell extracts were analyzed by western blotting with the indicated antibodies. Representative western blots (left panel) showing the protein level of p21 and phospho-RB. β-actin was used as a loading control. Depletion of p21 in PKP3-KO cells resulted in decreased p21 protein level similar to WT cells, but enhanced RB phosphorylation. The bar plots (right panels) depict the protein amounts (+ s.d.; n=3) normalized to β-actin and relative to siCtrl-treated WT cells (first lane in western blot). Statistical significance was determined by one-way ANOVA with Tukey's multiple comparisons test.

Taken together, these data show that PKP3 inhibits p21 mRNA and protein levels by a yet unknown mechanism. Furthermore, PKP3 prevents the nuclear localization of p21 by association, which controls its function as an inhibitor of RB phosphorylation. In the following chapter, the mechanism underlying the PKP3-dependent regulation of p21 protein level will be analyzed.

4.2.5. PKP3 modulates a RUNX3-EGFR axis

Expression of p21 is regulated by a number of transcription factors, including c-MYC (Abbas and Dutta, 2009) and RUNX3 (Figure 44A), an effector of transforming growth factor-β (TGF-β) signaling (Ito and Miyazono, 2003). To analyze whether mRNA expression of c-MYC or RUNX3 were altered in PKP3-KO cells, mRNA levels of c-MYC and RUNX3 were investigated along with the reference gene *EIF3K* in WT, PKP3-KO, and WT+PKP3 cells (Figure 44B). C-MYC Ct levels revealed no PKP3-dependence. In contrast, RUNX3 Ct values were significantly decreased in PKP3-KO cells and increased in WT+PKP3 cells, indicative of elevated RUNX3 mRNA levels in PKP3-KO cells. To confirm these data, protein levels were analyzed (Figure 44C). In agreement with mRNA levels, c-MYC protein levels were unaltered, whereas RUNX3 protein levels were dramatically enhanced in PKP3-KO cells. This suggests that elevated RUNX3 may be responsible for increased p21 and reduced phospho-RB levels in PKP3-KO cells.
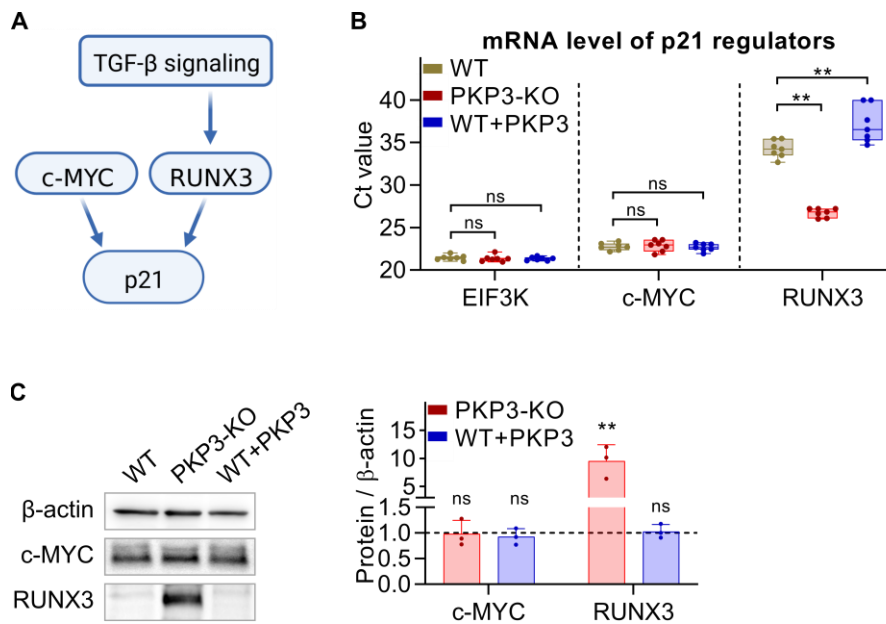
Figure 44 │ PKP3 inhibits RUNX3 mRNA and protein levels. (A) A schematic of the regulation of p21 by c-MYC and RUNX3, which is an effector of TGF-β signaling (created with biorender.com, modified from (Ito and Miyazono, 2003; Abbas and Dutta, 2009). **(B)** For analyzing mRNA levels of p21 regulators, WT, PKP3-KO, and WT+PKP3 cells were grown for 24 h in LCM and processed for qRT-PCR. EIF3K was used as an invariant endogenous control. Whereas Ct values of c-MYC were unaltered, analysis of RUNX3 mRNA levels revealed dramatically decreased Ct values in PKP3-KO and increased Ct values in WT+PKP3 cells compared to WT cells. The boxplot depicts the Ct values (n=7). The Whiskers extend to the minimum and maximum values. Statistical significance was determined by one-way ANOVA with Tukey's multiple comparisons test. **(C)** For analysis of the protein levels, WT, PKP3-KO, and WT+PKP3 cells were grown for 24 h in LCM and lysed in SDS lysis buffer. Total cell extracts were analyzed by western blotting with the indicated antibodies. Representative western blots (left panel) showing the protein levels of c-MYC and RUNX3. β-actin was used as a loading control. Whereas c-MYC protein level was unaltered, RUNX3 protein level was highly increased in PKP3-KO cells compared to WT cells. The bar plot (right panel) depicts the protein amounts (+ s.d.; n=3) normalized to β-actin and relative to WT cells (first lane in western blot). Statistical significance was determined by one-way ANOVA with Tukey's multiple comparisons test.

To more directly evaluate the putative link between RUNX3 and p21 expression, WT and PKP3-KO cells were transfected with non-targeting or RUNX3-directed siRNAs (Figure 45). RUNX3 siRNAs diminished RUNX3 protein level in PKP3-KO cells although the level as still somewhat elevated compared to WT cells. Importantly, downregulation of RUNX3 in PKP3-KO cells resulted in decreased abundance of p21 protein which was similar to the level measured in WT cells. This confirmed the assumption that RUNX3 regulates p21 expression in murine keratinocytes. Furthermore, RB phosphorylation was increased in RUNX3-depleted PKP3-KO cells, though it did not reach the level observed in WT cells. This might be due to the short time frame of the knockdown experiment. Nonetheless, this partial rescue of RB phosphorylation after RUNX3 knockdown in PKP3-KO cells suggests that PKP3-dependend elevation of RUNX3 promotes p21 expression, which results in impaired RB phosphorylation.
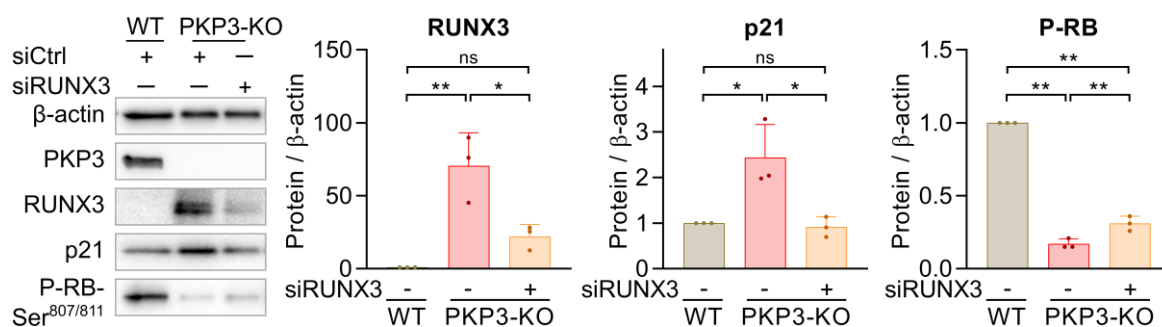
Figure 45 │ **RUNX3 protein increases p21 protein level but decreases RB phosphorylation.** For analyzing RUNX3 depletion, WT and PKP3-KO cells were transfected with non-targeting (siCtrl) or RUNX3-directed (siRUNX3) siRNAs, grown for 72 h in LCM, and lysed in SDS lysis buffer. Total cell extracts were analyzed by western blotting with the indicated antibodies. Representative western blots (left panel) showing the protein levels of RUNX3, p21, and phospho-RB. β-actin was used as a loading control. Depletion of RUNX3 in PKP3-KO cells resulted in decreased RUNX3 and p21 protein levels similar to WT cells, but enhanced RB phosphorylation. The bar plots (right panels) depict the protein amounts (+ s.d.; n=3) normalized to β-actin and relative to siCtrl-treated WT cells (first lane in western blot). Statistical significance was determined by one-way ANOVA with Tukey's multiple comparisons test.

Next, I wondered which signaling pathway contributes to the regulation of a RUNX3-p21 axis in murine keratinocytes. It has been reported that RUNX3 is regulated by TGF-β (Ito and Miyazono, 2003) and its inactivation is frequently associated with a kirsten rat sarcoma virus (KRAS)-mutated background, e.g. in human lung adenocarcinoma (Lee *et al.*, 2013). As KRAS protein becomes activated by EGF stimulation (Jancik *et al.*, 2010), a putative link between EGFR signaling and RUNX3 expression might be assumed. To analyze whether EGFR signaling via RAS-MEK-ERK might controls RUNX3 and p21 protein levels, WT cells were treated with gefitinib, a selective EGFR tyrosine kinase inhibitor (Figure 46A). As expected, gefitinib considerably reduced ERK1/2 phosphory-lation. Importantly, RUNX3 and p21 protein levels were significantly increased, suggesting a regulation via the EGFR-ERK signaling pathway. In accordance with enhanced RUNX3 and p21 protein levels, RB and phospho-RB were decreased in gefitinib-treated WT cells.
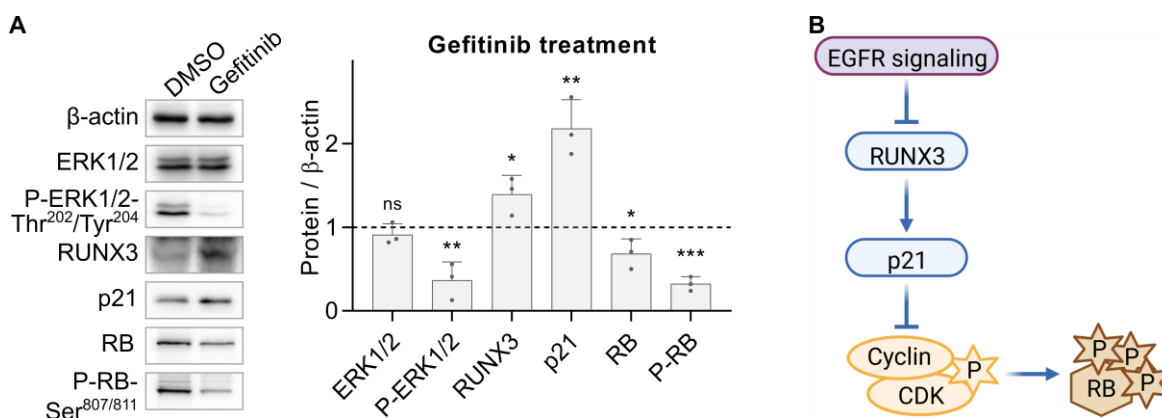
Figure 46 │ **EGFR signaling regulates RUNX3 and p21 protein levels and RB phosphorylation. (A)** For analysis of the effect of EGFR signaling, WT cells were grown for 24 h in LCM, treated with gefitinib (10 µM) for 24 h to inhibit EGFR, and lysed in SDS lysis buffer. Total cell extracts were analyzed by western blotting

with the indicated antibodies. Representative western blots (left panel) showing the protein levels of effectors downstream the EGFR. β-actin was used as a loading control. Impact of inhibitor was verified by impaired ERK phosphorylation. EGFR inhibition in WT cells resulted in enhanced RUNX3 and p21 protein levels, but decreased RB protein level and phosphorylation. The bar plot (right panel) depicts the protein amounts (+ s.d.; n=3) normalized to β-actin and relative to DMSO-treated WT cells (first lane in western blot). Statistical significance was determined by a student's unpaired two tailed *t*-test. **(B)** A schematic of the regulation of RUNX3, p21, and RB by EGFR signaling (created with biorender.com) demonstrates that EGF signaling blocks RUNX3 and p21 expression, which promotes RB phosphorylation.

Taken together, these results show that PKP3 inhibits p21 expression via RUNX3 regulation. Furthermore, mitogenic signaling via EGFR is required to block RUNX3 and p21 expression and allow RB phosphorylation and G1-S phase transition (Figure 46B).

4.2.6. PKP3 promotes EGFR signaling

In the first part of this thesis, it has been demonstrated that EGFR signaling controls PKP3 phosphorylation by RSKs, thereby modulating PKP3 function in desmosome formation, maturation, and adhesion. Furthermore in the previous chapter, it has been shown that EGFR signaling contributes to RUNX3 and p21 regulation of the RB pathway, which is linked to extra-desmosomal PKP3. To further elucidate the role of PKP3 in EGFR signaling, I asked whether PKP3 can regulate EGFR signaling and, if so, at which level this may occur (Figure 47A). First, the EGFR protein levels and phosphorylation were determined in WT, PKP3-KO, and WT+PKP3 cells (Figure 47B). The loss of PKP3 (PKP3-KO cells) resulted in decreased total EGFR protein level and its phosphorylation at multiple tyrosine residues. In contrast, WT+PKP3 cells had improved EGFR phosphorylation, which correlated with increased activation of its downstream targets MEK1/2, ERK1/2, and RSK. Importantly, RSK phosphorylation was impaired in PKP3-KO cells, which might indicate a regulation by PKP3. To further examine the role of PKP3 as a scaffold to promote EGFR signaling, putative binding partners of PKP3 were identified by immunoprecipitations. PKP3-GFP was affinity purified from WT+PKP3 cells (Figure 47C). EGFR and MEK1/2 did not co-purify with PKP3, whereas ERK1/2 and RSK1 co-precipitated, suggesting an association between these kinases and PKP3.
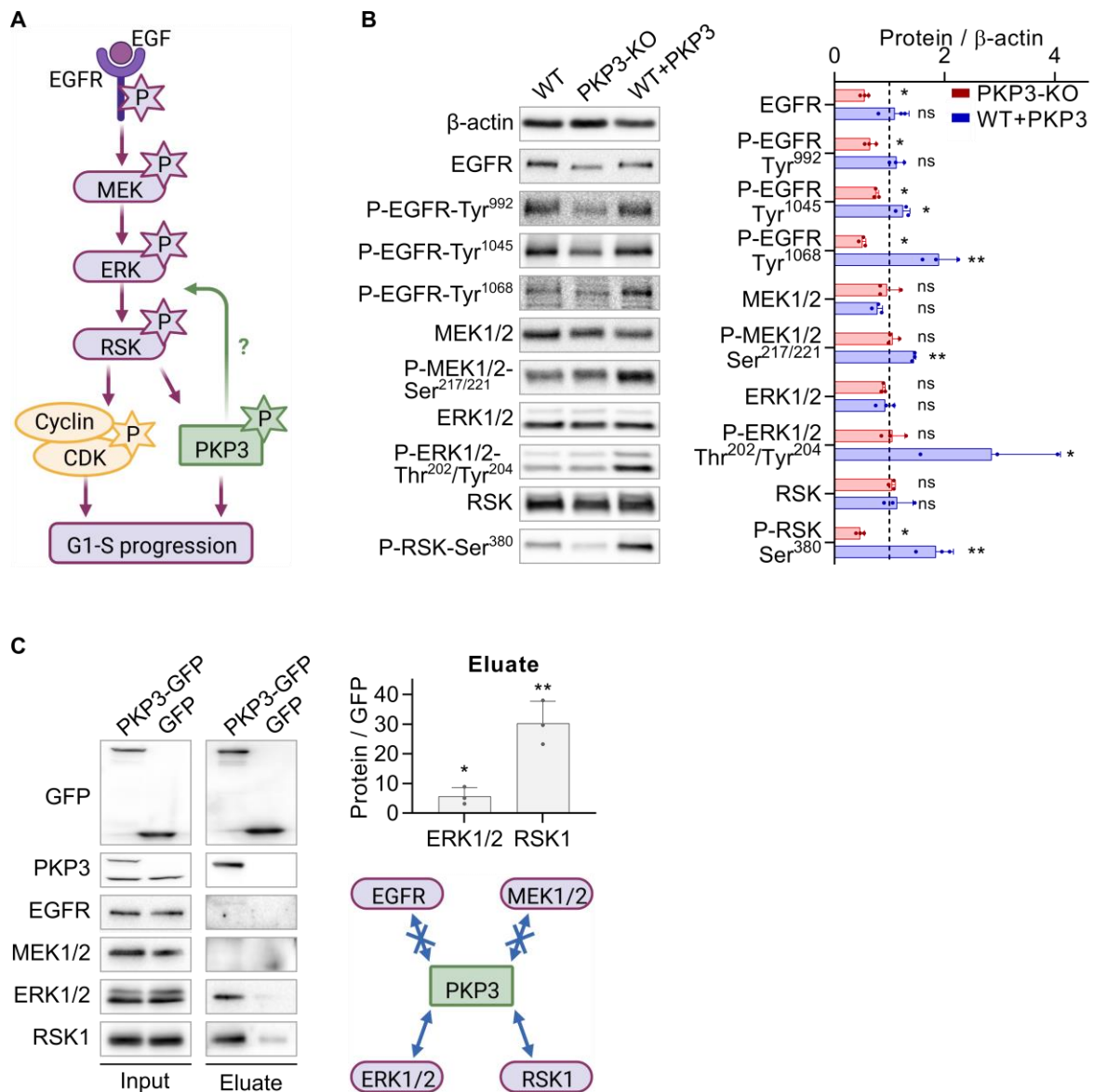
Figure 47 │ PKP3 promotes EGFR signaling. (A) A schematic of the regulation of G1-S phase progression by EGFR signaling (created with biorender.com) demonstrates that PKP3 might regulates the EGFR signaling pathway via the MEK-ERK-RSK axis. **(B)** For analysis of the protein levels, WT, PKP3-KO, and WT+PKP3 cells were grown for 24 h in LCM and lysed in SDS lysis buffer. Total cell extracts were analyzed by western blotting with the indicated antibodies. Representative western blots (left panel) showing the phosphorylation and levels of proteins involved in the EGFR signaling pathway. β-actin was used as a loading control. EGFR protein level and phosphorylation were decreased in PKP3-KO cells, but slightly increased in WT-PKP3 cells compared to WT cells. Whereas MEK1/2 and ERK1/2 phosphorylation was unaltered in PKP3-KO cells, RSK phosphorylation was significantly impaired in PKP3-KO cells and enhanced in WT+PKP3 cells. The bar plot (right panel) depicts the protein amounts (+ s.d.; n=3) normalized to β-actin and relative to WT cells (first lane in western blot). Statistical significance was determined by one-way ANOVA with Tukey's multiple comparisons test. **(C)** For analyzing putative PKP3 binding partners, PKP3-GFP or GFP were precipitated from ectopically expressing WT cells using GFP-trap agarose and probed for interaction by western blotting with the indicated antibodies. Representative western blots (left panel) showing total protein lysates labeled input, and immunoprecipitates which are eluated from the beads after the immunoprecipitation labeled eluate. In the PKP3 blot, the lower lane represents endogenous PKP3, the upper lane reflects PKP3-GFP. Whereas EGFR and MEK1/2 did not co-purify with PKP3, ERK1/2 and RSK1 co-precipitated. The bar plot (upper right panel) depicts the level of eluate proteins (+ s.d.; n=3) normalized to precipitated GFP and relative to the values of GFP-only cells (second lane in western blot). Statistical significance was determined by a student's unpaired two tailed *t*-test. The schematic (lower right panel, created with biorender.com) shows the role of PKP3 as a putative interaction partner of proteins involved in the EGFR signaling pathway.

But was the lack of RSK activity in PKP3-KO cells responsible for reduced RB phosphorylation? To more directly analyze this putative link, RSK depletion by siRNA-mediated knockdown in WT cells was performed in order to reduce RB phosphorylation. WT cells were transfected with non-targeting, RSK1-, or RSK2-directed siRNAs (Figure 48). RSK1 depletion significantly reduced RB phosphorylation, whereas RSK2 depletion did not affect RB protein level or phosphorylation. This suggests that RSK1 may be a key driver in RB regulation by PKP3.
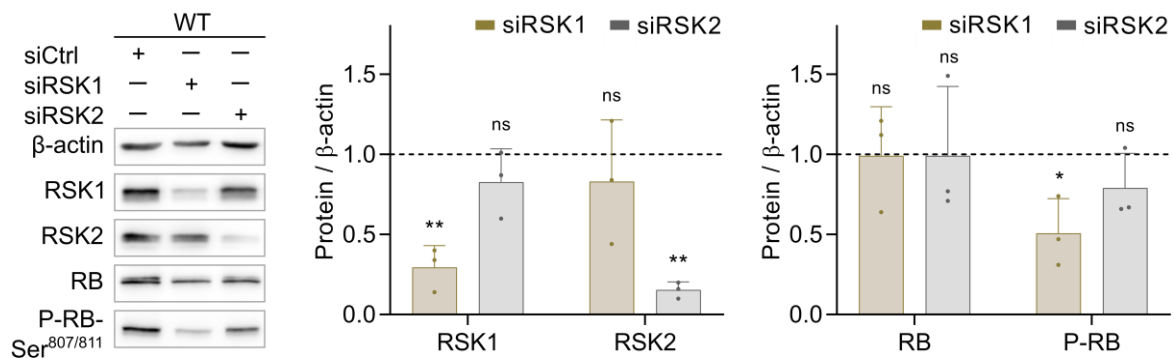
Figure 48 │ RSK1 promotes RB phosphorylation. For analyzing RSK depletion, WT cells were transfected with non-targeting (siCtrl), RSK1, or RSK2 (siRSK1, siRSK2, respectively) directed siRNAs, grown for 72 h in LCM, and lysed in SDS lysis buffer. Total cell extracts were analyzed by western blotting with the indicated antibodies. Representative western blots (left panel) showing the protein levels of RSK1, RSK2, RB, and phospho-RB. β-actin was used as a loading control. Knockdown of RSK1 or RSK2 was verified by impaired RSK1 and RSK2 protein levels, respectively. Depletion of RSK1 in WT cells resulted in decreased RB phosphorylation, whereas RSK2 did not affect RB protein level and phosphorylation compared to siCtrl-treated WT cells. The bar plots (right panels) depict the protein amounts (+ s.d.; n=3) normalized to β-actin and relative to siCtrl-treated WT cells (first lane in western blot). Statistical significance was determined by one-way ANOVA with Tukey's multiple comparisons test.

Collectively these results uncover a role of PKP3 as a scaffold in EGFR signaling. PKP3 improved RSK1 phosphorylation thereby enhancing signaling downstream of EGFR. In contrast, the loss of PKP3 resulted in the dysregulation of EGFR signaling with reduced RSK activity, which contributes to impaired RB phosphorylation and cell cycle progression.

4.2.7. Summary

In summary of this chapter, non-transformed murine keratinocytes were used to analyze the extra-desmosomal role of PKP3 as a scaffold for signaling and its contribution to proliferation. The loss of PKP3 (PKP3-KO cells) leads to a delayed progression from G0/G1 to S phase of the cell cycle, resulting in reduced proliferation whereas PKP3-GFP expressing WT cells reveal elevated proliferation. Since differentiation is not enhanced or accelerated, permanent exit of PKP3-KO cells from the cell cycle can be precluded. PKP3 expression correlates directly with RB phosphorylation, which is a key event to allow S phase entry, and E2F-dependent target gene expression, including genes required for cell

cycle progression. Mechanistically, PKP3 interacts with phosphorylated RB in the cytoplasm, which may contribute to reducing RB in the nucleus and decrease the inhibitory RB-E2F interaction in the nucleus. Increased levels of the key cyclin-dependent kinases CDK4 and CDK6 does not rescue RB phosphorylation in PKP3-KO cells, suggesting that these kinases are not fully active. Furthermore, expression of the CDK inhibitor p21 inversely correlates with PKP3 levels. Reducing p21 protein levels by knockdown in PKP3-KO cells rescues RB phosphorylation supporting the idea that CDKs are not fully active in PKP3-KO cells. In addition, the transcription factor RUNX3 was identified as a key factor in controlling p21 expression in PKP3-KO cells. RUNX3 is inversely correlated with PKP3 expression levels and is suppressed by an EGFR-ERK signaling axis. Finally, I show that PKP3 promotes EGFR-dependent signaling, as indicated by increased RSK- and ERK phosphorylation and an association of PKP3 with these kinases. Taken together, this chapter of the thesis focused on the regulation of PKP3 in terms of proliferation and identifies a role of PKP3 in promoting a ERK/RSK-RUNX3-p21-RB-E2F1 signaling axis that controls proliferation in non-transformed murine keratinocytes.

5. DISCUSSION

Desmosomes have long been considered as more or less static structures that provide strong adhesion to force-exposed tissues such as the skin epidermis and the heart. However, epidermal regeneration depends on proliferation and cell movement implicating the requirement for dynamic modulation of adhesion. In the epidermis, proliferation is restricted to the basal layer whereas suprabasal layers are crucial for barrier formation (Sumigray and Lechler, 2015) implicating that desmosomal adhesion must differ between these layers. While cell type specific expression of desmosomal cadherins and PKPs has been known for years, little is known about how PKP isoforms impact on desmosomal properties and how desmosomal localization of these isoforms is regulated. Furthermore, PKPs perform additional functions in the nucleus and the cytoplasm that are not well characterized. Owing to their dual function in regulating desmosome adhesion and extra-desmosomal signaling, regulation of their localization is of special interest. Thus, this thesis focused on the role of PKP3 in adhesion as well as proliferation, and reports several novel findings that considerably improve the understanding of PKP3's function and regulation.

5.1. PKP3 and EGFR signaling are mutually dependent on each other

Promoting tissue integrity, PKP1-3 assist in linking desmosomal cadherins to intermediate filaments at desmosome junctions. PKP1 is absolutely essential for epidermal adhesion as revealed by neonatal lethality in PKP1-KO mice and severe skin disease in humans (Rietscher *et al.*, 2016; Doolan *et al.*, 2020). In contrast, PKP3 deficiency causes mild skin blistering and an increased risk of inflammatory reactions pointing to a putative function during skin barrier formation (Sklyarova *et al.*, 2008). Furthermore, PKP1 and PKP3 have distinct functions in intercellular adhesion that is reflected by their complementary expression levels during keratinocyte differentiation. PKP3, which outbalances PKP1 in the basal layer, confers dynamics to desmosomes, whereas PKP1, which predominates in the suprabasal layers, imparts stability (Keil *et al.*, 2016). These complementary functions suggest a differentiation-specific and coordinated regulation in keratinocytes. Although the ratio of both proteins varies during keratinocyte differentiation, PKP1 and PKP3 are co-expressed, suggesting that they are regulated by distinct growth factors and signaling pathways. Whereas PKP1 is phosphorylated by AKT2 via IGF-1/insulin signaling (Wolf *et al.*, 2013), I showed that PKP3 phosphorylation at AGC-kinase consensus sites was not affected by insulin signaling, suggesting that the IGF-1/insulin pathway does not regulate PKP3. In contrast, PKP3 phosphorylation was induced by RSKs via EGF

signaling, which promoted PKP3 recruitment to the lateral plasma membranes. The proposed model shows how PKP1 and PKP3 are regulated to balance stability and dynamic of the epidermis (Figure 49). The basal layer of the epidermis is composed of cells maintained in a proliferative state (Alonso and Fuchs, 2003), which requires dynamic cell-cell interactions. In contrast, the barrier function of the suprabasal layer depends on strong and stable cellular adhesion (Sumigray and Lechler, 2015). This change in cell contacts from basal to suprabasal layers can be achieved by altered composition and post-translational modifications such as phosphorylation. PKP1 and PKP3 display complementary expression patterns in the epidermis with PKP3 highly expressed in basal cells and increasing amounts of PKP1 in suprabasal cells. In basal cells, IGF-1/insulin mediated modification of PKP1 prevents the formation of PKP1-dependent hyper-adhesive desmosomes since phosphorylated PKP1 by AKT2 relocalizes from desmosomes to the cytoplasm. In the cytoplasm, PKP1 interacts with the translation initiation complex to promote protein synthesis thereby stimulating proliferation and maintaining cells in a proliferation competent state (Wolf *et al.*, 2010; Wolf *et al.*, 2013). At the same time, PKP3 in response to EGF signaling and phosphorylation by RSKs initiates the formation of dynamic desmosomes in the basal layer of the epidermis by lateral localization of phosphorylated PKP3. This results in stable but dynamic cell adhesion in the basal cells. Upon transition to the suprabasal layers, the impact of EGF- and IGF-1/insulin signaling decreases through diminished receptor expression and activation (Gazel and Blumenberg, 2013; Joly-Tonetti *et al.*, 2021). Thus, un-phosphorylated PKP1 localizes mainly at lateral contacts, which displaces PKP3 into tricellular regions. This allows formation of stable PKP1-dependent desmosomes and promotes the barrier function of the suprabasal layer. As EGFR is also expressed in suprabasal layers and EGFR-dependent signaling in the granular layer induces tight junction formation (Rubsam *et al.*, 2017), EGF signaling might promote epidermal sealing by directing phosphorylated PKP3 into the tricellular junctions of desmosomes. Finally, the proposed model highlights the differential functions of PKP1 and PKP3 in regulating keratinocyte adhesion versus proliferation, and how these functions are independently but coordinately regulated by distinct signaling pathways.
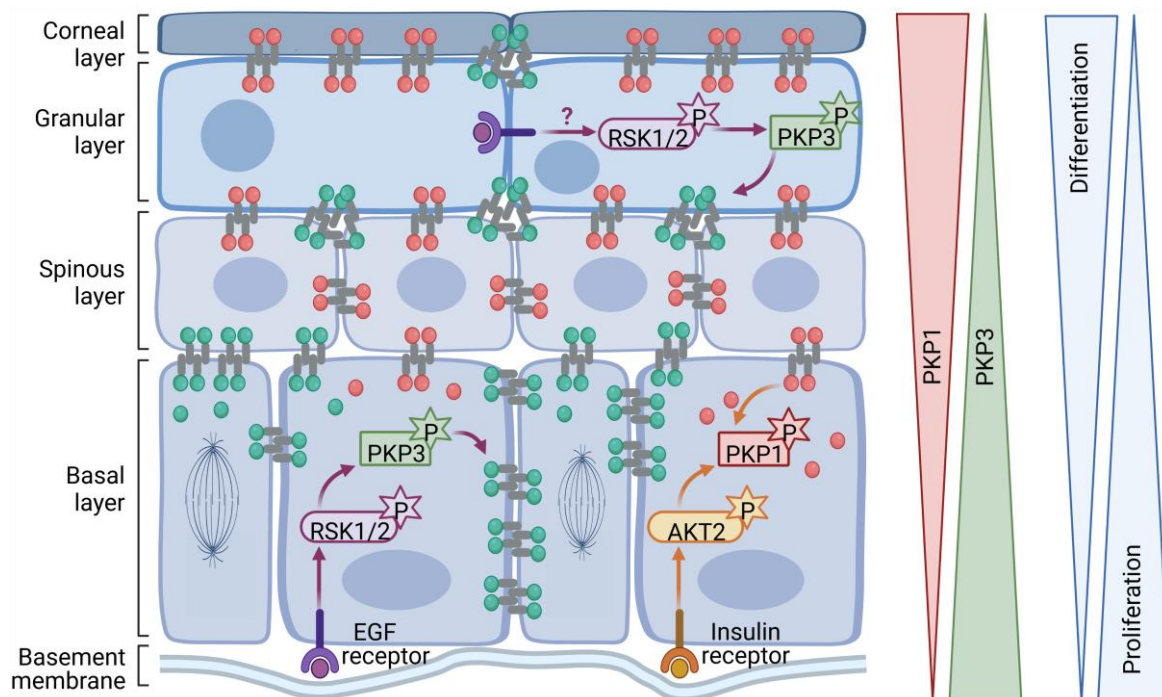
Figure 49 │ Proposed model depicting the regulation of PKP1 and PKP3 by insulin and EGF signaling in the epidermis. Created with biorender.com. PKP1 and PKP3 display complementary expression patterns in the epidermis with PKP1 (red) primarily expressed in the superficial epidermal layers, whereas PKP3 (green) shows increased expression in the basal layer. In basal cells, PKP1 is regulated by insulin signaling via AKT2. Phosphorylated PKP1 relocalizes from lateral desmosomes into the cytoplasm (indicated as red bubbles), which promotes proliferation by stimulating translation. In contrast, PKP3 is regulated by EGF signaling via RSK1/2-meadiated phosphorylation. Phosphorylated PKP3 localizes at lateral contacts, which increase cell-cell adhesion when desmosomal PKP1 is low. This results in dynamic intercellular adhesion in the high-proliferative basal epidermal layer. In suprabasal cells with high PKP1 expression, attenuation of insulin signaling results in lateral localization of unphosphorylated PKP1 with increased desmosome number an onset of hyper-adhesion. Thereby, PKP3 is displaced from lateral into tricellular regions, which might be facilitated by EGFR signaling in the granular layer. This results in stabilization of cellular adhesion in the differentiated suprabasal epidermal layers.

This thesis not only highlights that PKP3 itself is regulated by RSKs downstream of EGFR signaling, but also reveals a scaffold role of PKP3 in modulating EGFR signaling. I showed that loss of PKP3 decreased EGFR and RSK phosphorylation, whereas PKP3 overexpression resulted in increased EGFR, MEK, ERK, and RSK phosphorylation. Furthermore, PKP3 interacted with ERK1/2 and RSK1, suggesting a link between PKP3 and mitogenic signaling downstream of the EGFR.

EGFR signaling leads to activation of CDKs by ERK phosphorylation (Chambard *et al.*, 2007), which maintains keratinocytes in the basal layer in a proliferative state. In ovarian cancer cells, PKP3 silencing results in decreased phosphorylation of ERK1/2, whereas PKP3 overexpression leads to increased ERK1/2 phosphorylation and cell proliferation ratio (Lim *et al.*, 2019). The molecular mechanism how PKP3 modulates proliferation via EGFR signaling is so far not understood. RSK1 not only regulates the desmosomal function of PKP3, the kinase also contributes to proliferation (Anjum and Blenis, 2008), which I

confirmed by demonstrating a direct effect of RSK1 level on RB phosphorylation. An interaction of ERK near the C-terminus of RSK1 initiates its activation (Smith *et al.*, 1999), resulting in RSK1 autophosphorylation at Ser^{380} (Romeo *et al.*, 2012). Subsequent full activation of RSK1 allows phosphorylation of downstream targets, including PKP3. In PKP3-KO cells, RSK phosphorylation at Ser^{380} was significantly decreased. This suggests reduced RSK1 autophosphorylation possibly driven by impaired ERK binding to RSK1. PKP3 interacted with ERK1/2 as well as RSK1, and PKP3 overexpression stimulated ERK and RSK phosphorylation. Thus, PKP3 may act as scaffold for the kinases to extend signaling downstream of EGFR.

As EGFR signaling is a driver for cancer progression (Sigismund *et al.*, 2018), EGFR inhibitors are an important therapeutic option for patients with malignant tumors. However, cutaneous side-effects are frequently observed during therapy (Holcmann and Sibilia, 2015). Understanding EGFR signaling in the epidermis not only with respect to proliferation and survival pathways but also with respect to cell-cell adhesion may help to understand these unwanted effects. This thesis unravels the EGFR-dependent molecular regulation of PKP3's function in adhesion as well as proliferation and might provide results from basic research, which may eventually contribute to improved treatment options for skin cancer patients.

5.2. PKP3 is phosphorylated by RSKs

Kinase cascades and phosphorylation of target proteins are well known to modulate the localization and function of numerous proteins. However, concerning desmosomes, the current knowledge of post-translational modifications and their impact is limited. Desmoplakin, the linker protein between desmosomal cadherins and the keratin network, is the best studied desmosomal protein with respect to phosphorylation. Its C-terminus is phosphorylated by PKC (Stappenbeck *et al.*, 1994; Amar *et al.*, 1999; Kroger *et al.*, 2013) or glycogen synthase kinase 3 (GSK3) (Albrecht *et al.*, 2015), which seems to modulate desmoplakin's interaction with keratins. Although numerous phosphorylation sites have been detected in the desmoplakin N-terminus which interacts with the PKPs and plakoglobin and recruits desmoplakin to the desmosomes (Kowalczyk *et al.*, 1997; Bornslaeger *et al.*, 2001), the impact of responsible kinases have not been characterized so far. However, the large negatively charged phosphate group might disrupt the molecular composition within the desmosomal plaque, resulting in disordered binding with a lower affinity and reduced cell-cell adhesion. Thus, phosphorylation of desmoplakin coordinates cytoskeletal dynamics and cellular adhesion.

For PKP3, phosphorylation at Ser[285] has been shown to promote its association with stratifin, which resulted in the cytoplasmic accumulation of phosphorylated PKP3 and limited exchange with desmosomal PKP3 (Roberts *et al.*, 2013). The decreased desmosomal PKP3 exchange correlated with increased adhesion and impaired migration. Cytoplasmic localization of PKP3 is further driven by its phosphorylation at Tyr[195] by c-Src kinase (Neuber *et al.*, 2015). Tyr[195]-phosphorylated PKP3 relocalized from desmosomes into the cytoplasm. As phosphorylated PKP3 was released from the desmosomes, a role in desmosome disassembly might be suggested. However, Tyr[195] phosphorylation was transient and the modification was only detected after EGFR activation when at the same time tyrosine phosphatases were inactivated. The detailed mechanism and consequences of this modification remain to be determined. In contrast, PKP3 phosphorylation at Ser[134/135] by RSKs might support desmosome assembly in keratinocytes (Müller *et al.*, 2020). Mutations of the RSK phosphorylation site (serine to alanine and serine to glutamic acid) reflect the effects of RSK inhibition and overexpression, respectively. PKP3-Ser[134/135]Ala mutant showed punctate lateral desmosomes and less tricellular PKP3, whereas the phospho-mimetic mutant PKP3-Ser[134/135]Glu localized at tricellular junctions, suggesting that PKP3 phosphorylated at Ser[134/135] positively correlates with cellular adhesion. These findings demonstrate that RSK mediated phosphorylation of the desmosomal protein PKP3 supports adhesion whereas in most cases described so far phosphorylation compromised intercellular adhesion. Thus, PKP3 phosphorylation both positively and negatively regulates desmosome assembly (Figure 50).
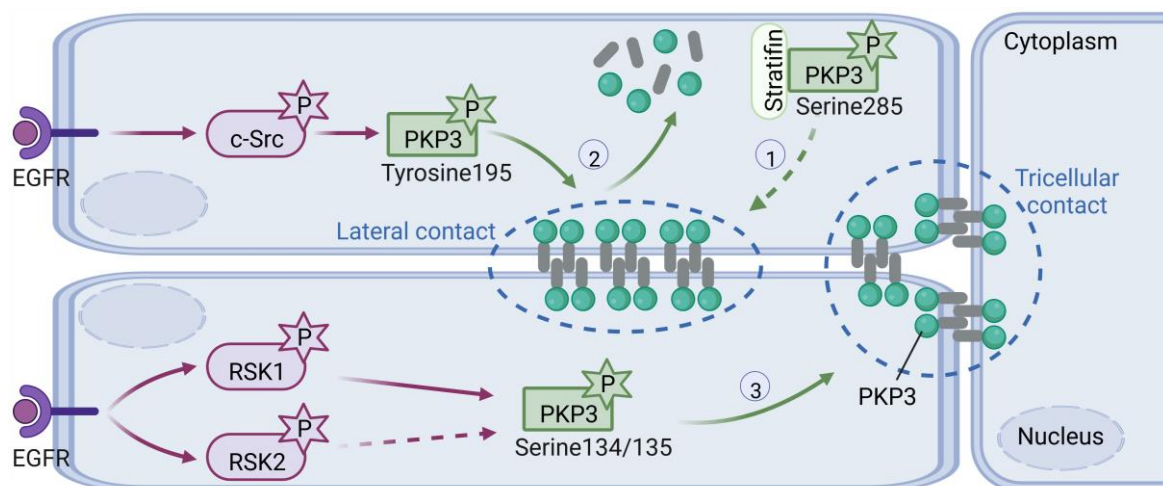
Figure 50 │ Phosphorylation of PKP3 modulates its localization. Created with biorender.com. (1) Phosphorylation of PKP3 at Ser[285] by stratifin results in accumulation of cytoplasmic PKP3 and limited exchange with desmosomes (shown by a dashed arrow line), which correlates with increased adhesion but decreased migration (Roberts *et al.*, 2013). (2) Cytoplasmic accumulation of PKP3 is also driven by its phosphorylation at Tyr[195] by EGFR-signaling activated c-Src kinase, resulting in decreased desmosomal PKP3 localization (Neuber *et al.*, 2015), suggesting desmosome disassembly. (3) In contrast, EGFR-signaling

activated RSK1/2 phosphorylate PKP3 at Ser[134/135], which promotes its localization in tricellular regions, resulting in increased cellular adhesion (Müller *et al.*, 2020).

5.3. PKP3 regulates proliferation in a differentiation-independent manner

Epidermal homeostasis is essential for maintaining tissue integrity and is regulated by stem cells in epithelial tissues (Sotiropoulou and Blanpain, 2012). Stem cells replace the keratinocytes that are lost through normal differentiation or through cell death following injury. A balance between the proliferating self-renewing cells in the epidermal basal layer and the differentiated cells in the suprabasal layers has to be maintained to avoid a variety of skin diseases, including cancer progression (Pierard, 2012). The molecular mechanisms that orchestrate proliferation and differentiation in the epidermis remain incompletely understood. Extra-cellular signals, including growth factors, and cell-intrinsic information regulate the decision between going through a division cycle or arresting cell division (Wang, 2021). If cells arrest, they can undergo reversible quiescence by entering temporarily the non-proliferative state G0 or the cells irreversible enter G0 phase, which induces terminal differentiation with the simultaneous inability to proliferate (Marescal and Cheeseman, 2020). Both quiescent and terminal differentiated cells are characterized by a prolonged G0/G1 phase, impaired E2F activity, high levels of hypo-phosphorylated RB, and increased CDKN activity (Buttitta and Edgar, 2007). Despite these similarities, quiescent cells actively prevent differentiation allowing them to reenter the cell cycle.

Using PKP3-KO and PKP3-overexpressing cells, a clear correlation of PKP3 expression and cellular proliferation was demonstrated. WT+PKP3 cells showed increased proliferation, which was characterized by a reduced number of cells in G0/G1 phase. In contrast, the loss of PKP3 (PKP3-KO cells) led to impaired proliferation and a prolonged G0/G1 phase, resulting in a delay in S phase entry. As the protein levels of differentiation markers was unaffected or reduced in the PKP3-KO cells, these cells entered a state of transient quiescence instead of starting the differentiation program prematurely. This implicates a function of PKP3 in stem cell maintenance of the epidermis by its positive effect on G0/G1-S phase transition of the cell cycle.

5.4. PKP3 mediates the RB pathway to promote cell cycle progression

The mechanisms that maintain the balance between proliferation and differentiation primarily affect cell cycle progression. RB protein is the central cell cycle regulator that controls the G1-S phase transition (Giacinti and Giordano, 2006). As PKP3 contributes to G1 to S phase progression, an extra-desmosomal role of PKP3 in regulating the RB

pathway has to be assumed. Furthermore, PKP3 promoted EGFR signaling and was itself regulated by EGFR signaling. The first pulse of EGFR signaling induces exit from quiescence into G1 phase by increasing the expression of cyclins and the activation of CDKs, which finally leads to RB phosphorylation and the progression through the restriction point (Wee and Wang, 2017). In non-transformed murine keratinocytes, the RB pathway was clearly regulated by PKP3 expression. The loss of PKP3 (PKP3-KO cells) led to decreased levels of total RB and especially, phospho-RB. In contrast, PKP3 overexpression resulted in up-regulation of total RB and phospho-RB. This suggests a PKP3-dependent regulation of RB.

RB phosphorylation is mediated by cyclin-CDK complexes (Harbour *et al.*, 1999; Topacio *et al.*, 2019). While the CDK4 protein level was not affected by PKP3, CDK6 was down-regulated in PKP3-KO cells. However, the level of phospho-CDK6-Thr[177] which is supposed to represent the active form, was essentially unaltered. Furthermore, overexpression of CDK6 did not enhance RB phosphorylation in PKP3-KO cells, suggesting that lack of CDK6 was not the major driver of prolonged cell cycle exit. Furthermore, increased CDK2 protein levels in the PKP3-KO cells excluded a lack of CDK2 being responsible for reduced RB hyper-phosphorylation. However, it cannot be excluded that CDKs might not be fully active in the absence of PKP3 since additional factors besides threonine phosphorylation may be required. Alternatively, PKP3 may intervene downstream of cyclin-CDK complexes.

PKP3 not only increased the total RB level and its phosphorylation, it also bound to RB and its interaction depended on the subcellular localization. Using immunoprecipitations, an association between PKP3 and RB as well as phospho-RB was demonstrated. In murine keratinocytes, stably overexpressed PKP3 showed cytoplasmic as well as nuclear localization, which enables protein interactions in both compartments. Cell fractionation and immunofluorescence studies revealed that the majority of total RB localized in the nucleus, whereas minor amounts representing phospho-RB accumulated in the cytoplasm. Nonetheless, PKP3 interaction occurred, at least primarily, in the cytoplasm. This suggests, that PKP3 interacted primarily with phospho-RB *in vivo*. However, phosphorylation was not a prerequisite for PKP3 binding, since a RB mutant lacking all CDK phosphorylation sites (Narasimha *et al.*, 2014) was still able to bind PKP3. Mechanistically, this means (1) that the interaction is regulated by intracellular localization which depends on RB post-translational modification and (2) that PKP3 binds and retains phospho-RB in the cytoplasm thereby preventing its de-phosphorylation and/or inhibitory function in the nucleus to improve E2F activity and thus promote proliferation.

RB can interact with other proteins via two sites: the A and B domains in the RB pocket which binds the E2F transcription factor, and the side surface of the pocket domain which mediates interactions via a conserved LxCxD/E motif (in which x represents any amino acid residue) in the target proteins (Dahiya *et al.*, 2000; Kalejta *et al.*, 2003; Wang *et al.*, 2012). An interaction between RB and LxCxD/E motif carrying proteins may promote E2F detachment and thus cell cycle progression (Ramanujan *et al.*, 2021). The conserved LxCxD/E motif is not present in PKP3. However, a similar motif comprising the sequence LSCSR (LTCSR in mouse) might represent a RB binding site although the non-conservative exchange of an acidic amino acid (D/E) to a basic amino acid (R) in the motif could interfere with RB binding. Future studies could address the role of this motif by generating a mutant PKP3 lacking this motif and testing for its RB association.

In this thesis, I have identified a novel function of PKP3 in promoting proliferation via the RB-E2F pathway and unraveled the molecular mechanism of its extra-desmosomal function in G1-S phase transition.

5.5. PKP3 regulates the RB pathway via an EGFR-RUNX3-p21 axis

Alterations in the RB pathway are typically associated with dysregulation of the cell cycle. A key regulator involved in inhibiting the RB pathway is p21, which is encoded by *CDKN1A* gene. p21 mediates RB degradation and inhibits CDK activities (Harper *et al.*, 1995; Broude *et al.*, 2007) . Furthermore, p21 not only influences proliferation via protein-protein interactions with cyclins and/or CDKs, but can also interact directly with E2F1, reducing its transcriptional activity (Dimri *et al.*, 1996).

In murine keratinocytes, the p21 protein level was inversely correlated with RB phosphorylation. Moreover, PKP3 suppressed p21 mRNA and protein levels, its inhibitory effect on RB phosphorylation, and its nuclear localization. The regulatory function of p21 is mediated by its intracellular localization (Abbas and Dutta, 2009; Georgakilas *et al.*, 2017). Nuclear p21 acts as a tumor suppressor by inactivating cyclins and/or CDKs, which prevents cell cycle progression (Al Bitar and Gali-Muhtasib, 2019). Elevated nuclear p21 levels in PKP3-KO cells point to a central role in mediating the prolonged G0/G1 phase in these cells.

As p21 mRNA was increased in PKP3-KO cells, the transcriptional regulation was analyzed. One of the best known p21 suppressors is c-Myc, which is highly expressed in cancer cells. Overexpression of c-Myc leads to activation of oncogenes, but suppression of cell cycle inhibitors, including p21 (Jung *et al.*, 2010). Although PKP3-KO cells showed increased p21 levels, c-Myc mRNA and protein levels were not altered by PKP3. In

contrast, RUNX3 was found as a key mediator of p21 expression in murine keratinocytes. The tumor suppressor RUNX3 promoted p21 protein level, led to impaired RB phosphorylation, and was strongly increased in PKP3-KO cells. RUNX3 activity is closely associated with TGF-β signaling (Ito and Miyazono, 2003), but in addition deletion of RUNX3 in mouse lung causes the development of lung adenomas and accelerated KRAS-induced progression into adenocarcinomas (Lee *et al.*, 2013), suggesting a modulation between RUNX3 and EGFR signaling. I confirmed a positive correlation between RUNX3 and p21 levels and showed that EGFR signaling suppressed RUNX3 and p21. These results link PKP3 to the control of an EGFR-RUNX3-p21 signaling axis to promote RB phosphorylation and cell cycle progression (Figure 51).

Moreover, the data unravel the molecular mechanism of PKP3's function as an oncogene which has been described in various tumors. However, despite PKP3's role as an oncogene facilitating tumor cell growth, there are some examples where PKP3 was downregulated in tumor tissue (Papagerakis *et al.*, 2003; Takahashi *et al.*, 2012). The role of PKP3 may depend on tissue and cell type and on the activation of distinct signaling pathways. This might support the hypothesis that PKP3 is a "dual role cancer driver gene", which can exhibits oncogene or tumor suppressive behavior depending on the biological context (Colaprico *et al.*, 2020). Despite distinct functions in adhesion and signaling, the basic principle that intracellular localization determines function is conserved between PKP1 and PKP3. Desmosomal PKP1 acts as a tumor suppressor by promoting desmosomes stability (Keil *et al.*, 2016), whereas cytoplasmic PKP1 acts as an oncogene, where it stimulates proliferation by enhancing protein synthesis in an eIF4A-dependent pathway (Wolf *et al.*, 2010). This is controlled by IGF-1/insulin and AKT2 signaling (Wolf *et al.*, 2013). In contrast, recruitment of PKP3 to the cell border is driven by EGF signaling to facilitate desmosome assembly. PKP3 acts as a tumor suppressor in desmosomes, where it stabilizes intercellular adhesion by its association with RSKs. Cytoplasmic PKP3 regulates the RB pathway via an EGFR-RUNX3-p21 axis, which promotes proliferation and exhibits the role of PKP3 as an oncogene. Thus, it may be a general principle that PKPs are dual role cancer driver genes with tumor suppressive functions when localized in desmosomes and oncogenic characteristic in the cytoplasm or nucleus.
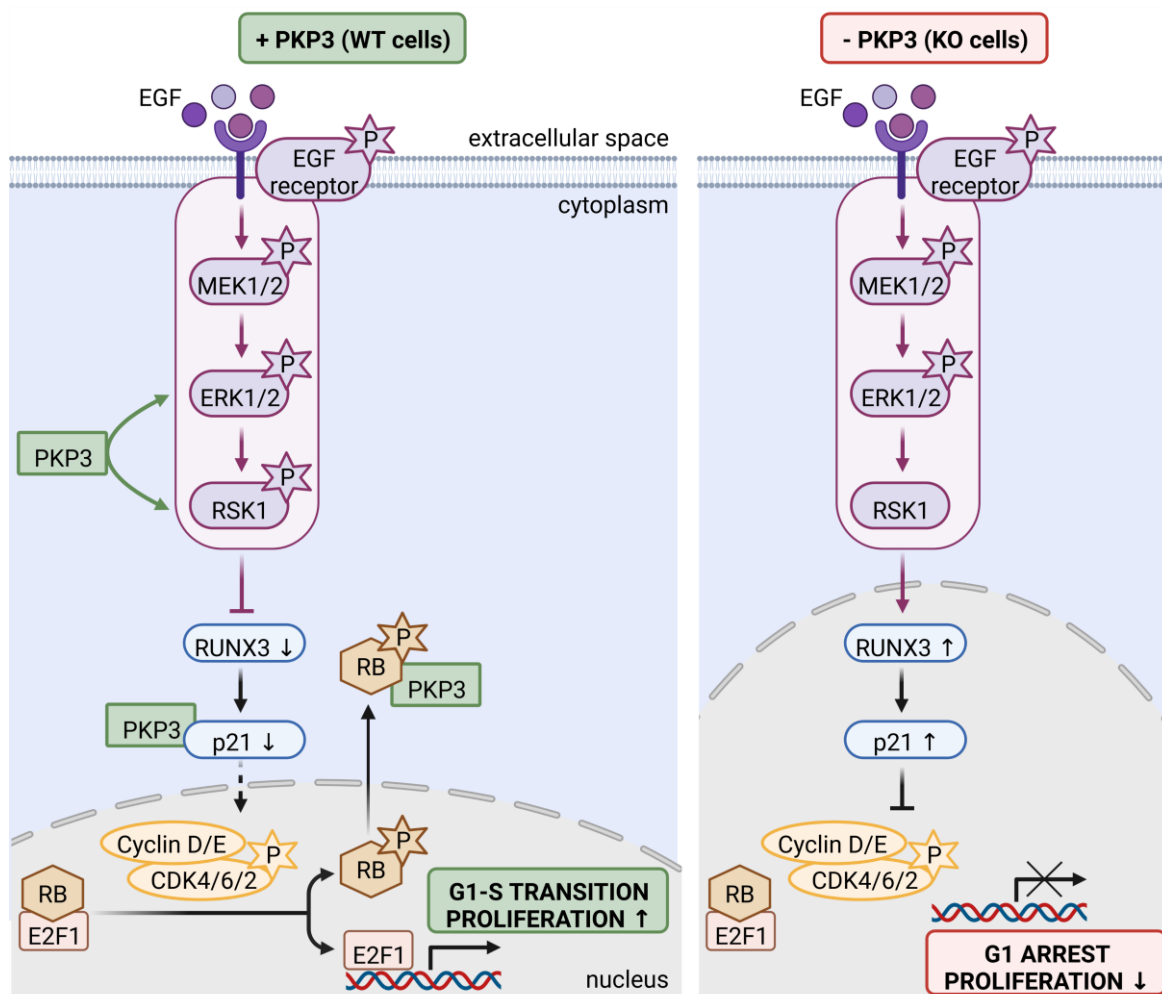
Figure 51 │ **Proposed model depicting the regulation of cell cycle progression by PKP3.** Created with biorender.com. In PKP3-expressing WT cells (left panel), PKP3 supports EGFR signaling via a feedforward mechanism, which suppressed RUNX3 level and its transcriptional target p21. This promotes the phosphorylation and activation of cyclin-CDK complexes, RB phosphorylation, and E2F1 release. PKP3 also sequesters phosphorylated RB in the cytoplasm to promote E2F1 activity, resulting in G1-S phase transition and enhanced proliferation. In contrast, the loss of PKP3 (PKP3-KO cells, right panel) results in impaired RSK1 phosphorylation, which increases RUNX3 and p21 levels. Elevated nuclear p21 prevents RB phosphorylation and E2F1 target gene expression, leading to G1 arrest and reduced proliferation.

5.6. Future perspective: Crosstalk between cellular junctions and signaling pathways in regulating adhesion and proliferation

The stratified epidermis requires adhesive contact remodeling to maintain its structural integrity. Although adherens junctions and desmosomes are separate structures with different protein compositions, it is well accepted that adherens junctions cooperate with desmosomes in providing tight intercellular adhesion (Sumigray and Lechler, 2015; Rubsam *et al.*, 2018). However, the exact molecular crosstalk between these two adhesive structures in the epidermis is not precisely understood. Both the classical cadherins of adherens junctions and the desmosomal cadherins associate through their cytoplasmic

domains with interacting proteins that mediate for cytoskeletal binding and strong adhesion (Garcia *et al.*, 2018; Zimmer and Kowalczyk, 2020). These proteins include members of the armadillo and armadillo-related families such as the desmosomal proteins plakoglobin and PKP1-3, as well as the adherens junction proteins β-catenin and p120-catenin. Furthermore, these proteins can be incorporated into both adherens junctions and desmosomes (Cowin *et al.*, 1986; Bierkamp *et al.*, 1999; Rickelt *et al.*, 2010), suggesting a synergistic contribution to adhesive strength. In addition, PKP3 has been characterized as a protein with a broad repertoire of interaction partners, as it directly interacts with plakoglobin, desmoplakin, all desmogleins and desmocollins (Bonne *et al.*, 2003). Furthermore, PKP3 associates with E-cadherin to initiate desmosome assembly (Gosavi *et al.*, 2011) or to promote adherens junction maturation (Todorovic *et al.*, 2014). This shows a direct or indirect involvement of PKP3 in regulating cell-cell adhesion by desmosomes and/or adherens junctions to maintain epidermal integrity.

Intercellular adhesion is also constantly subjected to modulation, especially during epithelial mesenchymal transitions (EMT) in which epithelial cells acquire mesenchymal features (Ribatti *et al.*, 2020). EMT is accompanied by the loss of adherens junctions and the simultaneously increase of mesenchymal markers. In contrast to the strictly regulated EMT required during development and tissue regeneration, deregulated EMT occurs during cancer progression where cells leave the epithelial layer in order to migrate to other tissues (Son and Moon, 2010). In skin cancer, the loss of desmoplakin and E-cadherin promotes EMT (Hodorogea *et al.*, 2019). Furthermore, a link between PKP3 and EMT in human cancer progression has been reported (Aigner *et al.*, 2007). The transcription factor ZEB1 not only prevented the formation of adherens junctions by repressing E-cadherin, but also induced the disassembly of desmosomal structures. E-cadherin and PKP3 as EMT-associated genes were also confirmed in colorectal cancer (Jackstadt *et al.*, 2013). This suggests that adherens junctions and desmosomes synergistically coordinate mechanics and signaling to orchestrate tissue function, whereas deregulation leads to subsequent changes in normal cellular mechanisms which might facilitate cancer progression.

The function of junctional proteins is further modulated by their subcellular localization. Several studies have already shown that proteins of the adherens junctions, especially β-catenin, play an important role in controlling proliferation and differentiation due to their extra-desmosomal role in the cytoplasm and/or nucleus. Cytoplasmic stabilization of β-catenin is essential for the activation of the canonical Wnt signaling pathway. The Wnt mediated protection of β-catenin from degradation allows shuttling of β-catenin into the nucleus to induce Wnt target gene expression (MacDonald *et al.*, 2009; Yu *et al.*, 2021).

Furthermore, β-catenin enables a crosstalk between Wnt and Hippo signaling pathways (Kim and Jho, 2014) and might be a convergent point between EGFR and Wnt signaling pathways (Hu and Li, 2010). This crossregulation of multiple signaling pathways is essential for balanced cell growth. For PKP3, a nuclear shuttling following Wnt pathway activation increased the expression of Wnt target genes (Hong *et al.*, 2021), suggesting a similar role as established for the structurally related β-catenin. The present thesis highlights the role of PKP3 as a component of the desmosome where PKP3 can regulate intercellular adhesion in an EGFR signaling dependent manner. Furthermore, extra-desmosomal PKP3 acts as an intracellular signal scaffold in the EGFR and RB signaling pathways to promote proliferation. Although future work will be needed to examine the exact mechanisms, PKP3 might be a central player in several signaling pathways involved in modulating fundamental cellular processes, including proliferation, differentiation, and adhesion.

6. REFERENCES

Abbas T and Dutta A (2009). "P21 in cancer: Intricate networks and multiple activities." *Nat Rev Cancer*. 9(6): 400-414. DOI: 10.1038/nrc2657.

Aigner K, Descovich L, Mikula M, Sultan A, Dampier B, Bonne S, van Roy F, Mikulits W, Schreiber M, Brabletz T, Sommergruber W, Schweifer N, Wernitznig A, Beug H, Foisner R and Eger A (2007). "The transcription factor zeb1 (deltaef1) represses plakophilin 3 during human cancer progression." *FEBS Lett*. 581(8): 1617-1624. DOI: 10.1016/j.febslet.2007.03.026.

Al Bitar S and Gali-Muhtasib H (2019). "The role of the cyclin dependent kinase inhibitor p21(cip1/waf1) in targeting cancer: Molecular mechanisms and novel therapeutics." *Cancers (Basel)*. 11(10) DOI: 10.3390/cancers11101475.

Albrecht LV, Zhang L, Shabanowitz J, Purevjav E, Towbin JA, Hunt DF and Green KJ (2015). "Gsk3- and prmt-1-dependent modifications of desmoplakin control desmoplakin-cytoskeleton dynamics." *J Cell Biol*. 208(5): 597-612. DOI: 10.1083/jcb.201406020.

Alonso L and Fuchs E (2003). "Stem cells of the skin epithelium." *Proc Natl Acad Sci U S A*. 100 Suppl 1: 11830-11835. DOI: 10.1073/pnas.1734203100.

Amar LS, Shabana AH, Oboeuf M, Martin N and Forest N (1999). "Involvement of desmoplakin phosphorylation in the regulation of desmosomes by protein kinase c, in hela cells." *Cell Adhes Commun*. 7(2): 125-138. DOI: 10.3109/15419069909034396.

Anjum R and Blenis J (2008). "The rsk family of kinases: Emerging roles in cellular signalling." *Nat Rev Mol Cell Biol*. 9(10): 747-758. DOI: 10.1038/nrm2509.

Ardito F, Giuliani M, Perrone D, Troiano G and Lo Muzio L (2017). "The crucial role of protein phosphorylation in cell signaling and its use as targeted therapy (review)." *Int J Mol Med*. 40(2): 271-280. DOI: 10.3892/ijmm.2017.3036.

Bass-Zubek AE, Godsel LM, Delmar M and Green KJ (2009). "Plakophilins: Multifunctional scaffolds for adhesion and signaling." *Curr Opin Cell Biol*. 21(5): 708-716. DOI: 10.1016/j.ceb.2009.07.002.

Bektas M, Jolly PS, Berkowitz P, Amagai M and Rubenstein DS (2013). "A pathophysiologic role for epidermal growth factor receptor in pemphigus acantholysis." *J Biol Chem*. 288(13): 9447-9456. DOI: 10.1074/jbc.M112.438010.

Bierkamp C, Schwarz H, Huber O and Kemler R (1999). "Desmosomal localization of beta-catenin in the skin of plakoglobin null-mutant mice." *Development*. 126(2): 371-381. DOI: 10.1242/dev.126.2.371.

Boehm JS, Zhao JJ, Yao J, Kim SY, Firestein R, Dunn IF, Sjostrom SK, Garraway LA, Weremowicz S, Richardson AL, Greulich H, Stewart CJ, Mulvey LA, Shen RR, Ambrogio L, Hirozane-Kishikawa T, Hill DE, Vidal M, Meyerson M, Grenier JK, Hinkle G, Root DE, Roberts TM, Lander ES, Polyak K and Hahn WC (2007). "Integrative genomic approaches identify ikbke as a breast cancer oncogene." *Cell*. 129(6): 1065-1079. DOI: 10.1016/j.cell.2007.03.052.

Bonne S, Gilbert B, Hatzfeld M, Chen X, Green KJ and van Roy F (2003). "Defining desmosomal plakophilin-3 interactions." *J Cell Biol*. 161(2): 403-416. DOI: 10.1083/jcb.200303036.

Bonne S, van Hengel J, Nollet F, Kools P and van Roy F (1999). "Plakophilin-3, a novel armadillo-like protein present in nuclei and desmosomes of epithelial cells." *J Cell Sci*. 112 (Pt 14): 2265-2276. DOI: 10.1242/jcs.112.14.2265.

Bornslaeger EA, Godsel LM, Corcoran CM, Park JK, Hatzfeld M, Kowalczyk AP and Green KJ (2001). "Plakophilin 1 interferes with plakoglobin binding to desmoplakin, yet together with plakoglobin promotes clustering of desmosomal plaque complexes at cell-cell borders." *J Cell Sci.* 114(Pt 4): 727-738. DOI: 10.1242/jcs.114.4.727.

Bosveld F, Markova O, Guirao B, Martin C, Wang Z, Pierre A, Balakireva M, Gaugue I, Ainslie A, Christophorou N, Lubensky DK, Minc N and Bellaiche Y (2016). "Epithelial tricellular junctions act as interphase cell shape sensors to orient mitosis." *Nature.* 530(7591): 495-498. DOI: 10.1038/nature16970.

Breuninger S, Reidenbach S, Sauer CG, Strobel P, Pfitzenmaier J, Trojan L and Hofmann I (2010). "Desmosomal plakophilins in the prostate and prostatic adenocarcinomas: Implications for diagnosis and tumor progression." *Am J Pathol.* 176(5): 2509-2519. DOI: 10.2353/ajpath.2010.090737.

Broude EV, Swift ME, Vivo C, Chang BD, Davis BM, Kalurupalle S, Blagosklonny MV and Roninson IB (2007). "P21(waf1/cip1/sdi1) mediates retinoblastoma protein degradation." *Oncogene.* 26(48): 6954-6958. DOI: 10.1038/sj.onc.1210516.

Broussard JA, Getsios S and Green KJ (2015). "Desmosome regulation and signaling in disease." *Cell Tissue Res.* 360(3): 501-512. DOI: 10.1007/s00441-015-2136-5.

Burks HE, Matossian MD, Rhodes LV, Phamduy T, Elliott S, Buechlein A, Rusch DB, Miller DFB, Nephew KP, Chrisey D, Collins-Burow BM and Burow ME (2021). "Zeb2 regulates endocrine therapy sensitivity and metastasis in luminal a breast cancer cells through a non-canonical mechanism." *Breast Cancer Res Treat.* 189(1): 25-37. DOI: 10.1007/s10549-021-06256-x.

Buttitta LA and Edgar BA (2007). "Mechanisms controlling cell cycle exit upon terminal differentiation." *Curr Opin Cell Biol.* 19(6): 697-704. DOI: 10.1016/j.ceb.2007.10.004.

Caspi M, Zilberberg A, Eldar-Finkelman H and Rosin-Arbesfeld R (2008). "Nuclear gsk-3beta inhibits the canonical wnt signalling pathway in a beta-catenin phosphorylation-independent manner." *Oncogene.* 27(25): 3546-3555. DOI: 10.1038/sj.onc.1211026.

Chambard JC, Lefloch R, Pouyssegur J and Lenormand P (2007). "Erk implication in cell cycle regulation." *Biochim Biophys Acta.* 1773(8): 1299-1310. DOI: 10.1016/j.bbamcr.2006.11.010.

Chen X, Bonne S, Hatzfeld M, van Roy F and Green KJ (2002). "Protein binding and functional characterization of plakophilin 2. Evidence for its diverse roles in desmosomes and beta -catenin signaling." *J Biol Chem.* 277(12): 10512-10522. DOI: 10.1074/jbc.M108765200.

Colaprico A, Olsen C, Bailey MH, Odom GJ, Terkelsen T, Silva TC, Olsen AV, Cantini L, Zinovyev A, Barillot E, Noushmehr H, Bertoli G, Castiglioni I, Cava C, Bontempi G, Chen XS and Papaleo E (2020). "Interpreting pathways to discover cancer driver genes with moonlight." *Nat Commun.* 11(1): 69. DOI: 10.1038/s41467-019-13803-0.

Costa S, Cerrone M, Saguner AM, Brunckhorst C, Delmar M and Duru F (2021). "Arrhythmogenic cardiomyopathy: An in-depth look at molecular mechanisms and clinical correlates." *Trends Cardiovasc Med.* 31(7): 395-402. DOI: 10.1016/j.tcm.2020.07.006.

Cowin P, Kapprell HP, Franke WW, Tamkun J and Hynes RO (1986). "Plakoglobin: A protein common to different kinds of intercellular adhering junctions." *Cell.* 46(7): 1063-1073. DOI: 10.1016/0092-8674(86)90706-3.

Dahiya A, Gavin MR, Luo RX and Dean DC (2000). "Role of the lxcxe binding site in rb function." *Mol Cell Biol.* 20(18): 6799-6805. DOI: 10.1128/MCB.20.18.6799-6805.2000.

REFERENCES

Dani C, Blanchard JM, Piechaczyk M, El Sabouty S, Marty L and Jeanteur P (1984). "Extreme instability of myc mrna in normal and transformed human cells." *Proc Natl Acad Sci U S A*. 81(22): 7046-7050. DOI: 10.1073/pnas.81.22.7046.

Delva E, Tucker DK and Kowalczyk AP (2009). "The desmosome." *Cold Spring Harb Perspect Biol*. 1(2): a002543. DOI: 10.1101/cshperspect.a002543.

Dimri GP, Nakanishi M, Desprez PY, Smith JR and Campisi J (1996). "Inhibition of e2f activity by the cyclin-dependent protein kinase inhibitor p21 in cells expressing or lacking a functional retinoblastoma protein." *Mol Cell Biol*. 16(6): 2987-2997. DOI: 10.1128/MCB.16.6.2987.

Doolan BJ, Gomaa NS, Fawzy MM, Dogheim NN, Liu L, Mellerio JE, Onoufriadis A and McGrath JA (2020). "Ectodermal dysplasia-skin fragility syndrome: Two new cases and review of this desmosomal genodermatosis." *Exp Dermatol*. 29(6): 520-530. DOI: 10.1111/exd.14096.

Dunn SJ, Osborne JM, Appleton PL and Nathke I (2016). "Combined changes in wnt signaling response and contact inhibition induce altered proliferation in radiation-treated intestinal crypts." *Mol Biol Cell*. 27(11): 1863-1874. DOI: 10.1091/mbc.E15-12-0854.

Durinck S, Moreau Y, Kasprzyk A, Davis S, De Moor B, Brazma A and Huber W (2005). "Biomart and bioconductor: A powerful link between biological databases and microarray data analysis." *Bioinformatics*. 21(16): 3439-3440. DOI: 10.1093/bioinformatics/bti525.

Engeland K (2022). "Cell cycle regulation: P53-p21-rb signaling." *Cell Death Differ*. 29(5): 946-960. DOI: 10.1038/s41418-022-00988-z.

Fischer-Keso R, Breuninger S, Hofmann S, Henn M, Rohrig T, Strobel P, Stoecklin G and Hofmann I (2014). "Plakophilins 1 and 3 bind to fxr1 and thereby influence the mrna stability of desmosomal proteins." *Mol Cell Biol*. 34(23): 4244-4256. DOI: 10.1128/MCB.00766-14.

Furukawa C, Daigo Y, Ishikawa N, Kato T, Ito T, Tsuchiya E, Sone S and Nakamura Y (2005). "Plakophilin 3 oncogene as prognostic marker and therapeutic target for lung cancer." *Cancer Res*. 65(16): 7102-7110. DOI: 10.1158/0008-5472.CAN-04-1877.

Gao L, Li X, Guo Q, Nie X, Hao Y, Liu Q, Liu J, Zhu L, Yan L and Lin B (2020). "Identification of pkp 2/3 as potential biomarkers of ovarian cancer based on bioinformatics and experiments." *Cancer Cell Int*. 20: 509. DOI: 10.1186/s12935-020-01602-3.

Garcia MA, Nelson WJ and Chavez N (2018). "Cell-cell junctions organize structural and signaling networks." *Cold Spring Harb Perspect Biol*. 10(4) DOI: 10.1101/cshperspect.a029181.

Garrod D and Chidgey M (2008). "Desmosome structure, composition and function." *Biochim Biophys Acta*. 1778(3): 572-587. DOI: 10.1016/j.bbamem.2007.07.014.

Garrod DR, Berika MY, Bardsley WF, Holmes D and Tabernero L (2005). "Hyper-adhesion in desmosomes: Its regulation in wound healing and possible relationship to cadherin crystal structure." *J Cell Sci*. 118(Pt 24): 5743-5754. DOI: 10.1242/jcs.02700.

Gaudry CA, Palka HL, Dusek RL, Huen AC, Khandekar MJ, Hudson LG and Green KJ (2001). "Tyrosine-phosphorylated plakoglobin is associated with desmogleins but not desmoplakin after epidermal growth factor receptor activation." *J Biol Chem*. 276(27): 24871-24880. DOI: 10.1074/jbc.M102731200.

Gazel A and Blumenberg M (2013). "Transcriptional effects of inhibiting epidermal growth factor receptor in keratinocytes." *Dermatologica Sinica*. 31(3): 107-119. DOI: 10.1016/j.dsi.2012.11.003.

Georgakilas AG, Martin OA and Bonner WM (2017). "P21: A two-faced genome guardian." *Trends Mol Med*. 23(4): 310-319. DOI: 10.1016/j.molmed.2017.02.001.

REFERENCES

Ghosh R, Gilda JE and Gomes AV (2014). "The necessity of and strategies for improving confidence in the accuracy of western blots." *Expert Rev Proteomics*. 11(5): 549-560. DOI: 10.1586/14789450.2014.939635.

Giacinti C and Giordano A (2006). "Rb and cell cycle progression." *Oncogene*. 25(38): 5220-5227. DOI: 10.1038/sj.onc.1209615.

Giard DJ, Aaronson SA, Todaro GJ, Arnstein P, Kersey JH, Dosik H and Parks WP (1973). "In vitro cultivation of human tumors: Establishment of cell lines derived from a series of solid tumors." *J Natl Cancer Inst*. 51(5): 1417-1423. DOI: 10.1093/jnci/51.5.1417.

Goodarzi P, Falahzadeh K, Nematizadeh M, Farazandeh P, Payab M, Larijani B, Tayanloo Beik A and Arjmand B (2018). "Tissue engineered skin substitutes." *Adv Exp Med Biol*. 1107: 143-188. DOI: 10.1007/5584_2018_226.

Gosavi P, Kundu ST, Khapare N, Sehgal L, Karkhanis MS and Dalal SN (2011). "E-cadherin and plakoglobin recruit plakophilin3 to the cell border to initiate desmosome assembly." *Cell Mol Life Sci*. 68(8): 1439-1454. DOI: 10.1007/s00018-010-0531-3.

Gottlieb AB, Chang CK, Posnett DN, Fanelli B and Tam JP (1988). "Detection of transforming growth factor alpha in normal, malignant, and hyperproliferative human keratinocytes." *J Exp Med*. 167(2): 670-675. DOI: 10.1084/jem.167.2.670.

Gurjar M, Raychaudhuri K, Mahadik S, Reddy D, Atak A, Shetty T, Rao K, Karkhanis MS, Gosavi P, Sehgal L, Gupta S and Dalal SN (2018). "Plakophilin3 increases desmosome assembly, size and stability by increasing expression of desmocollin2." *Biochem Biophys Res Commun*. 495(1): 768-774. DOI: 10.1016/j.bbrc.2017.11.085.

Hannus M, Beitzinger M, Engelmann JC, Weickert MT, Spang R, Hannus S and Meister G (2014). "Sipools: Highly complex but accurately defined sirna pools eliminate off-target effects." *Nucleic Acids Res*. 42(12): 8049-8061. DOI: 10.1093/nar/gku480.

Harbour JW, Luo RX, Dei Santi A, Postigo AA and Dean DC (1999). "Cdk phosphorylation triggers sequential intramolecular interactions that progressively block rb functions as cells move through g1." *Cell*. 98(6): 859-869. DOI: 10.1016/s0092-8674(00)81519-6.

Harper JW, Elledge SJ, Keyomarsi K, Dynlacht B, Tsai LH, Zhang P, Dobrowolski S, Bai C, Connell-Crowley L, Swindell E and et al. (1995). "Inhibition of cyclin-dependent kinases by p21." *Mol Biol Cell*. 6(4): 387-400. DOI: 10.1091/mbc.6.4.387.

Hartsock A and Nelson WJ (2008). "Adherens and tight junctions: Structure, function and connections to the actin cytoskeleton." *Biochim Biophys Acta*. 1778(3): 660-669. DOI: 10.1016/j.bbamem.2007.07.012.

Hatzfeld M (2007). "Plakophilins: Multifunctional proteins or just regulators of desmosomal adhesion?" *Biochim Biophys Acta*. 1773(1): 69-77. DOI: 10.1016/j.bbamcr.2006.04.009.

Hatzfeld M, Haffner C, Schulze K and Vinzens U (2000). "The function of plakophilin 1 in desmosome assembly and actin filament organization." *J Cell Biol*. 149(1): 209-222. DOI: 10.1083/jcb.149.1.209.

Hatzfeld M, Keil R and Magin TM (2017). "Desmosomes and intermediate filaments: Their consequences for tissue mechanics." *Cold Spring Harb Perspect Biol*. 9(6) DOI: 10.1101/cshperspect.a029157.

Hatzfeld M, Wolf A and Keil R (2014). "Plakophilins in desmosomal adhesion and signaling." *Cell Commun Adhes*. 21(1): 25-42. DOI: 10.3109/15419061.2013.876017.

REFERENCES

Higashi T and Chiba H (2020). "Molecular organization, regulation and function of tricellular junctions." *Biochim Biophys Acta Biomembr.* 1862(2): 183143. DOI: 10.1016/j.bbamem.2019.183143.

Hodorogea A, Calinescu A, Antohe M, Balaban M, Nedelcu RI, Turcu G, Ion DA, Badarau IA, Popescu CM, Popescu R, Popp C, Cioplea M, Nichita L, Hulea I and Brinzea A (2019). "Epithelial-mesenchymal transition in skin cancers: A review." *Anal Cell Pathol (Amst).* 2019: 3851576. DOI: 10.1155/2019/3851576.

Hofmann I, Casella M, Schnolzer M, Schlechter T, Spring H and Franke WW (2006). "Identification of the junctional plaque protein plakophilin 3 in cytoplasmic particles containing rna-binding proteins and the recruitment of plakophilins 1 and 3 to stress granules." *Mol Biol Cell.* 17(3): 1388-1398. DOI: 10.1091/mbc.e05-08-0708.

Holcmann M and Sibilia M (2015). "Mechanisms underlying skin disorders induced by egfr inhibitors." *Mol Cell Oncol.* 2(4): e1004969. DOI: 10.1080/23723556.2015.1004969.

Hong JY, Zapata J, Blackburn A, Baumert R, Bae SM, Ji H, Nam HJ, Miller RK and McCrea PD (2021). "A catenin of the plakophilin-subfamily, pkp3, responds to canonical-wnt pathway components and signals." *Biochem Biophys Res Commun.* 563: 31-39. DOI: 10.1016/j.bbrc.2021.05.043.

Hsu CK, Lin HH, Harn HI, Hughes MW, Tang MJ and Yang CC (2018). "Mechanical forces in skin disorders." *J Dermatol Sci.* 90(3): 232-240. DOI: 10.1016/j.jdermsci.2018.03.004.

Hu T and Li C (2010). "Convergence between wnt-beta-catenin and egfr signaling in cancer." *Mol Cancer.* 9: 236. DOI: 10.1186/1476-4598-9-236.

Ishida-Yamamoto A and Igawa S (2015). "The biology and regulation of corneodesmosomes." *Cell Tissue Res.* 360(3): 477-482. DOI: 10.1007/s00441-014-2037-z.

Ito Y and Miyazono K (2003). "Runx transcription factors as key targets of tgf-β superfamily signaling." *Current Opinion in Genetics & Development.* 13(1): 43-47. DOI: 10.1016/s0959-437x(03)00007-8.

Jackstadt R, Roh S, Neumann J, Jung P, Hoffmann R, Horst D, Berens C, Bornkamm GW, Kirchner T, Menssen A and Hermeking H (2013). "Ap4 is a mediator of epithelial-mesenchymal transition and metastasis in colorectal cancer." *J Exp Med.* 210(7): 1331-1350. DOI: 10.1084/jem.20120812.

Jancik S, Drabek J, Radzioch D and Hajduch M (2010). "Clinical relevance of kras in human cancers." *J Biomed Biotechnol.* 2010: 150960. DOI: 10.1155/2010/150960.

Janiszewska M, Primi MC and Izard T (2020). "Cell adhesion in cancer: Beyond the migration of single cells." *J Biol Chem.* 295(8): 2495-2505. DOI: 10.1074/jbc.REV119.007759.

Jiao W, Lin HM, Datta J, Braunschweig T, Chung JY, Hewitt SM and Rane SG (2008). "Aberrant nucleocytoplasmic localization of the retinoblastoma tumor suppressor protein in human cancer correlates with moderate/poor tumor differentiation." *Oncogene.* 27(22): 3156-3164. DOI: 10.1038/sj.onc.1210970.

Joly-Tonetti N, Ondet T, Monshouwer M and Stamatas GN (2021). "Egfr inhibitors switch keratinocytes from a proliferative to a differentiative phenotype affecting epidermal development and barrier function." *BMC Cancer.* 21(1): 5. DOI: 10.1186/s12885-020-07685-5.

Jung YS, Qian Y and Chen X (2010). "Examination of the expanding pathways for the regulation of p21 expression and activity." *Cell Signal.* 22(7): 1003-1012. DOI: 10.1016/j.cellsig.2010.01.013.

REFERENCES

Kalejta RF, Bechtel JT and Shenk T (2003). "Human cytomegalovirus pp71 stimulates cell cycle progression by inducing the proteasome-dependent degradation of the retinoblastoma family of tumor suppressors." *Mol Cell Biol*. 23(6): 1885-1895. DOI: 10.1128/MCB.23.6.1885-1895.2003.

Kanehisa M, Goto S, Kawashima S, Okuno Y and Hattori M (2004). "The kegg resource for deciphering the genome." *Nucleic Acids Res*. 32(Database issue): D277-280. DOI: 10.1093/nar/gkh063.

Keil R, Rietscher K and Hatzfeld M (2016). "Antagonistic regulation of intercellular cohesion by plakophilins 1 and 3." *J Invest Dermatol*. 136(10): 2022-2029. DOI: 10.1016/j.jid.2016.05.124.

Keysar SB, Le PN, Anderson RT, Morton JJ, Bowles DW, Paylor JJ, Vogler BW, Thorburn J, Fernandez P, Glogowska MJ, Takimoto SM, Sehrt DB, Gan GN, Eagles-Soukup JR, Serracino H, Hirsch FR, Lucia MS, Thorburn A, Song JI, Wang XJ and Jimeno A (2013). "Hedgehog signaling alters reliance on egf receptor signaling and mediates anti-egfr therapeutic resistance in head and neck cancer." *Cancer Res*. 73(11): 3381-3392. DOI: 10.1158/0008-5472.CAN-12-4047.

Kim M and Jho EH (2014). "Cross-talk between wnt/beta-catenin and hippo signaling pathways: A brief review." *BMB Rep*. 47(10): 540-545. DOI: 10.5483/bmbrep.2014.47.10.177.

Kimura TE, Merritt AJ and Garrod DR (2007). "Calcium-independent desmosomes of keratinocytes are hyper-adhesive." *J Invest Dermatol*. 127(4): 775-781. DOI: 10.1038/sj.jid.5700643.

Klijn JG, Berns PM, Schmitz PI and Foekens JA (1992). "The clinical significance of epidermal growth factor receptor (egf-r) in human breast cancer: A review on 5232 patients." *Endocr Rev*. 13(1): 3-17. DOI: 10.1210/edrv-13-1-3.

Kowalczyk AP, Bornslaeger EA, Borgwardt JE, Palka HL, Dhaliwal AS, Corcoran CM, Denning MF and Green KJ (1997). "The amino-terminal domain of desmoplakin binds to plakoglobin and clusters desmosomal cadherin-plakoglobin complexes." *J Cell Biol*. 139(3): 773-784. DOI: 10.1083/jcb.139.3.773.

Krane JF, Murphy DP, Carter DM and Krueger JG (1991). "Synergistic effects of epidermal growth factor (egf) and insulin-like growth factor i/somatomedin c (igf-i) on keratinocyte proliferation may be mediated by igf-i transmodulation of the egf receptor." *J Invest Dermatol*. 96(4): 419-424. DOI: 10.1111/1523-1747.ep12469799.

Kroger C, Loschke F, Schwarz N, Windoffer R, Leube RE and Magin TM (2013). "Keratins control intercellular adhesion involving pkc-alpha-mediated desmoplakin phosphorylation." *J Cell Biol*. 201(5): 681-692. DOI: 10.1083/jcb.201208162.

Lee MJ and Yaffe MB (2016). "Protein regulation in signal transduction." *Cold Spring Harb Perspect Biol*. 8(6) DOI: 10.1101/cshperspect.a005918.

Lee YS, Lee JW, Jang JW, Chi XZ, Kim JH, Li YH, Kim MK, Kim DM, Choi BS, Kim EG, Chung JH, Lee OJ, Lee YM, Suh JW, Chuang LS, Ito Y and Bae SC (2013). "Runx3 inactivation is a crucial early event in the development of lung adenocarcinoma." *Cancer Cell*. 24(5): 603-616. DOI: 10.1016/j.ccr.2013.10.003.

Li S, Jiang C, Pan J, Wang X, Jin J, Zhao L, Pan W, Liao G, Cai X, Li X, Xiao J, Jiang J and Wang P (2015). "Regulation of c-myc protein stability by proteasome activator reggamma." *Cell Death Differ*. 22(6): 1000-1011. DOI: 10.1038/cdd.2014.188.

Li Y, Ju K, Wang W, Liu Z, Xie H, Jiang Y, Jiang G, Lu J, Dong Z and Tang F (2018). "Dinitrosopiperazine-decreased pkp3 through upregulating mir-149 participates in nasopharyngeal carcinoma metastasis." *Mol Carcinog*. 57(12): 1763-1779. DOI: 10.1002/mc.22895.

Liberzon A, Birger C, Thorvaldsdottir H, Ghandi M, Mesirov JP and Tamayo P (2015). "The molecular signatures database (msigdb) hallmark gene set collection." *Cell Syst.* 1(6): 417-425. DOI: 10.1016/j.cels.2015.12.004.

Lim V, Zhu H, Diao S, Hu L and Hu J (2019). "Pkp3 interactions with mapk-jnk-erk1/2-mtor pathway regulates autophagy and invasion in ovarian cancer." *Biochem Biophys Res Commun.* 508(2): 646-653. DOI: 10.1016/j.bbrc.2018.11.163.

Lorch JH, Klessner J, Park JK, Getsios S, Wu YL, Stack MS and Green KJ (2004). "Epidermal growth factor receptor inhibition promotes desmosome assembly and strengthens intercellular adhesion in squamous cell carcinoma cells." *J Biol Chem.* 279(35): 37191-37200. DOI: 10.1074/jbc.M405123200.

Lutful Kabir FM, Alvarez CE and Bird RC (2015). "Canine mammary carcinomas: A comparative analysis of altered gene expression." *Vet Sci.* 3(1) DOI: 10.3390/vetsci3010001.

MacDonald BT, Tamai K and He X (2009). "Wnt/beta-catenin signaling: Components, mechanisms, and diseases." *Dev Cell.* 17(1): 9-26. DOI: 10.1016/j.devcel.2009.06.016.

Marescal O and Cheeseman IM (2020). "Cellular mechanisms and regulation of quiescence." *Dev Cell.* 55(3): 259-271. DOI: 10.1016/j.devcel.2020.09.029.

Matsui T and Amagai M (2015). "Dissecting the formation, structure and barrier function of the stratum corneum." *Int Immunol.* 27(6): 269-280. DOI: 10.1093/intimm/dxv013.

McClatchey AI and Yap AS (2012). "Contact inhibition (of proliferation) redux." *Curr Opin Cell Biol.* 24(5): 685-694. DOI: 10.1016/j.ceb.2012.06.009.

Mendonsa AM, Na TY and Gumbiner BM (2018). "E-cadherin in contact inhibition and cancer." *Oncogene.* 37(35): 4769-4780. DOI: 10.1038/s41388-018-0304-2.

Miroshnikova YA, Le HQ, Schneider D, Thalheim T, Rubsam M, Bremicker N, Polleux J, Kamprad N, Tarantola M, Wang I, Balland M, Niessen CM, Galle J and Wickstrom SA (2018). "Adhesion forces and cortical tension couple cell proliferation and differentiation to drive epidermal stratification." *Nat Cell Biol.* 20(1): 69-80. DOI: 10.1038/s41556-017-0005-z.

Mittnacht S and Weinberg RA (1991). "G1/s phosphorylation of the retinoblastoma protein is associated with an altered affinity for the nuclear compartment." *Cell.* 65(3): 381-393. DOI: 10.1016/0092-8674(91)90456-9.

Müller L, Hatzfeld M and Keil R (2021). "Desmosomes as signaling hubs in the regulation of cell behavior." *Front Cell Dev Biol.* 9: 745670. DOI: 10.3389/fcell.2021.745670.

Müller L, Rietscher K, Keil R, Neuholz M and Hatzfeld M (2020). "Plakophilin 3 phosphorylation by ribosomal s6 kinases supports desmosome assembly." *J Cell Sci.* 133(8) DOI: 10.1242/jcs.238295.

Munoz WA, Lee M, Miller RK, Ahmed Z, Ji H, Link TM, Lee GR, Kloc M, Ladbury JE and McCrea PD (2014). "Plakophilin-3 catenin associates with the etv1/er81 transcription factor to positively modulate gene activity." *PLoS One.* 9(1): e86784. DOI: 10.1371/journal.pone.0086784.

Nanney LB, Ellis DL, Levine J and King LE (1992). "Epidermal growth factor receptors in idiopathic and virally induced skin diseases." *Am J Pathol.* 140(4): 915-925.

Narasimha AM, Kaulich M, Shapiro GS, Choi YJ, Sicinski P and Dowdy SF (2014). "Cyclin d activates the rb tumor suppressor by mono-phosphorylation." *Elife.* 3 DOI: 10.7554/eLife.02872.

Nekrasova O and Green KJ (2013). "Desmosome assembly and dynamics." *Trends Cell Biol.* 23(11): 537-546. DOI: 10.1016/j.tcb.2013.06.004.

REFERENCES

Nestor-Bergmann A, Stooke-Vaughan GA, Goddard GK, Starborg T, Jensen OE and Woolner S (2019). "Decoupling the roles of cell shape and mechanical stress in orienting and cueing epithelial mitosis." *Cell Rep.* 26(8): 2088-2100 e2084. DOI: 10.1016/j.celrep.2019.01.102.

Neuber S, Jager S, Meyer M, Wischmann V, Koch PJ, Moll R and Schmidt A (2015). "C-src mediated tyrosine phosphorylation of plakophilin 3 as a new mechanism to control desmosome composition in cells exposed to oxidative stress." *Cell Tissue Res.* 359(3): 799-816. DOI: 10.1007/s00441-014-2063-x.

Neuber S, Muhmer M, Wratten D, Koch PJ, Moll R and Schmidt A (2010). "The desmosomal plaque proteins of the plakophilin family." *Dermatol Res Pract.* 2010: 101452. DOI: 10.1155/2010/101452.

Nguyen AV and Soulika AM (2019). "The dynamics of the skin's immune system." *Int J Mol Sci.* 20(8) DOI: 10.3390/ijms20081811.

Niessen CM (2007). "Tight junctions/adherens junctions: Basic structure and function." *J Invest Dermatol.* 127(11): 2525-2532. DOI: 10.1038/sj.jid.5700865.

Papagerakis S, Shabana AH, Depondt J, Gehanno P and Forest N (2003). "Immunohistochemical localization of plakophilins (pkp1, pkp2, pkp3, and p0071) in primary oropharyngeal tumors: Correlation with clinical parameters." *Hum Pathol.* 34(6): 565-572. DOI: 10.1016/s0046-8177(03)00174-6.

Park JW, Hwang SR and Yoon IS (2017). "Advanced growth factor delivery systems in wound management and skin regeneration." *Molecules.* 22(8) DOI: 10.3390/molecules22081259.

Pierard GE (2012). "Cell proliferation in cutaneous malignant melanoma: Relationship with neoplastic progression." *ISRN Dermatol.* 2012: 828146. DOI: 10.5402/2012/828146.

Ramanujan A, Bansal S, Guha M, Pande NT and Tiwari S (2021). "Lxcxd motif of the apc/c coactivator subunit fzr1 is critical for interaction with the retinoblastoma protein." *Exp Cell Res.* 404(2): 112632. DOI: 10.1016/j.yexcr.2021.112632.

Ribatti D, Tamma R and Annese T (2020). "Epithelial-mesenchymal transition in cancer: A historical overview." *Transl Oncol.* 13(6): 100773. DOI: 10.1016/j.tranon.2020.100773.

Richards SA, Dreisbach VC, Murphy LO and Blenis J (2001). "Characterization of regulatory events associated with membrane targeting of p90 ribosomal s6 kinase 1." *Mol Cell Biol.* 21(21): 7470-7480. DOI: 10.1128/MCB.21.21.7470-7480.2001.

Rickelt S, Rizzo S, Doerflinger Y, Zentgraf H, Basso C, Gerosa G, Thiene G, Moll R and Franke WW (2010). "A novel kind of tumor type-characteristic junction: Plakophilin-2 as a major protein of adherens junctions in cardiac myxomata." *Mod Pathol.* 23(11): 1429-1437. DOI: 10.1038/modpathol.2010.138.

Rietscher K (2018). "Regulation of pkp1´s function in intercellular adhesion, proliferation and barrier formation." doctoral thesis, Martin-Luther-Universität Halle-Wittenberg.

Rietscher K, Keil R, Jordan A and Hatzfeld M (2018). "14-3-3 proteins regulate desmosomal adhesion via plakophilins." *J Cell Sci.* 131(10) DOI: 10.1242/jcs.212191.

Rietscher K, Wolf A, Hause G, Rother A, Keil R, Magin TM, Glass M, Niessen CM and Hatzfeld M (2016). "Growth retardation, loss of desmosomal adhesion, and impaired tight junction function identify a unique role of plakophilin 1 in vivo." *J Invest Dermatol.* 136(7): 1471-1478. DOI: 10.1016/j.jid.2016.03.021.

Roberts BJ, Reddy R and Wahl JK, 3rd (2013). "Stratifin (14-3-3 sigma) limits plakophilin-3 exchange with the desmosomal plaque." *PLoS One.* 8(10): e77012. DOI: 10.1371/journal.pone.0077012.

Romeo Y, Zhang X and Roux PP (2012). "Regulation and function of the rsk family of protein kinases." *Biochem J.* 441(2): 553-569. DOI: 10.1042/BJ20110289.

Ruan S, Shi J, Wang M and Zhu Z (2021). "Analysis of multiple human tumor cases reveals the carcinogenic effects of pkp3." *J Healthc Eng.* 2021: 9391104. DOI: 10.1155/2021/9391104.

Rubin SM (2013). "Deciphering the retinoblastoma protein phosphorylation code." *Trends Biochem Sci.* 38(1): 12-19. DOI: 10.1016/j.tibs.2012.10.007.

Rubsam M, Broussard JA, Wickstrom SA, Nekrasova O, Green KJ and Niessen CM (2018). "Adherens junctions and desmosomes coordinate mechanics and signaling to orchestrate tissue morphogenesis and function: An evolutionary perspective." *Cold Spring Harb Perspect Biol.* 10(11) DOI: 10.1101/cshperspect.a029207.

Rubsam M, Mertz AF, Kubo A, Marg S, Jungst C, Goranci-Buzhala G, Schauss AC, Horsley V, Dufresne ER, Moser M, Ziegler W, Amagai M, Wickstrom SA and Niessen CM (2017). "E-cadherin integrates mechanotransduction and egfr signaling to control junctional tissue polarization and tight junction positioning." *Nat Commun.* 8(1): 1250. DOI: 10.1038/s41467-017-01170-7.

Sadagurski M, Yakar S, Weingarten G, Holzenberger M, Rhodes CJ, Breitkreutz D, Leroith D and Wertheimer E (2006). "Insulin-like growth factor 1 receptor signaling regulates skin development and inhibits skin keratinocyte differentiation." *Mol Cell Biol.* 26(7): 2675-2687. DOI: 10.1128/MCB.26.7.2675-2687.2006.

Schafer KA (1998). "The cell cycle: A review." *Vet Pathol.* 35(6): 461-478. DOI: 10.1177/030098589803500601.

Schindelin J, Arganda-Carreras I, Frise E, Kaynig V, Longair M, Pietzsch T, Preibisch S, Rueden C, Saalfeld S, Schmid B, Tinevez JY, White DJ, Hartenstein V, Eliceiri K, Tomancak P and Cardona A (2012). "Fiji: An open-source platform for biological-image analysis." *Nat Methods.* 9(7): 676-682. DOI: 10.1038/nmeth.2019.

Schmidt A and Jager S (2005). "Plakophilins--hard work in the desmosome, recreation in the nucleus?" *Eur J Cell Biol.* 84(2-3): 189-204. DOI: 10.1016/j.ejcb.2004.12.020.

Seeger MA and Paller AS (2015). "The roles of growth factors in keratinocyte migration." *Adv Wound Care (New Rochelle).* 4(4): 213-224. DOI: 10.1089/wound.2014.0540.

Shamloo B and Usluer S (2019). "P21 in cancer research." *Cancers (Basel).* 11(8) DOI: 10.3390/cancers11081178.

Shir A, Ogris M, Wagner E and Levitzki A (2006). "Egf receptor-targeted synthetic double-stranded rna eliminates glioblastoma, breast cancer, and adenocarcinoma tumors in mice." *PLoS Med.* 3(1): e6. DOI: 10.1371/journal.pmed.0030006.

Sigismund S, Avanzato D and Lanzetti L (2018). "Emerging functions of the egfr in cancer." *Mol Oncol.* 12(1): 3-20. DOI: 10.1002/1878-0261.12155.

Sklyarova T, Bonne S, D'Hooge P, Denecker G, Goossens S, De Rycke R, Borgonie G, Bosl M, van Roy F and van Hengel J (2008). "Plakophilin-3-deficient mice develop hair coat abnormalities and are prone to cutaneous inflammation." *J Invest Dermatol.* 128(6): 1375-1385. DOI: 10.1038/sj.jid.5701189.

Smith JA, Poteet-Smith CE, Malarkey K and Sturgill TW (1999). "Identification of an extracellular signal-regulated kinase (erk) docking site in ribosomal s6 kinase, a sequence critical for activation by erk in vivo." *J Biol Chem*. 274(5): 2893-2898. DOI: 10.1074/jbc.274.5.2893.

Son H and Moon A (2010). "Epithelial-mesenchymal transition and cell invasion." *Toxicol Res*. 26(4): 245-252. DOI: 10.5487/TR.2010.26.4.245.

Sotiropoulou PA and Blanpain C (2012). "Development and homeostasis of the skin epidermis." *Cold Spring Harb Perspect Biol*. 4(7): a008383. DOI: 10.1101/cshperspect.a008383.

Stappenbeck TS, Lamb JA, Corcoran CM and Green KJ (1994). "Phosphorylation of the desmoplakin cooh terminus negatively regulates its interaction with keratin intermediate filament networks." *J Biol Chem*. 269(47): 29351-29354. DOI: 10.1016/S0021-9258(18)43881-1.

Stokke T, Erikstein BK, Smedshammer L, Boye E and Steen HB (1993). "The retinoblastoma gene product is bound in the nucleus in early g1 phase." *Exp Cell Res*. 204(1): 147-155. DOI: 10.1006/excr.1993.1019.

Sumigray KD and Lechler T (2015). "Cell adhesion in epidermal development and barrier formation." *Curr Top Dev Biol*. 112: 383-414. DOI: 10.1016/bs.ctdb.2014.11.027.

Takahashi H, Nakatsuji H, Takahashi M, Avirmed S, Fukawa T, Takemura M, Fukumori T and Kanayama H (2012). "Up-regulation of plakophilin-2 and down-regulation of plakophilin-3 are correlated with invasiveness in bladder cancer." *Urology*. 79(1): 240 e241-248. DOI: 10.1016/j.urology.2011.08.049.

Takasawa A, Kojima T, Ninomiya T, Tsujiwaki M, Murata M, Tanaka S and Sawada N (2013). "Behavior of tricellulin during destruction and formation of tight junctions under various extracellular calcium conditions." *Cell Tissue Res*. 351(1): 73-84. DOI: 10.1007/s00441-012-1512-7.

Todorovic V, Koetsier JL, Godsel LM and Green KJ (2014). "Plakophilin 3 mediates rap1-dependent desmosome assembly and adherens junction maturation." *Mol Biol Cell*. 25(23): 3749-3764. DOI: 10.1091/mbc.E14-05-0968.

Topacio BR, Zatulovskiy E, Cristea S, Xie S, Tambo CS, Rubin SM, Sage J, Koivomagi M and Skotheim JM (2019). "Cyclin d-cdk4,6 drives cell-cycle progression via the retinoblastoma protein's c-terminal helix." *Mol Cell*. 74(4): 758-770 e754. DOI: 10.1016/j.molcel.2019.03.020.

Valladares-Ayerbes M, Diaz-Prado S, Reboredo M, Medina V, Lorenzo-Patino MJ, Iglesias-Diaz P, Haz M, Pertega S, Santamarina I, Blanco M, Quindos-Varela M, Figueroa A and Anton-Aparicio LM (2010). "Evaluation of plakophilin-3 mrna as a biomarker for detection of circulating tumor cells in gastrointestinal cancer patients." *Cancer Epidemiol Biomarkers Prev*. 19(6): 1432-1440. DOI: 10.1158/1055-9965.EPI-10-0123.

van den Heuvel S and Harlow E (1993). "Distinct roles for cyclin-dependent kinases in cell cycle control." *Science*. 262(5142): 2050-2054. DOI: 10.1126/science.8266103.

Wang LL, Meng QH, Jiao Y, Xu JY, Ge CM, Zhou JY, Rosen EM, Wang HC and Fan SJ (2012). "High-mobility group boxes mediate cell proliferation and radiosensitivity via retinoblastoma-interaction-dependent and -independent mechanisms." *Cancer Biother Radiopharm*. 27(5): 329-335. DOI: 10.1089/cbr.2012.1199.

Wang Z (2021). "Regulation of cell cycle progression by growth factor-induced cell signaling." *Cells*. 10(12) DOI: 10.3390/cells10123327.

REFERENCES

Ward CW, Lawrence MC, Streltsov VA, Adams TE and McKern NM (2007). "The insulin and egf receptor structures: New insights into ligand-induced receptor activation." *Trends Biochem Sci*. 32(3): 129-137. DOI: 10.1016/j.tibs.2007.01.001.

Watt FM (1989). "Terminal differentiation of epidermal keratinocytes." *Curr Opin Cell Biol*. 1(6): 1107-1115. DOI: 10.1016/s0955-0674(89)80058-4.

Wee P and Wang Z (2017). "Epidermal growth factor receptor cell proliferation signaling pathways." *Cancers (Basel)*. 9(5) DOI: 10.3390/cancers9050052.

Welcker M, Orian A, Jin J, Grim JE, Harper JW, Eisenman RN and Clurman BE (2004). "The fbw7 tumor suppressor regulates glycogen synthase kinase 3 phosphorylation-dependent c-myc protein degradation." *Proc Natl Acad Sci U S A*. 101(24): 9085-9090. DOI: 10.1073/pnas.0402770101.

Wolf A, Krause-Gruszczynska M, Birkenmeier O, Ostareck-Lederer A, Huttelmaier S and Hatzfeld M (2010). "Plakophilin 1 stimulates translation by promoting eif4a1 activity." *J Cell Biol*. 188(4): 463-471. DOI: 10.1083/jcb.200908135.

Wolf A, Rietscher K, Glass M, Huttelmaier S, Schutkowski M, Ihling C, Sinz A, Wingenfeld A, Mun A and Hatzfeld M (2013). "Insulin signaling via akt2 switches plakophilin 1 function from stabilizing cell adhesion to promoting cell proliferation." *J Cell Sci*. 126(Pt 8): 1832-1844. DOI: 10.1242/jcs.118992.

Yin T and Green KJ (2004). "Regulation of desmosome assembly and adhesion." *Semin Cell Dev Biol*. 15(6): 665-677. DOI: 10.1016/j.semcdb.2004.09.005.

Yu F, Yu C, Li F, Zuo Y, Wang Y, Yao L, Wu C, Wang C and Ye L (2021). "Wnt/beta-catenin signaling in cancers and targeted therapies." *Signal Transduct Target Ther*. 6(1): 307. DOI: 10.1038/s41392-021-00701-5.

Yu G, Wang LG, Han Y and He QY (2012). "Clusterprofiler: An r package for comparing biological themes among gene clusters." *OMICS*. 16(5): 284-287. DOI: 10.1089/omi.2011.0118.

Yu G, Wang LG and He QY (2015). "Chipseeker: An r/bioconductor package for chip peak annotation, comparison and visualization." *Bioinformatics*. 31(14): 2382-2383. DOI: 10.1093/bioinformatics/btv145.

Zanzoni A, Spinelli L, Ribeiro DM, Tartaglia GG and Brun C (2019). "Post-transcriptional regulatory patterns revealed by protein-rna interactions." *Sci Rep*. 9(1): 4302. DOI: 10.1038/s41598-019-40939-2.

Zihni C, Mills C, Matter K and Balda MS (2016). "Tight junctions: From simple barriers to multifunctional molecular gates." *Nat Rev Mol Cell Biol*. 17(9): 564-580. DOI: 10.1038/nrm.2016.80.

Zimmer SE and Kowalczyk AP (2020). "The desmosome as a model for lipid raft driven membrane domain organization." *Biochim Biophys Acta Biomembr*. 1862(9): 183329. DOI: 10.1016/j.bbamem.2020.183329.

7. APPENDIX

7.1. Supplementary figures

```
         10         20         30         40         50
MQDGNFLLSA LQPEAGVCSL ALPSDLQLDR RGAEGPEAER LRAARVQEQV
         60         70         80         90        100
RARLLQLGQQ PRHNGAAEPE PEAETARGTS RGQYHTLQAG FSSRSQGLSG
        110        120        130        140        150
DKTSGFRPIA KPAYSPASWS SRSAVDLSCS RRLSSAHNGG SAFGAAGYGG
        160        170        180        190        200
AQPTPPMPTR PVSFHERGGV GSRADYDTLS LRSLRLGPGG LDDRYSLVSE
        210        220        230        240        250
QLEPAATSTY RAFAYERQAS SSSSRAGGLD WPEATEVSPS RTIRAPAVRT
        260        270        280        290        300
LQRFQSSHRS RGVGGAVPGA VLEPVARAPS VRSLSLSLAD SGHLPDVHGF
        310        320        330        340        350
NSYGSHRTLQ RLSSGFDDID LPSAVKYLMA SDPNLQVLGA AYIQHKCYSD
        360        370        380        390        400
AAAKKQARSL QAVPRLVKLF NHANQEVQRH ATGAMRNLIY DNADNKLALV
        410        420        430        440        450
EENGIFELLR TLREQDDELR KNVTGILWNL SSSDHLKDRL ARDTLEQLTD
        460        470        480        490        500
LVLSPLSGAG GPPLIQQNAS EAEIFYNATG FLRNLSSASQ ATRQKMRECH
        510        520        530        540        550
GLVDALVTSI NHALDAGKCE DKSVENAVCV LRNLSYRLYD EMPPSALQRL
        560        570        580        590        600
EGRGRRDLAG APPGEVVGCF TPQSRRLREL PLAADALTFA EVSKDPKGLE
        610        620        630        640        650
WLWSPQIVGL YNRLLQRCEL NRHTTEAAAG ALQNITAGDR RWAGVLSRLA
        660        670        680        690        700
LEQERILNPL LDRVRTADHH QLRSLTGLIR NLSRNARNKD EMSTKVVSHL
        710        720        730        740        750
IEKLPGSVGE KSPPAEVLVN IIAVLNNLVV ASPIAARDLL YFDGLRKLIF
        760        770        780        790
IKKKRDSPDS EKSSRAASSL LANLWQYNKL HRDFRAKGYR KEDFLGP
```

Figure S1 │ Putative binding sites of phospho-AKT substrate antibody in human PKP3. RXXpS/pT motif (phospho-AKT substrate antibody) are depicted in blue. Start and end of the armadillo repeat domain are indicated by blue arrows.
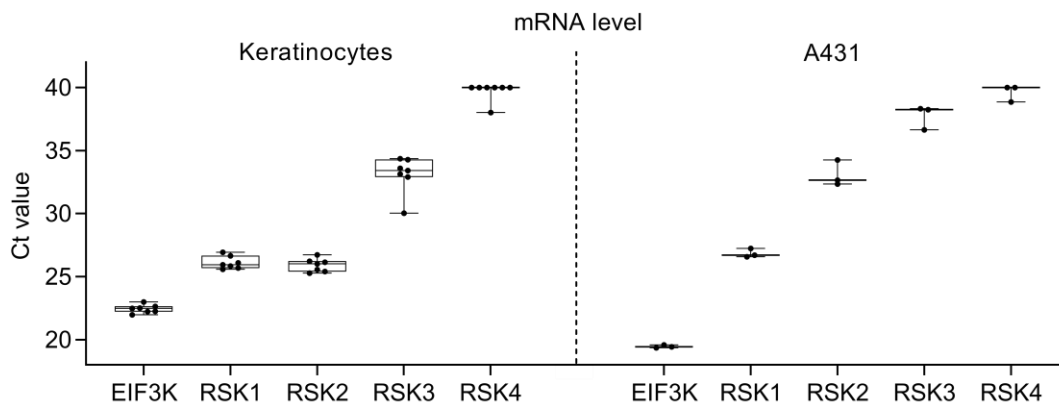
Figure S2 │ RSK1-4 mRNA levels in murine keratinocytes and A431 cells. For analyzing RSK mRNA levels, murine keratinocytes grown for 24 h in HCM and A431 cells grown for 24 h in standard DMEM were processed for qRT-PCR. EIF3K was used as an invariant endogenous control. Whereas RSK1 and RSK2 were abundant in keratinocytes and A431 cells, RSK3 and RSK4 were hardly detectable. The boxplot depicts the Ct values (keratinocytes n=7; A431 cells n=3). The Whiskers extend to the minimum and maximum values.
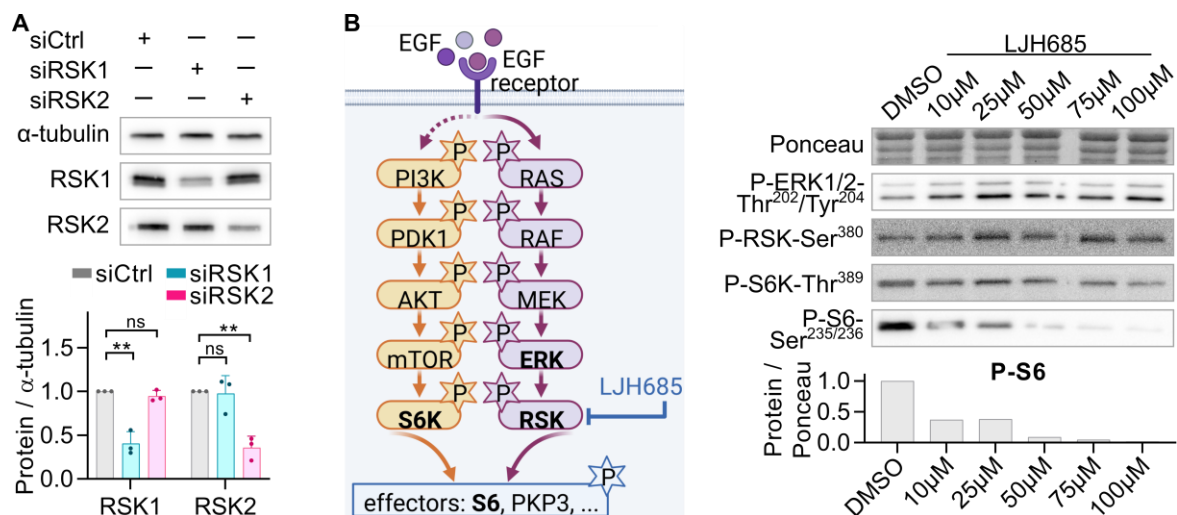
Figure S3 │ Validation of knockdown and inhibitor impact. (A) For analysis of knockdown efficiencies, murine keratinocytes transfected with non-targeting (siCtrl), RSK1, or RSK2 (siRSK1, siRSK2, respectively) directed siRNAs were switched to HCM at 48 h after transfection, and kept in HCM for another 24 h. In parallel with processing of immunofluorescence studies, cells were lysed in SDS lysis buffer. Total cell extracts were analyzed by western blotting with the indicated antibodies. Representative western blots (upper panel) showing the protein levels of RSK1 and RSK2. α-tubulin was used as a loading control. Knockdown of RSK1 or RSK2 was verified by impaired RSK1 and RSK2 protein levels, respectively. The bar plot (lower panel) depicts the protein amounts (+ s.d.; n=3) normalized to α-tubulin and relative to siCtrl-treated keratinocytes (first lane in western blot). Statistical significance was determined by one-way ANOVA with Tukey's multiple comparisons test. **(B)** The function and specificity of the RSK inhibitor LJH685 was analyzed by western blotting. The schematic (left panel, created with biorender.com) shows the impact of LJH685 on PI3K/AKT (orange colored) and RAS/RAF/MAPK (purple colored) signaling pathways with indicated analyzed targets (marked in bold). Murine keratinocytes were grown in HCM for 24 h before treatment with LJH685 (from 10 μM to 100 μM) for 1 h. Cells were lysed in SDS lysis buffer. Total cell extracts were analyzed by western blotting with the indicated antibodies. Representative western blots (upper right panel) showing the phosphorylation levels of ERK1/2, RSK, S6K, and S6. Ponceau S staining was used as a loading control. Impact of inhibitor LJH685 was verified by a decrease of S6 phosphorylation in a concentration-dependent manner. The bar plot (lower right panel) depicts the amount of phospho-S6 (n=1) normalized to Ponceau S staining and relative to DMSO-treated keratinocytes (first lane in western blot).
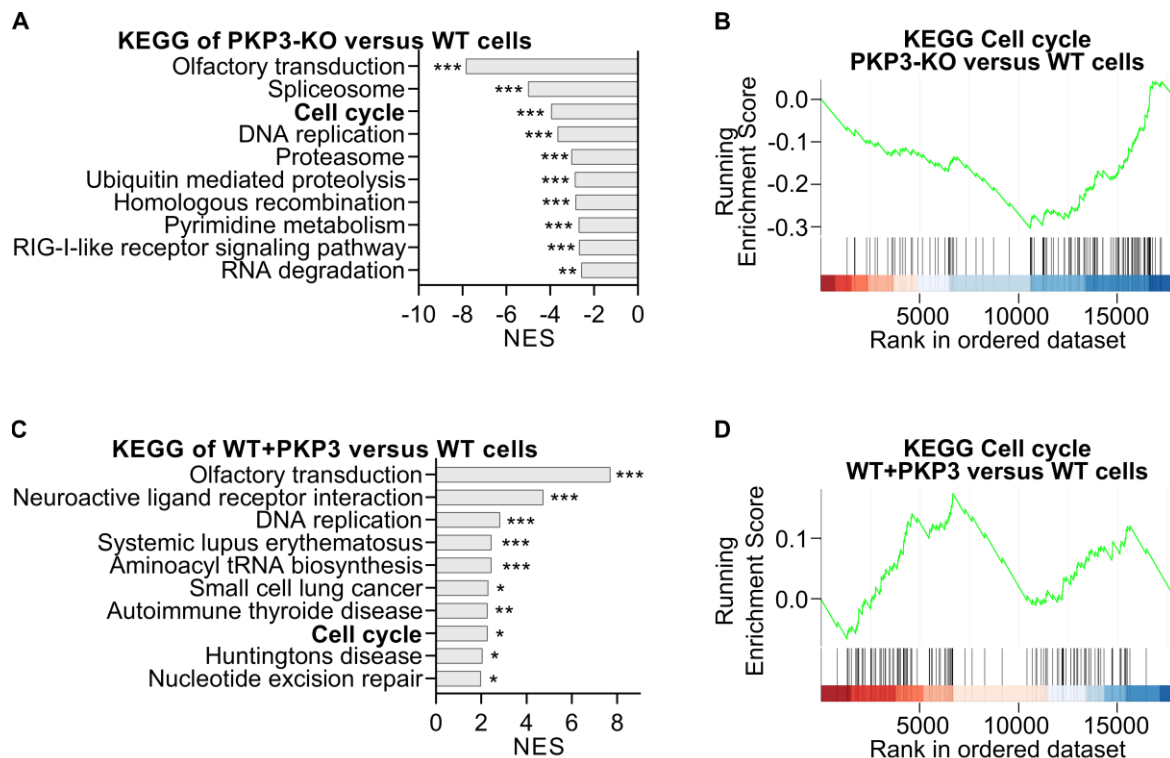
Figure S4 │ GSEA-based KEGG links PKP3 to cell cycle regulation. WT, PKP3-KO, and WT+PKP3 cells were grown for 24 h in LCM and prepared for RNA sequencing. Based on a list of all protein coding genes ranked according to log_2 fold changes, a GSEA was performed mapping the KEGG database. The GSEA-based KEGG shows that downregulated protein coding genes in PKP3-KO cells and upregulated protein coding genes in WT+PKP3 cells were mainly involved in cell cycle regulation. Calculation of log_2 fold changes and GSEA were kindly performed by Dr. Markus Glaß (Core Facility Imaging of the Medical Faculty, Martin Luther University). **(A, C)** The bar plots depict the normalized enriched scores (NES) of (A) the top ten most negatively enriched gene sets among protein coding genes in PKP3-KO versus WT cells or (C) the top ten most positively enriched gene sets among protein coding genes in WT+PKP3 versus WT cells. A positive NES reflects enrichment of the gene set at the top of the ranked list, i.e. gene sets overrepresented among induced genes. A negative NES indicates enrichment of the gene set at the bottom of the ranked list, i.e. gene sets overrepresented among repressed genes. The adjusted p-value estimates the statistical significance of the NES for a single gene set. The representative gene set which is further analyzed in (B) and (D) is marked in bold. **(B, D)** The GSEA enrichment plots for "KEGG Cell cycle" for (B) PKP3-KO versus WT cells and (D) WT+PKP3 versus WT cells shows the running enrichment score (green curve), which increases as a gene within the set is present while the GSEA walks down the rank ordered list of log_2 fold changes of protein coding genes. Vertical black lines indicate the positions of genes in the ranked dataset. Genes on the far left (red) correlates with the most upregulated cell cycle-associated genes, whereas genes on the far right (blue) correlates with the most downregulated cell cycle-associated genes.
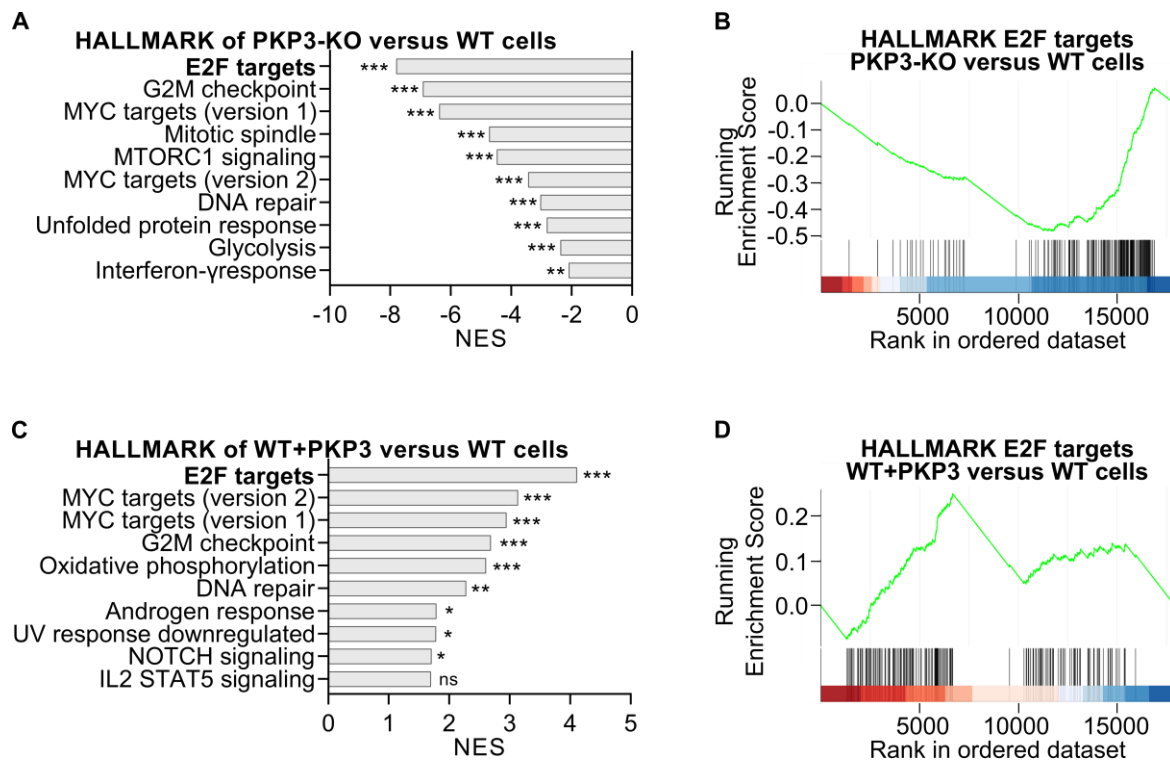
Figure S5 │ GSEA-based HALLMARK links PKP3 to E2F targets. WT, PKP3-KO, and WT+PKP3 cells were grown for 24 h in LCM and prepared for RNA sequencing. Based on a list of all protein coding genes ranked according to $\log_2$ fold changes, a GSEA was performed mapping the HALLMARK database. The GSEA-based HALLMARK shows that downregulated protein coding genes in PKP3-KO cells and upregulated protein coding genes in WT+PKP3 cells were mainly associated with E2F targets. Calculation of $\log_2$ fold changes and GSEA were kindly performed by Dr. Markus Glaß (Core Facility Imaging of the Medical Faculty, Martin Luther University). **(A, C)** The bar plots depict the normalized enriched scores (NES) of (A) the top ten most negatively enriched gene sets among protein coding genes in PKP3-KO versus WT cells or (C) the top ten most positively enriched gene sets among protein coding genes in WT+PKP3 versus WT cells. A positive NES reflects enrichment of the gene set at the top of the ranked list, i.e. gene sets overrepresented among induced genes. A negative NES indicates enrichment of the gene set at the bottom of the ranked list, i.e. gene sets overrepresented among repressed genes. The adjusted p-value estimates the statistical significance of the NES for a single gene set. The representative gene set which is further analyzed in (B) and (D) is marked in bold. **(B, D)** The GSEA enrichment plots for "HALLMARK E2F targets" for (B) PKP3-KO versus WT cells and (D) WT+PKP3 versus WT cells shows the running enrichment score (green curve), which increases as a gene within the set is present while the GSEA walks down the rank ordered list of $\log_2$ fold changes of protein coding genes. Vertical black lines indicate the positions of genes in the ranked dataset. Genes on the far left (red) correlates with the most upregulated E2F targets-associated genes, whereas genes on the far right (blue) correlates with the most downregulated E2F targets-associated genes.
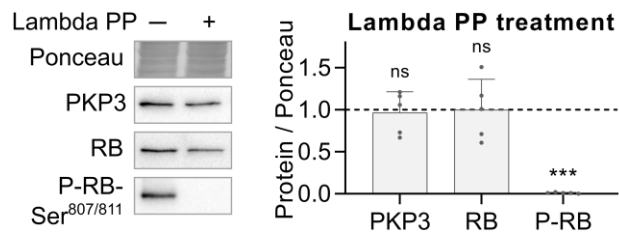
Figure S6 │ Validation of phospho-RB-Ser^807/811 antibody specificity. To validate the phospho-RB-Ser[807/811] antibody in murine keratinocytes, WT cells were grown for 24 h in LCM, lysed in IP buffer II, homogenized and cleared by centrifugation. The entire cell lysate was incubated with Lambda PP at 30°C for 30 min. Total cell extracts were analyzed by western blotting with the indicated antibodies. Representative western blots (left panel) showing the protein level of PKP3, RB, and phospho-RB. Ponceau S staining was used as a loading control. Specificity of the phospho-RB-Ser[807/811] antibody for phospho-RB was confirmed by abolished phospho-RB signal, whereas Lambda PP treatment did not affect PKP3 or RB levels. The bar plot (right panel) depicts the protein amounts (+ s.d.; n=5) normalized to Ponceau S staining and relative to keratinocytes without Lambda PP treatment (first lane in western blot). Statistical significance was determined by a student's unpaired two tailed *t*-test.

7.2. Abbreviations

ANOVA	one-way analysis of variance
AU	area units
BCA	bicinchoninic acid
BiFC	bimolecular fluorescence complementation
BrdU	5-bromo-2'-desoxyuridine
BSA	bovine serum albumin
CDK	cyclin-dependent kinase
CDKN	cyclin-dependent kinase inhibitor
CDT	chromatin licensing and DNA replication factor
CHX	cycloheximide
CIP	contact inhibition of proliferation
CIP/KIP	cyclin-dependent kinase interacting protein/kinase inhibitory protein
c-Src	cellular sarcoma
C_t	cycle threshold
DMEM	Dulbecco's modified Eagle medium
DMSO	dimethyl sulfoxide
DNM1L	dynamin-1-like protein
DSP	desmoplakin
DTT	dithiothreitol
ECL	enhanced chemiluminescence
EDTA	ethylenediaminetetraacetic acid
EGF	epidermal growth factor
EGFP	enhanced green fluorescent protein
EGFR	epidermal growth factor receptor
EGTA	ethylene bis(oxyethylenenitrilo)tetraacetic acid
eIF	eukaryotic translation initiation factor
EIF3K	eukaryotic translation initiation factor 3 subunit k
EMT	epithelial mesenchymal transitions
ERK	extracellular-signal regulated kinase
ETS	E twenty-six
ETV	E twenty-six variant transcription factor
FCS	fetal calf serum
FEN	flap endonuclease
FUCCI	fluorescent ubiquitination-based cell cycle indicator
FW	forward primer
FXR	fragile X mental retardation syndrome-related protein
G3BP	rat sarcoma virus GTPase-activating protein-binding protein
GEM	geminin
-GF	without growth factors
GFP	green fluorescent protein
GSEA	gene set enrichment analysis
GSK	glycogen synthase kinase
h	human
HA	human influenza hemagglutinin
HCM	high calcium medium

IF	immunofluorescence
IGF-1	insulin like growth factor 1
INK4	inhibitors of cyclin-dependent kinase 4
IgG	immunoglobulin G
IP	immunoprecipitation
JAK	janus kinase
KO	knockout
KRAS	kirsten rat sarcoma virus
LCM	low calcium medium
MAPK	mitogen activated protein kinase
MCM	minichromosome maintenance complex component
MEK	mitogen-activated protein kinase kinase
miRNA	microRNA
MKC	murine keratinocytes
mRNA	messenger RNA
MT	microtubule stabilization
mTOR	mechanistic target of rapamycin
NES	normalized enriched scores
NP-40	nonidet P 40
ORF	open reading frame
p	promoter
P	phospho
PABPC	polyadenylate-binding protein
PBS	phosphate-buffered saline
PBSE	phosphate-buffered saline with ethylenediaminetetraacetic acid
PDK	3-phosphoionositide-dependent protein kinase
PI3K	phosphoinositide 3-kinase
PKC	protein kinase C
PKP	plakophilin
PP	protein phosphatase
RAF	rapidly accelerated fibrosarcoma
RAP1 GTPase	rat sarcoma virus-related protein 1 guanosine triphosphatase
RAS	rat sarcoma virus
RB	retinoblastoma
REV	reverse primer
RIPA	radioimmunoprecipitation assay
RSK	ribosomal S6 kinase
RUNX	runt-related transcription factor
S6K	s6 kinase
SDS	sodium dodecyl sulfate
SDS-PAA	sodium dodecyl sulfate polyacrylamide
SDS-PAGE	sodium dodecyl sulfate polyacrylamide gel electrophoresis
SNAI	snail family transcriptional repressor
STAT	signal transducer and activator of transcription
TBS	tris-buffered saline
TBST	tris-buffered saline with Tween 20

TEMED	tetramethylethylenediamine
TGF-β	transforming growth factor-β
TYMS	thymidylate synthase
3'-UTR	3'-untranslated regions
WB	western blotting
WT	wildtype
ZEB	zinc finger E-box binding homeobox

7.3. List of figures

7.4. List of tables

DANKSAGUNG

„Eine der Lektionen, die ich in den verschiedenen Phasen meiner Karriere gelernt habe, ist, dass Wissenschaft nicht alleine gemacht wird. Fortschritte werden erst durch Gespräche und den Austausch mit anderen erzielt."

(Carol W. Greider, Molekularbiologin)

CURRICULUM VITAE

Personal Details

Name: Lisa Müller
Birth: 01.11.1990, Halle
Nationality: German

Education

1996-1999	Grundschule "Kastanienallee", Halle
1999-2000	Grundschule "Am Gimritzer Damm", Halle
2000-2009	Gymnasium "Georg-Cantor", Halle – Abitur

Scientific Education

2010-2013	B.Sc. studies in Biology at the Martin Luther University Halle Wittenberg
2013	Bachelor thesis under supervision of PD Dr. Dietmar Weinert at the Martin Luther University Halle Wittenberg; title: "Untersuchungen zur Gedächtnisleistung von *Phodopus sungorus*: Vergleich von arrhythmischen und Wildtyp-Tieren"
2013-2015	M.Sc. studies in Biology at the Martin Luther University Halle Wittenberg
2015	Master thesis under supervision of PD Dr. Dietmar Weinert at the Martin Luther University Halle Wittenberg; title: "Der Einfluss circadianer Rhythmen auf das Sozialverhalten von Dsungarischen Kurzschwanzzwerghamstern (*Phodopus sungorus*)"
2016-2017	Research assistant in the laboratory of Prof. Dr. Mechthild Hatzfeld at the Martin Luther University Halle Wittenberg
2017-2022	Doctoral studies in the laboratory of Prof. Dr. Mechthild Hatzfeld at the Martin Luther University Halle Wittenberg

LIST OF PUBLICATIONS, PRESENTATIONS, AND POSTERS

Publications

Müller L, Keil R, Hatzfeld M (2023). "Plakophilin 3 facilitates G1/S phase transition and enhances proliferation by capturing RB protein in the cytoplasm and promoting EGFR signaling*." Cell Reports.* 42: 112031. DOI: 10.1016/j.celrep.2023.112031.

Müller L, Hatzfeld M and Keil R (2021). "Desmosomes as signaling hubs in the regulation of cell behavior." *Frontiers in Cell and Developmental Biology*. 9: 745670. DOI: 10.3389/fcell.2021.745670.

Weiße J, Rosemann J, **Müller L**, Kappler M, Eckert AW, Glaß M, Misiak D, Hüttelmaier S, Ballhausen WG, Hatzfeld M, Hämmerle M and Gutschner T (2021). "Identification of lymphocyte cell-specific protein-tyrosine kinase (lck) as a driver for invasion and migration of oral cancer by tumor heterogeneity exploitation." *Molecular Cancer*. 20(1): 88. DOI: 10.1186/s12943-021-01384-w.

Müller L, Rietscher K, Keil R, Neuholz M and Hatzfeld M (2020). "Plakophilin 3 phosphorylation by ribosomal s6 kinases supports desmosome assembly." *Journal of Cell Science.* 133(8) DOI: 10.1242/jcs.238295.

Presentations

Müller L: "Plakophilin 3 is a central regulator of proliferation and G1-S phase transition", Annual symposium of the DFG priority programme 1782, 10/04/2022-10/06/2022, Aachen, Germany.

Müller L: "A novel role of the desmosomal regulator plakophilin 3 in proliferation and cell cycle progression", International meeting of the DFG priority programme 1782, 10/04/2021-10/06/2021, online.

Müller L: "Role of plakophilin 3 in desmosome assembly and cell proliferation", Young investigator retreat of the DFG priority programme 1782, 11/18/2019-11/19/2019, Würzburg, Germany.

Müller L: "Quantification of immunostainings", Young investigator retreat of the DFG priority programme 1782, 11/18/2019-11/19/2019, Würzburg, Germany.

Posters

Müller L and Hatzfeld M: „Plakophilin 3 is a central regulator of proliferation and G1/S phase transition", 1st Alpine desmosome disease meeting, 10/12/2022-10/14/2022, Grainau, Germany.

Rietscher K, **Müller L**, Neuholz M and Hatzfeld M: „Regulation of plakophilin 3 by EGF signaling", International meeting of the DFG priority programme 1782, 07/04/2018-07/06/2018, Halle, Germany.

EIDESSTATTLICHE ERKLÄRUNG

Hiermit erkläre ich, dass ich die vorliegende Arbeit selbständig und ohne fremde Hilfe verfasst habe. Alle von mir verwendeten Quellen und Hilfsmittel wurden vollständig angegeben. Die aus den verwendeten Werken wörtlich oder inhaltlich entnommenen Stellen wurden als solche kenntlich gemacht.

Mit der vorliegenden Arbeit bewerbe ich mich erstmals um die Erlangung des Doktorgrades.

Halle, September 2022

Lisa Müller